ADVANCING THE ENGINEERING UNDERSTANDING OF COFFEE EXTRACTION

BY

BORJA ROMAN CORROCHANO

A thesis submitted to
The University of Birmingham
For the degree of
DOCTOR OF ENGINEERING

School of Chemical Engineering
College of Physical and Engineering Sciences
The University of Birmingham
December 2015

ABSTRACT

This Engineering Doctorate thesis seeks to advance the fundamental engineering understanding of coffee extraction. This aim is based on the current need of the coffee industry to optimise soluble coffee process (as stress on water and energy is dramatically increasing), and the growing popularity of On-Demand coffee systems.

Firstly, the macrostructure, microstructure and extraction parameters of roast and ground coffee were investigated. Coffee grinds were shown to be non-spherical (sphericity ~ 0.75) particles whose sizes follow bimodal distributions. A combination of helium pycnometry and mercury porosimetry revealed that coffee microstructure is formed by micro-pores (~ 40 μm) and nano-pores (10-20 nm). The overall porosity was between 0.50 and 0.65. From the mercury hysteresis curves, the tortuosity of the grinds were measured and were between 3 and 7. This microstructural data was used to estimate the effective diffusion coefficients of representative molecules that form the coffee soluble solids, and they resulted to be in the range of 10^{-10} – 10^{-12} $m^2\ s^{-1}$.

The kinetics of extraction of coffee soluble solids was measured in a stirred vessel and a packed bed extraction rig for a variety of process conditions. The experimental results were compared with the simulations obtained with a multi-scale extraction model that considers extraction as a combination of transport phenomena occurring at the particle scale (~μm) and the packed bed scale (~cm). The continuously bimodal nature of the considered coffee grinds was accounted for in the model by simultaneously solving the concentration profile in two particles (fine and coarse particles). A single diffusing species, i.e. coffee soluble solids, was considered.

In the case of the stirred vessel (longer extraction times), it was shown that the extraction curve could not be fully described with a single effective diffusion coefficient. This is due to the chemical heterogeneity (fast and slow diffusing molecules) of coffee soluble solids. Effective diffusion coefficients in the range of 10^{-11} m^2 s^{-1} were shown to offer the better fit if a single effective diffusion coefficient is to be used (*MPE* = 6-17 %). When four effective diffusion coefficients (representing the whole size spectrum of the species forming coffee soluble solids) were considered, the agreement between the model simulations and the experiments improved significantly (*MPE* = 5-8 %). In the case of the packed bed extraction, it was shown that the model predicted quite accurately literature extraction data for caffeine, chlorogenic acids and trigonelline in the espresso regime.

Regarding the hydrodynamics of coffee packed beds, a new methodology to estimate the permeability of roast and ground coffee in steady state was developed. Permeability of beds typically used in espresso practice resulted to lie between 10^{-13}-10^{-14} m^2. The lack of agreement between the experimental results and the theoretical estimates obtained with permeability models based on Kozeny-Carman equation, was attributed to the effect of hydrodynamic forces on coffee grinds.

ACKNOWLEDGEMENTS

I would like to express my gratitude towards my academic supervisors, Prof. Serafim Bakalis, and Prof. Peter Fryer for the opportunity they gave me and their continuous guidance through the project.

I would like to express my sincere gratitude to my industrial supervisor, Dr. John Melrose. His commitment to the project, patience, motivation, and willingness to enlighten me with his immense knowledge have been instrumental to accomplish this thesis.

Within Mondelez International, I would also like to thank Dr. Mark Norton, who was of great help during the first steps of this project. I thank Andrew Bentley for allowing me to use the extraction rig that he himself designed and built. I would also like to express my gratitude to my work group in Mondelez International for continuous support, and endless cups of coffee. Especial thanks go to Marcela Montoya Guerra, for sharing with me her work and expertise on flaked coffee, but almost more importantly for her support, and for listening to me when I needed it. I thank Dr. Tülay Massey for her encouragement especially during the writing period. I thank Dr. Sylvia Gaysinsky, Etienne Arman, and Dr. Mehdi Almant for being always willing to help and stimulating scientific discussions.

Within the University of Birmingham, I would like thank Dr. Richard Greenwood for guidance, encouragement and the multiple currys and pints we have shared. My thanks also go to John Hooper and Lynn Draper for their help with administrative

procedures, and Dr. James Bowen and Theresa Morris for training and assistance with Science City and SEM equipment, respectively.

I would also like to thank my friends Maria, Nuno and Diana for all the fun we have had all these years and their support. My thanks also go for my friends in Birmingham, Banbury and Spain.

I would also like to thank Dr. Patricia Perez Esteban, Patri, for having proof-read this manuscript at least twice, for listening to all my presentations at least 30 times each, for allowing me to do most part of this journey with her, for her incredible patience when dealing with my emotional rollercoasters, and, above all, for believing in me unconditionally. My gratitude is truly more than words can express. Gracias.

Last but not least, thanks to my lovely family, parents Gabriel and Resu and brother Alberto. Soís la mejor familia que uno pudiera desear, muchísimas gracias por todo vuestro apoyo, cariño y compresión durante toda mi vida y en especial durante estos años. Gracias.

TABLE OF CONTENTS

LIST OF FIGURES

LIST OF TABLES

NOMENCLATURE

a, b, c, d	Fitting constants for the experimental flow rate
A	Area
Bi	Biot number
C_b	Concentration inside the bulk
$C_{b\ eq}$	Concentration at equilibrium in the bulk
$C_{s,0}$	Initial concentration inside the solid
C_s	Concentration inside the solid
$C_{s\ eq}$	Concentration at equilibrium inside the solid
$C_{aliquot}$	Concentration of an aliquot
C_{bed}	Concentration in the bed
C^*	Dimensionless concentration
Ca	Capillary number
c	Generic diffusion tensor in COMSOL Multiphysics
d_{pore}	Pore diameter
D_b	Bulk diffusion coefficient
D_{eff}	Effective diffusion coefficient
d	Diameter
$d_{[3,2]}$	Sauter mean diameter of a particle size distribution
$d_{[4,3]}$	Volume mean diameter of a particle size distribution
d_{fine}	Mode of the fine size class of a particle size distribution
d_{coarse}	Mode of the coarse size class of a particle size distribution
d_a	Mass coefficient
H_m	Microstructural hindrance factor
h	Distance penetrated by water in a porous particle
i	Denotes a given size class in the extraction model
J_i	Mass flux coming out of size class i
k_{obs}	First order kinetic constant
K	Solid-liquid partition coefficient
L_0	Initial height of the bed

L_t	Bed height reduction at each time point
L_{actual}	Height of the bed after consolidation
m	Mass
M	Extracted mass
n	Number of moles
n	Exponential parameter in the bed porosity-bed tortuosity equation
n	Number of taken aliquotes
P	Pressure
P_{trans}	Pressure read by the pressure transducer
Q	Flow rate
r	Radial coordinate
Re	Reynolds number
R	Radius of a particle
r_h	Hydraulic radious
S	Swelling factor of the grinds (swollen volume / dry volume)
S	Strength
sc	Total number of considered size classes in the extraction model
sp	Total number of considered species in the extraction model
S_v	Surface-to-volume ratio of a packing material
Sc	Schmidt number
Sh	Sherwood number
T	Temperature
t^*	Dimensionless extraction time
t	Time
t_R	Relaxation time
u	Generic variable in PDE in COMSOL Multiphysics
$V_{distribution}$	Volume of the grind
$v_{distribution}$	Specific volume of the grind
v_{closed}	Specific volume of closed pores
v_{open}	Specific volume of open pores
v_{solid}	Specific volume of a coffee blend
V_{coffee}	Volume of coffee
V_T	Volume fraction of mercury entrapped

v_{in}	Intruded volume of mercury
v_{ex}	Extruded volume of mercury
$V_{s,eq}^{ext}$	Volume of the particles after extraction
V_b	Volume of the bulk phase
V_w	Original volume of water added in extraction experiments
V_{wp}	Volume of water absorbed by the coffee particles
V_s	Removed volume from the bulk solution by sampling
V_{cum}	Cumulative volume
$V_{aliquot}$	Volume of an aliquot
v	Fluid velocity
X_{50}	Median diameter of a particle size distribution
y^*	Dimensionless extraction yield
y	Extraction yield
$y_0\,(\Psi_j)$	Long time limit extraction yield

Greek letters

$\alpha_{chamber}$	Diameter-length ratio of a brewing chamber
α	Coffee-water relation
β	Denotes a given species in the extraction model
γ	Surface tension
$\Delta P_{elements}$	Pressure drop caused by the elements of the rig
ΔP_{bed}	Pressure drop across the bed
ε_{open}	Open porosity
ε_{closed}	Closed porosity
$\varepsilon_{particle}$	Porosity of a particle
ε_{bed}	Porosity of a packed bed
$\varepsilon_{bed\,ss}$	Porosity of a packed bed at the steady state
θ	Contact angle
κ	Permeability of a coffee packed bed
κ_r	Relative permeability of a coffee packed bed

λ	Consolidation degree
λ	solute-pore radius ratio
μ	Dynamic viscosity
ρ_{solid}	Intrinsic solid density of roast coffee
ρ_{bed}	Density of the packed bed
$\rho_{particle}$	Density of a coffee grind
$\tau_{particle}$	Tortuosity of a particle
$\tau_{particle\ CPSM}$	Tortuosity as determined by CPSM model
τ_{bed}	Tortuosity of a packed bed
ν	Volume percentage of a size class
Φ	Sphericity
χ	Absorbed water per unit mass of fresh coffee
χ_0	Initial coffee moisture
Ψ_j	Coffee grind, with j= A-H

Abbreviations

CPSM	Corrugated pore structure model
DP	Degree of polymerisation
HF	High flowrate
LF	Low flowrate
HD	High density
LD	Low density
MPE	Mean percentage error
MW	Molecular weight
RGC	Roast and ground coffee
exp	Experimental
pre	Predicted
ET	Early time
LT	Long time
AS	Analytical solution
NS	Numerical solution

ss	Soluble solids
HR	Hydraulic resistance
max	Maximum

Chapter 1: Introduction

1.1. Background and objectives

The global popularity of coffee beverages can be attributed to their delightful flavour and aroma, along with the physiological effects of caffeine, which is regarded as the most used pharmacologically active substance (Petracco, 2005a). As a matter of fact, a well-known legend has it that it was precisely the effects of caffeine that led to the discovery of coffee as a food product in the 13th century. Kaldi, an Ethiopian goatherd, noticed that his goats started to jump and dance energetically after having chewed some (coffee) berries from a bush. A monk from a monastery nearby spotted the goat's behaviour and took some of the berries, roasted and brewed them. Upon consumption of the beverage, the monks were able to stay more alert during their night prayers (Smith, 2001).

Coffee is the second most-traded commodity in the world after oil, with a global market worth $32 billion annually (around 600 billion cups per annum) (International Coffee Organisation, 2016). From the practical point of view, producing a cup of coffee is a rather simple activity performed around 20000 times each second around the globe. However, delving into the underpinning physical-chemical mechanisms that drive the resulting organoleptic profile of a coffee beverage is an extremely complex challenge. The attributes of the green coffee beans, i.e. botanical (Arabica or Robusta) and geographical origin, as well as the applied roasting process, play a crucial role since they determine the nature and abundance of the some 1800 species that form a roast coffee bean (Petracco, 2001). However, the chosen extraction method to transfer these species from the coffee matrix into the cup also shapes the final chemical profile of the beverage, and thus its sensory attributes. In this respect, there are virtually as many coffee

extraction methods as cultures in the world. Amongst the well-known ones are espresso (Italy), Moka (Southern Europe), and drip filter (North America, Northern Europe). Coffee *aficionados* are well aware of the very different attributes of the beverages produced with each technique. This is the result of the interaction of the coffee complex physical-chemical nature (microstructure, chemistry and molecular size of the species), and the different extraction conditions (temperature, particle size, flow rate, extraction time, coffee weight) applied for each technique. Optimisation of the extraction conditions for each particular method is then aimed at obtaining the appropriate extraction profile in order to meet consumers' tastes.

Coffee extraction is not well understood yet. The process has been typically regarded as a *black box*: extraction conditions are mainly optimised using trial and error approaches combined with sensory evaluation. For example, in the case of espresso coffee, the quality of the cup largely depends on the *barista's* ability and intuition to select the appropriate set of extraction variables, e.g. coffee weight, particle size distribution, bed tamping. As a matter of fact, the traditional *barista's* rule states that '*to prepare an espresso cup correctly, it is necessary to set the right temperature and pressure, then to adjust the hydraulic resistance (by grinding and compacting), until the right volume of beverage is obtained at the right time'* (Petracco, 2005b). In an attempt to gain insights into the underlying mechanisms of the operation, the physical-chemical properties of the beverages have been measured and that information linked to sensory data (see Andueza et al. (2003), and references therein). Also, chemical analyses have been extensively carried out to measure the concentration of substances contained in coffee beverages, such as caffeine, melanoidins, and oils, that may affect human health (see e.g. Zhang et al. (2012)).

The current fast-paced Western lifestyle has led the consumers to demand more convenient food products, and coffee is not an exception. In order to fulfil this demand, the 20th century saw two of the greatest revolutions in coffee history: the appearance of soluble coffee in supermarket's shelves and On-Demand coffee systems.

Soluble (also known as instant) coffee is produced at the industrial scale by extracting roast and ground coffee that is subsequently either freeze-dried or spray-dried to produce a coffee powder. Upon hydration, the powder dissolves in hot water to create a beverage. Although the first known patent for soluble coffee was awarded in 177, as cited in Nestle's website (Nestle, 2013), it was during the first half of the 20th century when soluble coffee bloomed. Its popularity increased during this time partly due to the U.S. army consuming it during the World War II. Despite significant optimisation, coffee soluble processing is still water and energy intense, with some 30 litres of water consumed per *kg* of spray-dried soluble coffee produced (Humbert et al., 2009); this is equivalent to a consumption of 90 *ml* of water per cup of coffee assuming 3 *g* of coffee per cup. Only in the UK approximately 38000 tons of soluble coffee are produced per year (W. Griffiths, Personal communication, 2015). As stress on water and energy resources is dramatically rising, one of the coffee industry challenges is to reduce the usage of such resources without compromising the feasibility of the process, and in general, the attributes of the final product.

On-Demand coffee systems are formed by individual capsules (containing between 5 and 10 *g* of roast and ground coffee) that are extracted in small automatic brewers especially designed for that purpose. Amongst other factors, such as the capsule storage system guaranteeing the freshness of the roast and ground coffee, the increasing

popularity of On-Demand systems can be attributed to the fact that superior beverages are produced at the touch of a button: no special skills or extremely expensive equipment are required to produce beverages of a comparable quality to those produced by professionals. It can be then said that On-Demand systems bring a closer *coffee shop experience* to customers' living rooms. Since 1977, when Eric Favre invented and patented the *Nespresso*® system (Favre, 1979), over a hundred different On-Demand machines have been launched (C. Choukroun, Personal communication, 2015). Thus, On-Demand systems are a fast-growing, competitive market, which represent a substantial part of the business of the main actors in the coffee business this is, Nestle and Jacobs Douwe Egberts.

Coffee extraction has been traditionally regarded as an art rather than as a genuine process engineering unit operation occurring in small-scale extractors that are available in practically every household. Therefore, the aim of this Engineering Doctorate thesis is to advance the fundamental engineering understanding of coffee extraction. The thesis is particularly focused on the extraction of soluble solids from roast and ground coffee. This will contribute to the efficient design and optimisation of industrial soluble process and On-Demand products. To achieve this objective, a combination of experimental techniques were employed to characterise the physical properties and extraction behaviour of coffee. A multi-scale model that considers extraction as a combination of transport phenomena occurring at the particle scale ($\sim\mu m$) and the packed bed scale ($\sim cm$) was used to assist the interpretation of the experimental results, and analyse the sensitivity of extraction to the considered process parameters.

1.2. Relevance to Mondelez International

Mondelez International, Inc (formerly Kraft Foods), the industrial sponsor of this project, is one of the largest food, beverage and snack company in the world. Its net revenues ascended in 2014 to $34 billion. The company divides its business in 5 categories (Chocolate, Biscuits, Cheese & Grocery, Gum & Candy, and Beverages), with Beverages accounting for 16 % of the net revenue. The coffee business accounts for about 20 % of the global market and includes iconic brands such us *Kenco*, *Gevalia*, *Jacobs*, and *Carte Noir*. With the aim to meet the taste of the coffee drinkers around the world, more than 300 coffee blends are marketed under these brands.

Tassimo® is Mondelez's On-Demand system. It allows producing a range of coffee, tea and cocoa beverages, which makes the system one of the more versatile in the market. To ensure that optimal products are delivered every time, the extraction conditions (temperature, flow rate) are adjusted to the requirements of each beverage. This information is encompassed in a barcode located on the lid of the capsule that is read by the brewer. Mondelez's On-Demand portfolio also includes compatible capsules manufactured for other On-Demand systems (*Nespresso*®, *Senseo*®).

As of 6th of July 2015, Mondelez's coffee business and the Dutch coffee company D.E Master Blenders 1753 merged to create the world's largest *pure play* coffee company, Jacobs Douwe Egberts (JDE). In order to remain successful in the coffee increasingly competitive environment, it is of chief importance for the business to gain a deeper engineering understanding of the extraction operation in order to optimise products and processes in a fast, reliable and effective way.

1.3. Thesis layout

In this Chapter, the motivation, objectives and industrial relevance of this thesis have been presented.

Chapter 2 (Literature review) provides a comprehensive overview of the current state-of-the art of coffee extraction, and other fields that are relevant to coffee processing: physicochemical changes produced in the coffee beans upon roasting and grinding, the experimental and modelling approaches applied so far to study coffee extraction, and the fundamental theoretical principles underpinning solid-liquid extraction and flow in packed beds.

Chapter 3 (Material and methods) provides detailed information of the different coffee samples used throughout the study, the experimental extraction set-ups, and the variety of techniques applied to measure and characterise relevant coffee properties. The used extraction and permeability models are also described here. Finally, this Chapter also includes a general description of the implementation of the extraction models in the Computational Fluid Dynamic software used in this thesis (COMSOL Multiphysics®), and a mesh sensitivity analysis.

Chapter 4 (Particle fundamental characterisation) discusses the results obtained from the analysis of the properties of the grinds that are relevant to extraction, and are required to parametrise the extraction models presented in Chapter 3.

Chapter 5 (Extraction at the particle scale) examines the experimental extraction results collected in a stirred vessel set-up, for a variety of process conditions (stirring rate, particle size distribution, particle shape, temperature). These results are compared

with the predictions obtained with the extraction model at the particle scale. The model is also used to analyse the sensitivity of the extraction curves to process parameters.

Chapter 6 (Hydrodynamics of coffee packed beds) discusses the measured permeability of coffee beds in steady state as a function of particle size distribution, bed density, particle shape, temperature, and aspect ratio of the extraction cell. The theoretical predictions obtained with the proposed permeability models in Chapter 3 are then compared with the experimental values. Also, the observed non-steady state fluid flow during the earlier stages of extraction is discussed and hypotheses to explain the behaviour are proposed.

Chapter 7 (Extraction at the bed scale) presents the experimental extraction results collected in the packed bed extraction set-up, as a function of particle size distribution, flow rate, and coffee weight. These results are compared with the predictions obtained with the extraction model at the bed scale. A sensitivity study is then carried out to investigate subtle effects of the process parameters, e.g. flow rate, that are difficult to test at the experimental level. The experimental data is then used to analyse how the selection of process parameters can lead to the celebrated over-extracted and under-extracted *espresso* coffees. Also, through Chapter 7, the controversial effect of pressure on the final attributes of the beverage is discussed.

Chapter 8 summarises the conclusions of this thesis and proposes directions to carry out future work in the field.

1.4. Publications and presentations

Publications:

- **Corrochano, B.R.**, Melrose, J.R., Bentley, A.C., Fryer, P.J., and Bakalis, S. (2014). A new methodology to estimate the steady-state permeability of roast and ground coffee in packed beds. *Journal of Food Engineering, 150,* 106-116.
- Melrose, J.R, **Corrochano, B.R**, Norton, M, Silanes Kenny, J., Fryer, P.J, Bakalis, S. (2012). Optimising coffee brewing using a multi-scale approach. In ASIC (Ed.), *24th Conference of the Association for Science and Information on Coffee* (pp. 510–512). San Jose, Costa Rica.

Poster presentations:

- 12th International Congress on Engineering and Food, 14-18th June 2015. Quebec, Canada. (Two posters)
- 25th Conference of the Association for Science and Information on Coffee, 8-13th September 2014. Armenia, Colombia.
- 9th World Congress of Chemical Engineering, 18-13 August 2013. Seoul, Korea.
- Annual Meeting of the Institute of Food Technologists, 12-16 July 2013. Chicago, USA.
- 24th Conference of the Association for Science and Information on Coffee, 17-18th November 2012. San Jose, Costa Rica.

Oral presentations:

- 11th Annual Formulation Engineering Conference, 7-9th April 2014. Birmingham, UK.

- 10th Annual Formulation Engineering Conference, 8-10th April 2013. Birmingham, UK.
- 9th European Congress of Chemical Engineering, 21-25th April 2013. The Hague, Netherlands.
- 9th Annual Formulation Engineering Conference, 17-18th April 2012. Birmingham, UK.

Chapter 2: Literature review

2.1. Introduction

The aim of this Chapter is twofold: contextualise extraction in the frame of coffee processing, and provide a comprehensive review of the state-of-the-art of coffee extraction.

Section 2.2 presents an overview coffee processing. Roasting and grinding are briefly defined and reviewed in Section 2.2.1 and 2.2.2, respectively. Section 2.2.3 compiles the state-of-art on the practical understanding of coffee extraction and how process parameters affect the final quality of the drink. Section 2.2.4 reviews the typical composition and nature of the soluble solids that form part of a cup of coffee.

Section 2.3 introduces the engineering approach to solid-liquid extraction and reviews current knowledge of coffee extraction from this perspective. This section is divided in Extraction at the particle scale (Section 2.3.1), Extraction at the bed scale (Section 2.3.2), and Hydrodynamics of coffee packed beds (Section 2.3.3).

Section 2.4 presents the conclusions of the literature review and the identified gaps in the knowledge are discussed.

2.2. Coffee processing

The term coffee processing encompasses here all the operations to which green coffee beans are subjected with the final objective of producing a coffee beverage. A simplified schematic overview of coffee processing is displayed in Figure 2.1. The minimum required operations to produce a coffee beverage are roasting, grinding, and extraction (also known as brewing). In broad terms, the whole picture of coffee

processing is completed by an optional decaffeination step (prior to roasting), and a post drying step of the extract if the product being manufactured is soluble coffee.

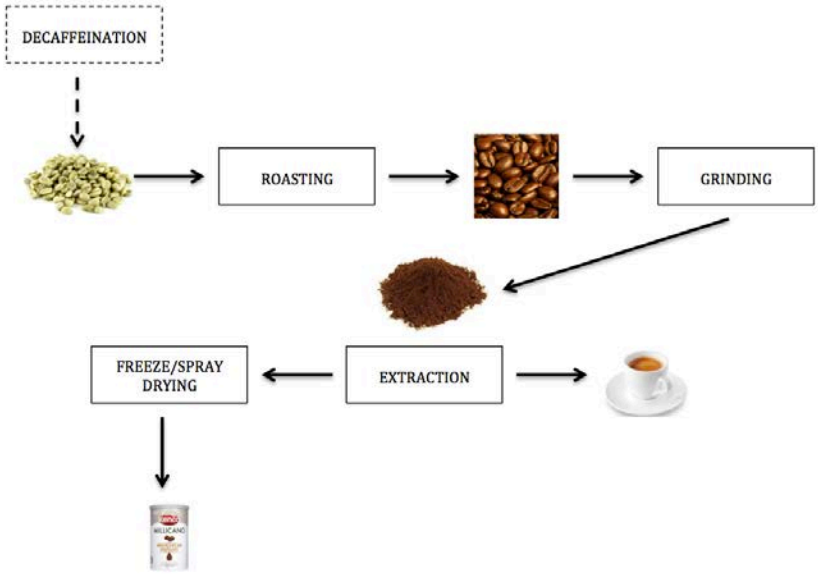

Figure 2.1: Schematic of coffee processing. The discontinuous lines indicate that the considered step is not mandatory to produce a coffee drink

Until the beginning of the 20th century, even roasting green coffee beans at the household was common practice (Sivetz and Desrosier, 1979a). However, increasing demand, desire of convenience, and acceleration of the pace of life, promoted the transformation of coffee processing from domestic operations to industrial scale processes. Therefore, the majority of the consumed coffee nowadays has been industrially processed to some degree. The need of the coffee industry to understand the processes profoundly in order to manufacture consistent products in an efficient way has come with this change of paradigm.

The next Sections present a general overview of the three basic steps of coffee processing.

2.2.1. Roasting

Roasting consists in the dry heat treatment of green beans (Bonnländer et al., 2005). The result of this operation is well-known: green beans, which posses a hard texture and a rather weak, greenly (not particularly appealing) aroma, are transformed into dark, brittle roasted beans of highly appreciated and rich aroma. Roasting can be therefore summarised as the process that brings about the required changes that make coffee suitable for the subsequent grinding and extraction.

From an engineering point of view, roasting is a complex process that involves heat and mass transfer coupled to chemical reactions and structural mechanics. Depending on the desired characteristics of the bean and the roasting equipment, temperatures up to 160-240 $°C$ and processing times between 8 and 20 minutes are commonplace (Fabbri et al., 2011). A general review of industrial roasting units can be found elsewhere (Eggers and Pietsch, 2001). Bonnländer et al. (2005) described the roasting steps as a function of the temperature achieved within the bean. These can be broadly summarised in (i) drying step (20-130 $°C$): the initial moisture of the green bean is eliminated and the colour of the beans starts shifting from green to light yellow-brown; (ii) chemical reactions (130-220 $°C$): the main reactions leading to flavour and aroma development occur in this temperature range. The mechanical properties of the beans also vary dramatically as their volume increases and they become brittle.

The coffee bean constituents can be divided in non-volatile and volatile species. Figure 2.2 displays the families of non-volatile species and the comparison between their typical composition in green and roasted Arabica coffee beans. The percentages shown in Figure 2.2 may vary for different roasting conditions.

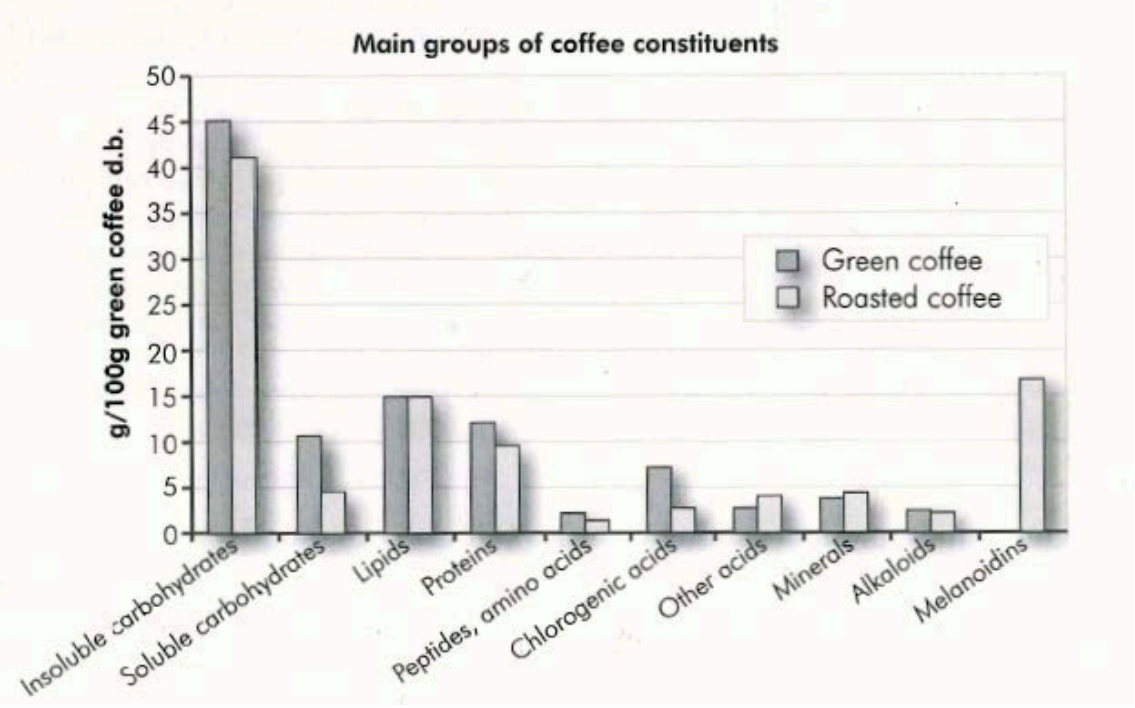

Figure 2.2: Typical composition of green and roasted Arabica coffee beans (Bonnländer et al. (2005))

The fractions of the non-volatile species that end up extracted into the beverage are typically referred to as *soluble solids*. The amount of soluble solids in a coffee extract greatly depends on the selected extraction conditions. In terms of sensory attributes, they are responsible for the sourness, bitterness and astringency of the beverage, as well as for its viscosity (related to mouthfeel) (Buffo and Cardelli-Freire, 2004). They are also instrumental in the visual appearance of the cup: the concentration of proteinaceous material is correlated to the foam ability and carbohydrates to the foam stability of espresso coffees (Nunes et al., 1997). In this respect, roasting improves the extractability of the protein and carbohydrate fraction. Leloup and Liardon (1993, cited in Bradbury 2001), showed that the solubility of molecules containing arabinose, galactose and mannose increased from 1 *g* per 100 *g* in green to 6 *g* per 100 *g* in roasted coffee. Nunes and Coimbra (2001) found that the extracted polysaccharides from roast coffee were between 22 and 93 % higher than from green coffee. Whereas the amount of extracted

proteins increased with roasting degree, carbohydrates increased up to a maximum and then started decreasing for darker roasted coffees (Nunes et al., 1997).

The production of melanoidins is one of the most significant chemical changes in the non-volatile species produced upon roasting. Melanoidins are polymeric products of the Maillard reaction: this is, the non-enzymatic browning reaction between carbohydrates and species with a free amino group. They have been defined as macromolecular, nitrogenous, brown species (Bekedam, 2008) and are typically present in all the heat-processed foods, e.g. coffee, malt, beer, breakfast cereals, cocoa. They conform an heterogeneous group of molecules regarding their molecular weight (3-100 *kDa*) and chemical properties (Homma, 2001). Significant efforts have been devoted to unveil their formation mechanisms and structure (Bekedam, 2008), but they still remain relatively unknown. Their concentration in coffee beverages is typically inferred from the difference between the total dissolved solids and the mass of these species that can be quantified. Alternatively, spectrophotometry at 405 *nm* can be also applied in order to determine the concentration of melanoidins. The importance of the melanoidins is mainly linked to their capacity to bind aroma molecules (Hofmann et al., 2001) and their antioxidant capacity (Bartel et al., 2015; Borrelli et al., 2002; Ludwig et al., 2012).

Regarding the volatile compounds (referred to as aroma), they are responsible for the flavour profile of the beverage. More than 800 compounds belonging to a wide range of chemical families have been identified in roasted coffee as aroma compounds (Grosch, 2001). However, approximately only 25-30 contribute significantly to the perceived aroma profile (Mayer et al., 2000). These species are typically grouped as a function of their characteristic flavour notes (sweetish/caramel, earthy,

sulphurous/roasty, smoky, fruity and spicy) (Mayer et al., 2000). The mechanisms of aroma formation involve a complex network of chemical reactions that are not still well understood. In addition to aroma, CO_2 is also generated as a by-product of some of these reaction routes, e.g. Maillard reaction, pyrolysis, Strecker degradation (Buffo and Cardelli-Freire, 2004). Although part of the generated gas leaves the bean during roasting, significant amounts can remain entrapped and pressurised within the bean structure (Nicoli and Savonitti, 2005). The entrapped amount largely depends on bean type as well as on process conditions; between 6 and 16 *mg* of CO_2 per *g* of coffee have been reported (Wang and Lim, 2013). Upon grinding, CO_2 is partly liberated from the bean but amounts between 4 and 12 $mg\ g^{-1}$ (depending on grind fineness) are retained by the grinds (Anderson et al., 2003; Wang and Lim, 2014). Before packing, roasted coffee is left in silos (tempering process) to reduce the CO_2 content and avoid swelling of the package or even explosion. Valuable volatile compounds are also lost in the process. Thus, the kinetics of degassing of roast and ground coffee has been investigated in order to maintain a fine balance between the remaining amount of CO_2 in the beans and quality (Anderson et al., 2003; Wang and Lim, 2014). These studies revealed that the degassing process seems to occur according to a complex mechanism involving Fickian diffusion, Knudsen diffusion and pressure flow. Degassing is rather slow with characteristic times of approximately 10 hours. Upon water penetration into the coffee particles during extraction, this gas is presumably released and contributes (upon mixing with the extracted soluble solids) to the formation of the iconic layer of foam on top of espresso coffees.

From the structural point of view, substantial changes in the macrostructure and microstructure of the beans are produced upon roasting. At the macrostructure level,

the density of the bean is reduced from 1100-1300 to 500-700 $kg\ m^{-3}$ (Geiger et al., 2002). Part of the formed volatile compounds, CO_2, and moisture leave the bean resulting in a weight decrease. This is commonly referred to as the *roasting loss* and is one of the parameters commonly used to characterise the extent of roasting. Moreover, since temperatures during roasting may exceed the glass transition temperature of the polymeric cell wall material (approximately 175 $°C$ for 10-11 % moisture (Geiger et al., 2002)), the pressure forces exerted by the gases formed inside the coffee cells results in the volume expansion of the beans (Geiger et al., 2002).

At the microstructure level, the volume expansion and loss of mass results in changes in the bean porosity and pore size distribution. The microstructure of porous solids plays a key role in mass transfer. In the particular case of coffee processing, mass transfer is at the heart of degassing after roasting, oxygen transport into the grinds (affecting product shelf life) and extraction performance. Therefore, significant effort has been devoted towards the elucidation of coffee microstructure and its dependency on roasting conditions. Pittia et al. (2011) measured the porosity of green and roasted coffee using X-Ray micro-tomography, and reported values of 0.041-0.064 and 0.397-0.420, respectively. Applying the same technique, Frisullo et al. (2012) followed the evolution of the microstructure of coffee beans with roasting time. Values of 0.10 were reported for green beans whereas after 5 minutes they observed a porosity of 0.36. Schenker et al. (2000) studied the influence of the combination of temperature and roasting times on the microstructure of beans roasted to the same degree. In their work (using mercury porosimetry experiments), it was found that higher temperatures and shorter times resulted in greater porosity and median pore sizes (0.528 and 13.45 *nm*,

respectively) as compared to lower temperatures and longer times (0.474 and 11.22 *nm,* respectively).

2.2.2. Grinding

In order to increase the exposed surface area per unit volume, the beans are subjected to a grinding step. Due to the brittleness stemming from the roasting stage, the applied stresses disrupt the bean structure reducing their size from several millimetres down to (typically) few hundred microns. As will be seen in Table 2.1, the desired degree of grinding depends on the chosen extraction technique. Sizes ranging from 100-150 μm (for the traditional Turkish coffee) up to 1000 μm (for French press) are common practice.

The most commonly used grinding devices in coffee processing are disc grinders and roller grinders. Disc grinders are typically used at smaller scales (households and coffee shops). Particle size reduction is achieved by the impact of blades at high speed on the beans. Roller grinders are preferably used at the industrial level. In this case, particle size reduction is achieved by the forces exerted by two rotating rollers when the beans pass through the gap left between them. The resulting particle size distribution depends on the configuration of the grinder, e.g. distance between the discs or separation between the rollers, type of rollers, number of rollers and the mechanical properties of the beans. The mechanical properties of the beans have been shown to mainly depend on moisture content, and to a lesser extend on roasting degree and bean type (Arabica or Robusta) (Pittia and Rosa, 2001).

Particle size distribution plays a relevant role in both the kinetics of extraction and the hydrodynamics of coffee packed beds. However, the fracture mechanisms of

roasted coffee beans have been barely considered in the published literature. Petracco and Marega (1991) proposed a finite element model to simulate coffee grinding. The main finding of their work is that due to the biological cellular coffee structure, ground coffee shows a naturally occurring polydispersed particle size distribution. Grinding tends to generate finer particles (< 20 μm) and coarser particles; the particle size distributions have been shown to be bimodal or even trimodal when measured by laser diffraction (Petracco, 2005b).

2.2.3. Extraction

Extraction is broadly defined as the process whereby species are transferred between two phases. In the particular case of coffee processing, extraction usually refers to the removal of caffeine from green beans or to the mobilisation of soluble solids and aroma from roast and ground coffee to produce a coffee extract. This coffee extract may already constitute a coffee beverage for consumption or may undergo a drying step to manufacture soluble coffee (see Figure 2.1). This Section reviews coffee extraction in the context of coffee beverages. At this stage, only the studies aimed at empirically optimising specific extraction techniques (essentially the majority of the published work) are considered. Investigations regarding the fundamental understanding of the mechanisms of extraction will be reviewed in Section 2.3.

Numerous extraction methods are available nowadays. The choice of a particular method is largely driven by cultural habits as much as by personal taste. The effectiveness of an extraction technique to transfer soluble solids and aroma species from the coffee particles to the cup shapes the chemical profile of the extract and thus its sensory profile. Regarding quality, the sensory attributes of a coffee extract can be partly

inferred from its extraction yield and concentration of total soluble solids (typically referred to in the coffee jargon as drink strength). Extraction yield is defined as the amount of material extracted into the cup per used unit mass of roast and ground coffee. As it can be seen in Table 2.2, coffee beverages are formed by a mixture of soluble solids that includes smaller molecules such as caffeine, chlorogenic acids, and minerals, and larger molecules such as melanoidins, protein material and polysaccharides. Lower yield beverages may present a higher proportion of smaller molecules as compared to higher yield brews; smaller molecules are extracted faster than larger molecules since the diffusion coefficient is inversely proportional to the hydrodynamic radius (according to the Stokes-Einstein equation). At the basics of flavour, the ideal extraction yield has been reported to lie between 18 and 22 % (Navarini et al., 2009). However, this figure will vary for different bean types and roasting degrees. Flavour profiles of lower and higher yield brews, referred to as under- and over-extracted drinks, have been described as acid-sweet, and astringent, respectively, and may be related to the relative proportion of smaller/larger molecules present in the drinks (Petracco, 2001). Aroma species in the beverages (typically in the range of 10^{-6}-10^{-3} g per kg of roasted coffee (Grosch, 2001)), hardly contribute to the measured value of extraction yield. Thus, a more accurate elucidation of the aroma profile requires specific analytical methods, e.g. solid-phase micro-extraction gas-chromatography couple with gas spectrometry (see Caporaso et al. (2014) and Gloess et al. (2013)).

The drink strength is defined as the percentage of soluble solids present in a coffee beverage. Since the density of coffee beverages can be approximated to that of water (Navarini et al., 2004), the drink strength can be also interpreted as the mass of soluble solids extracted into the cup per unit volume of drink. For a fixed mass of roast

and ground coffee processed, the strength of the drink decreases exponentially as the volume of the drink increases (Navarini et al., 2004). Sensory studies have revealed that higher strength values increased the mouthfeel of the drink (Navarini et al., 2004), and enhanced perception of flavour attributes (Andueza et al., 2007). In this respect, coffee beverages have been traditionally classified as a function of the drink volume *ristretto* < 20 *ml*; *espresso* 30-50 *ml*; and *lungo* > 50 *ml* (Navarini et al., 2004).

Producing an optimal cup of coffee involves the fine balance between the chemistry in the cup (indicated by extraction yield, aroma profile), the intensity of the attributes and mouthfeel (indicated by the drink strength). Achieving these features requires: (i) determination of the optimal extraction yield for the considered beans (origin, roasting degree); and (ii) selection of the process parameters (temperature, flow rate, particle size distribution) so that the appropriated drink volume and extraction yield are achieved in a given extraction time. Considerable research on the empirical optimisation of extraction techniques has been carried out. A first attempt to standardise and optimise coffee extraction was undertaken in the decade of 1950 at the Coffee Brewing Institute (USA) with the *Brewing Control Chart* as shown in Figure 2.3.

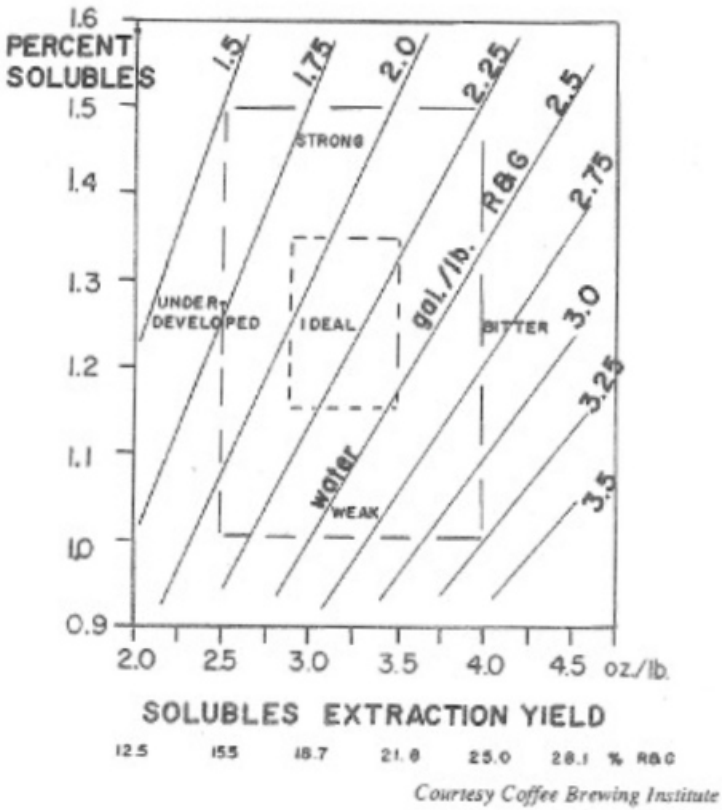

Figure 2.3: Brewing Control Chart. Concentration of the beverage (*y*-axis) vs. extraction yield (*x*-axis); the straight lines show the different water/coffee relations that may be used for extraction (Sivetz and Desrosier, 1979b)

The chart represents the dependence of the sensory characteristics of a coffee beverage as a function of its percentage of soluble solids (*y*-axis) (roughly equivalent to drink strength), extraction yield (*x*-axis) and used water/coffee relationship (straight lines). According to American consumers' standards, an *ideal* region for brews produced (presumably) with filter machines and percolators was defined in the chart (concentration of 1.15-1.35 % and extraction yield of 18-22 %). For higher/lower concentrations, coffee beverages were classified as strong/weak, whereas higher/lower extraction yields results in bitter (over-extracted)/underdeveloped (under-extracted) drinks. Although the chart is overall a useful illustrative tool, it misses the information regarding the relevant kinetics of extraction. For example, it can be seen that the chances of producing a beverage that lies in the *ideal* region are maximised when a

water/coffee relation between 1.75-2.75 $gal\ lb^{-1}$ is used. However, the use of these ratios does not guarantee an ideal beverage: the ultimate factor that determines whether that would occur or not is the relationship between the extraction kinetics at the particle scale and the total extraction time (given by the flow rate) to obtain the volume of beverage. In order to have a more accurate understanding of this, it is mandatory to know the mechanisms of extraction.

A general overview of the extraction yield and drink strength of coffee beverages produced with some of the most popular extraction methods, as well as the required technical conditions are reported in Table 2.1. This illustrates the great variability across extraction techniques. A description of the specific extraction devices can be found in the provided references.

Table 2.1: Overview of the characteristics and technical conditions of some popular extraction techniques

Brewing method	***Mass of RGC (g)***	***Flow rate (ml s^{-1})/ Volume (ml)***	***Extraction time (s)***	***Particle size (µm)***	***Temperature (°C). Inlet - Outlet***	***Strength (mg ml^{-1})***	***Yield (%)***	***Reference***
EM	[1]14.5 ± 0.2	2/51.4 ± 1.2	25-30		92 – 79.6 ± 3	59.48 ± 1.78	21.01 ± 0.6	
HP	6.7 ± 0.1	n.s/25.7 ± 0.6	n.s	~ 50 % between 250-500	92 – 87.6 ± 1.8	69.69 ± 1.78	25.01 ± 0.7	a
IE	6.9 ± 0.1	n.s/25.7 ± 0.6	n.s		92 – 82.5 ± 4.3	66.14 ± 1.83	24.40 ± 0.9	
ESA	[1]16.01 ± 0.01	[3]2.10/60	28.07 ± 0.2	~400		~56	~20.8	
LSA	[1]16.01 ± 0.01	[3]6.45/240	37.2 ± 0.3	~600		~13	~19.3	
EFA	[1]16.0 ± 0.6	[3]2.37/60	25.3 ± 0.7	n.s		~47	~17.6	
LFA	[1]16.0 ± 0.6	[3]6.80/240	35.3 ± 0.1	n.s		~13	~20.0	
NE	5.5 ± 1.1	[3]1.25/30	24 ± 2	n.s		~40	~22.2	
M	7.5 ± 0.1	[3,4]0.49/110	224 ± 12	~400	90/92 – 60.9/68.3	~21	~31.2	b
FP	27.493 ± 0.003	n.a/500	240 ± 2	1000-1025		~14	~26.2	
KK	27.500 ± 0.003	n.a/500	370 ± 10	1000-1025		~12	~21.9	
F	100.02 ± 0.03	[3]5.17/1800	348 ± 2	1000-1025		~10	~18.5	
EM	7.12 ± 0.4	0.95 ± 0.30/22.04 ± 3.92	[3]23.2 ± 8.00	n.s	n.s	77.13 ± 22.59	23.88 ± 1.96	[2]c
EM	7.5	[3]1.90/40	21±3	450-550	92 - 86 ± 2	34.59 - 42.74	19.0 - 25.3	d
POD	7	[3]1.02/25	23-26	n.s	87/104 (average)	48.15 to 59.05	18.6 to 21.8	e
ECF	7	n.s/25	n.s	~ 50 % between 250-500	75/85 – 67-78	60.46 – 67.78	21.3 - 23.3	f
F	25	[3]1.92/230	120		90 – 66.40 ± 0.65	12.20 ± 0.91	11.23 ± 0.84	
NEA	15.4	[3]0.25/75	300	350	90 - 61 ± 1.50	48.97 ± 4.01	24.17 ± 1.98	g
M	11.13	[3,4]0.34/62	180		Above 100 - 80.23 ± 3.75	56.57 ± 7.05	30.99 ± 3.87	
EM	7.5	[3]1/25	25		83 - 68 ± 1.50	73.66 ± 8.90	25.97 ± 3.14	

EM: Espresso Machine; **HP**: On-Demand Hyper Espresso (Illy Caffe); **IE**: On-Demand I-Espresso (Illy Caffee); **ESA**: Espresso Semi Automatic Machine; **LSA**: Lungo Semi-Automatic machine; **EFA**: Espresso Fully Automatic Machine; **LFA**: Lungo Fully Automatic Machine; **NE**: On-Demand Nespresso (Nestle); **M**: Moka; **FP**: French Press; **KK**: Karlsbader Kanne; **F**: Filtered Coffee; **POD**: On-Demand Coffee Pod; **ECF**: On-Demand Espresso Caffè Firenze; **NEA**: Neapolitan coffee. **1**:Amount for a double espresso; **2**: Average values of a field study in Italian coffee shops; **3**: Estimated from reported volumes, flow rates and extraction times; **4**: Brewing times in Moka preparation may include the pre-brewing time required to generate the steam that pushes the water through the bed.

All the volumes correspond to the measured mass of the brew assuming a brew density of 1 $g\ cm^{-3}$. Values ± standard deviation. **n.s**: not stated in the study; **n.a**: not applicable.

References: (a) Parenti et al. (2014); (b) Gloess et al. (2013); (c) Romani et al. (2004); (d) Andueza, De Peña, et al. (2003); (e) Albanese et al. (2009); (f) Masella et al. (2014); (g) Caporaso et al. (2014)

Table 2.1 shows that the selection of extraction parameters largely depends on the specific technique, and the variability in their magnitude is considerable. For example, no pressure systems, e.g. filter coffee or French press, tend to use coarser particle sizes (1000 μm) than pressure systems, e.g. espresso, Moka (250 – 600 μm). Coarser particle sizes effectively result in a slower extraction. Thus the former methods require longer extraction times in order to achieve an acceptable extraction yield. This also results in greater produced volumes. These variations in the extraction parameters affect the organoleptic properties of the drink. For example, as the average coffee consumer knows, filter coffee (F) or lungo coffees (LSA, LFA) are considerably *weaker*, i.e. more diluted, (strength ~ 10.00-12.20 $mg\ ml^{-1}$ or roughly 1.0-1.2 % to refer it to Figure 2.3) than any of the espresso coffees (strength 35.53-77.13 $mg\ ml^{-1}$). Gloess et al. (2013) evaluated the sensory profile (body, aroma, acidity, bitterness and astringency) of the coffees produced with nine different extraction methods (reference *b* in Table 2.1). Higher scores of all the attributes were achieved the greater the drink strength. Another example of the influence of extraction conditions can be appreciated in the highest extraction yield achieved by the Moka system (M) (30.99 – 31.20 %). This may be due to the fact that the temperatures used in Moka systems (typically above 100 $°C$ (Navarini et al., 2009)) may hydrolyse insoluble polysaccharides that become extractable.

Furthermore, there is also a more subtle variability within the same extraction technique, e.g. espresso coffees present extraction yields ranging from 17.6 % to 25.05 % and brew strengths from 35.53 to 77.13 $mg\ ml^{-1}$. These differences undoubtedly have implications in the organoleptic attributes of the cup and thus determines consumers

acceptance. Moreover, understanding this variability is crucial to On-Demand systems (single-serve coffee capsules), as they own part of their popularity precisely to the expected consistency. Analysing the causes of the differences of in espresso coffees reported in Table 2.1 may be challenging as the data belong to different studies. For example, the particle size distributions were assessed using different methods (sieves, laser diffraction) and these results may vary. However, the variability of espresso coffee drinks has received much attention in the last years, and has been consistently researched by some groups. Cid's et al. group published a series of studies (see below) that investigated the influence of process conditions (temperature, particle size distribution, coffee to water ratio and water pressure) on the characteristics and consumer acceptance of espresso coffee with a combination of physicochemical and sensory analyses. The main conclusions of these studies are summarised as follows:

- Influence of temperature (Andueza, Maeztu, et al., 2003): increasing the extraction temperature from 88 to 98 $°C$ resulted in an increase in yield from 19 % to 22 %. Extraction at 96 and 98 $°C$ resulted in an intensification of the astringent and bitter perception, and the concentration of the aroma compounds responsible for the woody/papery, burnt/roasted and acrid notes. The better judges acceptability was found at 92 $°C$.

- Influence of particle size distribution (Andueza, De Peña, et al., 2003): three particle size distributions (coarse, fine and very fine) of a 20:80 Arabica/Robusta blend were produced and its size analysed by sieving. The coarse peaks of the bimodal particle size distributions resulted to be between 450 and 550 μm approximately. Extraction yield and drink strength increased from 19 to 24 %,

and from 35.53 to 45.29 *mg* ml^{-1} respectively, when the particle size distribution was varied from coarse to very fine. The effect of particle size in extraction yield seems to be more significant than that of temperature in the considered range of 88-98 *°C* in Andueza, Maeztu, et al. (2003) (previously reviewed). The very fine grind was shown to increase the perception of woody/papery, burnt/roasty, acrid and rubbery notes. It was therefore concluded that the coffee produced with the very find grinds was over-extracted. Since the coarse grind did not allow '*a good development of the aroma*', the fine grind was found to be the optimal.

- Influence of coffee to water ratio (Andueza et al., 2007): espresso coffees (40 *ml*) were produced from 6.5, 7.5 and 8.5 *g* of roast and ground coffee. Whereas the extraction yield was virtually the same for the three considered coffee weights (20-21 % for 100 % Arabica coffees and 19-21 % for a 20:80 Arabica/Robusta blend), the drinks strength increased from 32 to 40 *mg* ml^{-1}. This resulted in an intensification of the astringent and bitter perception, and the concentration of the aroma compounds responsible for the burnt earthy/musty and acrid notes. Despite the fact that the espresso produced from 6.5 or 7.5 *g* of roast and ground coffee showed significantly different viscosity, no different in the perceived body of the drink was found.

- Influence of water pressure (Andueza et al., 2002): three different pressures (7, 9 and 11 *atm*) were used for the preparation of espresso coffees from 100 % Arabica coffee at the same temperature. Similar extraction yields (21 %) and drink strengths (35-37 *mg* ml^{-1}) were found for the range of pressures. Based on the sensory evaluation, 9 *atm* was found to be the optimal pressure.

The presented series of research is a comprehensive experimental investigation on the influence of extraction conditions on espresso quality. However, the lack of a more fundamental approach restricts the applicability of the results to other systems. Additionally, the aspects related with the hydrodynamics of the system were somewhat overlooked. For all the reported experiments, 40 *ml* of coffee were extracted in 21 ± 3 seconds, which resulted in average flow rates between 1.67 – 2.22 $ml\ s^{-1}$. For all cases, except when the effect of pressure was being tested, it was claimed that the extraction pressure was kept at 9 *bar*. In an espresso machine, the flow rate is set by the hydraulic resistance of the coffee bed, which depends on the geometric characteristics of the extraction chamber, fluid viscosity and bed permeability. The latter is determined by the porosity of the bed and the particle size. This points out that, in order to maintain the flow rate and pressure variables constant for coarse, fine and very fine particle sizes, the hydraulic resistance of the bed should have been adjusted by, for example, different degrees of compression of the bed, i.e. adjust the porosity of the bed. This will be illustrated in more detail in Section 2.3.3, where the hydrodynamics of packed beds is reviewed.

2.2.4. Typical composition of coffee soluble solids

During extraction, only a percentage of the total used mass of the roast and ground coffee is transferred to the cup (extraction yield). For commercial extraction systems, this has been shown to lie between 18 and 31 % (Table 2.1). The term *coffee soluble solids* refers to the species that are incorporated into the beverage in a fluid state. Thus, the definition excludes fragments of the coffee bean that may end up in the cup and can be separated from the beverage upon filtration.

The composition of a standard espresso beverage is displayed in Table 2.2. From the molecular weight point of view, the beverage contains smaller, lower molecular weight (< 1 *kDa*) species (lipids, chlorogenic acids, caffeine, minerals) and larger higher molecular weight (> 1 *kDa*) species (carbohydrates, melanoidins, proteins). This particularity of coffee soluble solids governs extraction behaviour: while the chemical nature of the species determines their thermodynamic properties (and thus its water solubility), their diffusion coefficient is given by the molecular size. Additionally, the representative percentages given in Table 2.2 will vary with extraction yield: as shown in Table 2.1, longer extraction times result in greater yields, as they allow the slower diffusing molecules to be extracted.

Table 2.2: Composition of an espresso beverage (adapted from Petracco (2005c))

Concentration (mg ml^{-1})	***Arabica***	***% Total extracted solids***
Total solids (after filtration)	47.3	100
Total lipids	2.5	5.3
Unsaponifiable lipids	0.4	0.8
Chlorogenic acids	4.3	9.1
Carbohydrates	8.0	16.9
Total element nitrogen	1.8	3.8
Caffeine	2.6	5.5
Ash	7.2	15.2
Elemental potassium	3.2	6.8
[1]Melanoidins	17.3	36.6

1 Percentage not reported in the original reference. It has been here estimated as the difference between the total soluble solids after filtration and the sum of the rest of the compounds

It is relatively straightforward to portray a clear picture of the nature of the low molecular weight material forming a coffee beverage, but the high molecular weight species are relatively unknown. Regarding the carbohydrate fraction, despite the fact that green coffee has significant amounts of mono- and disaccharides (up 9 % of the dry weight may be sucrose) (Bee et al., 2005), it is known that only traces of these remain

after roasting (Bonnländer et al., 2005). This has been confirmed by various investigations of the extracted polysaccharides in roast and ground coffee. For instance, Nunes and Coimbra (2001) found that in extracts produced at 80 *°C*, galactomannans accounted for 68-69 % of the total carbohydrate content whereas arabinogalactans represented 25-30 %. In the article, an average degree of polymerisation (DP) of 20 for the galactomannans fraction was estimated and they claimed that this value compared well to the range of 13-45 found by other authors. This DP is also in line with the range of 14.8-26.2 (Bradbury, cited in Bradbury, 2001)). These estimated DPs confirm the degradation of the smaller carbohydrate units. Leloup et al. (1997) studied the molecular weight distribution of the carbohydrates extracted from roast and ground coffee at 180 *°C* (typical temperature in the soluble coffee process) and the profile is shown in Figure 2.4.

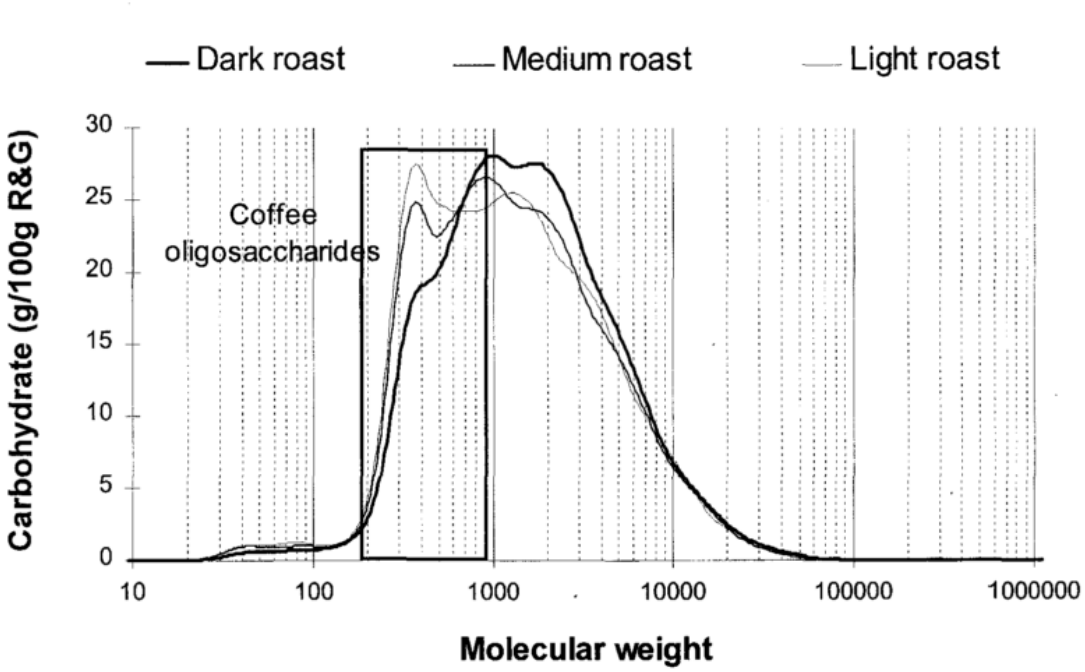

Figure 2.4: Carbohydrate molecular weight distribution of coffee extracts obtained at 180 *°C* from ground coffee roasted at different levels (Leloup et al., 1997)

According to Figure 2.4, the molecular weight ranged from approximately 0.1 to 30 *kDa* and the modal molecular weight was found to increase with roasting degree. The extremes of the profile are comparable to the values found by the same authors for coffee extracts at 95 *°C* (0.2-50 *kDa* for arabinogalactans and 0.8-80 *kDa* for galactomannans) Leloup and Liardon (1993, cited in Bradbury 2001). Thus, Figure 2.4 may represent an indication of the molecular weight profile of coffee beverages produced with consumer-scale extraction methods although with some limitations. It must be taken into account that considerably lower temperatures (75-95 °C; see Table 2.1) are typically used in these methods and those may not be able to solubilise higher molecular weight carbohydrates. On the other hand, hydrolysis reactions take place at 180 *°C* and therefore some of the carbohydrates that would have also been extracted at the lower temperatures may be fractionated.

Regarding melanoidins, they make an heterogeneous group of molecules regarding both molecular weight (3-100 *kDa*) and chemical properties (Homma, 2001). Bekedam (2008) was able to isolate a high (59 %) and low (41 %) melanoidins fraction using a diafiltration membrane with a cut-off value 3 *kDa*.

2.3. Coffee extraction as an engineering process: solid-liquid extraction from plant materials

Extraction has been reviewed so far in the context of the practical implications in the final quality of the drink. The aim of this Section is to describe coffee extraction from the engineering standpoint and review the state-of-the art in the field.

In this regard, solid-liquid extraction is a widely used operation applied to separate valuable molecules from plant materials in the food, nutraceuticals, pharmaceutical, cosmetic, flavour and fragrance industries (Kassing et al., 2010). At the consumer scale, solid-liquid extraction takes place, for example, when infused beverages (coffee, tea) are made. Aguilera (2003) divided the solid-liquid extraction process in six fundamental steps. A schematic is displayed in Figure 2.5.

1. Penetration of the fluid into the solid
2. Solubilisation and/or breakdown of the components
3. Transport of solutes within the solid porous microstructure
4. Incorporation of the solute from the surface of the solid to the bulk solution
5. Movement of the extract with respect to the solid
6. Separation and discharge of the extract

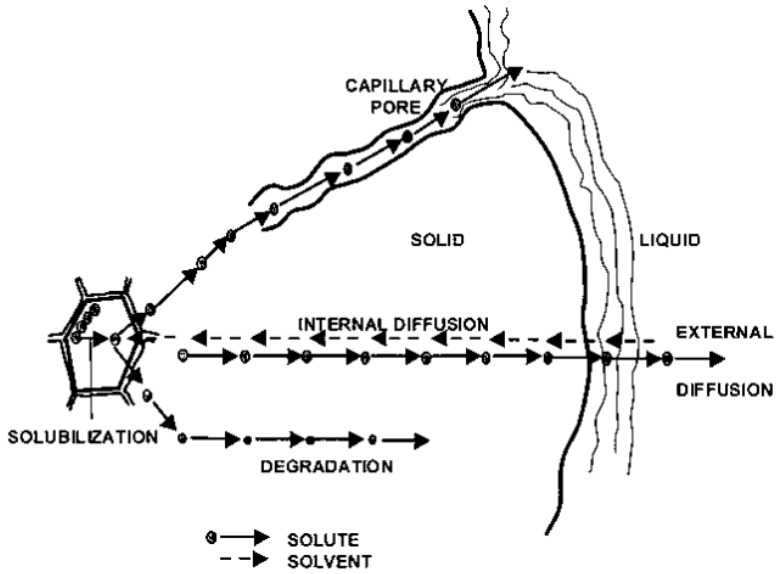

Figure 2.5: Steps involved in solid-liquid extraction processes from plant materials (Aguilera, 2003)

From an engineering perspective, solid-liquid extraction can be defined as the combination of multiple transport phenomena that occur across different scales. Solvent

penetration, solubilisation/breakdown and migration of the solutes occur at the particle scale. The particle size used in extraction represents a compromise between the mass transfer rate and the generated pressure drop across the packed bed (or subsequent filtration step if batch extractors are used). In industrial extraction processes typical particle sizes are between 2000-5000 μm (Schwartzberg, 1987). In coffee consumer applications smaller particles (100-1000 μm) can be afforded at the basis of quality (Table 2.1). Moreover, plant materials have a cellular structure. Vegetable cells show a complex microstructure formed by a membrane, cell wall and conduits (plasmodesmata) that connect one cell to another for the exchange of water and other nutrients (Aguilera and Stanley, 1990). Common cell and plasmodesmata conduit sizes are in the range of 20-50 μm and 20-80 nm, respectively. Thus, the particle scale may be further divided into the micro- and nano-scale. On the other hand, movement of the extract and discharge from the extractor occurs at the process scale, which may range from a few centimeters, e.g. an espresso packed bed, to 4-6 m in industrial processes (Schwartzberg, 1987).

2.3.1. Extraction at the particle scale

Molecular diffusion is the main mechanism whereby colloidal and nanoscale dissolved material is transported at the particle scale in extraction processes (Aguilera, 2003). The mechanism is characterised by a spatial chemical potential gradient (usually approximated to a concentration gradient) and a bulk diffusion coefficient, which is defined from Fick's first law:

$$J = D_b\left(\frac{\partial C}{\partial x}\right) \qquad \text{Eq. 2.1}$$

Where J is the diffusion flux ($kg\ m^{-2}\ s^{-1}$), D_b the bulk diffusion coefficient ($m^2\ s^{-1}$) and ($\partial C/\partial x$) the concentration gradient ($kg\ m^{-4}$). For the most common solvent-solute systems, the bulk diffusion coefficient is tabulated in reference textbooks, but it can also be estimated from available correlations, e.g. Stokes-Einstein equation.

In solid-liquid extraction processes the bulk diffusion coefficient is replaced by an effective diffusion coefficient. This is intended to encompass all the effects caused by the solid phase and other compounds (soluble or insoluble) that may delay the diffusion rate of a given solute. These effects may be classified as: (i) required finite time for the liquid to ingress in the solid and desorb the solute from the solid matrix; (ii) re-adsorption of the solute on the solid matrix or interactions with other co-solutes, e.g. formation of complexes (Schwartzberg and Chao, 1982); (iii) modification of the diffusion length due to swelling of the polymeric matrix (Mateus and Rouvet, 2007); and (iv) microstructural effects caused a combination of the hindering effects of the surface and throats of the pores, and tortuosity effects, that result in longer paths for the diffusing species (Aguilera, 2003; Samprovalaki et al., 2012).

Solid-liquid extraction is typically a non-steady state phenomenon. The time-dependent concentration gradient of a given species inside the solid can be obtained by solving Fick's second law (shown in Eq. 2.2 in spherical coordinates; for other geometries and concentration dependent diffusion coefficients the relevant forms of Fick's second law can be found in Crank, (1975)) with appropriate boundary conditions. This allows the computation of the kinetics of extraction, i.e. mass extracted of a given compound over time, which is the crucial information for optimisation of extraction process.

$$\frac{\partial C_S}{\partial t} = D_{eff}\left(\frac{\partial^2 C_S}{\partial r^2} + \frac{2}{r}\frac{\partial C_S}{\partial r}\right) \qquad \text{Eq. 2.2}$$

Where D_{eff} is the effective diffusion coefficient ($m^2\ s^{-1}$), C_S the concentration of the solute inside the solid ($kg\ m^{-3}$) and r the radial coordinate (m). Much effort has been devoted towards obtaining analytical solutions to Eq. 2.2 for the classical boundary conditions (Crank, 1975; Stapley, 2002). However, the resulting infinite Fourier series are tedious to implement, as they require a large numbers of terms in the summation to converge, especially at earlier times (see Chapter 3), and, in some cases, the evaluation of parameters from trigonometric equations. This has certainly promoted the use of simplified models to analyse extraction systems (empirical models, long-time approximation), and the use of numerical solutions. Moreover, numerical solutions are the only alternative for more complex scenarios relevant to coffee extraction, e.g. multi-particle systems; the analytical solutions are here limited to simple boundary conditions, e.g. constant concentration at the boundary, that may not accurately represent the real system (Stapley, 2002).

The next Sections will review two approaches to the determination of the relevant effective diffusion coefficients required to perform the extraction simulations.

- Effective diffusion coefficients fitted from experimental data

Effective diffusion coefficients have been traditionally derived by fitting experimental extraction data (concentration or extraction yield vs. time) to solutions of the relevant models. An extensive compilation of bulk and derived effective diffusion coefficients for food systems is available in Schwartzberg and Chao (1982). In the case of coffee, kinetic studies are almost exclusively limited to caffeine extraction from green

beans, e.g. Espinoza-Perez et al. (2007) and references therein. The low number of publications on the kinetics of extraction from roast and ground coffee is certainly surprising, provided the popularity of coffee beverages. The majority of these studies are also limited to caffeine extraction. They are based on a steady state first-order kinetic expression (Eq. 2.3) proposed by Spiro and Siddique (1981) for caffeine extraction from tea leaves, which was extended afterwards to caffeine extraction from roast coffee (Spiro and Selwood, 1984). They built the model by defining three transport steps that occur at the same rate at the steady state: diffusion inside particles, partition between the particle and the bulk solution at the boundary and transfer through the external boundary layer. Since steady state was assumed for the derivation of the model, the concentration profile inside the particle was assumed to be linear.

$$\ln\left(\frac{C_{eq}}{C_{eq}-C_b(t)}\right)=k_{obs}t \qquad \text{Eq. 2.3}$$

Where C_{eq} and C_b are the concentration in the bulk phase at equilibrium and at any given time ($kg\ m^{-3}$), k_{obs} the experimental first order kinetic parameter (s^{-1}) and t the experimental time (s). Spiro and co-workers carried out a comprehensive and systematic investigation (see below) based on Eq. 2.3 regarding the effect of process conditions on the kinetics of caffeine extraction from tea and roast coffee. In the particular case of coffee, their conclusions can be summarised as follows:

- Effect of particle size (Spiro and Selwood, 1984): the estimated effective diffusion coefficient at 25.8 $°C$ was found to lie between 1.6 and $3.0\times10^{-11}\ m^2\ s^{-1}$ without a defined trend with respect to particle size (95 – 4130 μm). These values are approximately 30 times smaller than the value for the bulk diffusion of caffeine at

the same temperature. This was attributed to microstructural restrictions and caffeine forming complexes with other compounds. The value found at 84.1 *°C* was 17.3×10^{-11} m^2 s^{-1}.

- Effect of the hydrodynamics of the system (Spiro and Page, 1984): in order to evaluate the effect of the external mass transfer boundary layer, extraction experiments from grinds glued to a rotating disc were conducted. The estimated diffusion coefficient was found to be independent of the rotating speed of the disc, i.e. hydrodynamic conditions, and was thus concluded that the effect of the external boundary layer was negligible and the main limiting step was diffusion inside the grinds.

- Effect of roasting (Spiro and Hunter, 1985): the estimated effective diffusion coefficient was found to increase from 17×10^{-11} m^2 s^{-1} for green and light roasted coffee to 24×10^{-11} m^2 s^{-1} to dark roasted coffee (17 % mass loss). This was attributed to the dependency of coffee microstructure (porosity) on roasting conditions, as investigated years later by several authors (see Section 2.2.1)

- Hindrance factor (Spiro et al., 1989): this investigation was intended to unveil the mechanisms that hinder diffusion inside the grains. This has been traditionally carried out by means of a hindrance factor (ratio of the bulk to the estimated effective diffusion coefficient) or its reciprocal, the microstructural correction factor (del Valle et al., 2006). At 80 *°C*, Spiro reported a hindrance factor of 11.1 for caffeine extracted from roast and ground coffee. When caffeine was extracted from water-filled swollen coffee particles (containing the coffee soluble solids)

the hindrance factor was reduced to 5.4. The difference was attributed to the finite time required for water ingress, caffeine dissolution and water inflow hindering the outflow of caffeine. However, the time scale of these phenomena is expected to be short: roast and ground coffee is a hydrophilic material and water penetration is expected to be fast. Furthermore, as the authors acknowledged, caffeine is very soluble at 80 *°C* with a solid-liquid partition coefficient of circa 1. Therefore, this decrease in the hindrance factor may be mostly due a modification of the microstructure due to swelling (Mateus and Rouvet, 2007). In the case of water-filled swollen coffee particles emptied of soluble solids but containing caffeine, the hindrance factor decrease was found to be 3.7. The difference was attributed to the chemical interactions between caffeine and other species resulting in complexes. However, loading spent coffee grinds with caffeine from a caffeine aqueous solution to obtain the grinds containing only caffeine may result in a different spatial distribution of the compound in the particle, e.g. more caffeine in the intercellular space, so this factor may also include microstructural factors. The remaining factor of 3.7 was attributed mainly to coffee swollen microstructure.

- Effect of temperature on the hindrance factor (Spiro and Chong, 1997): the derived hindrance factors for roast and ground coffee at 25.5 *°C* resulted to be bigger by a factor of 2.7 than those derived at 80 *°C*. In the case of green coffee this ratio was found to be 3. This increase was attributed to a lower dissolution rate of caffeine at lower temperatures, as well as to the greater tendency to form complexes and being absorbed onto the matrix. However, it is also possible that a

less pronounced swelling effect of the polymeric matrix at lower temperatures occurred.

Jaganyi and Madlala (2000) extended Spiro's and co-workers investigation and carried out a comparative study of the effective diffusion coefficient at 80 $°C$ for caffeine and various minerals for medium roast coffees (particle size 1700 – 2000 μm) of five different origins. The results highlight that the derived coefficient varies with coffee origin and species: values for caffeine were found to lie between 15.8-20.5×10^{-11} $m^2\ s^{-1}$ (hindrance factor between 14 and 11) and between 18.7-37.0×10^{-11} $m^2\ s^{-1}$ for K^+ (hindrance factor between 27 and 14); hindrance values as high as 48 were reported for Mn^{2+}. Moreover, the dependency of the effective diffusion coefficient on the solid matrix and the specific chemistry of the system can be more dramatically illustrated by comparing coefficients derived from extraction of the same solute from two different food matrices. For instance, values of the effective diffusion coefficient for caffeine in South African black tea were considerably smaller (3.43×10^{-11} $m^2\ s^{-1}$ at 80 $°C$; hindrance factor of 62) (Jaganyi and Price, 1999) than those previously reported for caffeine in roast and ground coffee (hindrance factor of 11.1).

Regarding the performance of the model, Eq. 2.3 predicted experimental data reasonably well at longer times, but it consistently failed to predict early time data. Furthermore, the predicted zero intercept was considerably missed in all experimental data sets, and an ad-hoc non-zero intercept was added to the model for a better fit. Years later, it was found that Eq. 2.3 with a non-zero intercept results from considering only the first term of the Fourier series solution (Spiro, 1997; Stapley, 2002). This approximation is precisely valid at longer times, as the higher order terms of the

summation are very close to zero. The main advantage this kind of expressions is the straightforward mathematical treatment of the problem as compared to the analytical (Crank, 1975b) or numerical solutions of Fick's second law.

However, the main limitation is that the whole extraction curve cannot be predicted. Moreover, if the effective diffusion coefficient varies with time, the derived value depends dramatically on the model used to fit experimental extraction data. This is exemplified with the effective diffusion coefficients found for the total soluble solids extracted from roast and ground coffee: using the steady state first-order kinetic model derived by Spiro, Zanoni et al (1992) the values found (5.99×10^{-13} – 4.24×10^{-12} $m^2\ s^{-1}$ at 90 °*C*) between one and two order of magnitude lower than those fitted by Voilley and Simatos (1979) (0.8×10^{-11} – 1.1×10^{-11} $m^2\ s^{-1}$ at 70-85 °*C*) using a Fourier series solution to Fick's Second law. In Zanoni's and co-workers investigation, the first experimental point was taken after 1 minute. Thus, Spiro (1993) attributed the lower coefficients found by Zanoni et al. to the fact that after this time the soluble solids are dominated by larger species.

Other pieces of work regarding the kinetics of extraction from roast and ground coffee at the particle scale include the removal of CO_2 (Anderson et al., 2003), stripping of aroma compounds (Mateus et al., 2007), or cyclically pressurised extraction (Pacheco Ortiz et al., 2015).

- The microstructural approach to the effective diffusion coefficient

As reviewed in the previous point, at higher temperatures (when the solute is easily dissolved in the solvent), the solid microstructure can be assumed to be the dominant effect on the effective diffusion coefficient. Under these circumstances, an

estimate of the effective diffusion coefficient can be obtained as a function of measurable microstructural parameters, thus without the need of fitting experimental extraction data. The most celebrated correlation is shown in Eq. 2.4 (E.L. Cussler, 2009a):

$$D_{eff} = D_b \frac{\varepsilon_{particle}}{\tau_{particle}} f(\lambda) \qquad \text{Eq. 2.4}$$

Where $\varepsilon_{particle}$ is the particle porosity (-), $\tau_{particle}$ is the tortuosity of the diffusion path (-) and $f(\lambda)$ is a polynomial function of the solute-pore radius ratio (λ) that accounts for the friction between them; note that $f(\lambda)$ approximates unity when the solute is very small compared to the pore radius. This correlation estimates the effective diffusion coefficient as a function of average microstructural parameters. Other expressions available in the literature aim to incorporate architectural effects of the solid (Aguilera, 2003).

Porosity is relatively straightforward to measure via optical or porosimetry techniques. Values for coffee grains ranging from 0.40 to 0.53 have been previously reported (Section 2.2.1). Tortuosity is a more challenging parameter to measure, since models describing the porous structure accurately are required. However, tortuosity can be derived from Eq. 2.4 if the effective diffusion coefficient value is estimated from experimental extraction data, and the porosity of the material is known. Typical values of tortuosity for adsorbents and porous catalysts have been reported to lie between 2 and 6 (Aguilera, 2003). Also, attempts have been carried out to derive empirical expressions to estimate the tortuosity as a function of measurable parameters. For example, as cited in Carniglia (1986), Wakao and Smith proposed an empirical correlation ($1/\varepsilon_{particle}$) but it is not sustained as a general form by large a body of empirical data. Carniglia (1986) derived an empirical model as a function of particle

porosity, and an empirical pore shape factor involving the total pore volume, surface and pore diameter. The main drawback of the model is that the determination of an empirical pore shape factor requires nitrogen adsorption and mercury porosimetry measurements. Salmas and Androutsopoulos (2001) proposed an expression to evaluate the tortuosity of porous catalysts based on the Corrugated Pore Structure Model (CPSM). In the model, a corrugated pore is formed by a given number of cylindrical segments of the same length and different diameter. Tortuosity was then defined as a function of the number of cylindrical segments forming a pore (nominal pore length), as this parameter is related to the frequency of the pore diameter variation per unit length, and as a function of the extent of that variation itself (pore size distribution). The effect of these parameters on the tortuosity is illustrated in Figure 2.6.

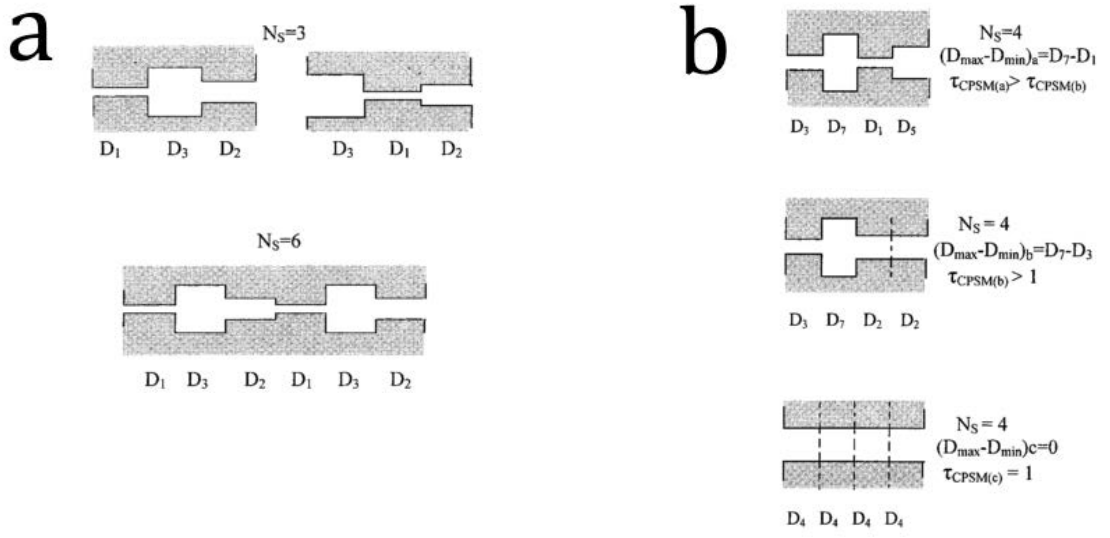

Figure 2.6: Examples of the effect of the nominal pore length (a) and pore size distribution (b) on the Corrugated Pore Structure Model tortuosity (Salmas and Androutsopoulos, 2001)

In Figure 2.6a, the pore size distribution and the sum of the volumes and surface area of the two corrugated pores formed by 3 segments (above) are identical to that of the corrugated pore formed by 6 segments (below). However, in the former case, the

frequency in diameter variation per unit length of pore is greater and so is its tortuosity according to the model. It can be seen that a limiting tortuosity of 1 would be obtained for a corrugated pore formed by a single segment. In Figure 2.6b is shown that the complexity of the corrugated pores decreases as the pore size distribution becomes more homogenous. A limiting tortuosity value of 1 is obtained for a corrugated pore formed by any number of segments with no difference between the maximum and minimum diameter.

The application of the model to commercial catalyst samples yielded tortuosity values between 1.12 and 10.07. This range compares well with the typical values derived from the measurement of effective diffusion coefficients. In order to obtain estimates with this model, fitting sorption hysteresis data is required. However, to extend the applicability of the model, the estimated tortuosity values were correlated to mercury porosimetry intrusion-extrusion hysteresis data. It was found that catalysts with a greater estimated tortuosity resulted in higher percentages of entrapped mercury after the intrusion-extrusion cycle, and a correlation was derived.

The link between mass transfer processes in coffee technology and coffee microstructure has not been explicitly studied to the best of our knowledge. However, Eq. 2.4 has been previously used to derive the effective diffusion coefficients of various oils in food and vegetable systems. Uquiche et al (2004) investigated the supercritical extraction of oleoresin from pelletised red peppers flakes. Porosity was measured by mercury porosimetry and a value of 0.17 was derived. Tortuosity was estimated from an analysis of the fractal dimensions of the solid and resulted to be 2.41. The resulting effective diffusion coefficient was shown to provide simulations that compared

acceptably with experimental data. Using the same methodology, Uquiche et al (2005) shown the effect of the pre-processing conditions on the microstructure (and thus on the effective diffusion coefficient) of pelletised jalapeno peppers; porosity values between 0.25 and 0.31 and tortuosity values between 1.11 and 7.48 were reported. del Valle et al (2006) estimated effective diffusion coefficients for supercritical extraction of prepressed rapeseeds, flaked rosehip seeds and olive husks. In addition to the tortuosity values derived from fractal analysis, they used the hysteresis in the intrusion-extrusion mercury porosimetry curves to derive tortuosity values according to the model proposed by Salmas and Androutsopoulos (2001). The fractal tortuosity values were found to be considerably lower (1.6-2.0) than those derived from mercury porosimetry (7.3-15.5). The effective diffusion coefficients estimated with the former were found to be an order of magnitude larger, and resulted in simulations that compared considerably better with the experimental kinetic data. However, as acknowledged by the authors, fractal analysis is based on 2D images and therefore not on the pore structure of the solid.

It is also relevant to note from the previous studies (e.g. Uquiche et al. (2005)) that the estimated hindrance factors based on the microstructural measurements were found to lie between 4 and 29, which are considerably greater than the value of 4 attributed by Spiro et al (1989) to roast and ground coffee microstructure.

2.3.2. Extraction at the bed scale

The kinetics of extraction from coffee packed beds has not received much attention in the literature. Table 2.3 shows a summary of the relevant references where extraction profiles over time from coffee packed beds can be found. Most of the studies

are empirical or semi-empirical or they merely display the measured data. In fact, the main objective of most of these studies is not unveiling the mechanisms of extraction, but the measurement is performed to serve other purposes, e.g. evaluate the antioxidant capacity of the coffee beverage as a function of extraction time. Thus, the lack of systematisation makes drawing conclusions challenging and their applicability to other systems limited.

Table 2.3: Studies on the kinetics of extraction in various extraction systems

Extraction method	***Studied compounds***	***Model***	***Reference***
Filter machine	Aroma compounds	No	Lee et al., 1992
Espresso machine	Total soluble solids	Fit to a power law equation	Navarini et al., 2004
Espresso machine, On-Demand	Caffeine, Chlorogenic acids, Trigonelline	No	Navarini et al., 2008
Espresso and filter machine	Melanoidins, Caffeine, Chlorogenic acids	No	Ludwig et al., 2012
Espresso machine	Total solids, protein, lipids / Caffeine, trigonelline, nicotinic acid	No	Caprioli et al., 2012, 2014
Percolation	Caffeine, N-methylpyridinium, Trigonelline, Chlorogenic acids	No	Lang et al., 2013
On-Demand	Aroma compounds	2 parameter hyperbolic equation	Mestdagh et al., 2014
Various On-Demand systems	Antioxidant compounds	2 parameter hyperbolic equation	Bartel et al., 2015
Filter machine	Total soluble solids	Multi-scale model	Moroney et al., 2015

Lee et al. (1992) studied the extraction of aroma species at flow rates of 50 and 250 $ml\ min^{-1}$. In both cases they found that the concentration of the collected aliquots decreased exponentially with time. Increasing the flow rate effectively decreases the required extraction time to produce a given volume of drink. This was shown to decrease the extraction yield of some of the compounds (probably the slower-diffusing

ones), whereas others remained unaffected. Mestdagh et al. (2014) observed that the cumulative extraction profiles of various aroma molecules varied greatly with the polarity of the considered molecule. For instance, 2,3-butanodione (polar) exhibited the typical first-order profile whereas the extraction of β-damascenone (non-polar) was slower and the profile a straight line. It must be also noted that the molecular weight of the former is considerably lower (86 $g\ mol^{-1}$ as opposed to 190 $g\ mol^{-1}$) and that may also contribute to the observed faster extraction.

From a more general perspective, the wide use of packed beds to extract natural products in the food, cosmetic and pharmaceutical industry (Huang et al., 2012) has promoted the development of mathematical models to assist in the design, optimisation and control of large scale extraction processes. These models typically consist of a set of partial differential equations (derived from differential mass balances), boundary conditions and solute-solvent equilibrium relationships that describe the mass transfer at the particle and bed scale. Modelling at the particle scale was reviewed in Section 2.3.1; thorough reviews of extraction models with supercritical fluids can be found elsewhere (del Valle and de la Fuente, 2006; Huang et al., 2012; Oliveira et al., 2011; Sovová and Stateva, 2011). Adaptations of these models can be used, in principle, to describe the kinetics of coffee extraction from packed beds. In coffee technology, this type of models have not been used with the exception of the recent publication by Moroney et al. (2015). They present a multi-scale extraction model (similar to the one developed in Chapter 3) to describe the operation of filter coffee machines. However, their approach is based on global mass transfer coefficients, as opposed to solving the concentration profile in coffee particles via Fick's second law.

2.3.3. Hydrodynamics of coffee packed beds

Hydrodynamics of coffee packed beds are relevant at both the industrial and consumer scale. At the industrial scale, soluble coffee processes typically employ a battery of extraction columns (Schwartzberg, 1987), whereas at the consumer scale, the most popular extraction methods require hot water flow through a packed bed (see Section 2.2.3). Industrial extraction columns have been operated on the basis of selecting a particle size *coarse enough* to maintain an acceptable pressure drop and avoid blockages in the extractor. On the other hand, consumer extraction methods are designed with the aim to achieve a certain flow rate that results in an optimal extraction time for the considered grind. Considering the broad applicability of packed beds in the chemical and food industry and the available knowledge on the subject, it is somewhat surprising that the topic has received very limited attention in the case of coffee technology.

Observations by Petracco and Liverani, (1993) showed that the flow rate profile through an espresso-like bed was in the non-steady state regime and it was attributed to a time-dependent geometry coffee bed. The flow rate shot up during the first 2-3 seconds of the extraction and then exponentially decayed by approximately 60-85 % in a time scale of approximately 20 seconds. It was also observed that the flow rate through the bed increased when higher pressures were applied until a point in which either the flow rate would not increase or would even decrease. This was attributed to a consolidation effect on the bed whereby its porosity (and thus its permeability) decreased. A similar behaviour has been described in the chromatography literature (Hekmat et al., 2011). Cappuccio and Liverani (1999) studied the dependence of flow

rate on temperature and pressure using standard coffee pods, containing the same mass of coffee with the same particle size distribution. A response-surface method experiment was carried out and a polynomial equation derived. The results confirmed the observations made by Petracco and Liverani (1993) regarding the drop in flow rate when pressure is increased above a certain level. Furthermore, other observations highlighted in both studies was that flow rate considerably increased when colder temperatures, i.e. 4 $°C$ as opposed to 90 $°C$, were used. These studies provided mainly qualitative information, but they did not provide conclusive results as to the order of magnitude of the permeability

A more fundamental approach to the hydrodynamics of packed beds can be taken by considering Darcy's law (Carman, 1997). This elementary relationship derived in 1856 by the French engineer Henry Darcy states that, at the steady state and low particle Reynolds numbers (Re_p < 10), the pressure drop across a packed bed is proportional to the flow rate that travels through it. The proportionality constant is referred here as the hydraulic resistance of the medium and it depends on the geometric characteristics of the bed (cross-section area and length), fluid viscosity, and packing material (permeability). The latter is defined as the ability of a porous medium to allow the transport of a fluid through it.

Much effort has been devoted to the development of theoretical correlations to predict the permeability as a function of measurable parameters of the bed. The main difficulty is that models describing the porous media are required. One of the most common approaches portrays the medium as a bundle of capillaries formed by the solid particles in which the Hagen-Poiseulle equation is applied. Cell models, on the other

hand, portray the bed as a collection of spherical or cylindrical elements surrounded by a fluid envelope (Li and Park, 1998). The Kozeny-Carman equation is arguably one of the most used correlations based on the bundle of capillaries approach (Carman, 1997). It expresses the permeability of the bed as a function of particle size, porosity and a constant that encompasses the pore shape effect and the tortuosity of the medium. This expression was originally derived for packed beds of mono-sized spheres. However, this is a rather rare case in most engineering practical applications. Therefore, most of the efforts in the investigations that have employed this correlation are directed towards the fitting of the constant for beds packed with a range of materials (Macdonald et al., 1979; Nemec and Levec, 2005). Others have developed empirical and theoretical models to elucidate the dependency of the bed tortuosity on bed porosity (Dias et al., 2006; Lanfrey et al., 2010). Moreover, another difficulty arises when two immiscible fluid phases co-exist in the bed. The concept of *relative permeability* is then required to describe the flow. For instance, in the case of water flowing through a bed in the presence of gas, the relative permeability is a non-linear function of the water saturation degree adopting the value of 1 when only water is present and 0 when no water is present (Weerts et al., 2005).

Works concerned with the general operation of Moka (stove-top) machines do include a section dedicated to the assessment of bed permeability using the direct application of Darcy's law. In essence, all the studies tried to correlate, on the implicit assumption of steady sate, the obtained flow of drink, measured using different methods, to a vapour pressure head driving the flow. However, neither the particle size distribution of the tested samples nor the bed bulk density was explicitly given in any of the studies. Thus, it is assumed that commercially available samples, packed at a bed

bulk density slightly higher than the tapped density of the distributions, were used in the experiments. Gianino, (2007) derived a permeability of 2.3×10^{-12} m^2. King, (2008) reported values of fluid conductance of 1.00×10^{-10} $m^3\ Pa^{-1}\ s^{-1}$, which can be translated, using the characteristics of their experimental set-up, to a permeability of 8.98×10^{-13} m^2. This is in good agreement with Navarini et al. (Navarini et al., 2009), who derived a time-dependent permeability ranging from 7.0×10^{-14} to 4.00×10^{-13} m^2. Specific information about the operation of stove-top coffee makers can be found in any of the aforementioned publications. Despite the fact that these studies provided an idea about the order of magnitude of permeability, the analysis of the influence of key variables, namely bed bulk density and particle size distribution, was out of the scope of the study.

The estimation of porosity in packed beds has been extensively studied in the engineering literature. An average constant porosity value is usually adopted, assuming therefore a homogenous bed structure. However, techniques, such as Magnetic Resonance Imaging or X-ray-Computer Tomography, have shown that the coordination index between particles decreases in the regions close to the wall, and in such spaces, porosity presents the upper limiting value of 1. Between four and five particle diameters away from the wall, the porosity tends to the average bulk value, being this transition normally modelled with a damped oscillatory function (Sederman et al., 2001).

In the previously reviewed articles dealing with extraction from packed beds (del Valle et al., 2006; Uquiche et al., 2004), the porosity of the bed was estimated from measurements of the packing material and the bed density. On a more theoretical level, four factors have been identified to influence the value of the average bed porosity: particle size distribution (monodisperse or polydisperse), particle shape (spherical or

non-spherical), absolute particle size (coarse or fine, non-cohesive or cohesive), and compaction history of the bed. An extensive review of previous experimental and modelling works dealing with packed bed porosity may be found elsewhere (Latham et al., 2002). The first investigations and models to understand packing behaviour involved the simple cases of uniform, non-cohesive spheres. Theoretical geometric calculations showed that a minimum value of bed porosity (0.26) would be achieved if the particles were displayed in a crystalline-like face-centered cubic (fcc) lattice whereas a bed porosity of 0.125 would be achieved for the same scenario when considering a binary mixture (Bear, 1988). In reality, depending on the compaction history of the bed, two possible configurations of mono-sized particles have been reported: random loose packing (bed porosity greater than 0.40) and random close packing (bed porosity of 0.36) (Scott, 1960). When smaller particles are added to the bed, the skeleton formed by the coarse particles accommodates them until the volumetric fraction of coarse particles is approximately 70 % (Yu and Standish, 1993); this varies slightly with fine-to-coarse particle ratio. At this point, further addition of particles results in an increment of the overall porosity as segregation may occur, as there are no extra spaces available for the fine particles. The effect of particle shape may be straightforward but difficult to quantify: greater porosity values are obtained as the shape deviates from spherical. The Power´s roundness scale (Peronius and Sweeting, 1985) and sphericity have been the most used parameters for that purpose. Regarding the absolute particle size, it has been acknowledged in the literature that for particles approximately below 100 μm inter-particle forces, such as Van der Waals and electrostatic forces, may dominate over gravitational forces. Therefore, finer particles are cohesive and that influences their packing behaviour (Zou et al., 2011).

Finally, another aspect of the hydrodynamic variables in coffee extraction is their influence on the final beverage. The effect of flow rate is straightforward as it sets the extraction time and water-coffee contact time. On the other hand, although *pressure* is typically listed in coffee literature (and also forms part of the collective imaginary) as one of the process parameters that greatly influence coffee extraction, its effect is not clear yet. Some studies have compared espresso coffees produced in pressure ranges from 7 to 11 *atm* (Andueza et al., 2002; Caprioli et al., 2012, 2014). Based on sensory evaluation of the obtained beverages, both studies concluded that 9 *atm* seemed to be the optimal pressure for espresso coffee extraction. However, from a simple fundamental analysis of flow in packed beds based in Darcy's equation, the pressure drop across a packed bed is a consequence of a flow rate travelling through a system of certain hydraulic resistance. It is difficult to elucidate how the effect of pressure can be independently studied, i.e. varying the pressure but maintaining a constant flow rate, particle size, bed density constant. Unfortunately, this is not specifically detailed in the referred publications.

2.4. Conclusions

A comprehensive review of the coffee extraction literature has been carried out in this Chapter. It has been shown that the majority of the published work relies solely on chemical and sensory analysis in order to optimise extraction conditions. The published work in which the mechanisms of extraction are investigated are mainly limited to caffeine extraction. Despite the importance of extraction yield and drink strength on the final quality of the cup and on the viability of soluble coffee manufacturing process, this has been hardly investigated before; thus the fundamental

understanding is still rather limited. Moreover, the used models are based on simplifying assumptions, e.g. first-order kinetics for single particles, which cannot be adapted to real scenario extractions at the consumer point of use, e.g. polydispersed particle size distribution.

The complexity of coffee extraction as a solid-liquid extraction process has also been described in this Chapter. Recently researchers have put special emphasis on the theoretical understanding of the solid microstructure on extraction rate via the effective diffusion coefficient. Coffee microstructure (and its dependency on roasting parameters) has been investigated and described by various authors, but this feature has never been included in a coffee extraction model.

The published research on the hydrodynamics of coffee packed beds is very scarce. Neither the phenomena that give rise to the observed non-steady state nor the relationship between coffee bed properties (particle size distribution and bed density) and flow rate-required pressure have been previously systematically investigated. Moreover, the influence of hydrodynamics variables (especially pressure) on the final quality of the beverage is limited and often misunderstood. Due to the relevancy of the hydrodynamic variables in the extraction devices design, these problems are addressed in this thesis (see Chapter 6).

Chapter 3: Material and Methods

3.1. Introduction

The aim of this Chapter is to provide detailed information on the experimental approaches developed and applied to study the range of phenomena that occur during the extraction of soluble solids from roast and ground coffee (RGC). Sections 3.2 presents the materials used i.e. RGC, water, extraction set-ups, and the analytical methods for the characterisation of fundamental properties of RGC, and Section 3.3 presents the experimental methods used to derive the relevant parameters needed in order to obtain simulations from the extraction and permeability mathematical models presented in Section 3.4. Section 3.5 presents the general details of the implementation of the mass transfer models in COMSOL Multiphysics®, as well as a mesh sensitivity study.

3.2. Materials

3.2.1. Roast coffee blends used in this study

The roast coffee blends used throughout this study are shown in Table 3.1:

Table 3.1: Roast coffee blends used in this study

Blend	***Origin***	***Roasting colour/Moisture content***	***Comments***	***Supplier***
1	100 % Arabica: Central America (30 %) and Brazil (70 %)	7.0 *La*	Default blend used	Mondelez International
2	100 % Arabica: Central America and Brazil	10.0 *La*	Flaked coffee	Mondelez International
3	100 % Arabica (50 % Colombia, 50 % Brazil) (Decaffeinated)	9 .0 *La* and 5.0 *La*	Blend used to test the influence of roasting colour	Mondelez International
4	Illycaffè's blend	9.5 *La*	Used in Illy's Hyperespresso On-Deman machine	Commercially available

La corresponds to 'Langue' colour units. These indicate the degree of light reflectance of a roast coffee samples. According to the standard calibration from Mondelez International, a value of 3.0 *La* corresponds to black colour, whereas a value of 23.0 *La* corresponds to a pale yellow. According to this, the range 3.0-4.0 *La* corresponds to a very dark roast, 5.0-6.0 *La* to a dark roast, 7.0-8.0 *La* to a medium-dark roast, and 9.0-10.0 *La* to a medium roast.

Exhaustive quality controls are routinely carried out at Mondelez International factories to ensure product consistency. However, due to the intrinsic nature of coffee, the characteristics of the beans, e.g. moisture content, roasting colour or bean chemistry, may lie within a narrow range of values. No investigation of this possible variability was carried out in the present study as it exceeds the scope of this thesis.

Blend 1 was the default coffee blend used in all the experiments, unless it is stated otherwise. The beans were periodically supplied throughout the duration of the project in 1 *kg* bags by Mondelez International (Banbury, UK), and grinded before each experiment was carried out.

Blend 2 and 3 were used to elucidate the potential effects of the process history of the beans (grinding technology, i.e. flaked coffee, roasting colour, and decaffeination), may produce on coffee microstructure, total extractable soluble solids, kinetics of extraction, and permeability of coffee packed beds. These blends were available as they were used in other research and commercial projects carried out at Mondelez International, in which the author, as member of the Coffee Technology Group, was partially involved. The author conducted most part of the experiments performed on Blend 2 (flaked coffee), following the general experimental protocol of analysing (at least) three samples, and reporting the results as an average and a standard deviation, accounting for error propagation (Section 3.3.1). Part of the measurements carried out on Blend 3 were commissioned at the School of Chemical Engineering at the University of Birmingham (Birmingham, UK) (mercury porosimetry), or Reading Scientific Services Ltd (University of Reading) (particle size distribution), or carried out at Mondelez International (Banbury, UK) (helium pycnometry) by other members of the research group. For some of these experiments, duplicates or triplicates were not performed, and this is acknowledged when the experimental results are presented.

With the aim to test the applicability of the proposed extraction models to commercial systems, simulations were obtained and compared with published experimental extraction results from a *Hyper Espresso On-Demand* machine developed by Illy® (Navarini et al., 2008) (Chapter 7). Whereas the majority of the technical information was provided within Navarini et al. (2008), average size parameters of the distribution were not specified. Thus, Illy's *Hyper Espresso On-Demand* capsules (Blend 4) were purchased at 'Amazon' (*www.amazon.co.uk)* to assess the particle size distribution of the grind.

3.2.2. Grinders and particle size distributions

Whole roast beans of Blend 1 were ground to different levels using both a disc grinder (Dalla Corte, Baranzate, Italy), and a roller grinder (Probat, Germany) to produce eight different grinds, named from A to H in Table 3.2. This grinding range was selected as it covers the whole spectrum that is typically used in coffee processing. Ψ_A resulted in a very finely ground powder similar to that used in Turkish coffee brewing style; Ψ_H resulted in a much coarser granulometry where pieces of the original bean of around 1000-1500 μm could be visually distinguished. The latter sizes are typically used in instant coffee production processes due to pressure drop restrictions in the industrial extraction columns.

Table 3.2: Grinds produced from Blend 1 using either a disc or a roller grinder

Grinds produced from Blend 1	***Grinder***
Ψ_A	Disc
Ψ_B	Disc
Ψ_C	Disc
Ψ_D	Disc
Ψ_E	Disc
Ψ_F	Roller
Ψ_G	Roller
Ψ_H	Roller

Whole beans of Blend 2 were used to produce flakes of roast coffee using a three-stage industrial-scale flaking mill (Flamenco, Bühler, Swizerland). The beans were fed to a pre-breaking section, where two tooth rollers (separated by a gap of approximately 800 μm) broke them down to a median particle size (X_{50}) of around 1000-1500 μm. The ground material was subsequently fed to a second flaking section, where two smooth rollers (separated by a gap of approximately 150 μm) compacted and flattened the particles. The compaction section (third stage) available in the mill was not used.

3.2.3. Water used in the experiments

In order to provide results with the largest scope for application in product and process development for the Mondelez International Coffee Global Centre of Excellence (Banbury, UK), all the experiments were performed with tap water as supplied from the network in Banbury (UK). The analysis of the chemical composition of a water sample (Table 3.3) was commissioned to Eurofins Scientific (UK).

Table 3.3: Chemical composition of Banbury (UK) tap water

Ion	***Concentration (mg dm^{-3})***
Cu^{2+}	0.028
Zn^{2+}	0.029
Na^{+}	21
K^{+}	3.4
Mg^{2+}	5.2
Ca^{2+}	87
$Fe^{2+/3+}$	<0.005
Cl^{-}	37

The hardness of Banbury tap water is 8.7 French degrees (1 French degree (°*F*) = 10 *mg* dm^{-3} $CaCO_3$). Although some studies have pointed out the possible influence of water mineral composition in some aspects of coffee extraction, such as brewing time (Navarini and Rivetti, (2010), and references therein), it was not taken into account in this thesis.

3.2.4. Scanning electron microscopy

Scanning electron microscopy (SEM) pictures of RGC were obtained in order to investigate the particle morphology. Two different microscopes were used: a Philips XL30 FEG ESEM, available at the School of Metallurgy and Materials at the University of

Birmingham, and a Hitachi tabletop TM-1000, available at the Mondelez International Coffee Global Centre of Excellence (Banbury, UK).

3.2.5. Stirred vessel set-up for the kinetics of extraction of soluble solids

A stirred vessel was used to investigate the kinetics of extraction of soluble solids at the particle scale. The set-up consisted of a 600 ml glass beaker heated by a hot plate (Ret Control-visc, IKA Labortechnik, Germany) with digital temperature and magnetic stirring rate control. The top of the beaker was covered with several layers of tin foil forming a lid to prevent water losses, which were considered negligible. The temperature of the bulk solution was monitored by means of an electronic thermometer introduced through the foil. The bulk solution was stirred using a magnetic agitator.

3.2.6. Packed bed extraction rig

A packed bed rig (Figure 3.1), designed and built at Mondelez International (Banbury, UK), was adapted to carry out fixed-time brewing cycles. Two main sections of the rig are to be distinguished:

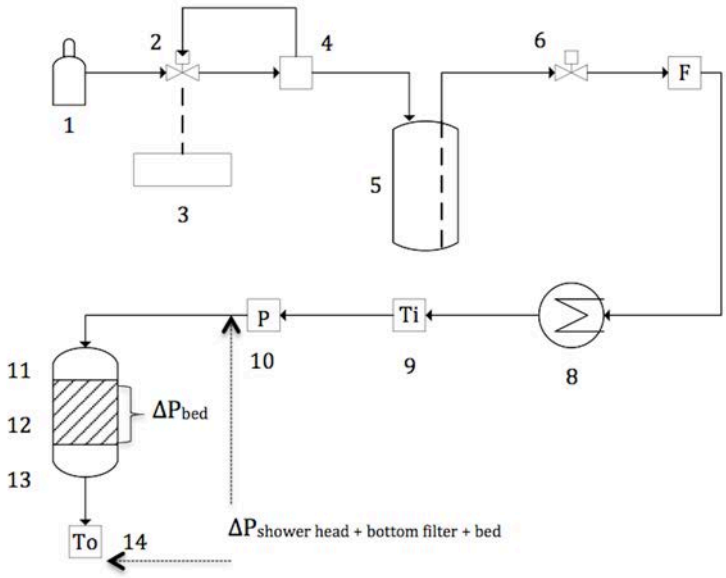

Figure 3.1: Custom pressure rig; (1) Compressed air source; (2) Electro-pneumatic valve; (3) Power supply for electro-pneumatic valve; (4) Regulator; (5) Keg-like water tank; (6) Valve; (7) Flow meter; (8) Boilers; (9) Inlet thermocouple; (10) Pressure transducer; (11) Shower head distributor; (12) Brewing chamber (containing the packed bed); (13) Bottom filter; (14) Outlet thermocouple

- Extraction section: It consists of an extraction cell built by assembling together three independent pieces as shown in Figure 3.2: (i) a bottom filter; (ii) a brewing chamber containing the coffee packed bed; and (iii) a shower head distributor. The aim of this extraction cell is to mimic the portafilter of a traditional espresso machine. Brewing chambers (Figure 3.2b) of two different diameter-length aspect ratios (2:1 and 6:1) were used in the experiments. The diameter and length of the 2:1 brewing chamber were 37 *mm* and 18.5 *mm*, respectively; the diameter and length of the 6:1 brewing chamber were 54 *mm* and 9 *mm*, respectively. Taking into account that the coarsest particle size used in these beds is 364 μm (see Table 4.1), the wall effect can be neglected (diameter of the bed/diameter of the particle ≤ 40 (Cheng, 2011)). The temperature before (T_i) and after (T_o) the extraction section was measured by two thermocouples. The pressure drop across the packed bed (ΔP_{bed}) was estimated from the

measurement provided by the pressure transducer (0-6 bar RS348-8087, RS Components, UK) (P_{trans}) located before the extraction cell. The pressure drop caused by the elements of the extraction cell, i.e. shower head distributor, brewing chamber wall and the bottom filter ($\Delta P_{elements}$) were measured (see Section 3.2.7) and subtracted from P_{trans}.

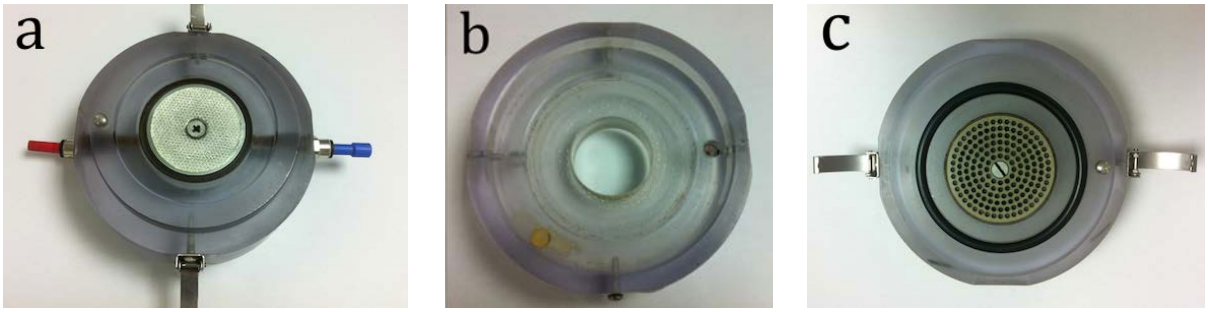

Figure 3.2: Extraction cell; (a) bottom filter; (b) brewing chamber with a 2:1 diameter/length; (c) shower head

- Pumping and heating section: A cylindrical keg-like water tank, with two pipe connection points at the top (IMI Cornelius, UK), was connected to a compressed air source (maximum pressure 6.00×10^5 *Pa*). The aperture of an electro-pneumatic valve (ITV2050-31F2BS3, SMC, USA) set the magnitude of the hydrostatic pressure achieved inside the tank and kept it constant. The brewing cycle started when the timed-valve (UDT Timer, Tempatron, UK) was opened. Flow rate was measured by means of an ultrasonic flow meter located after the tank (USC-731, Malema, USA).

The measured variables, i.e. temperature, pressure transducer and flow rate, were continuously recorded (10 measurements per second) with the aid of a custom-made data logging system. The software that operated the rig was developed with LabView (National Instrument, Germany).

3.2.7. Calibration of the pressure drop in the extraction rig

The pressure drop caused by the elements ($\Delta P_{elements}$) of the extraction cell located after the pressure transducer of the rig, i.e. shower head, wall of the brewing chamber and bottom filter, was measured. For that purpose, different flow rates were run through the extraction cell in the absence of a coffee packed bed, the pressure drop recorded, and a correlation obtained (Figure 3.3).

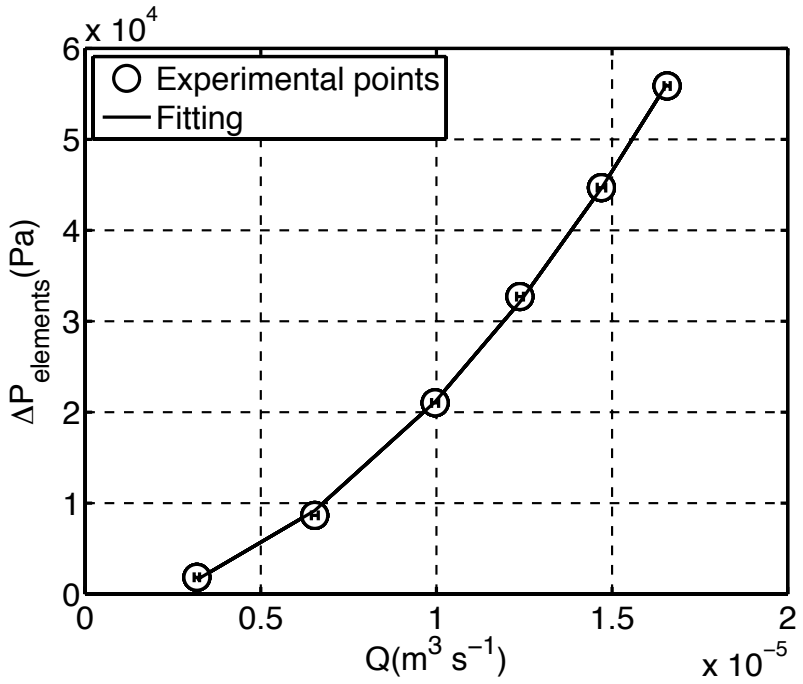

Figure 3.3: Calibration of the pressure drop (y-axis) caused by the shower head, wall of the brewing chamber and bottom filter for different flow rates, Q, (x-axis). The experiments were conducted in triplicate and the error bars represent ± the standard deviation of the repetitions. The experimental points were fitted to a second order polynomial expression of the flow rate (Q): $\Delta P_{elements} = 1.8\times10^{14}\ Q^2 + 5.3\times10^{8}\ Q + 1.9\times10^{3}$ ($R^2 = 0.99$). Error bars of $\Delta P_{elements}$ are too small to be shown

It can be seen in Figure 3.3 that the pressure drop in the empty extraction cell is a quadratic function of the flow rate. This indicates that the nozzles of the shower head give rise to a turbulent flow.

3.3. Methods

3.3.1. Statistical data treatment

The results are reported (numerically or graphically) as plus or minus (±) the standard deviation (σ) of the mean of a given measurement or experiment typically performed in three independent samples of each grind, unless otherwise stated. When the estimation of a parameter (c) involved algebraic operations between two or more previously measured parameters (a,b), each of those with an associated standard deviation (σ_a, σ_b), error propagation analysis was performed as follows in order to determine the standard deviation of the new estimated parameter (σ_c):

For addition and subtraction:

$$\sigma_c = \sqrt{(\sigma_a)^2 + (\sigma_b)^2} \qquad \text{Eq. 3.1}$$

For multiplication and division:

$$\frac{\sigma_c}{c} = \sqrt{\left(\frac{\sigma_a}{a}\right)^2 + \left(\frac{\sigma_b}{b}\right)^2} \qquad \text{Eq. 3.2}$$

3.3.2. Particle size distribution measurement

The particle size distributions of the grinds were measured by laser diffraction. Two methodologies were used, namely the *dry* and *wet* methods. The main difference lies in the dispersion process of the particles. In the *dry* method, the particles are fed to the measuring unit at a constant mass rate by means of a vibrating feeding device. A vacuum is then applied to drive the powder through the laser beam, providing an energy input to disperse the particles. This occurs due to particle-to-particle and particle-to-

wall collisions, and velocity gradients that give rise to centrifugal forces (Sympatec, 2015). In the *wet* method, however, the particles are fed manually to a beaker containing the dispersant liquid. Dispersion is typically achieved by stirring, application of ultrasound, and addition of a small quantity of surfactant.

The *dry* method is typically used across Mondelez International's manufacturing sites, as it results in quicker (approximately 30 seconds per measurement versus circa 10 minutes per measurement for the *wet* method), and more economically efficient measurements. On the other hand, the *wet* method is predominately used in the coffee patent literature, e.g. Ohresser et al. (2010). Since preliminary measurements showed that the results provided by these methods differ to some extent, there is a need to characterise the particle size distribution of the grinds using both methods.

The *dry* method was performed with a Helos laser diffraction sensor (Sympatec, Germany). Approximately 10-15 *g* of RGC were fed to the laser beam by a vibrating dosing unit (VIBRI/L, Sympatec, Germany) applying a vacuum of 95 *mBa*. The dispersing unit was a RODOS/M (Sympatec, Germany). The particle size distribution of three samples of each grind was assessed and the results averaged. A similar *dry* method was used to assess the particle size distribution of the grinds produced from Blend 3. In this case the used equipment was a Mastersizer 2000 (Malvern Instruments, UK), with a feeder for dry powders (Scirocco 2000). This measurement was comissioned at Reading Scientific Services Ltd (University of Reading).

The *wet* method was performed with a Mastersizer 2000 (Malvern Instruments, UK). Cold tap water (~ 15 °*C*) was used here as dispersant. Other fluids, e.g. butanol, are also typically used for this measurement (Ohresser et al., 2010). Past experiments

carried out at Mondelez International (Banbury, UK) have shown that the measured particle sizes exhibit certain sensitivity to the selection of the dispersant fluid. Approximately 0.40-070 *g* of RGC were mixed with water in a 25 *ml* beaker. Three droplets of TRITON™ X-100, a non-ionic surfactant, were added to facilitate dispersion and the slurry was manually stirred. The slurry was then transferred to a bigger beaker containing 800 *ml* of water, and the 25 *ml* beaker was rinsed with water to ensure that no particles were left behind. A vertical stirrer then started to agitate the slurry at 2000 *rpm* until the measurement was completed. Additionally, and prior to starting the measurement, sonication was applied to the slurry at amplitude of 50 *Hz* for 30 seconds to further enhance dispersion. The slurry was then left to settle (only with agitation) for 3 minutes and after this time the measurement commenced. Each sample was measured five times and the results averaged. The particle size distribution of four sample of each grind was assessed and the results averaged.

3.3.3. Particle sphericity

Particle sphericity (Φ) was estimated with a high-speed image analysis sensor (QICPIC, Sympatec, Germany) that records 2D images of the particles. The equipment is available at the School of Chemical Engineering at the University of Birmingham. Approximately 10-15 g of RGC were fed to the equipment by a vibrating dosing unit (VIBRI/L, Sympatec, Germany) and dispersed by a gravity-dispersing unit (GRADIS/L, Sympatec, Germany). The sphericity was automatically calculated by the equipment software as the ratio of the perimeter of an equivalent circle of the same area as the considered particle to the real perimeter of the particle. Three samples of each distribution were assessed and the results averaged.

3.3.4. Free flow and tapped density

The free flow density of the coffee grinds was measured by recording the required mass of RGC to fill a 200 cm^3 measuring cylinder. This cylinder was then transfer to a tapping machine (Stav 2003 Stamfvolumeter, Gemini BV, Germany) and 100 strokes were applied and the new volume recorded.

3.3.5. Helium pycnometry

Helium pycnometry measurements were conducted to estimate the specific volume of the considered grinds:

$$v_{distribution} = \frac{V_{distribution}}{m} \quad \text{Eq. 3.3}$$

Where $v_{distribution}$ is the specific volume of the grind ($m^3\ kg^{-1}$), $V_{distribution}$ is the volume of the grind as measured by helium pycnometry (m^3) and m the mass of RGC used for the measurement (kg).

These measurements were carried out at the School of Chemical Engineering at the University of Birmingham, and Mondelez International (Banbury, UK). All the measurements were carried out at room temperature, i.e. 18-20 $°C$. Three independent samples of each grind were assessed and the results averaged. The measurements carried out at the University of Birmingham (Blend 1 and 2) were performed with an AccuPyc II 1340 Helium Pycnometer, (Micromeritics). Between 0.1500-0.2500 g were weighed in an electronic balance with a precision of 10^{-4} g, and then placed into the pycnometer chamber. Air was evacuated in 50-purge cycles, 10 measurements of the volume of the solid performed, and the results averaged. The measurements carried out

at Mondelez International (Blend 3) were performed with an AccuPyc II 1330 Helium Pycnometer, (Micromeritics). Between 1.50-2.00 *g* were weighted and then placed into the pycnometer chamber. Air was evacuated in 5-purge cycles, 5 measurements of the volume of the solid performed, and the results averaged.

According to Mateus and Rouvet (2007), the solid specific volume of the considered blend (v_{solid}), i.e. that of the solid matrix and reciprocal of the solid density (ρ_{solid}), was considered to be the measured $v_{distribution}$ (Eq. 3.3) of a very fine grind. For example, for Blend 1, Ψ_A ($d_{[4,3]}$ = 95.9 μm as *dry* measured) was used for this purpose. The rationale behind this lies in the fact that the presence of intact cell pockets in such a fine grind is highly unlikely as their size, i.e. 25-40 μm (Schenker et al., 2000), is comparable to the radius of the particles. In coarser grinds, some of these intact cells cannot be accessed by helium during pycnometry experiments, and they were attributed to be the cause of the so-called closed porosity of the particles. Thus, for a given grind, the specific volume of the closed pores was estimated as follows:

$$v_{closed} = v_{solid} - v_{distribution} \qquad \text{Eq. 3.4}$$

Where v_{closed} is the specific volume of closed pores ($m^3\ kg^{-1}$), v_{solid} is the specific volume of the considered blend ($m^3\ kg^{-1}$), and $v_{distribution}$ is the specific volume of the grind ($m^3\ kg^{-1}$).

The closed porosity, defined as the proportion of the volume of a grind occupied by closed pores, was estimated as follows:

$$\varepsilon_{closed} = \frac{v_{closed}}{v_{closed} + v_{open} + v_{solid}} \qquad \text{Eq. 3.5}$$

Where ε_{closed} is the closed porosity (-), v_{closed} is the specific volume of closed pores ($m^3\ kg^{-1}$), v_{solid} is the specific volume of the considered blend ($m^3\ kg^{-1}$), and v_{open} ($m^3\ kg^{-1}$) is the specific volume of open pores. The details on how the specific volume of open pores was estimated will be given in Section 3.3.6.

3.3.6. Mercury porosimetry

Mercury porosimetry experiments (AutoPore IV 9500 Mercury Porosimeter, Micromeritics) were conducted to estimate the pore size distribution and the specific volume of open pores of the considered grinds. Between 0.2000 and 0.3500 g were weighted using an electronic balance with a precision of 10^{-4} g, and transferred into a cylindrical penetrometer suitable for powder samples. Mercury was fed to the penetrometer at progressively increasing pressures, from 0 to approximately 2×10^8 Pa, (intrusion cycle), and then released as the pressure was decreased (extrusion cycle). All the measurements were carried out at room temperature, i.e. 18-20 °C. Three independent samples of each grind were assessed and the results averaged.

The pore size distribution was estimated by Washburn's equation:

$$d_{pore} = -\frac{4\gamma}{P}\cos\theta \qquad \text{Eq. 3.6}$$

Where d_{pore} is the pore diameter (m) penetrated at the pressure P (Pa), γ is the surface tension ($N\ m^{-1}$) of mercury (Hg) at 20 °C, and θ is the contact angle between the Hg and the porous solid (°). Although the contact angle value depends on the solid surface, a value of 130 ° (common in most practical applications (Giesche, 2006)) has been assumed for this work.

The specific volume of open pores (v_{open}) in the grinds was estimated as the total amount of mercury inside the penetrometer by the end of the intrusion cycle minus the portion of that mercury volume that fills the inter-particle space. It was assumed that the biggest pore present on the surface of a particle was approximately 40 μm, based on the previously reported observations of the size of the cell pockets (Schenker et al., 2000). Thus, mercury was considered to start penetrating into the pores of the particles when the pressure in the penetrometer reached 3.72×10^4 Pa, which corresponds to a pore size of 33.07 μm, as estimated using Eq. 3.6. This is graphically explained in Figure 3.4, where a typical mercury cumulative intrusion-extrusion cycle against pressure is shown for grind Ψ_E as an example. The vertical dotted line delimits the inter particle space (left) and the pores of the particles (right), based on the aforementioned assumption of mercury having penetrated into the particles for measured pores sizes of 33.07 μm and below.

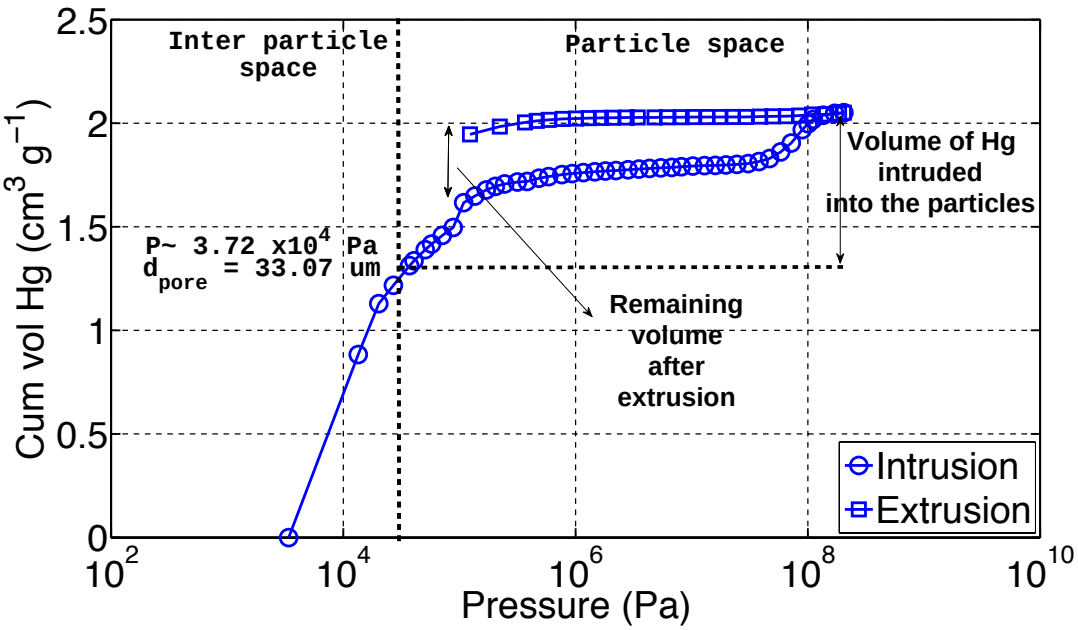

Figure 3.4: Cumulative mercury intrusion (○) – extrusion (□) volume (y-axis) for Ψ_E as a function of the applied pressure (x-axis). The lines are meant to guide the eye

Similarly to closed porosity, open porosity is defined as follows:

$$\varepsilon_{open} = \frac{v_{open}}{v_{closed} + v_{open} + v_{solid}} \quad \text{Eq. 3.7}$$

Where ε_{open} is the open porosity (-), v_{closed} is the specific volume of closed pores ($m^3\ kg^{-1}$), v_{solid} is the specific volume of the considered blend ($m^3\ kg^{-1}$), and v_{open} ($m^3\ kg^{-1}$) is the specific volume of open pores.

The total porosity of the grinds was estimated as the sum of the closed and open porosity:

$$\varepsilon_{particle} = \varepsilon_{open} + \varepsilon_{closed} \quad \text{Eq. 3.8}$$

Where $\varepsilon_{particle}$ is the total porosity of the grind (-), ε_{open} the open porosity (-) and ε_{closed} the closed porosity (-).

3.3.7. Estimation of particle tortuosity from the Corrugated Pore Structure Model (CPSM)

The average tortuosity of the grinds was estimated from the correlation obtained by Salmas and Androutsopoulos (2001) that relates the tortuosity predictions obtained with the Corrugated Pore Structure Model ($\tau_{particle,\ CPSM}$) for different catalyst particles, and the observed hysteresis from experimental mercury cumulative intrusion-extrusion cycles:

$$V_T = 1 - \frac{4.996}{1 + \exp\left[\frac{\left(\tau_{particle\ CPSM} + 5.8032\right)}{4.6242}\right]} \quad \text{Eq. 3.9}$$

Where $\tau_{particle,\ CPSM}$ is the particle tortuosity (-), and V_T is the entrapped fraction of mercury after the intrusion-extrusion cycles (-). This model was described more in-depth in Chapter 2 (Section 2.3.1)

In Figure 3.4, it can be seen that hysteresis in the mercury intrusion-extrusion cycles occurred for the grinds. In other words, when the extrusion cycle reached its end, i.e. $P = P_{atm}$, there was a fraction of the intruded mercury that remained entrapped within the particle microstructure. The porosimetry equipment only allowed reaching vacuum conditions during the intrusion cycle but not during the extrusion cycle. However, mercury intruded at atmospheric pressure and below this pressure can be considered as non-entrapped: this mercury would be filling pores above 10 μm, as estimated from Washburn's equation (Eq. 3.6), and said pores would be most likely located on the surface of the particles. It can be the safely assumed that this mercury would be easily extruded if vacuum conditions could be applied. Thus, V_T was estimated as follows:

$$V_T = \frac{\left(v_{ex} - v_{in}\right)_{P=P_{atm}}}{v_{open}} \qquad \text{Eq. 3.10}$$

Where v_{open} represents the total amount of mercury intruded into the particles ($m^3\ kg^{-1}$) and $(v_{ex}-v_{in})_{P\ =\ Patm}$ is the remaining mercury within the particles ($m^3\ kg^{-1}$) after extrusion, i.e. when $P = P_{atm}$.

3.3.8. Estimation of bulk diffusion coefficients of coffee soluble solids

Coffee soluble material consists of a complex mixture of solids within a wide range molecular weight (MW) (and thus radius) distribution. Coffee soluble solids are formed by smaller molecules (MW < 1 kDa), such as caffeine, chlorogenic acids and

minerals as well as by larger molecules (MW > 1 *kDa*), such as polysaccharides, proteins and melanoidins. Despite the little published information, the MW range of the larger molecules was shown in Chapter 2 to be quite broad.

Coffee soluble solids were firstly simplified into three MW categories (namely low, medium-high and high molecular weight), according to the published values of degree of polymerisation (DP) of polysaccharide fractions in coffee extracts (Nunes and Coimbra, 2001). It was assumed that within a category, all the compounds may show diffusion coefficients of the same magnitude and thus a compound of each category was selected as representative of the whole category. For the low molecular weight category caffeine was selected as the representative compound, as it is probably the most celebrated component of the coffee soluble solids, and its bulk diffusion coefficient is readily available in the literature and handbooks. For the medium-high and high MW categories, galactomannans, which constitute 69 % of the total carbohydrates of coffee brews (Nunes and Coimbra, 2001), were used as representative molecule. The reported DP values of 20 (for RGC extracts) and 45 (for soluble coffee) (Nunes and Coimbra, 2001) were assumed here to be representative of the medium-high and high molecular weight category, respectively. The diffusion coefficient of galactomannans polymers with a DP of 20 and 45 was estimated via the Stokes-Einstein equation. This relationship was also used to account for the effect of temperature in the diffusion coefficient, when required.

$$D_b = \frac{kT}{6\pi\mu r_h} \qquad \text{Eq. 3.11}$$

Where D_b is the bulk diffusion coefficient ($m^2\ s^{-1}$), k is the Boltzmann constant ($m^2\ kg\ s^{-2}\ K^{-1}$), T is the temperature (K), μ is the viscosity of the solvent ($Pa\ s$) and r_h is the hydrodynamic radius of the considered species (m).

The hydrodynamic radius of the considered galactomannans polymers was estimated via their radius of gyration (r_g). The radius of gyration is defined as the root-mean-square distance of the polymer segments from its centre of mass (Walstra, 2003), and depends on DP, monomer distribution in the chain, and the mannose-galactose proportion (Mazeau and Rinaudo, 2004; Petkowicz et al., 1999). Experimental and modelling studies relating DP and r_g have been carried out using special galactomannans with a regular and well-defined structure (extracted from the tree *Mimosa scrabella*); an example of these results is shown in Figure 3.5 (Mazeau and Rinaudo, 2004).

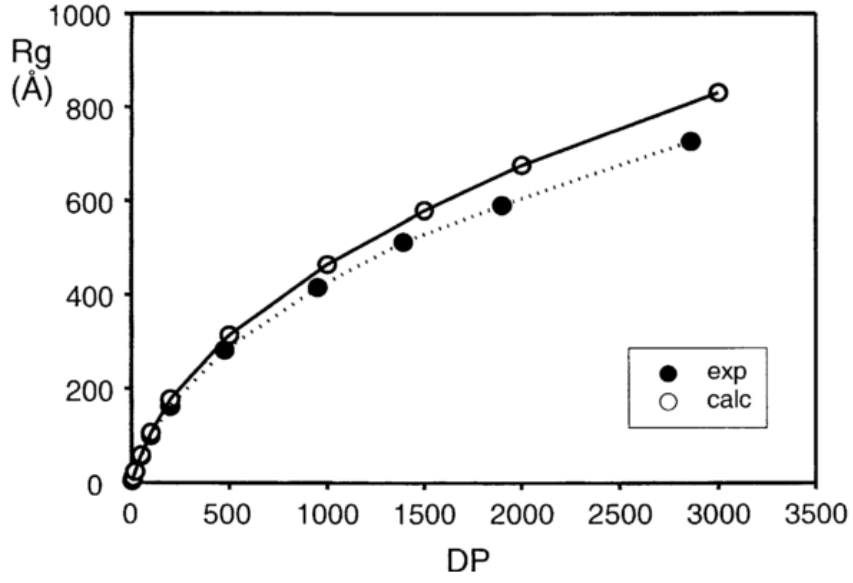

Figure 3.5: Comparison of light scattering experimental and modelling results for the radius of gyration (*y*-axis) for 1:1 galactomannans polymers as a function of their degree of polymerisation (*x*-axis) (Mazeau and Rinaudo, 2004). 'Exp' refers to the values measured from experiments and 'calc' to the values calculated with the models

Thus, assuming that the results obtained for these galactomannans are also applicable to coffee galactomannans, fragments with a DP of 20 and 45 show a radius of

gyration of 2 and 5.8 *nm*, respectively (Figure 3.5). The numerical data was extracted from the plot using the web-based freeware software WebPlotDigitizer (Rohatgi, 2015). The ratio between the hydraulic radius and the gyration radius (r_h/r_g) has been established for different solutions of synthetic polymers and was found to be in the range between 0.826 and 0.425 (Kok and Rudin, 1981). For unbranched polysaccharides, Walstra (2003) proposed a ratio of 0.67, and this value was adopted as representative to derive the hydraulic radius of coffee galactomannans from the estimated radius of gyration.

In addition to the available information in the literature, Dynamic Light Scattering (DLS) was also considered to estimate the hydrodynamic radius (r_h) coffee soluble solids. The finest and coarsest grinds tested in the kinetic experiments (Ψ_B and Ψ_H) were extracted at 80 $°C$ for 2 hours as described in Section 3.3.10, at a coffee-water relation of 25 $kg\ m^{-3}$ (effectively 5 g of RGC into 200 ml of water). Filtered aliquots of these extracts were sent to Malvern Instruments (UK) to perform the analysis. The measurement was carried out in triplicate at 25 $°C$ with a Malvern Zetasizer Nano ZS. A refractive index of 1.33 was assumed and the viscosity of the samples was approximated to be the viscosity of water.

For completeness, the results of the DLS measurements are reported here. Figure 3.6 shows the average results of three measurements of intensity of scattered light (y-axis), and the estimated diameter of the molecules in suspension (x-axis). For both grinds, the size distribution of the molecules was found to be monomodal, with a modal size of 188.7 *nm* for Ψ_B and 170.0 *nm* for Ψ_H (11 % smaller). According to the wide distribution of MW in the species forming coffee soluble solids (Chapter 2), a

distribution of molecular radii is expected, starting at a few nanometres. However, it is known that DLS is notoriously poor in highly polydispersed systems and its signal has a strong dependency on the larger species ($I \propto d^6$). Although it is clear that the information gathered in Figure 3.6 does not show the true picture of coffee soluble solids, it can be taken as an indication that a certain proportion of molecules in this size range forms part of the coffee soluble solids indeed.

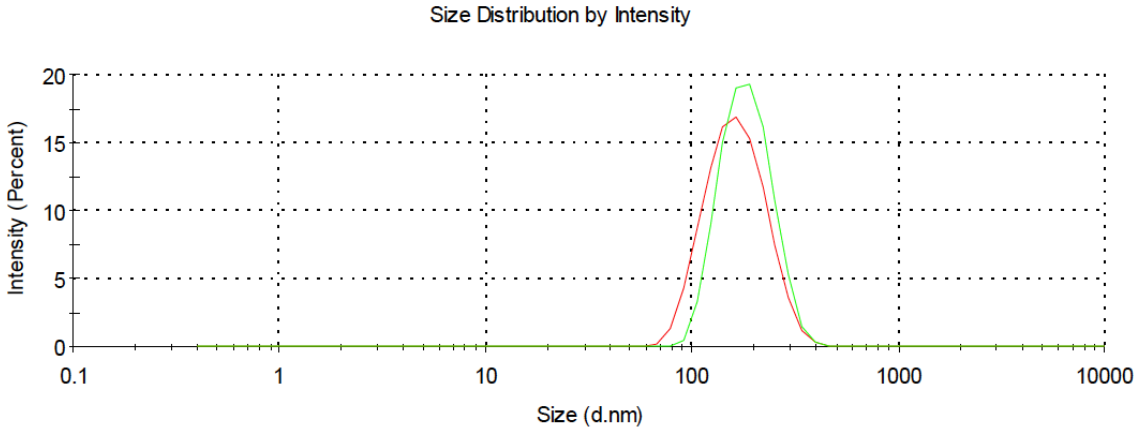

Figure 3.6: Intensity of light scattering (y-axis) and estimated diameter of the molecules in the extract (x-axis). Ψ_B (—); Ψ_H (—)

From the estimated DLS diameters, and assuming again that these measured molecules are well represented by galactomannans, the radius of gyration (r_g) was calculated from the ratio of 0.67 proposed by Walstra (2003) for unbranched polysaccharides. This value was used, in an inverse process as the one described before in this Section, to estimate the DP and the MW of the species measured by DLS. This resulted in DP of 149 for Ψ_B and 134 for Ψ_H. If a single unit of galactomannans shows a MW of 162 $g\ mol^{-1}$ (Dr. David Neville, Personal communication, 2015), the resulting MW for DLS measured molecules was found to be between 22000 and 24000 $g\ mol^{-1}$, which compares well with the upper-limit of MW reported previously as measured for extracts

obtained at 180 °*C* by Leloup et al. (1997) (Figure 2.4). The Stokes-Einstein equation (Eq. 3.11) was used to estimate D_b of these molecules.

Table 3.4 shows the D_b at 80 °*C*, as reported in the literature (caffeine), estimated from literature MW measurements of coffee carbohydrates, and as estimated from DLS measurements.

Table 3.4: Derived D_b at 80 °*C* for the three representative MW categories

Category	***Representative compound***	***D_b (80 °C) $m^2 s^{-1}$***	***Reference***
Low MW	Caffeine	18.9×10^{-10}	(Poling et al., 2008)
Medium-High MW	Galactomannans DP = 20	54.3×10^{-11}	This work; r_h derived from Mazeau and Rinaudo (2004)
High MW	Galactomannans DP = 45	18.7×10^{-11}	
Very High MW	—	$7.7\text{-}8.5\times10^{-12}$	This work; r_h derived from DLS

The values shown in Table 3.4 will be used to estimate the effective diffusion coefficients by applying a microstructural correction factor as per Eq. 2.4.

3.3.9. Soluble solids measurement in extract samples

The concentration of soluble solids of all the extract samples was measured with a refractometer (RFM340, Bellingham Stanley Ltd, UK). A linear relationship between Brix, as measured by the refractometer, and soluble solid concentration, as determined by oven-drying the extracts until constant weight, has been previously reported (Gloess et al., 2013), and was also established in Mondelez International (Banbury, UK). Figure 3.7 shows the percentage of soluble solids (*g* of soluble solids per 100 *g* of extract) as measured by oven-drying (*x*-axis), vs. the Brix as measured with the refractometer for a special 'coffee mode'.

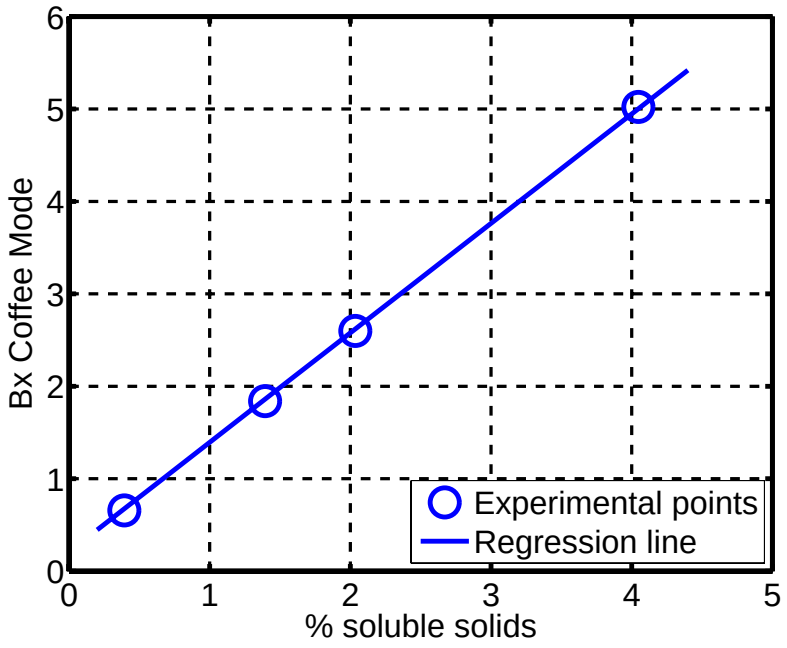

Figure 3.7:Reading of the refractometer in 'Brix coffee mode' (*y*-axis) as a function of the of soluble solids as measured by oven-drying (*x*-axis). *Brix coffee mode = 1.1842·% of soluble solids +0.2095* (R^2=1)

The density of coffee extracts can be approximated to that of water at the same temperature with a 1-3 % error for concentrated (espresso) extracts (Navarini et al., 2004). Thus, the measured mass percentage was approximated to a concentration (*g* of soluble solids per 100 cm^3 of extract).

The Brix of all the brew samples was measured in triplicate at room temperature (i.e. 20-22 *°C*) and the soluble solids concentration determined from the correlation shown in Figure 3.7.

3.3.10. Initial concentration of extractable soluble solids

The initial concentration of extractable soluble solids in each coffee grind was estimated as follows:

$$C_{s,0} = y_0\left(\Psi_j\right)\rho_{particle} \qquad \text{Eq. 3.12}$$

Where $C_{s,0}$ is the initial concentration of soluble solids ($kg\ m^{-3}$), $y_0\ (\Psi_j)$ is the long time limit extraction yield (-) (2 hours for Ψ_A, Ψ_B and Ψ_E; 4 hours for Ψ_F and Ψ_G; and 6 hours for Ψ_H) which can be obtained from a given grind after extraction in a very dilute system (maximum extraction yield), and $\rho_{particle}$ corresponds to the density of the grind ($kg\ m^{-3}$), i.e. $\rho_{particle} = \rho_{solid}\ (1 - \varepsilon_{particle})$. Preliminary kinetic experiments (Section 5.2) proved that the selected extraction times are well beyond the required times to achieve equilibrium.

Values of $y_0\ (\Psi_j)$ were determined in triplicate in a water bath at 80 $°C$ with mechanical agitation of 130 *rpm*. A very dilute solution of 10 $kg\ m^{-3}$ (in practice 2 g of RGC in 200 *ml* of water) was chosen so that the remaining mass of soluble solids inside the particles at equilibrium was small and therefore could be neglected. Three independent samples of each grind were assessed and the results averaged. Alternatively, it was found from equilibrium experiments carried out to derive the solid-liquid partition coefficient (Section 3.3.13), a maximum extraction yield for Ψ_A approximately 1 % higher than the maximum extraction yield found here with the dilute solution approximation. Therefore, in order to gain accuracy all the derived $y_0\ (\Psi_j)$ values were corrected accordingly.

3.3.11. Contact angle estimation

The water-roast and ground coffee contact angle measurement was commissioned at the Department of Chemical Engineering of Imperial College (London, UK), and the results are reproduced here. The contact angle was estimated with the sessile drop method by circle fitting water droplets deposited on coffee packed beds. Grinds Ψ_B and Ψ_E were arbitrarily chosen to carry out the measurement. The

measurement was conducted at 75 $°C$ and room temperature (not specified), and five repetitions were performed.

3.3.12. Water absorbed by roast and ground coffee

The volume of absorbed water per unit mass of RGC was measured in Ψ_A, Ψ_B, and Ψ_H at 80 $°C$. It was required for the estimation of the partition coefficient (Section 3.3.13), and the extraction yield (Section 3.3.14). All the assessed grinds were slurried in the water bath at a coffee-water relation of 25 $kg\ m^{-3}$. After a certain time had elapsed, the slurry was vacuum filtered (Filtration kit: Sartolab (Sartorious, Germany); Vacuum pump: (KNF, USA); Filter: Whatman glass microfiber, pore size 1.2 μm (Sigma-Aldrich, USA)) and the excess water on the surface of the particles was gently dried with tissue paper. It must be noted that the filtration process took between 3 and 4 minutes and that time was also considered as slurrying time. The wet coffee was then oven-dried at 103 $°C$ until constant weight was achieved (16-24 hours). The finest grind (Ψ_A) used for the estimation of the partition coefficient was slurried for 2 hours at 80 $°C$; Ψ_B was slurried for 4 and 20 minutes at 80 $°C$; and Ψ_H was slurried for 3, 20 and 120 minutes at 80 $°C$. Additionally, measurements after 4 and 3 minutes were performed for Ψ_B and Ψ_H, respectively, at 20 and 50 $°C$.

In order to express the amount of absorbed water per unit mass of *fresh* RGC, i.e. non-extracted RGC, it was taken into account that: (i) during the slurry RGC particles lost part of their mass since soluble solids were extracted; (ii) the oven-drying measured moisture also includes the original moisture of RGC; (iii) after the filtration step it was virtually impossible to recover all the wet particles from the slurry. The amount of absorbed water per unit mass of *fresh* coffee was calculated as follows:

$$\chi = \frac{m_{wet} - m_{dry} - m_{RGCeq}\chi_0}{m_{RGCeq}} \quad \text{Eq. 3.13}$$

Where χ is the absorbed water per unit mass of fresh coffee ($kg\ kg^{-1}$), m_{wet} is the recovered mass of wet RCG (kg), m_{dry} is the mass after drying in the oven (kg), χ_0 is the initial moisture per unit mass of *fresh* RGC ($kg\ kg^{-1}$) (also measured by oven-drying until constant weight) and $m_{RGC\ eq}$ is the original *fresh* mass of the recovered wet particles (kg). The proportionality between the original mass of RGC and the hypothetical dry mass measured for the same extraction yield was applied to estimate $m_{RGC\ eq}$ according as follows:

$$m_{RGCeq} = \frac{m_{dry}}{1 - y - \chi_0} \quad \text{Eq. 3.14}$$

3.3.13. Solid-liquid partition coefficient

The solid-liquid partition coefficient (K) is defined here as the bulk-to-solid concentration ratio at equilibrium:

$$K = \left(\frac{C_b}{C_s}\right)_{eq} \quad \text{Eq. 3.15}$$

Where $C_{b,eq}$ and $C_{s,eq}$ ($kg\ m^{-3}$) are the concentration of soluble solids in the bulk solution and inside the solid at equilibrium, respectively. The remaining material inside the solid may be present in solution in the pore space of the particle or still attached to the solid matrix. Note that for K defined in this fashion, $C_{s,eq}$ encompasses these two situations. While the measurement of $C_{b,eq}$ is straightforward, measuring $C_{s,eq}$ would involve filtration of the grounds and re-extraction to ensure that all the material has

been removed from within the particles. This would give rise to extremely dilute solutions difficult to quantify. Alternatively, and following Spiro's derivation (Spiro, 1997), a general mass balance was at equilibrium was established:

$$y_0\left(\Psi_j\right)m = C_{b,eq}V_b + C_{s,eq}V_{s,eq}^{ext} \qquad \text{Eq. 3.16}$$

Where $y_0(\Psi_j)$ is the maximum extraction yield (-), m is the mass of RGC (kg), $C_{b,eq}$ and $C_{s,eq}$ the concentration in each phase at equilibrium ($kg\ m^{-3}$) and V_b and $V_{s,eq}^{ext}$ the volume of the phases (m^3). $V_{s,eq}^{ext}$ represents the volume of the particles after extraction. If a possible swelling effect of the particle were to be taken into account, this volume would be expressed as the *dry* volume of the particles multiplied by a swelling factor (S).

The next steps in the derivation to obtain an equation without the equilibrium concentration in the solid phase (Eq. 3.17) were: (i) substituting Eq. 3.15 in Eq. 3.16; (ii) expressing V_b as the original volume of water (V_w) minus the volume absorbed by coffee particles; (iii) rearranging.

$$\frac{1}{C_{b,eq}} = \frac{1}{m}\frac{V_w}{y_0\left(\Psi_j\right)} + \frac{1}{y_0\left(\Psi_j\right)}\left(\frac{S}{K\rho_{particle}} - \chi\right) \qquad \text{Eq. 3.17}$$

Where V_w is the original volume of water added (m^3), S is the swelling factor of the grinds (swollen volume / dry volume) (-) and χ is the volume of water absorbed per unit mass of RGC ($m^3\ kg^{-1}$). Note that the derivation of Eq. 3.17 neglects the contribution of the extracted soluble solids to the volume of the bulk phase.

K was investigated at 20, 50 and 80 $°C$ for coffee soluble solids using the finest grind (Ψ_A). Similar experiments to those described in Section 3.3.10 were carried out at

variable coffee-water relations, ranging from 10 to 333 $kg\ m^{-3}$; effectively, in order to achieve each relation, the mass was varied from 2 to 67 g, whereas V_w was fixed at 200 cm^3 for all the experiments. K was derived from the intercept obtained with the linear regression of m vs. $1/C_{b,eq}$

3.3.14. Kinetics of the extraction of soluble solids at the particle scale

The kinetics of extraction at the particle scale was investigated in the stirred vessel set-up described in Section 3.2.5. At time zero RGC was introduced into the stirred vessel. At each time point, samples of approximately 5 *ml* were collected from the bulk solution with a syringe, filtered through a cellulose acetate syringe filter with a pore size of 0.45 μm (VWR) and the soluble solid concentration of the filtered sample measured in the refractometer as described in Section 3.3.9. The tips of the syringes were covered with a 100-μm filter mesh to prevent blocking the inlet when the coarser distributions were being assessed. The experimental extraction yield ($y_{exp}(t)$) (-) was calculated as follows:

$$y_{\exp}(t) = \frac{C_{b,\exp}(t)\left(V_w - V_{wp} - \sum_{j=1}^{n} V_s\right)}{m} \qquad \text{Eq. 3.18}$$

Where $C_{b,exp}$ is the experimental soluble solid bulk concentration measured at each time point ($kg\ m^{-3}$), V_w is the initial water volume in the stirred vessel (fixed at 500 *ml* for all the experimental conditions) (m^3), V_{wp} is the volume of water absorbed by the coffee particles (estimated in Section 3.3.12) (m^3), and m is the mass of RGC (kg). Based on the contact angle estimates that will be shown in Chapter 4, it was assumed that water was instantly absorbed into the particles. V_s is the removed volume from the bulk

solution when one sample is taken (m^3) i.e. 5 *ml*, and the summation represents the total removed volume at each time step.

The influence of stirring rate (200, 500, 900 and 1100 *rpm*), particle size distribution (grinds: Ψ_B, Ψ_E, Ψ_F, Ψ_G and Ψ_H), particle shape (traditional RGC and flaked coffee), and temperature (T) (20, 50 ± 1 and 80 ± 2 °*C*) were evaluated.

3.3.15. Packed bed preparation

All the packed beds used in this work were prepared following a standard procedure to ensure as much reproducibility as possible. Once the roast and ground coffee had been deposited into the extraction cell described in Section 3.2.6, the beds were manually levelled off and tapped 100 times to allow the particles to pack. Coffee was axially compressed afterwards with a metal tamper, reducing its volume until the volume of the brewing chamber was matched. In order to facilitate the compression process and ensure certain degree of accuracy, an auxiliary ring was placed on top of the brewing chamber to act as a mechanical stop of the tamper.

The applied force to pack the beds to the final density was estimated with an axial compression test carried out in a Z030 mechanical tester (Zwick/Roell, UK) at a compression rate of 0.1 $mm\ s^{-1}$ and maximum force of 300 *N*.

The porosity of the packed beds (ε_{bed}) was estimated as follows:

$$\rho_{bed} = \rho_{solid}\left(1-\varepsilon_{particle}\right)\left(1-\varepsilon_{bed}\right) \quad \text{Eq. 3.19}$$

Where ρ_{bed} is the density of the packed bed, i.e. weight of coffee divided by the volume of the bed ($kg\ m^{-3}$), ρ_{solid} is the intrisic solid density of roast coffee as determined by Helium pycnometry ($kg\ m^{-3}$), and $\varepsilon_{particle}$ the total porosity of the grind (-).

3.3.16. Estimation of the permeability of coffee packed beds in steady state

The permeability of coffee packed beds (κ) was estimated in the steady state flow regime using the extraction rig described in Section 3.2.6 and shown in Figure 3.1. As reviewed in Chapter 2, flow rate is a non-steady variable during coffee extraction. From all the possible dynamic phenomena that might occur, swelling of the particles seems to be the one with the longest time scale (approximately 600 seconds, according to Mateus and Rouvet (2007)). Thus, to achieve the steady state regime, water was circulated through the extraction cell for 600 seconds. By this time coffee was virtually fully extracted, and therefore the permeability in steady state corresponds to fully extracted beds.

The influence of the following process parameters on permeability was considered: (i) particle size distribution, (grinds: Ψ_B, Ψ_C, Ψ_D, Ψ_E); (ii) particle shape (flaked coffee); (iii) bed density (360, 400 and 480 $kg\ m^{-3}$); (iv) temperature (20 and 80 $°C$); (v) coffee blend (regular vs. decaffeinated RGC); and (vi) bed aspect ratio, i.e. diameter to length of the bed (2:1 and 6:1).

Preliminary experiments showed that the hydration conditions must be carefully chosen to avoid physical damage on the structure of the bed that can lead to undesirable effects such as macro-channelling. Hydrostatic pressures in the tank were then selected according to the initial bed bulk density of the packed beds and were 2.5, 3.0 and $4.5\times10^5\ Pa$ for initial bed bulk density of 360, 400 and 480 $kg\ m^{-3}$, respectively, and $1.5\times10^5\ Pa$ for initial bed bulk density of 480 $kg\ m^{-3}$ for the 6:1 D_{bed}/L_{bed}.

At the steady state regime, experimental flow rate-pressure drop data was collected. Figure 3.8 shows a schematic representation of the loop followed to acquire the experimental data. The hydrostatic pressure in the tank of the extraction rig was varied from $4.5\times10^5\,Pa$ to $0.5\times10^5\,Pa$ in steps of $0.5\times10^5\,Pa$, which effectively resulted in different flow rates through the bed (Figure 3.8). At each pressure step, the instant values of flow rate and pressure drop across the bed were recorded during 60 seconds and the values of the last 30 seconds averaged over time to form the steady state flow rate-pressure drop data sets.

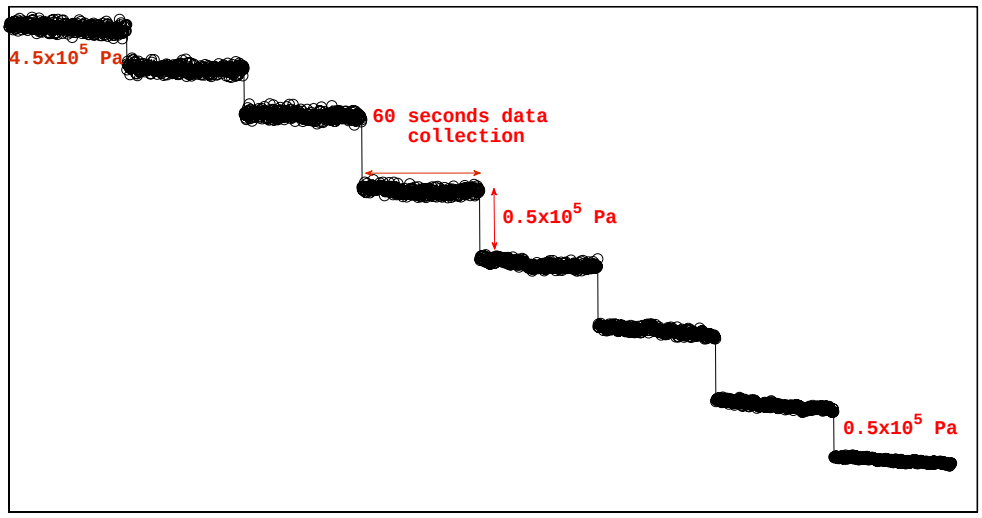

Figure 3.8: Schematic representation of the loop applied to acquire experimental Q-ΔP_{bed} data. The points represent the measured flow rate or pressure in the pressure transducer for each pressure in the tank during 60 seconds

The permeability of the bed was estimated by fitting the experimental steady state flow rate-pressure drop data to Darcy's equation. The validity of this expression will be shown in Chapter 6 with the estimates of the Reynolds particle numbers.

$$\Delta P_{bed} = \frac{L\mu}{\kappa A}Q \qquad \text{Eq. 3.20}$$

Where κ is the permeability of the packed bed (m^2), A the cross-section area of the brewing chamber (m^2), L the length of the bed (m), and μ the viscosity of water ($Pa\ s$). The pressure drop across the bed (ΔP_{bed}) (Pa) was obtained as follows:

$$\Delta P_{bed} = P_{trans} - \Delta P_{elements} \quad \text{Eq. 3.21}$$

Where P_{trans} is the pressure recorded by the transducer of the extraction rig (Pa), and $\Delta P_{elements}$ is the pressure drop caused by the elements of the extraction cell (Pa) (Section 3.2.7).

The permeability of three samples of each grind was assessed and the results averaged.

3.3.17. Packed bed consolidation

It was observed that, upon application of flow, the packed beds consolidated. The initial bed height decreased and RGC evolved from a fairly loose powder (when it is dry) to an agglomeration of particles. Dynamic bed consolidation was studied by measuring bed height reduction at different time points during 600 seconds.

The consolidation degree was calculated as follows:

$$\lambda\left(t\right)_{depth} = \frac{L_t}{L_0} \quad \text{Eq. 3.22}$$

Where L_0 is the initial height of the bed (m) and L_t is the bed height reduction at each time point (m). L_t was measured as shown in Figure 3.9a.

After 600 seconds had elapsed, the bed was carefully removed from the extraction cell and the actual height was measured as shown in Figure 3.9b. The consolidation degree was also calculated from this measurement as follows:

$$\lambda\left(t_{600}\right)_{length} = \frac{L_0 - L_{actual}}{L_0} \qquad \text{Eq. 3.23}$$

Where L_{actual} is the measured bed height (m).

The average steady state consolidation degree was then calculated as follows:

$$\lambda_{average} = \frac{\lambda\left(t_{600}\right)_{depth} + \lambda\left(t_{600}\right)_{length}}{2} \qquad \text{Eq. 3.24}$$

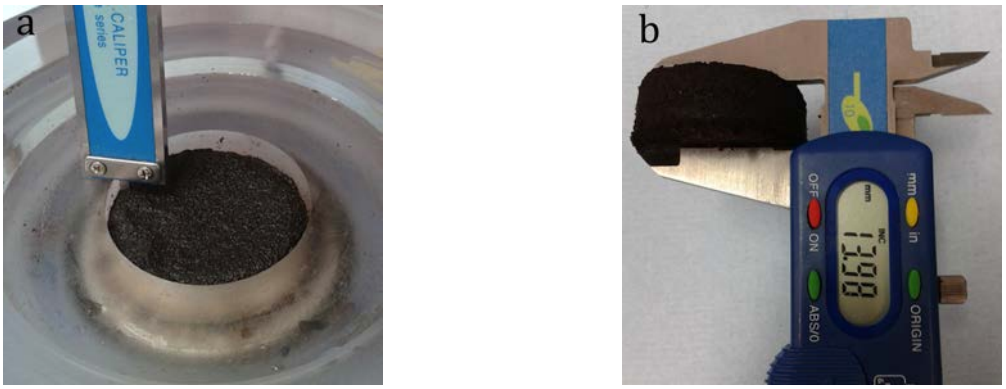

Figure 3.9: (a) Measurement of the height reduction (L_t) at a given time point; (b) measurement of the actual height of the bed ($_{Lactual}$) after 600 seconds

The steady state bed bulk porosity, when the bed was fully consolidated, was calculated accounting for consolidation as reported by Hekmat et al. (2011):

$$\varepsilon_{bedss} = \frac{\varepsilon_{bed} - \lambda_{average}}{1 - \lambda_{average}} \qquad \text{Eq. 3.25}$$

Where $\varepsilon_{bed\,ss}$ is the bed bulk porosity of the fully consolidated bed (-) and ε_{bed} the initial bulk porosity of the bed as calculated from Eq. 3.19 (-).

3.3.18. Kinetics of extraction of soluble solids at the bed scale

The kinetics of extraction of soluble solids from a packed bed was investigated using the rig described in Section 3.2.6 and shown in Figure 3.1. The packed beds were prepared following the procedure described in Section 3.3.15.

The influence of the following process parameters on the kinetics of extraction of soluble solids in a packed bed was considered: (i) flow rate regime (high (*HF*) and low flow (*LF*) rate regime); (ii) particle size distribution (Ψ_B, Ψ_C, Ψ_D and Ψ_E); and (iii) bed density (400 and 480 $kg\ m^{-3}$).

The pressure in the tank of the extraction rig was selected as a function of the considered grind and ρ_{bed}, so that the targeted flow rate regime was met. The extraction time was fixed at either 35 or 80 seconds and aliquots were collected for 5 or 10 seconds for *HF* and *LF*, respectively. The samples were weighted and the volume of the aliquot ($V_{aliquot}$) was determined under the approximation of the extract density being *circa* water density. After the samples were cooled down to room temperature the concentration of the collected aliquot ($C_{aliquot}$) ($kg\ m^{-3}$) was measured with a refractometer as described in Section 3.3.9. The extraction yield ($y_{exp}(t)$) (-) and brew strength ($S_{exp}(t)$) ($kg\ m^{-3}$) were then estimated as follows:

$$y_{\exp}(t) = \frac{\sum_{p=1}^{n} \left(C_{aliquot} V_{aliquot}\right)_p}{m} \qquad \text{Eq. 3.26}$$

$$S_{\exp}(t) = \frac{\sum_{p=1}^{n} \left(C_{aliquot} V_{aliquot}\right)}{\sum_{p=1}^{n} \left(V_{aliquot}\right)} \qquad \text{Eq. 3.27}$$

Where p represents the number of the aliquot and n the total number of aliquots taken during the experiment (7 for *HF* and 8 for *LF*).

3.4. Mathematical models

This section presents the derivation of the mass transfer (particle and bed scale) and hydrodynamic mathematical models that were used in the subsequent chapters to assist the analysis of experimental data or to provide simulations to gain insights of the system.

3.4.1. Extraction model at the particle scale – stirred vessel extraction model

This Section presents the proposed stirred vessel extraction model used to investigate the kinetics of extraction of soluble solids at the particle scale. As reviewed in Chapter 2, solid-liquid extraction may be divided in several steps that include solvent penetration into the solid, dissolution/breakdown of the compounds of interest, and diffusion through the porous solid towards the particle surface. The diffusion step is typically the rate-limiting step in coffee extraction (Spiro and Page, 1984). As a matter of fact, results of the roast and ground coffee-water contact angle measurement (that will be presented in Chapter 4) show that penetration into the particles is driven by capillary forces, and is very quick relative to the extraction time scale for soluble solids. Fickian diffusion is thus proposed as the transfer mechanism driving extraction.

Coffee porous particles are modelled as homogeneous spheres of a measured sphericity, whose volume does not change during extraction, i.e. no potential swelling effects are considered. The transport of given species only occurs in the radial direction of the particles (one dimensional transport) and is characterised by an effective diffusion coefficient (D_{eff}), which encompasses averaged information of the hindrance

effect exerted by the porous nature of the particles. So far, soluble solids as a whole have been considered. However, for the sake of completeness, the model is presented for a number of species. It is assumed that the concentration inside the coffee particles is dilute enough so that D_{eff} can be considered independent with respect to the concentration.

Thus, if a continuously bimodal particle size distribution is divided in *sc* size classes and coffee soluble solids are assumed to be formed by *sp* species, the model can be written as follows:

$$\frac{\partial C_{s,i}^{\beta}}{\partial t} = D_{eff,i}^{\beta}\left(\frac{\partial C_{s,i}^{\beta}}{\partial r^2} + \frac{2}{r}\frac{\partial C_{s,i}^{\beta}}{\partial r}\right) \qquad \text{Eq. 3.28}$$

$$t = 0\ ;\ C_{s,i}^{\beta} = C_{s,i,0}^{\beta}\ ;\ \left(0 \le r \le R_i\right) \qquad \text{Eq. 3.29}$$

$$t = t\ ;\ \mathrm{D}_{eff,i}^{\beta}\frac{\partial C_{s,i}^{\beta}}{\partial r} = 0\ ;\ \left(r = R_i\right) \qquad \text{Eq. 3.30}$$

$$t = t\ ;\ \mathrm{C}_{s,i}^{\beta}\frac{C_{b,i}^{\beta}}{K_i^{\beta}}\ ;\ \left(r = R_i\right) \qquad \text{Eq. 3.31}$$

Where *i* and *β* are a given size class and species, *t* is the time (*s*), *r* is the radial coordinate, and *R* is the average radius of the size class (*m*).

Eq. 3.28 represents Fick's second law of diffusion for multiple species in a porous medium characterised by D_{eff}; Eq. 3.29 assumes that the species are initially homogeneously distributed in the particle; Eq. 3.30 holds by symmetry at the centre of the particle; Eq. 3.31 assumes an equilibrium at the boundary of the particle as the

solution is *well-stirred* and consequently, the influence of the external mass transfer can be neglected. This was assumed according to Spiro and Jago (1982) and preliminary calculations of the Biot number. This is also experimentally validated in Chapter 5.

The mass flux of each species diffusing out of each size class can be calculated as follows:

$$J_i^{\beta} = -D_{eff,i}^{\beta} \left. \frac{\partial C_{s,i}^{\beta}}{\partial r} \right|_{r=R_i} \left(\frac{\upsilon_i m}{V_i \rho_{particle}} \right) \qquad \text{Eq. 3.32}$$

Where V is the volume (m^3) and ν the volume proportion of the considered size class (-), respectively. The first term is effectively the flux coming out of the average particle of the size class i and the second term, in brackets, multiplies this flux by the number of particles forming this class.

The simulated time-dependent concentration in the bulk of each extracted species can be calculated as shown in Eq. 3.33: Eq. 3.32 is multiplied by the surface area of the average particle of the considered size class and then integrated over time.

$$C_{b,pre}^{\beta}(t) = \frac{\int_0^{t_{exp}} \sum_{i=1}^{sc} J_i^{\beta} 4\pi \left(R_i \phi\right)^2 dt}{V_b} \qquad \text{Eq. 3.33}$$

Where Φ is the sphericity of the grind (-).

The simulated extraction yield in soluble solids can be then calculated as shown here:

$$y_{pre}(t) = \frac{\sum_{\beta=1}^{sp} C_{b,pre}^{\beta} V_b}{m} \qquad \text{Eq. 3.34}$$

The simplest case that can be implemented in the model aiming to represent extraction of multiple species from a particle size distribution, is considering a single diffusing species, i.e. $\beta = 1$, and a single size class, i.e. $sc = 1$ and $\nu = 1$. This scenario would involve assuming coffee soluble solids as a uniform species, and an average size parameter of the distribution, i.e. X_{50}, $d_{[3,2]}$ or $d_{[4,3]}$. More refine scenarios including more than a size class can be set. For example, a baseline multiparticle case can be built if the naturally-occurring continuous bimodal particle size distributions of ground coffee is approximated to be a discrete bimodal distribution formed by two size classes: fine size class, i.e. particle size ≤ 100 μm, and coarse class, i.e. rest of the particles in the distribution. The average size of the fine class is invariably found at circa the original biological coffee cell (~40 μm) for all the particle size distributions (Section 4.2.1); the average size of the coarse size class, which varies with grinding level, can be approximated to the volume mean diameter of the distribution, $d_{[4,3]}$.

3.4.2. Extraction model at the bed scale

This section presents the proposed equations to model soluble solid transport at the bed scale. Further simplifications were assumed in addition to the ones adopted for the transport at the particle scale: (i) convective transport occurs only in the axial direction of the bed; (ii) axial dispersion is negligible; (iii) the packed bed is fully wetted at $t = 0$ and thus the effect of the transient moving front through the bed at start-up is not considered. Note also that, at the particle scale, the concentration at the bulk solution (C_b) has to be replaced by the concentration in the pore space of the bed (C_{bed}), in the concentration boundary condition applied at $r = R_i$, i.e. Eq. 3.31.

Under these circumstances, the transport equation at the bed scale is as follows:

$$\frac{\partial C_{bed,i}^{\beta}}{\partial t} = \sum_{i=1}^{sc} \frac{3\left(1-\varepsilon_{bed}\right)}{\varepsilon_{bed} R_i} \upsilon_i J_i^{\beta} - u_p \frac{\partial C_{bed,i}^{\beta}}{\partial z} \qquad \text{Eq. 3.35}$$

Where the new variable introduced here (u_p) is the fluid velocity in the pore space of the bed ($m\ s^{-1}$).

When length and the thickness of the bed are of comparable magnitude, i.e. bed length ~ equal to 2 bed radius, it is possible to assume the simplification proposed in the review by del Valle and de la Fuente (2006), which states that the concentration in the bed varies linearly in the axial direction. This assumption effectively transforms Eq. 3.35 into an ordinary differential equation:

$$\frac{dC_{bed,i}^{\beta}}{dt} = \sum_{i=1}^{sc} \frac{3\left(1-\varepsilon_{bed}\right)}{\varepsilon_{bed} R_i} \upsilon_i J_i^{\beta} - \frac{Q C_{bed,i}^{\beta}}{V_{bed}\varepsilon_{bed}} \qquad \text{Eq. 3.36}$$

Where Q is the flow rate through the bed ($m^3\ s^{-1}$) and V_{bed} is the volume of the bed (m^3). In these circumstances C_{bed} is homogenous in space and only varies with time as the extraction from the bed, at a rate given by $Q\,C_{bed,i}^{m}/V_{bed}\varepsilon_{bed}$, proceeds.

From the main model variable ($C_{bed,i}^{m}$), the predicted cumulative yield (y_{pre}(t)) and strength (S_{pre}(t)) can be computed as follows:

$$y_{pre}\left(t\right) = \frac{\int_0^{t_{\exp}} \sum_{\beta=1}^{sp} \sum_{i=1}^{sc} C_{bed,i}^{\beta} Q dt}{m} \qquad \text{Eq. 3.37}$$

$$S_{pre}(t) = \frac{\int_0^{t_{exp}} \sum_{\beta=1}^{sp} \sum_{i=1}^{sc} C_{bed,i}^{\beta} Q dt}{\int_0^{t_{exp}} Q\, dt} \quad \text{Eq. 3.38}$$

3.4.3. Permeability models

This section presents the proposed permeability models that were used to investigate the hydrodynamics of coffee extraction at the bed scale. Since both models are based on the Kozeny-Carman equation (Carman, 1997), a brief introduction to its derivation is presented here.

The main foundation of the Kozeny-Carman equation is the assumption of the packed bed being a bundle of parallel capillaries, in which the Hagen-Poiseulle equation is applied. If the capillaries are assumed to be spherical this approach yields the following expression for the permeability (κ). (Endo et al., 2002; Rhodes, 2008):

$$\kappa = \frac{\varepsilon_{bed}^3}{2\tau_{bed}^2 S_v^2 \left(1-\varepsilon_{bed}\right)^2} \quad \text{Eq. 3.39}$$

Where ε_{bed} is the average bulk porosity of the packed bed (-), S_v is the surface-to-volume ratio of the packing material (m^{-1}), and τ_{bed} is the tortuosity of the bed (-); τ_{bed} is defined as the ratio of the actual tortuous length travelled by the fluid in the bed to the geometric, i.e. straight, length of the bed.

In the simplest case, where the packing material is formed by mono-sized spheres, implies that $S_v = 6/d_s$ and $\tau_{bed} = 1.58$; Eq. 3.39 is then reduced to Eq. 3.40, known as the Kozeny-Carman equation:

$$\kappa = \frac{\varepsilon_{bed}^3 \left(d_s\right)^2}{180\left(1-\varepsilon_{bed}\right)^2} \qquad \text{Eq. 3.40}$$

Where d_s is the diameter of the packing spheres (m) and 180 the Kozeny-Carman pre-factor.

The first permeability model to characterise coffee packed beds is derived from Eq. 3.40 and accounts for the fact that RGC exhibits a distribution of sizes and is a non-spherical material. Thus, d_s is replaced *by* $d_s = \Phi d_{[3,2]}$, where Φ is the sphericity of the material and $d_{[3,2]}$ is the average Sauter mean diameter, i.e. volume-to-surface ratio, of the distribution:

$$\kappa = \frac{\varepsilon_{bed}^3 \left(\phi d_{[3,2]}\right)^2}{180\left(1-\varepsilon_{bed}\right)^2} \qquad \text{Eq. 3.41}$$

The second permeability model derived here (Eq. 3.43) is an extension of the first one (Eq. 3.41). The main difference lies in the fact that it also accounts for the influence that a bimodal particle size distribution has on τ_{bed}. A semi-empirical tortuosity-bed bulk porosity correlation for beds of discrete bimodal distribution of spheres has been reported by Dias et al. (2006) and it is used in this work:

$$\tau_{bed} = \left(\frac{1}{\varepsilon_{bed}}\right)^n \qquad \text{Eq. 3.42}$$

Where n (-) is an adjustable parameter that depends on the packing method of the bed and varies from 0.4, for loose packed beds, to 0.5, for dense packed beds of spheres. Thus the second permeability model yields:

$$\kappa = \frac{\varepsilon_{bed}^3 \left(\phi d_{[3,2]}\right)^2}{72\left(\left(\frac{1}{\varepsilon_{bed}}\right)^n\right)^2 \left(1-\varepsilon_{bed}\right)^2} \qquad \text{Eq. 3.43}$$

3.5. Implementation of the mass transfer models in COMSOL Multiphysics®

The models of extraction at the particle and bed scale presented in Section 3.4 were solved using a commercially available Finite Element Method (FEM) software (COMSOL Multiphysics®, Sweden).

COMSOL Multiphysics® is a Computational Fluid Dynamics (CFD) package that incorporates *Application Modes*, e.g. chemical species transport, heat transfer, etcetera, encompassing the relevant Partial Differential Equations (PDE) and typical boundary conditions to model physical phenomena. The software offers the possibility of coupling two or more of these modes to carry out multiphysics simulations to model complex systems. Additionally, there is also the more versatile possibility of developing generic equation-based models under the *Mathematics application mode*, and this was the selected option in this work. A general overview of how the model was implemented in the software (Section 3.5.1) and a study to determine the optimal number of mesh elements (Section3.5.2) are presented in this Section.

3.5.1. Implementation of the mass transfer model at the particle scale

Coffee particles were pictured in the extraction model at the particle scale (Section 3.4.1) as equivalent spheres of a measured sphericity. However, it was chosen to implement them in the software as squares following previous examples of similar problems solved COMSOL Multiphysics® (Dixon et al., 2014). This offers two main advantages. Firstly, the absence of curve boundaries in the square geometry results in a more accurate mesh on the computational domain. Secondly, if the transport at the bed scale was to be solved accounting for the concentration profile in the axial direction (*z*-axis), i.e. Eq. 3.35, the concentration at the surface of the particle would be coupled to the axial-depending concentration in the pore space of the bed. From the operational point of view of the software, this coupling process would be carried out more easily in the case of the surface of the particle being a straight line (square geometry), compared to being a curved line (circular geometry). Fick's second law, i.e. Eq. 3.28, had then to be rescaled to account for the fact that, although the geometry of the solving domain is a square for the sake of convenience, the relevant transport problem is defined in spherical coordinates. To rescale Fick's second law, a more general form was considered (Aguilera, 2003):

$$\frac{\partial C_{s,i}^{\beta}}{\partial t} = \frac{1}{r^{\alpha-1}} \frac{\partial \left(r^{\alpha-1} D_{eff,i}^{\beta} \frac{\partial C_{s,i}^{\beta}}{\partial r} \right)}{\partial r} \qquad \text{Eq. 3.44}$$

where α = 1 for a slab; α = 2 for a cylinder; and α = 3 for a sphere.

From the *Mathematics application mode*, a *Coefficient Form PDE* was and the irrelevant terms of the equation, i.e. source and convective terms, were made zero in order to mimic Eq. 3.44, and this resulted in Eq. 3.45:

$$d_a \frac{\partial u}{\partial t} = \nabla \left(c \nabla u \right) \qquad \text{Eq. 3.45}$$

Where d_a is known as the mass coefficient (-) and multiplies the partial derivative of u with time, u is equivalent to C_s ($kg\ m^{-3}$) and c, which is effectively a diffusion tensor with four components, to D_{eff} ($m^2\ s^{-1}$) in Eq. 3.44, respectively.

It is then straightforward that, for the spherical case β = 3, Eq. 3.44 and Eq. 3.45 become identical when the substitutions $d_a = r^2$ and $c = D_{eff} r^2$ are implemented in the latter. In the square geometry, the r-coordinate in the model equations is represented by y-coordinate ($r = y$) (see Figure 3.11). It was then ensured that the simulated transport occurs only in the y-direction by assigning non-zero value only to the components of the diffusion tensor in the y-coordinate.

3.5.2. Study of the optimal mesh size

At the cost of computational time, accuracy in the solution is generally gained when the number of mesh elements in the computational domain is increased. In order to reach a compromise between computational time and accuracy, an optimisation study of the number of mesh elements was performed. The available analytical solution (AS) of Fick' second law for a constant concentration boundary condition ($C_s = C_b = 0$ at $r = R_i$) given as a Fourier series (Crank, 1975b), and a single size class, i.e. sc = 1, was considered as the reference case to test the accuracy of the numerical solution.

$$C^* = 1 - \frac{6}{\pi} \sum_{n=1}^{\infty} \frac{1}{n^2} \exp\left(-t^* \ n^2 \pi^2 \right) \qquad \text{Eq. 3.46}$$

Where C^* is the dimensionless concentration (-) defined as $C_b/C_{b,eq}$, n is the number of terms in the summation (-) and t^* is the Fourier dimensionless time (-) defined as $D_{eff}t/R^2$.

Firstly, the required number of terms in the summation of Eq. 3.46 was required to achieve convergence of the Fourier series, i.e. at $t^* = 0$, $C_b/C_{b,eq} = 0$, at earlier times. Figure 3.10 shows that convergence of the series dramatically improved when the number of terms was increased. It was then concluded that n = 500 offered an acceptable degree of convergence at earlier t^* values and thus this value was adopted to test the accuracy of the numerical solution.

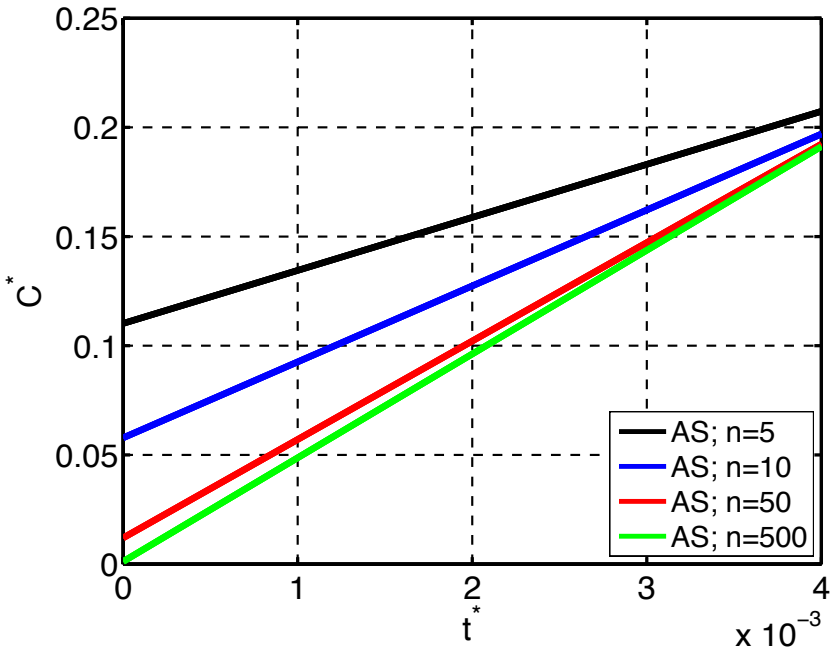

Figure 3.10: Convergence of the analytical solution (AS) of Fick's second law (Eq. 3.46) for different number of terms (n) of the summation

Secondly, the computational domain was discretised with a mapped mesh. This type of mesh was preferred over the classical tetrahedral free mesh since greater control over the mesh elements is gained with the former. A *fixed number of elements* distribution and a *predefined distribution type* were selected for the x-axis and y-axis,

respectively. A *predefined distribution type* (*y*-axis) allows varying the *element ratio* of the distribution, which is defined as the size ratio of the first to the last mesh element across the *y*-axis. The size of the rest of the mesh elements can follow either an arithmetic or geometric progression Figure 3.11 shows that, effectively, this results in a distribution of sizes of the mesh elements across the *y*-axis (*r* coordinate in the model equations), and it allows discretising sensitive zones of the geometry, e.g. the proximity to boundaries where high concentration gradients may occur, with smaller mesh elements improving therefore the accuracy of the numerical solution.

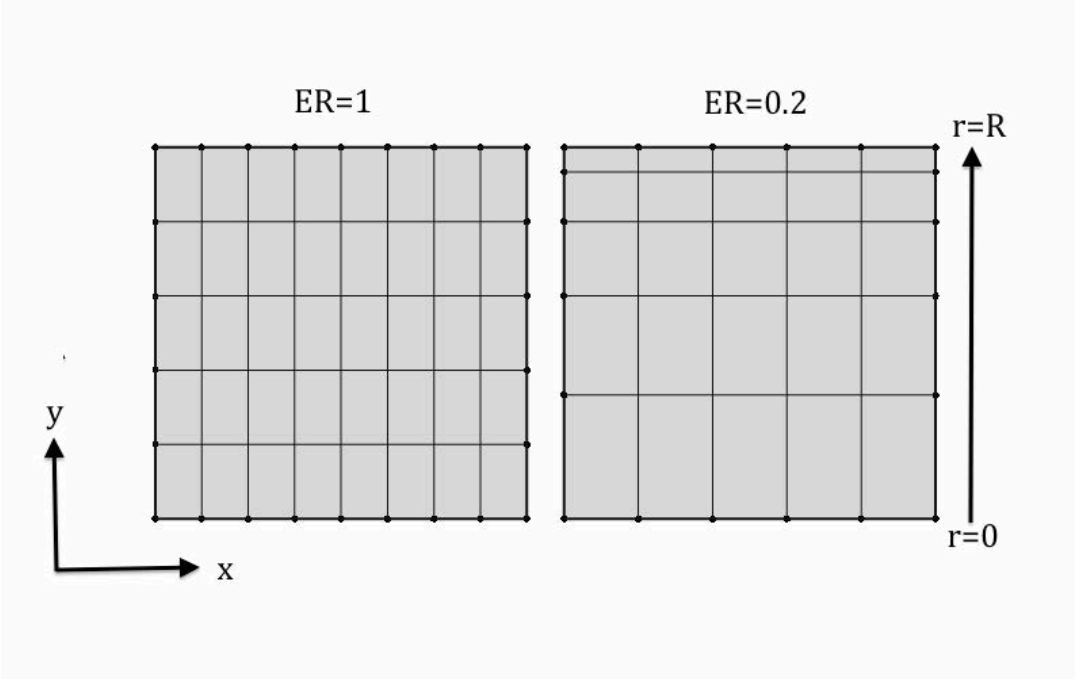

Figure 3.11: Square geometry implemented in COMSOL Multiphysics® to simulate extraction from RGC particles. Element ratios (ER) of 1 (right) and 0.2 (left) were compared

The considered number of mesh elements for this optimisation study was 0.33, 0.67 and 6.67 mesh elements (ME) per *μm* for both the *y* and *x*-axis at *element ratios* (ER) of 1 (uniform size in the mesh elements), and 0.2 (smaller size of the elements near the boundary) (Figure 3.11). Fick's second law, with the appropriate substitutions described in Section 3.5.1, and $C_s = C_b = 0$ at $r = R_i$, was solved numerically in the

aforementioned described computational domains and the solutions compared to the analytical solution.

Figure 3.12a shows the comparison of the analytical solution (AS) to the numerical solution (NS) for the proposed computational domains. It can be noticed that increasing the number of mesh elements and reducing the *element ratio* from 1 to 0.2 dramatically improved the accuracy of the numerical solution. Figure 3.12b shows the error of the numerical solution when compared to the analytical solution with n=500. The error for 0.67 ME per μm and ER of 0.2 was found to be around 1 %, whereas it was found to be around 0.1 % for 6.67 ME. However, it was found that the computational time increased by 7-fold when 6.67 ME were considered. Thus, it was determined that a good compromise situation was found for 0.67 ME at ER 0.2 and this computational domain was the one adopted for all the mass transfer models in this work.

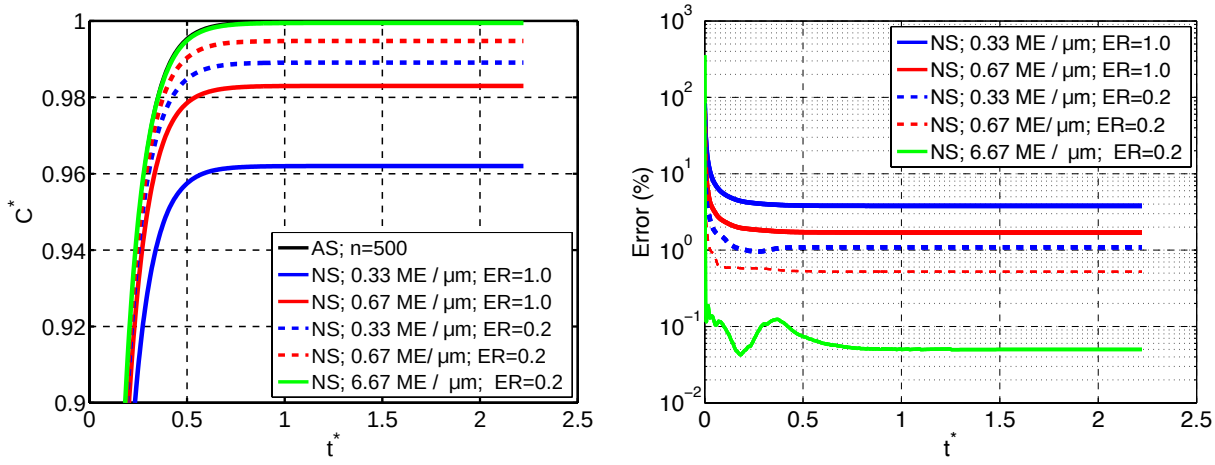

Figure 3.12: (a) Comparison of the convergence to the analytical solution (AS) of the numerical solution (NS) for a combination of different mesh elements (ME) and aspect ratios (AR); (b) Relative error between the AS and NS for the different considered situations

Chapter 4: Particle Fundamental Characterisation

4.1. Introduction

The main objective of this Chapter is to present the results of the fundamental characterisation study of the grinds produced from Blend 1. This was carried out in order to obtain measurements or estimations of the parameters of the mathematical models shown in Chapter 3. The characterisation work is divided into three different scales, which comprise different characteristics of the material:

- Macrostructure: particle size distribution, particle sphericity, and free flow and tapped density.

- Microstructure: intrinsic density and particle porosity, pore size distribution, and particle tortuosity.

- Extraction parameters: initial concentration of extractable soluble solids, microstructural hindrance factor, effective diffusion coefficient, water-roast and ground contact angle, absorbed water, and solid-liquid partition coefficient.

A secondary objective comprises the preliminary investigation of the dependency of some of these parameters on the process history of the beans (flaking process, heat treatments to obtain different roasting colours, and decaffeination). For this purpose, some of the measurements and estimates were also obtained for flaked coffee (Blend 2), and two samples of decaffeinated RGC produced with the same beans (Blend 3), but roasted to a different roasting colour (9.0 and 5.5. *La*).

4.2. Macrostructure

4.2.1. Particle size distributions

The particle size distribution of the coffee grinds was measured according to the *dry* and *wet* laser diffraction methods previously described in Section 3.3.2.

Figure 4.1 presents typical examples of the results obtained with the *dry* method for some of the grinds produced from Blend 1, and flaked coffee. The *y*-axis represents the density distribution of the particle sizes shown in the *x*-axis, which is displayed in a logarithmic scale. According to the results obtained with the *dry* method, it can be concluded that all the grinds (including the flakes) display a continuously bimodal particle size distribution. This characteristic of RGC has been previously reported elsewhere (Anderson et al., 2003; Corrochano et al., 2014; Petracco, 2005d).

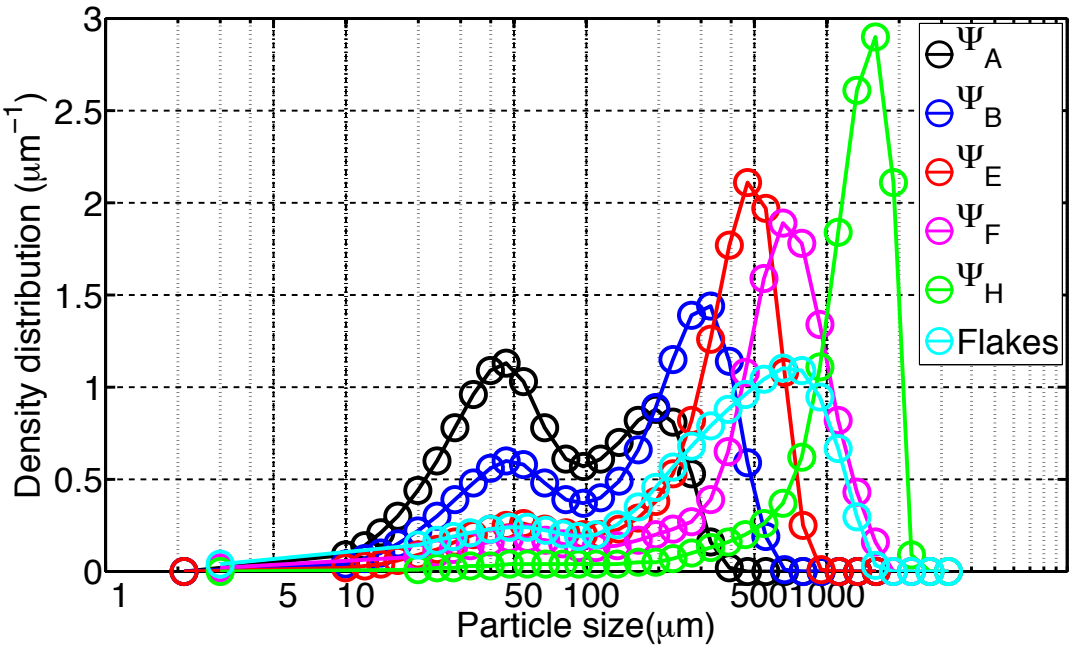

Figure 4.1: Density distribution (*y*-axis) vs. particle size (*x*-axis) for the considered grinds as *dry* measured. The lines are meant to guide the eye. The data represent the average of the measurement of three independent samples of each grind (error bars not shown; standard deviation is shown in Table 4.1)

For all the grinds, the fine peak is located at a particle size around 40-50 μm, which approximately corresponds to the size scale of a coffee cell pocket (Schenker et al., 2000), whereas the coarse peak shifts rightwards when the beans are ground to a coarser level. The inflection point that separates the fine and the coarse regions in the particle size distributions is located at around 100 μm for all the grinds. Therefore, as detailed in the model development (Chapter 3), if a baseline multiparticle case was to be implemented in the extraction model, i.e. sc = 2, a fine size class could be logically defined as the population of particles whose size is ≤ 100 μm (with an average diameter of 40 μm), while the coarse size class would be formed by the rest of the particles.

The particle size distribution of flaked coffee seems to display a different trend as compared to regular RGC, as observed in Figure 4.1. It can be seen that the density distribution of its fine size class (particle size ≤ 100 μm) is comparable to that of Ψ_E, but

for particles greater than 100 μm the height of the peak is considerably smaller and the distribution wider.

Figure 4.2 shows the corresponding cumulative curves of the distributions, where the *y*-axis represents the volume percentage of particles whose size lies under the size displayed in *x*-axis (logarithmic scale). The described tendency of flaked coffee can be also observed here: the particle size distribution of approximately 40-50 % of its volume is comparable to that of Ψ_E, whereas the rest of the volume seems to be formed by coarser particles.

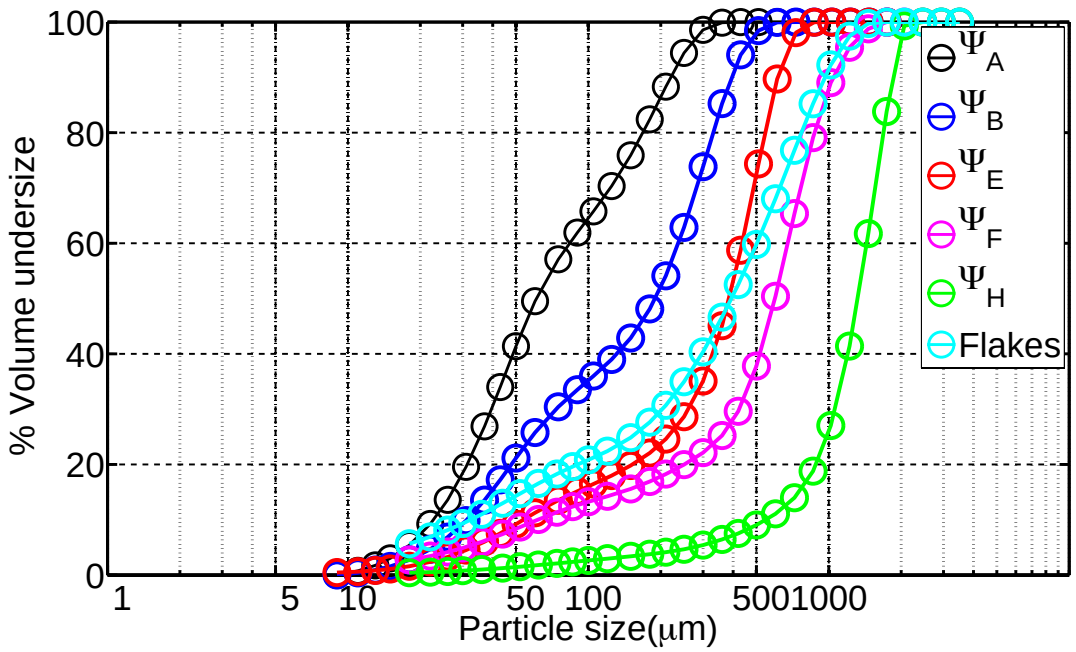

Figure 4.2: Volume percentage under size (*y*-axis) vs. particle size (*x*-axis) for the considered grinds *dry* measured. The lines are meant to guide the eye

In order to compare the *dry* and *wet* method, three samples of the grinds Ψ_B-Ψ_E were assessed according to the *wet* method. Figure 4.3 presents a typical example of a particle size distribution of a coffee grind (Ψ_B) as obtained with the *wet* method, and its comparison to the result from the *dry* method. The first identified difference between the *dry* and *wet* methods is that, for all the measured grinds, the *wet* results suggest that

RGC exhibit a trimodal particle size distribution. It can also be seen that the *wet* result displays a population of particles in the range of 1-10 μm that is not detected in the *dry* method (Figure 4.3). In other words, for a sample of the same grind, the *wet* method would detect finer particles as compared to the *dry* method.

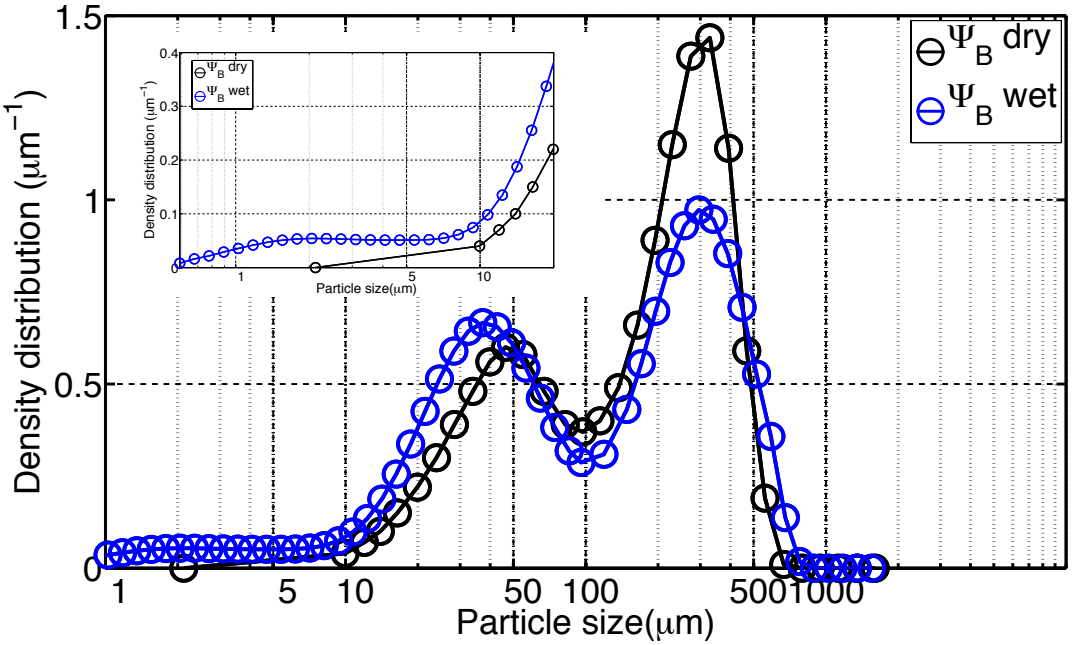

Figure 4.3: Comparison of the *dry* and *wet* particle size distribution measurements for grind Ψ_B. The small figure is a magnification of the 0-10 μm region. The lines are meant to guide the eye

A SEM microscopy image of grind Ψ_E (Figure 4.4) reveals what appears to be particles in the 1-10 μm size scale in the RGC grinds. They are typically located (and possibly bound to) on the surface of coarser particles. It is well-known that particles with sizes below 100-150 μm may exhibit a cohesive behavior mainly due to van der Waals forces (Zou et al., 2011). Besides, RGC oils could be holding these particles on the surface. The more effective dispersion procedure applied in the *wet* method (involving a liquid dispersant, surfactant, agitation, and sonication) may allow the detachment of such particles, and thus their detection in the measurement.

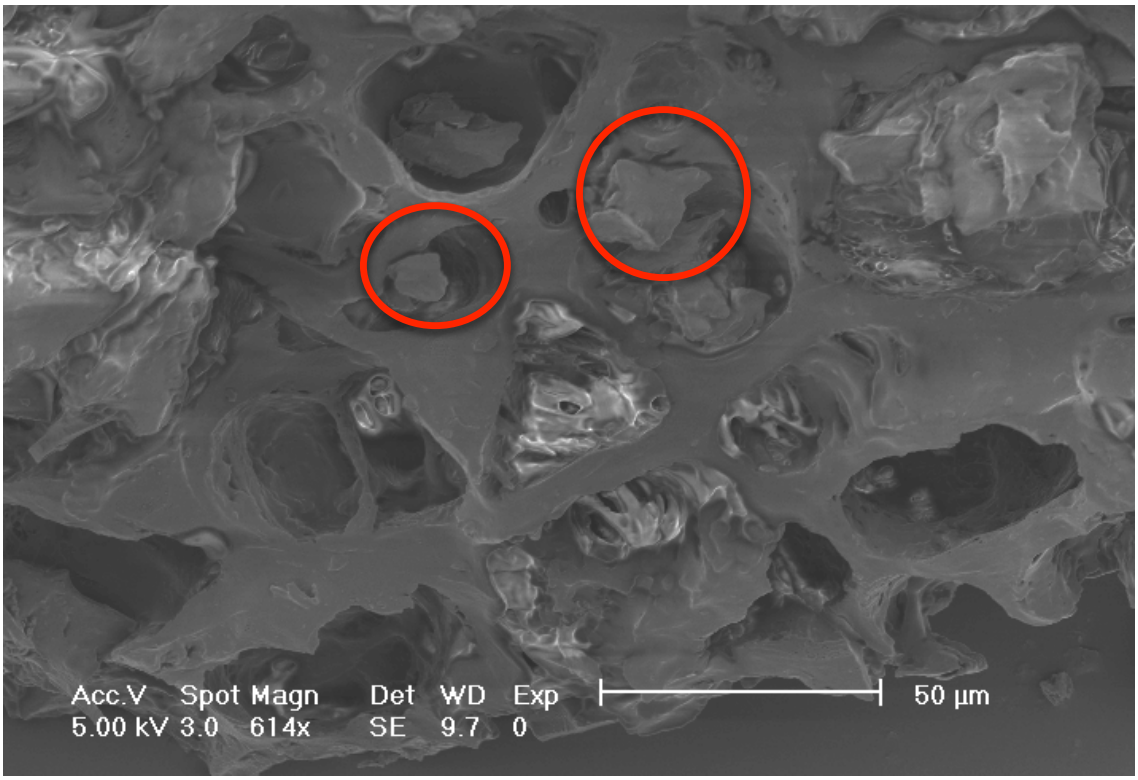

Figure 4.4: SEM picture of a coffee particle from Ψ_E showing small coffee fragments in the scale of 1-10 μm (circles)

The relevant average parameters of the distributions ($d_{[3,2]}$, $d_{[4,3]}$, % of fines, and X_{50}), as measured by both methods, are reported in Table 4.1 and Table 4.2. In Table 4.1 the value of the coarse peak is also included.

Table 4.1: Average parameters of the grinds as *dry* measured

Ψ_j	$d_{[3,2]} \times 10^{-6}$ (m)	$d_{[4,3]} \times 10^{-6}$(m)	[1]% fines	$X_{50} \times 10^{-6}$(m)	[2]Coarse peak $\times 10^{-6}$(m)
A	48.1 ± 0.1	95.9 ± 0.2	65.7 ± 0.1	61.1 ± 0.3	194.42
B	79.7 ± 0.5	198.8 ± 0.9	35.9 ± 0.2	189.6 ± 1.4	328.63
C	101.6 ± 0.2	260.1 ± 0.6	26.6 ± 0.2	265.1 ± 0.8	393.45
D	112.9 ± 1.1	325.2 ± 1.0	20.1 ± 0.1	336.1 ± 0.8	468.29
E	131.4 ± 2.1	363.6 ± 3.8	16.7 ± 0.3	383.0 ± 2.9	468.29
F	144.8 ± 12.0	592.5 ± 24.6	12.5 ± 1.5	601.6 ± 19.6	657.27
G	197.3 ± 14.7	808.3 ± 42.1	8.6 ± 0.9	820.8 ± 29.1	936.59
H	514.1 ± 7.8	1247.7 ± 14.6	2.7± 0.1	1297.2 ± 24.5	1593.86
Flakes	83.6 ± 1.1	454.2 ± 12.5	20.8 ± 0.2	394.4 ± 6.1	657.27
Blend 3 – 9.0 La	161.2 ± 0.8	374.0 ± 2.5	13.5 ± 0.1	372.0 ± 1.6	393.45
Blend 3 – 5.5 La	143.8 ± 0.7	365.0 ± 2.9	15.8 ± 0.1	367.5 ± 1.4	393.45

[1]: For Ψ_A- Ψ_D, and Blend 3, a particle size of 105 μm was the closest value to 100 μm displayed in the numerical output of the measurement. This value was taken as the inflection point to estimate the value % fines; 100 μm was displayed for the rest of the grinds and this value was used; [2]: The standard deviation for the coarse peak was 0.

Table 4.2: Average parameters of the grinds as *wet* measured

Ψ_j	$d_{[3,2]} \times 10^{-6}$(m)	$d_{[4,3]} \times 10^{-6}$(m)	[1]% fines	$X_{50} \times 10^{-6}$(m)
B	22.3 ± 2.5	173.0 ± 4.0	49.1 ± 0.7	112.8 ± 6.5
C	28.3 ± 6.5	226.9 ± 9.7	40.3 ± 2.0	196.7 ± 14.7
D	38.6 ± 1.3	294.8 ± 1.9	32.9 ± 0.4	279.2 ± 3.4
E	37.0 ± 3.8	348.2 ± 5.7	29.7 ± 1.0	338.4 ± 8.2

[1]: % of fines estimated as the population of particles below 105 μm

The graphical comparison of the *dry* and *wet* values (Figure 4.5), clearly reveals that both particle size distribution measurement methods indeed provide considerably different results, especially in the case of $d_{[3,2]}$, and the percentage of the fine size class. Whereas part of these differences may be due to some degree of intrinsic variability between the methods themselves, it is straightforward that the smaller parameters that resulted from the *wet* measurement are a direct consequence of the detection of the population of particles between 1-10 μm.

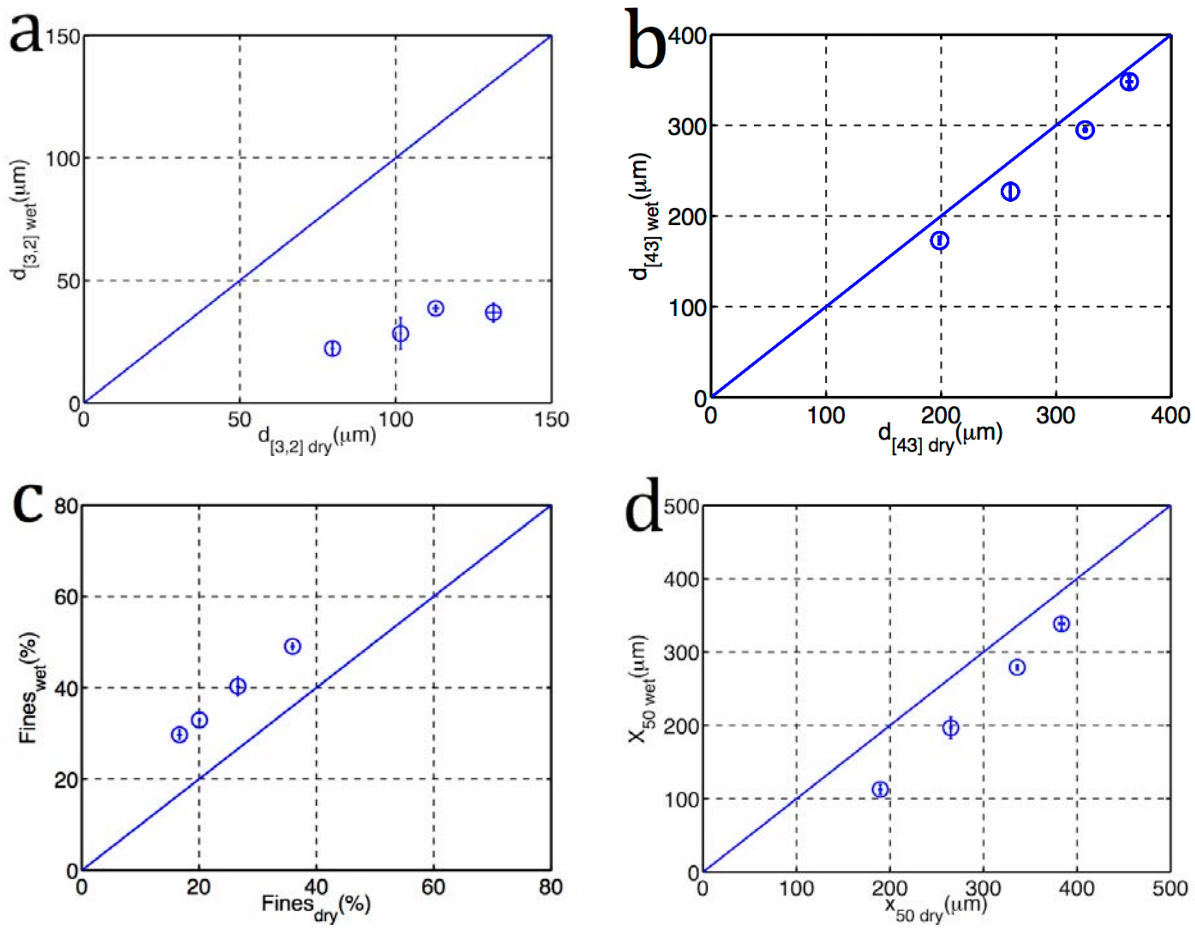

Figure 4.5: Comparison of the average parameters of Ψ_B-Ψ_E as *dry* and *wet* measured: (a) $d_{[3,2]}$; (b) $d_{[4,3]}$; (c) *% Fines*; (d) X_{50}. The straight lines represent y = x

Considering the remarkably different $d_{[3,2]}$ values obtained with both methods, and the sensitivity of the permeability to particle size ($\kappa \propto d^2_{[3,2]}$) (Chapter 3), a preliminary investigation on the nature of the 1-10 *µm* population of particles was considered to be relevant. Part of these detected 1-10 *µm* particles may be regular fragments of the coffee bean, this is, the insoluble coffee matrix, which is formed mainly by cellulose and contains the species that are dissolved during extraction. However, there is also the possibility of these particles being lumps of species not attached to the insoluble matrix that may be insoluble at the temperature at which the *wet* measurement is performed (approximately 15 *°C*), but soluble at the typical extraction

temperatures (80-95 $°C$). As a matter of fact, as later illustrated in Section 4.4.6, the solid-liquid partition coefficient was found to decrease from 0.61 at 80 $°C$ to 0.42 at 20 $°C$. In a real extraction scenario from a coffee packed bed, both possibilities would have different but relevant implications: the insoluble coffee matrix fragments would contribute to reduce the permeability of the bed, as they would increase its surface area per unit volume; on the other hand the soluble lumps would be irrelevant from this point of view since they may be (virtually) instantly dissolved by hot water, as it is the case in instant coffee. Additionally, despite the relatively low temperature at which the *wet* measurements were performed, extraction of some compounds occurred as evidenced by the characteristic light brown colour adopted by the water in which the grinds were dispersed. Thus, another type of particles contributing to this population could be oil droplets, as they have been previously reported to exhibit comparable sizes (between 1-10 μm) in coffee extracts (Petracco, 2005c).

To determine whether a fraction of the identified 1-10 μm population could correspond to lumps of soluble species at typical extraction temperatures but insoluble at the temperature of the measurement (15 $°C$), the particle size distribution of non-extracted and extracted grinds was measured and compared. To create the extracted grinds, approximately 0.5 g of Ψ_B and Ψ_E were slurried at 80 $°C$ in the set-up described in Section 3.3.10, for 1, 10 and 30 minutes. The particle size distribution of the slurries, i.e. extracted grinds and the liquid phase containing the dissolved species, was subsequently assessed according to the *wet* method. Figure 4.6 and Figure 4.7 show the comparison between the *wet* measurements performed on the non-extracted and the extracted grinds Ψ_B and Ψ_E.

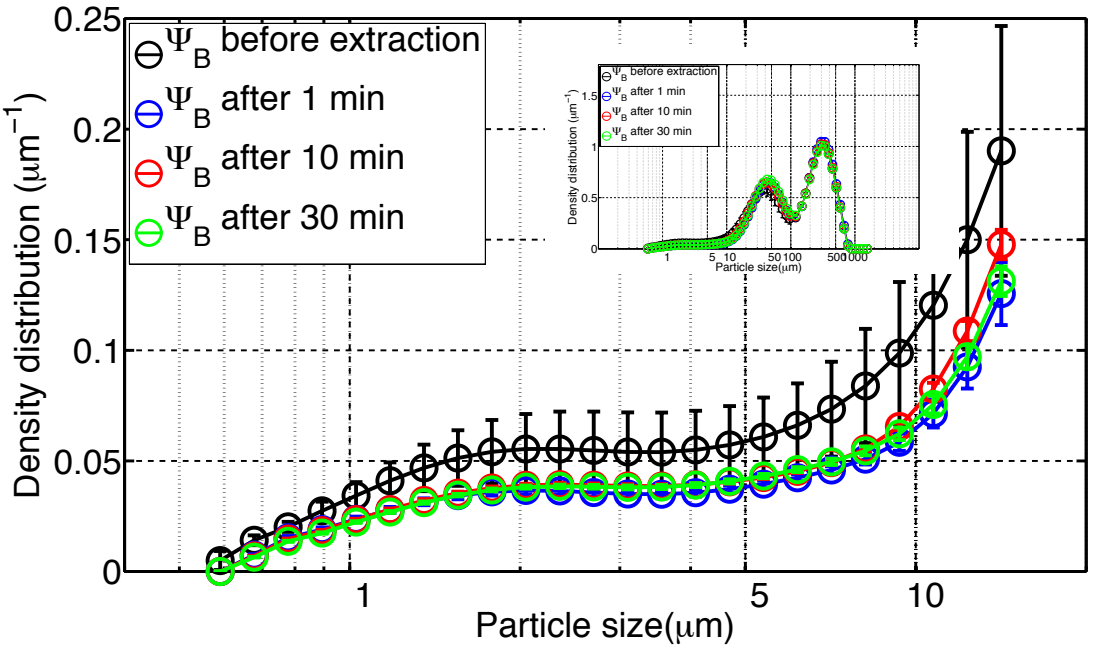

Figure 4.6: Comparison of the particle size distribution of non-extracted and extracted grinds at different times as *wet* measured for grind Ψ_B. The lines are meant to guide the eye

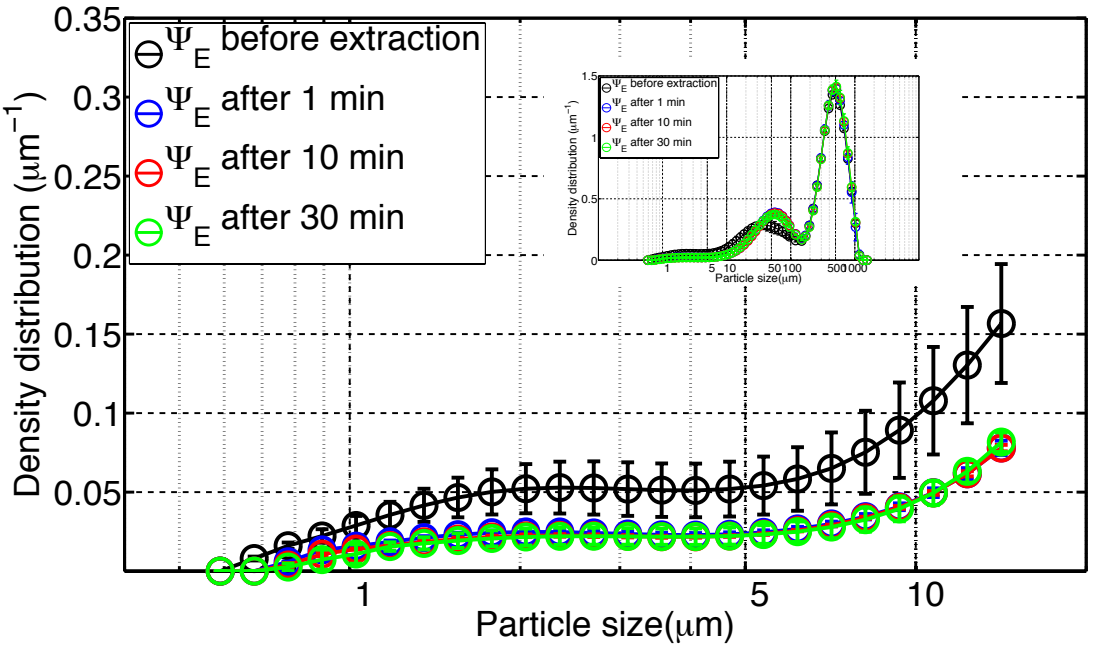

Figure 4.7: Comparison of the particle size distribution of non-extracted and extracted grinds at different times as *wet* measured for grind Ψ_E. The lines are meant to guide the eye

In Figure 4.6 and Figure 4.7 it can be observed that the 1-10 μm fraction in the extracted grinds decreases considerably, whereas the coarse peak remains virtually

unchanged. This may be an indication that part of the 1-10 μm fraction measured with the *wet* method in non-extracted grinds corresponds to lumps of species that in a real extraction scenario would be instantly dissolved.

The resulting $d_{[3,2]}$ and $d_{[4,3]}$ values for the non-extracted and extracted grinds are compared in Figure 4.8. Note that the parameters for the non-extracted grinds, i.e. t = 0 min, slightly differ from the ones reported in Table 4.2, and this is probably due to the fact that the measurements were performed with grinds produced from different bean batches of Blend 1; the study of the variability between batches was not considered in this thesis. For Ψ_B, $d_{[3,2]}$ values of the extracted grinds are approximately 1.3 times bigger than the values for the non-extracted grind, but virtually equal over time, whereas in the case of $d_{[4,3]}$, there is no significant difference between the non-extracted and the extracted grinds. For Ψ_E it seems that $d_{[3,2]}$ increases over time to values of approximately 1.9-fold, as compared to the non-extracted grind. This points out that upon wetting, the volume of the grains remains relatively constant for Ψ_B, whereas it increases by approximately 12 % for Ψ_E (as indicated by the observed tendency in $d_{[4,3]}$ in Figure 4.8). The surface area of the distribution would decrease in both cases (as observed by the increase of $d_{[3,2]}$), due to the dissolution of part of the population of 1-10 μm. The fact that the volume of the grains remains relatively constant, or increase only by 12 % contrasts with the observations from Mateus and Rouvet, (2007). They reported that for grinds of $d_{[4,3]}$ = 750-1050 μm, the volume of the particles increase between 20 and 23 % after wetting times of 10-15 minutes, and attributed it to a swelling effect of the coffee matrix polymers. However, Mateus and Rouvet used in their experiments distilled water (as opposed to tap water used in this thesis) and coffee beans with roasting degrees that differ form the one considered here. Further research

would be required to determine if the observed differences can be attributed to these factors.

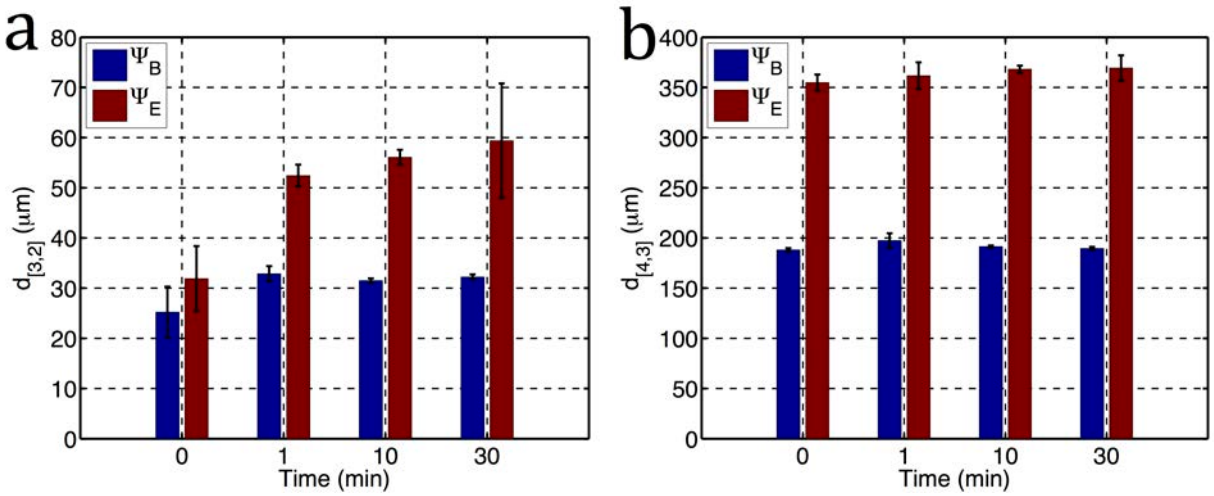

Figure 4.8: Comparison of the average size parameters of Ψ_B and Ψ_E over extraction time; (a) $d_{[3,2]}$; (b) $d_{[4,3]}$

The *dry* measurement is the typical choice in Mondelez International manufacturing sites, as it is a quicker and more economical measurement procedure. Therefore, the average value of the particle size distributions as *dry* measured will be adopted from now on, unless stated otherwise.

4.2.2. Particle sphericity

The sphericity (Φ) of three independent samples of each grind, Ψ_B-Ψ_E and flaked coffee, was estimated as the ratio of the perimeter of a circle with the same area as the projected area of the particle (recorded with a high-speed camera), and the actual perimeter of the particle. Figure 4.9 shows an example of the recorded particles from grind Ψ_B by the high-speed camera. In Figure 4.9 the heterogeneity in shape of the particles (circular, ellipsoidal, irregular), and the edges (rounded, angular) can be appreciated.

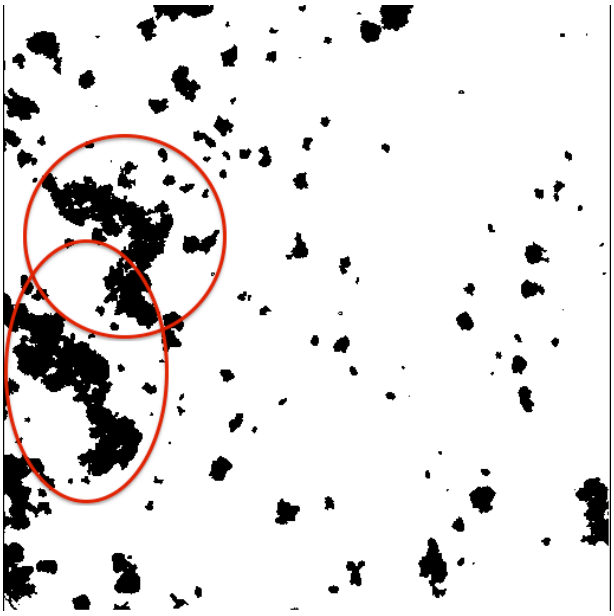

Figure 4.9: High-speed camera recorded images of coffee particles from Ψ_B. Circled particles most likely correspond to aggregates of material not properly dispersed

Figure 4.10 displays two typical examples of the estimated sphericity values of grind Ψ_B (a), and flaked coffee (b). All the other assessed grinds showed similar values, and also a decreasing tendency of sphericity with particle size. It can also be observed in Figure 4.10 that the last measured value of sphericity corresponds to a particle size that lies between 1000-2000 μm. The biggest particle size measured in grinds Ψ_B-Ψ_E with the reference *dry* method (Figure 4.1) is smaller than 1000 μm. Thus, these 1000-2000 μm particles could most likely correspond to aggregates (Figure 4.9) that were not properly dispersed by the disperser of the image analyser. According to manufacturer specifications, this disperser is designed for solids that do not require high dispersion. Thus, the 1000-2000 μm point was then excluded and the smallest measured sphericity was considered to be the value measured at around 600 μm. The median sphericity of each grind was estimated as the mean of the greatest and the smallest sphericity values (Table 4.3). Due to the approximate nature of the assessment method, the median

sphericity values were averaged and a representative sphericity value of 0.75 was considered for all the grinds produced from Blend 1.

Table 4.3: Mean sphericity values for RGC and flaked coffee

$\boldsymbol{\Psi_j}$	***Mean Φ***
B	0.72
C	0.71
D	0.74
E	0.82
Average	**0.75**
Flaked coffee	0.79

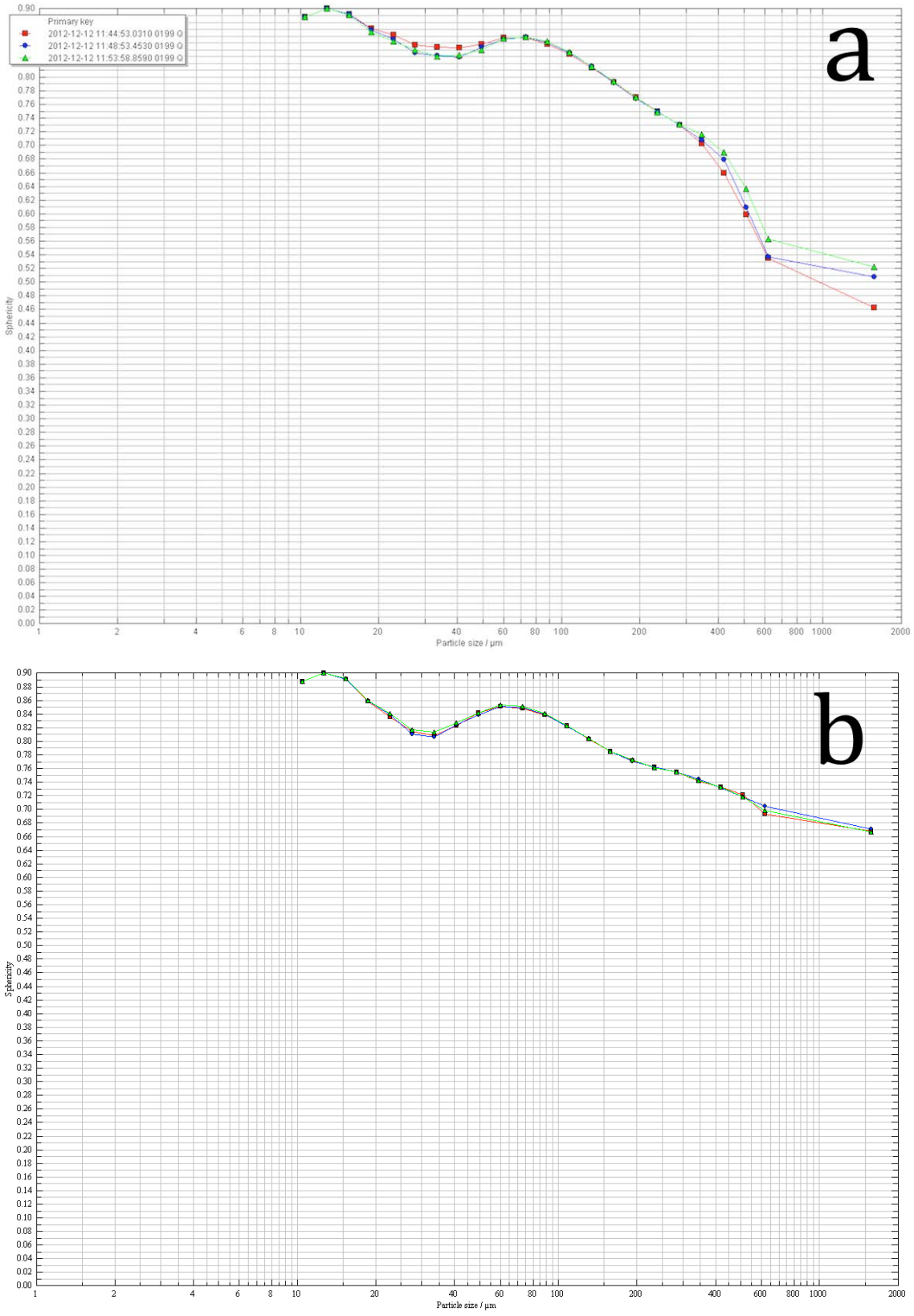

Figure 4.10: Estimated sphericity (y-axis) vs. particle size (x-axis); (a) RGC (grind Ψ_B); (b) Flaked coffee. It can be observed that the three measurements in both cases (as well as for the rest of the grinds) are virtually identical

The estimated sphericity for the flaked coffee is comparable to that of RGC despite the presumably very different morphology of the particles. As it will be discussed in Section 4.2.3, a visual inspection of RGC and flaked coffee showed that the shape of the particles (and thus the projected area) of RGC and flaked coffee does not seem to differ much, and thus similar results are produced with this measurement technique.

4.2.3. Comparison of regular and flaked coffee

The quantitative comparison of regular and flaked coffee did not seem to reveal significant differences with respect to their macrostructure, i.e. particle size distribution and sphericity, despite their presumably different morphology. In addition to particle size distribution and sphericity measurements, SEM pictures of regular and flaked coffee were obtained in order to carry out a qualitative comparison (Figure 4.11). On the one hand, it can be can see that regular RGC shows a sphere-like shape (Figure 4.11a, b), with easily distinguishable cell pockets on the surface of the particles (Figure 4.11a). These, as pointed out by Schenker et al. (2000), can be seen here to be in the range of 20-40 μm. On the other hand, flaked coffee seems to be the combination of larger flat circular particles with a smooth surface where cell pockets cannot be distinguished anymore, and smaller sphere-liked particles (Figure 4.11c, d). The intense compression to which the particles were subjected in the flaking step disrupted the structure of the pre-ground roast coffee to some extent. Particles whose size was below the gap set in between the rollers may have gone through the flaking step without being subjected to compression, and thus partly kept their original sphere-like shape. It can also be appreciated that in fact the projected areas of the regular and flaked coffee do not differ

dramatically, and hence, when this feature is used to estimate particle sphericity, it is not surprising to obtain similar values (see Section 4.2.2).

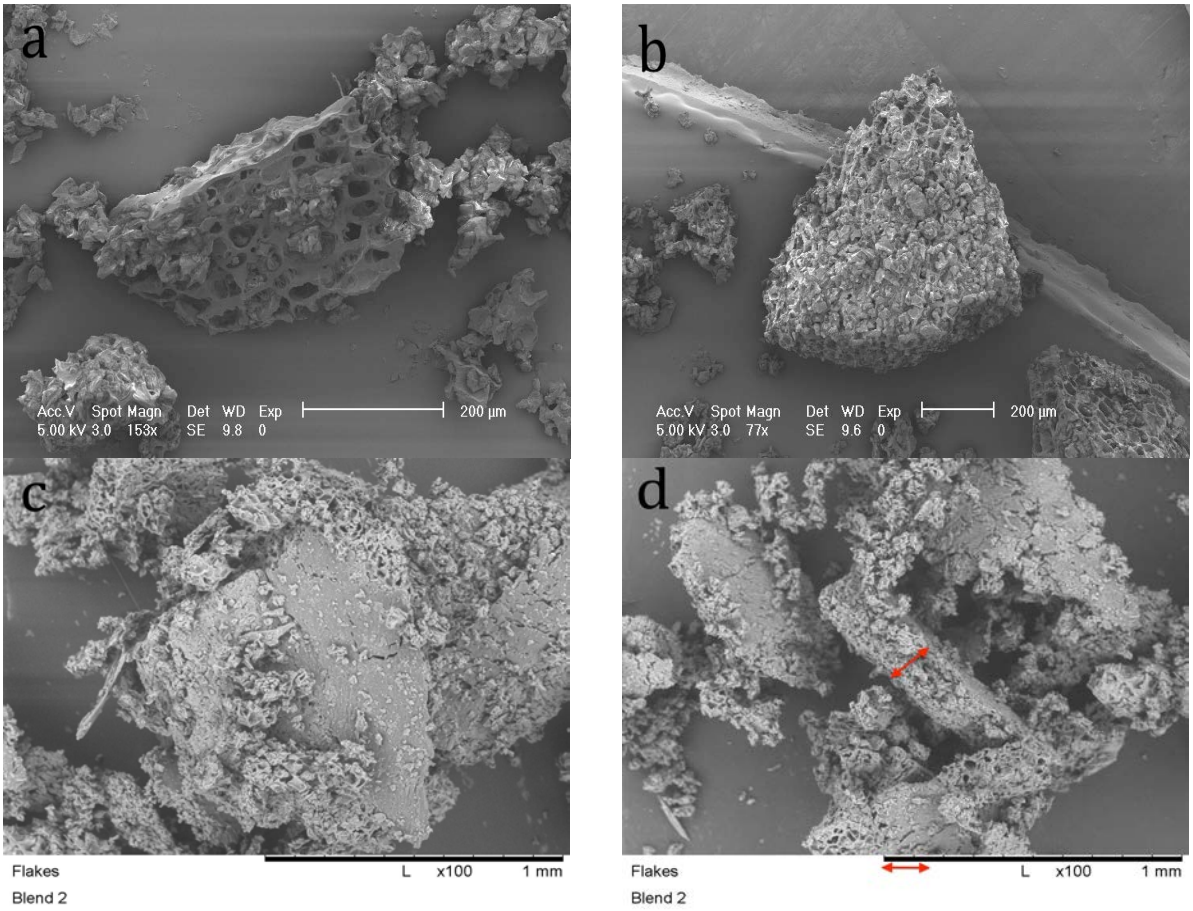

Figure 4.11: SEM pictures of regular RGC (grind Ψ_E) (a,b) and flaked coffee (c,d)

In Figure 4.11c displays the view of the surface area of a flake. It can be appreciate that it tends to be circular, and its characteristic size seems to be approximately between 800-1000 μm. In addition to this, in Figure 4.11d the thickness of a flake can be appreciated. Its size is in the range of 100-150 μm, as determined by the gap by which the two flaking rollers were separated, (approximately 150 μm). It must be noticed here that the laser diffraction method applied to assess the particle size distribution of the grinds is more likely to pick the size associated to the particle surface rather than the thickness. As a matter of fact, the particle size distribution of flaked

coffee as *dry* measured resulted in a $d_{[4,3]}$ = 454.24 μm, which is considerably larger than the observed thickness. However, due to its smaller size scale the relevant size magnitude for mass transfer is precisely the thickness of the flake, as the transport of species would predominately occur in this direction Thus, laser diffraction applied to the determination of the particle size distribution of flaked coffee must be carefully considered if it is to be used to parameterise mass transfer models.

4.2.4. Free flow and tapped density

The free flow and tapped density of the grinds Ψ_A-Ψ_E were measured and the results are displayed in Figure 4.12. The free flow density was found to be similar for Ψ_B-Ψ_E, with values between 266-270 $kg\ m^{-3}$; in the case of the finest grind (Ψ_A), this value was found to be 300 $kg\ m^{-3}$.

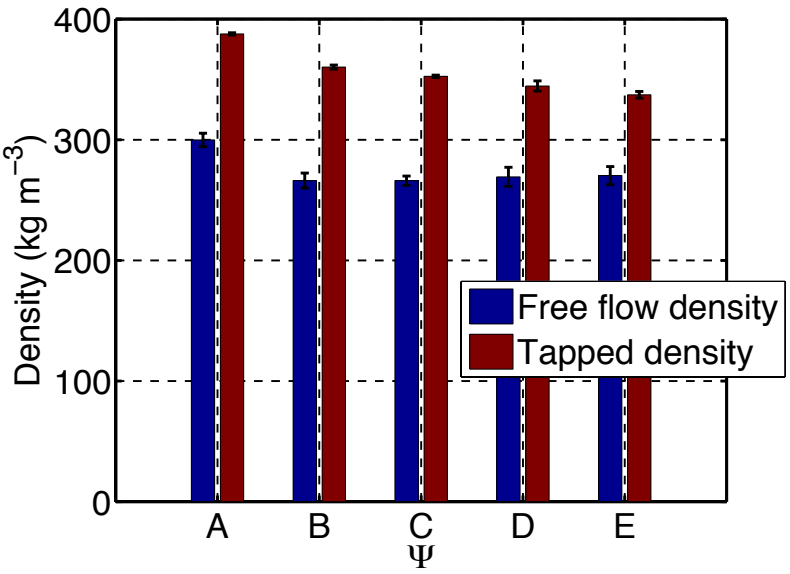

Figure 4.12: Free flow and tapped density for the considered grinds

The tapped density, however, was found to decrease for coarser grinds. This tendency qualitatively agrees with the theoretical predictions of the linear mixing model, which was proven to provide good estimates of the porosity of beds made of

binary spherical particles (Mota et al., 2001), and of two log-normal distributions (Yu and Standish, 1993). In the later reference, values of packing density (one minus the bed porosity) were predicted and compared to experimental results obtained for sand as per Sohn and Moreland, (1968), as a function of the percentage of the coarse size class, and for d_{fine}/d_{coarse} ratios ranging from 0.10 to 0.33. These ratios are comparable to those found in the coffee grinds used in this thesis (Ψ_A-Ψ_E), when estimated from fine and coarse peak values of the *dry* particle size distribution measurement (Table 4.1).

Bed porosity (ε_{bed}) of the tapped beds made from grinds Ψ_A-Ψ_E was inferred from the resuls shown by Yu et al., (1993) for two log-normal distributions, and the estimates are displayed in Table 4.4.

Table 4.4: ε_{bed} values of the tapped grinds as estimated from the results of a linear mixing model (Yu and Standish, 1993)

Ψ_j	d_{fine}/d_{coarse}	% coarse	ε_{bed}
A	0.21	34.6	0.28
B	0.12	64.1	0.24
C	0.10	73.3	0.25
D	0.09	79.9	0.25
E	0.09	83.3	0.26

For a given d_{fine}/d_{coarse}, the minimum bed porosity was achieved when the coarse size class was around 60 %, which is a percentage comparable to that of Ψ_B. At this percentage, the gaps left in between the coarser particles are optimally filled by the finer particles. Segregation effects appear when the percentage of the coarse size class is either increased or decreased. Increasing the percentage of the coarse size class results in insufficient fine particles available to fill the gaps left by the coarser particles; on the contrary, decreasing the percentage of the coarse size class would result in not enough gaps available to accommodate all the finer particles. Consequently, the predicted bed

porosity increases for coarser grinds, and is consistent with the tendency observed from the tapped bed density results. In the hypothetical case of having two grinds with comparable percentage of the coarse size class but different d_{fine}/d_{coarse}, the model predicts smaller porosity values for lower ratios. This can be attributed to the fact that the more different the size classes are, the bigger the gaps left in between the coarser particles, and thus the more fine particles could be accommodated.

Ψ_A, however, does not fit into the linear mixing model predictions. According to its d_{coarse}/d_{fine}, and percentage of the coarse size class, the model predicts the greater bed porosity amongst all the studied grinds, when in fact the measured tapped density shows just the contrary. One possible reason is that, as pointed out by Peronius and Sweeting (1985), the value of the bed porosity increases with the circularity of the particles. The circularity of the particles was shown in Section 4.2.2 to be higher for finer particle sizes, and this might explain the observed behaviour for Ψ_A.

Coffee grinds show a very different shape as compared to the material used to validate the model predictions, i.e. sand. Therefore, although the predictions seem to agree qualitatively for Ψ_B-Ψ_E, a closer exam should have to be carried out from the quantitative point of view. Another factor that is not taken into account by this model is the cohesiveness of the powders. Zou et al. (2011) showed that the porosity of beds formed by glass beads increased for particle sizes below 150 μm, and this was attributed to inter-particle cohesive forces. Visual inspection of Ψ_A proved that the particles were considerably more cohesive than coarser grinds, although according to the highest value of tapped density, this did not seem to influence the packing behaviour of this grind. Lastly, it should be pointed out that the considered grinds may exhibit slightly different

particle porosity values (Section 4.3.1), and hence the density of the particles might differ. Thus, some of the observed differences in tapped density may be due to the particle density and not due to the fashion in which the particles themselves are packed.

4.2.5. Conclusions of the macrostructure analysis

The results from the macrostructure analysis of the coffee grinds allow for drawing several conclusions. Coffee grinds with a broad range of sizes ($d_{[4,3]}$ = 95.9-1247.7 μm, as *dry* measured) were produced from Blend 1, and their particle size distribution assessed according to the *dry* and *wet* method. For the same grind, the results obtained from each method showed significant differences in the values of $d_{[3,2]}$, and percentage of fines, but resulted in relatively comparable values of $d_{[4,3]}$. Whereas the grinds were found to be bimodal according to the *dry* measurements, *wet* measurements displayed trimodal distributions. In addition to small fragments of insoluble coffee cell matrix, it was shown that the extra peak that appeared in the *wet* results (most likely due to a more effective dispersion system in this method) could be also formed by lumps of soluble species, as indicated by the observed drop in the 1-10 μm range for extracted grinds, and possibly oil droplets. Assessing the particle size distribution of extracted grinds for different periods of time did not seem to reveal swelling effects of the same magnitude and in the same time scale as those reported elsewhere (Mateus and Rouvet, 2007), as shown by the constant value of $d_{[4,3]}$ over time.

The estimated sphericity values were similar for all the grinds and also for flaked coffee. The similarity between regular and flaked coffee may be due to the used measurement technique that is based on 2D images. From SEM images it was concluded

that RGC and flaked coffee differ mainly in the thickness of the particle, and was postulated that this is the relevant size scale from the mass transfer point of view.

Tapped density was found to decrease for coarser grinds, and the observed behaviour was in good agreement with the proposed models in the literature that estimate the packing density of beds made of two log-normal distributions. However, to validate this observation, the shape of the particles, as well as the porosity of the particles (which may differ from grind to grind), needs be taken into account.

4.3. Microstructure

4.3.1. Intrinsic density and particle porosity

The solid density (ρ_{solid}), i.e. that of the solid matrix, was calculated as the reciprocal of the solid volume (v_{solid}), which was considered to be the volume measured by helium pycnometry in a very fine grind. Since whole beans of Blend 2 could not be obtained to produce a grind similar to Ψ_A, the solid volume of this blend was considered to be that measured in the flaked coffee as received. The thickness of the flakes was shown in Section 4.2.3 to be comparable to the size scale of Ψ_A. Thus, the assumption of the absence of isolated cell pockets within these particles may also apply for the case of the flaked coffee.

The obtained values of ρ_{solid} are comparable for all the assessed blends, including flaked coffee (Table 4.5). It can also be noticed for Blend 3 that roasting to a darker colour seems to slightly decrease ρ_{solid}. This is consistent with the fact that more intense thermal processes enhance the chemical reactions that occur during the roasting step of the beans and thus greater formation of gaseous products.

Table 4.5: Solid density (ρ_{solid}) of the coffee blends considered in the study

	Blend	***ρ_{solid} (kg m^{-3})***	***Grinds used***
	1	1337.0 ± 2.3	Ψ_A; $d_{[4,3]}$ = 95.9 μm
	2	1337.0 ± 6.9	Flaked coffee, as received
3	*9.0 La*	1348.0 ± 1.1	$d_{[4,3]}$ = 106 μm
	5.5 La	1340.0 ± 1.1	$d_{[4,3]}$ = 135 μm

The total particle porosity ($\varepsilon_{particle}$) was calculated as the sum of the closed (ε_{closed}), and the open (ε_{open}) porosity of the grinds. ε_{closed} was defined as the volume percentage of closed pores in a given grind. The specific volume of closed pores was assumed to be the difference between the specific volume of the grind being assessed and the solid volume, estimated as previously described in this Section. These volumes were measured via helium pycnometry. ε_{open} was defined as the volume percentage of open pores in a given grind. The volume of open pores was assumed to be the total volume of intruded mercury in the pores of the particles, and its value was taken from the cumulative mercury porosimetry curves; Figure 4.13 shows typical examples of these curves. Note that the volume of mercury filling the inter-particle space (penetrometer) was subtracted from the intruded volume of mercury; the exact details of the methodology are given in Section 3.3.6. It can be seen that the cumulative volume of intruded mercury increases at pore sizes of 30000-10000 *nm* (30-10 μm); it remains virtually flat in the range of 10000 to 30 *nm*, and increases again at 30-10 *nm*. The later increment is more pronounced for coarser grinds (see, for example, Ψ_H). This points out the size scale of the pores present in RGC particles, and will be more clearly seen and discussed in Section 4.3.2 with the aid of the differential mercury intrusion curves.

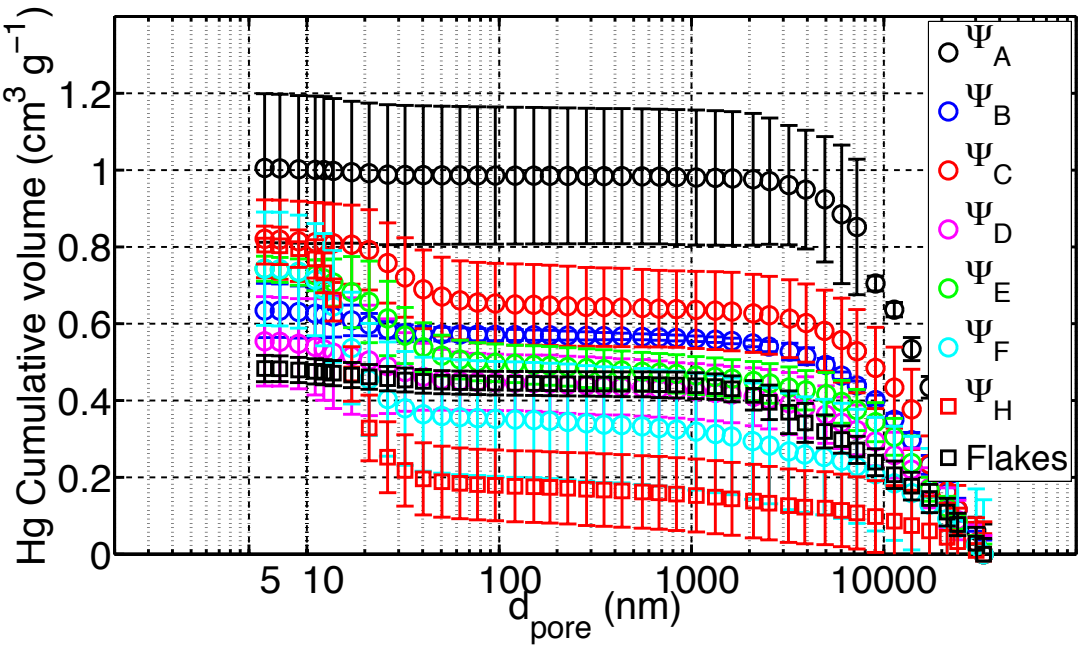

Figure 4.13: Cumulative intruded volume of Hg in the particle pore space (*y*-axis) vs. pore diameter of the intruded pores (*x*-axis)

Figure 4.14 shows the estimated open, closed, and total porosity of the grinds produced from Blend 1 (Ψ_A – Ψ_H), where the *y*-axis represent the porosity, and the *x*-axis the $d_{[4,3]}$ of the particle size distribution as *dry* measured. It is observed that open porosity increases (ε_{open} → 0.37 to 0.57), and closed porosity decreases (ε_{closed} → 0.28 to 0), when beans are more finely ground ($d_{[4,3]}$ of the particle size distributions decreases). Finer grinds result in greater surface-to-volume ratios. Therefore a greater proportion of the total cell pockets are broken and exposed on the surface of the particles, and thus are not (potentially) isolated within the particle microstructure contributing to the closed porosity. However, the apparent decreasing tendency of total porosity ($\varepsilon_{particle}$ → 0.65 to 0.50) for the finer grinds suggests that grinding the coffee beans to a size scale comparable to that of the cell pockets may break some of them until these cell pockets eventually disappear.

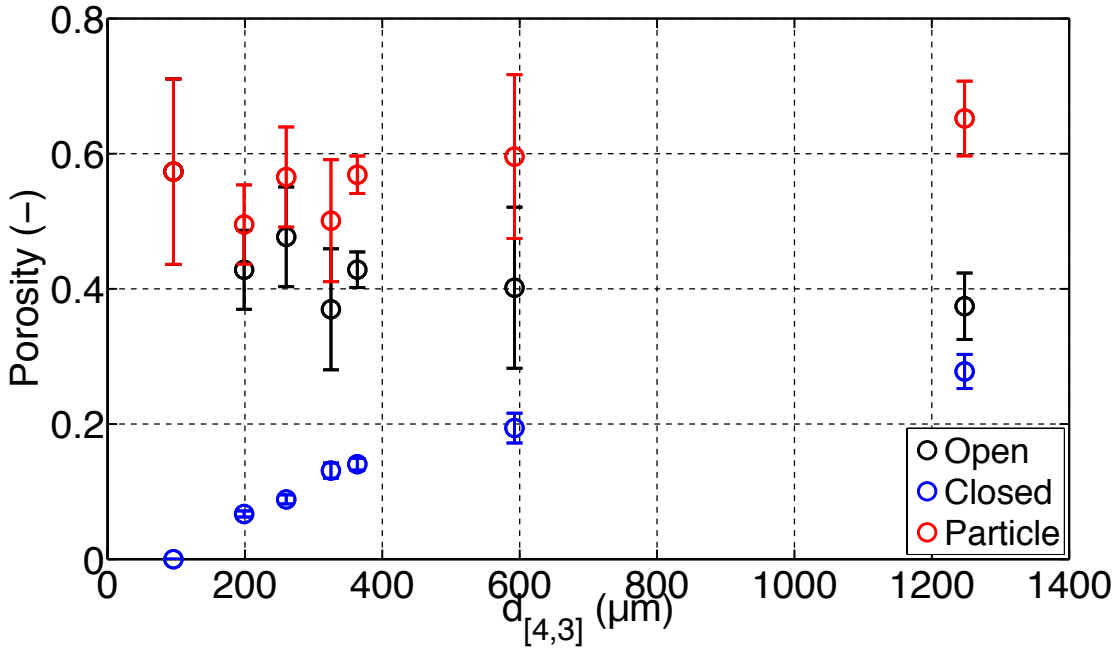

Figure 4.14: Open, closed and total porosity (y-axis) vs. the $d_{[4,3]}$ *dry* measured (x-axis) of the grinds from Blend 1 (Ψ_A – Ψ_H)

The open, closed, and total porosity evaluated for flaked coffee, and Blend 3 at the two different roasting colours are shown in Table 4.6. A sample of Blend 1 with a similar $d_{[4,3]}$ to the ones evaluated here is also included for comparison purposes.

Table 4.6: Particle porosity values (ε) of the coffee blends considered in the study

Blend		ε_{open}	ε_{closed}	$\varepsilon_{particle}$
1 (Ψ_E)		0.43 ± 0.03	0.14 ± 0.01	0.57 ± 0.03
Flaked coffee (Blend 2)		0.39 ± 0.06	0	0.39 ± 0.06
[1]3	9.0 La	0.35	0.14	0.49
	5.5 La	0.39	0.17	0.56

[1]:ε_{open} was estimated from a single mercury porosimetry measurement

Flaked coffee showed a lower value of porosity when compared to regular roast and ground coffee (Blends 1 and 3). As seen in Figure 4.4, most part of the cell pockets (main contributors by volume to the total porosity of coffee) originally present on the surface of the regular RGC cannot be distinguished in flaked coffee. They may have been destroyed as particles are flattened by the effect of the rotating rollers through which

the pre-ground coffee passes. This value compares well to porosity values obtained for flakes made from other vegetable materials previously reported in the literature (del Valle et al., 2006; Uquiche et al., 2005).

Roasting to darker colours (from 9.0 to 5.0 *La*) appears to increase the total porosity of the particles. As with the previous observation for ρ_{solid}, this can be explained as the effect of more material reacting into gaseous products due to the more intense thermal processes applied. The effect of roasting colour on the porosity of the particles might be another reason as to why flaked coffee, which was produced from the blend with the lightest roasting colour (Blend 2; roasting colour = 10.0 *La*), showed lower values of porosity. Another observation of the effect of the thermal processes applied to the beans on bean porosity development was reported by Schenker et al. (2000): roasting coffee beans to the same colour but using different roasting profiles, i.e. high temperature-short time or low temperature-long time, resulted in higher values of bean porosity (0.53 vs. 0.47, as measured with mercury porosimetry) for the high temperature process.

Finally, the decaffeination process seems to have no effect on particle porosity, as the reported values for Blend 1 and Blend 3 are comparable. However, this could specifically depend on the applied decaffeination process, and more in-depth experimentation would be required to reach more solid conclusions.

4.3.2. Pore size distribution

The pore size distribution of the particles was obtained from the mercury porosimetry experiments. Figure 4.15 shows the differential pore size distribution for the grinds produced from Blend 1 (Ψ_A-Ψ_H), and flaked coffee. The *y*-axis represents the

volume of mercury intruded in the population of pores of the size represented in the *x*-axis. As anticipated in Section 4.3.1, here it can be more clearly seen that all the investigated grinds showed a bimodal pore size distribution with pores around 10-30 *nm* (1), and 5000-40000 *nm* (5-40 *μm*) (2). The former may correspond to the cell wall pores, and plasmodesmata conduits that typically connect one vegetable cell to another (Aguilera and Stanley, 1990), whereas the later may correspond to the cell pockets themselves. These observations are in good agreement with Schenker et al. (2000), who reported similar cell pockets sizes, and overall mean pore sizes between 11 and 13 *nm*. It must be noted, however, that according to the Washburn equation (Eq. 3.6), the minimum pore size that can be determined by mercury porosimetry depends on the maximum pressure that the equipment can achieve. In this respect, pore sizes much smaller (between 0.35 and 0.50 nm) than those observed here have been estimated for other plant tissues by techniques such as solute exclusion (Carpita et al., 1979).

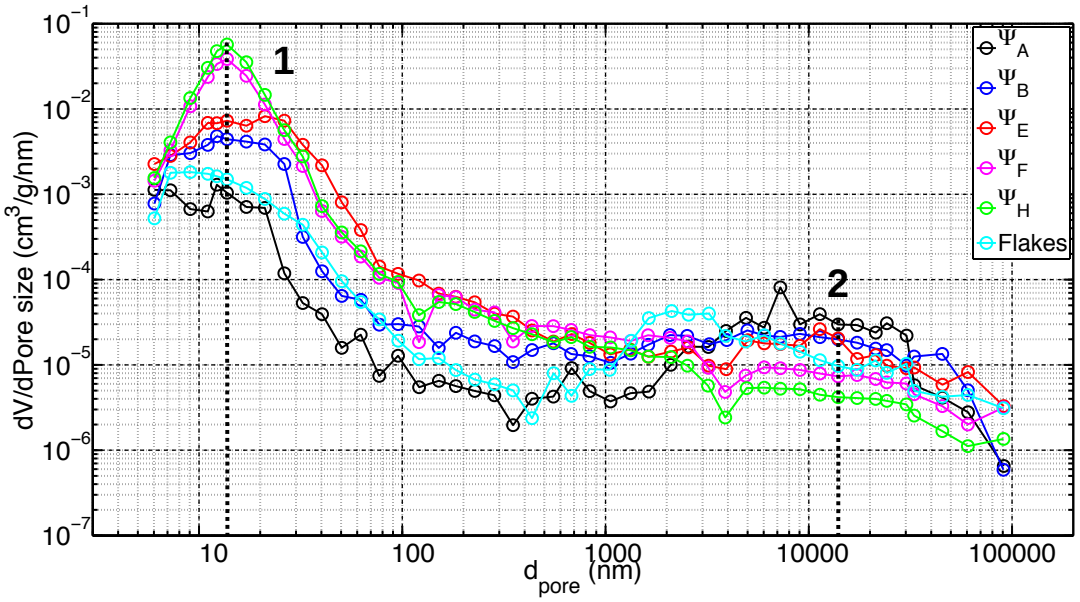

Figure 4.15: Differential mercury porosimetry intrusion. The *y*-axis represents the intruded amount of mercury in each pore size represented in the *x*-axis. The results are the average of the measurement of three independent samples (for clarity, error bars are not shown; average relative standard deviation: Ψ_A = 103 %; Ψ_B = 67 %; Ψ_E = 43 %; Ψ_F = 20 %; Ψ_H = 16 %; *Flakes* = 53 %). Ψ_C, Ψ_D and Ψ_G were not assessed

Due to the great difference in size between the two identified populations of pores (3 orders of magnitude), the pore volume distribution would be expected to be dominated by the bigger pores (5-40 μm). However, as observed in Figure 4.15, the biggest peak occurs in the nano-pore region (10-30 *nm*). This effect can be attributed to the ink-bottle microstructure of RGC (Schenker et al., 2000): some of the smaller pores are shielding larger pores, which can be only filled with mercury when enough pressure to fill the surrounding smaller pores is reached. In such a case, the volume of these larger pores would be accounted for in the pore size distribution as having the same size as the shielding pores, this is, the volume of the larger pores would be underestimated. Another indication of this effect may be the fact that, as observed Figure 4.15, when the original microstructure of the bean is substantially modified, by either grinding (from Ψ_H to Ψ_A), or flaking (flakes), the nano-pore peak (1) decreases, whereas peak (2) increases. This suggests that part of these ink-bottle connections are broken, and a

greater part of the cell pockets become unshielded, and accessible at or from the surface of the particles; this is consistent with the observed increase in open porosity for the finer grinds (Section 4.3.1). It can be also appreciated that the flaked coffee, in spite of showing a similar particle size distribution to Ψ_E (Section 4.2.1), presents a pore size distribution that is closer to that of the finest grind (Ψ_A).

As shown in Section 4.3.1, the effect of the roasting colour on the pore size distribution of the particles was tested with the two samples of Blend 3. Figure 4.16 displays the differential pore size distribution for both samples. It can be seen that the peak in the nanopores region occurs at approximately 20 *nm* for the medium roast (9.0 *La*), and at 30 *nm* for the very dark roast (5.0 *La*). Therefore, roasting to darker colours seems to increase both the total porosity of the particles, and also the size of the pores.

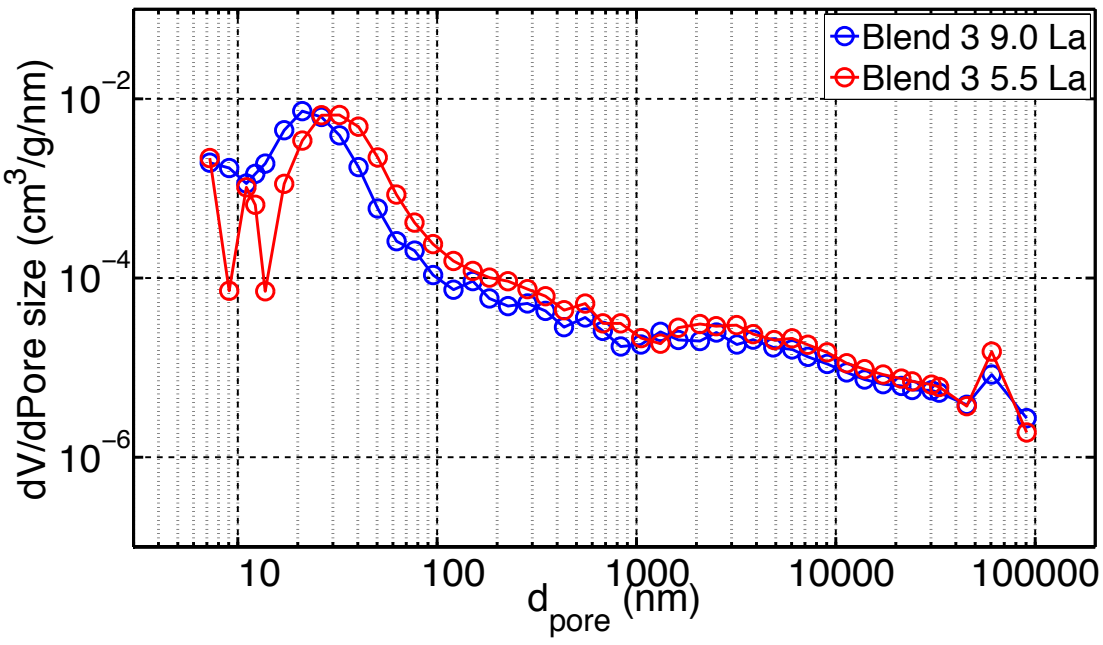

Figure 4.16: Differential mercury porosimetry intrusion for Blend 3 with a medium (9.0 *La*) or a very dark roast (5.5 *La*)

4.3.3. Particle tortuosity

The tortuosity of the particles was estimated with the expression derived by Salmas and Androutsopoulos (2001) using the 'Corrugated Pore Structure Model' (CPSM), which relates the entrapped mercury within the particles after the intrusion-extrusion cycles to the tortuosity of the particle. A more detailed description of the model was shown in Section 2.3.1. The procedure to estimate the entrapped amount of mercury after the intrusion-extrusion cycles was detailed in Section 3.3.6.

Figure 4.17 shows the intrusion-extrusion curves for Ψ_B and Ψ_H. It can be seen that the hysteresis effect in the intrusion-extrusion curves is more pronounced in the coarser, i.e. less intensively ground, grind (Ψ_H). Less intense grinding steps allows the coffee to maintain a greater percentage of its original ink-bottle microstructure, which is thought to cause the observed hysteresis between the intrusion-extrusion cycles.

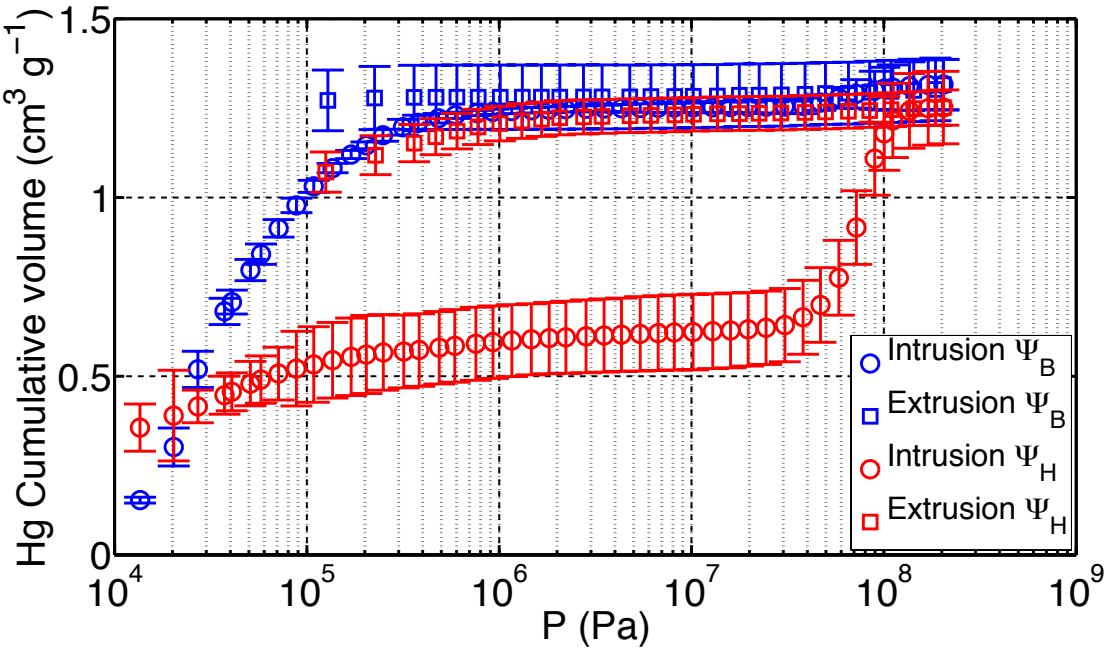

Figure 4.17: Hysteresis between the intrusion (○) and the extrusion (□) cycles for Ψ_B and Ψ_H

Figure 4.18 shows the estimated tortuosity values (according to CPSM) for Ψ_A-Ψ_H. It can be seen that tortuosity increases with $d_{[4,3]}$, which is consistent with the observation of the increasing complexity of the microstructure based on the pore size distribution measurements (Figure 4.15). These tortuosity values are likely to represent an average value of the whole coffee microstructure. On the one hand, the tortuosity experienced by a molecule located in the cell pockets at the surface of the particles (Figure 4.4a) may be close to 1, as these cell pockets are at least 2-3 orders of magnitude bigger than the diffusing molecules, which were estimated in Section 3.3.8 to be between 1-189 *nm*. On the other hand, it is likely that a molecule located at the centre of the particle, and that has to diffuse through various throats of the ink-bottle microstructure before reaching the bulk solution, experiences a higher tortuosity effects than those represented by the estimates in Figure 4.18.

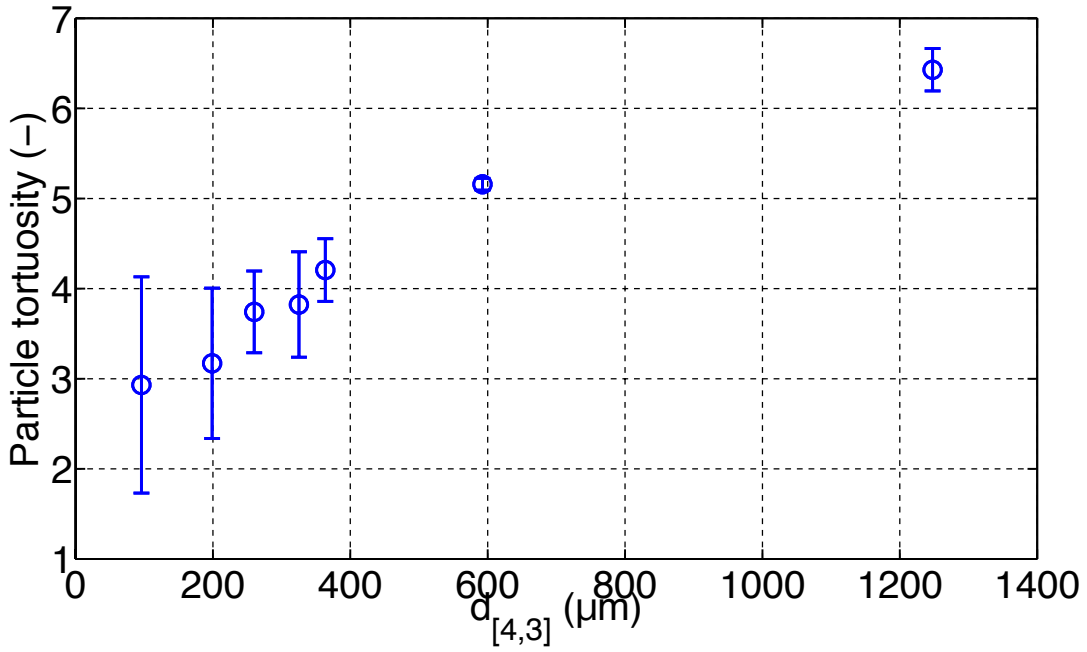

Figure 4.18: Estimated particle tortuosity (according to the CPSM) (y-axis) vs. the $d_{[4,3]}$ *dry* measured (x-axis) of the grinds produced from Blend 1 (Ψ_A – Ψ_H)

The particle tortuosity estimated for flaked coffee, and Blend 3 at the two different roasting colours are shown in Table 4.7. A sample of Blend 1 with a similar $d_{[4,3]}$ to the ones evaluated here is also included for comparison purposes. Despite the apparently much simpler microstructure of flaked coffee as compared to Ψ_E (Figure 4.15), it can be seen that they present similar tortuosity values. It is also true that the estimated value for flaked coffee is not far from the values estimated for the finest grinds, i.e. $\tau_{particle\ CPSM}$ = 2.9 ± 1.2 for Ψ_A, and 3.2 ± 0.8 for Ψ_B, to which flaked internal structure resembles more.

On the other hand, the estimated values for the decaffeinated coffee (Blend 3) are similar for both roasting colours. However, they are higher than the values estimated for regular RGC with a similar particle size distribution, i.e. $\tau_{\ particle\ CPSM}$ = 4.2 ± 0.4 for Ψ_E and 5.2 ± 0.8 Ψ_F. In principle, and based on the solid density, porosity, and pore size distribution results previously presented in Sections 4.3.1 and 4.3.2, there is no apparent reason to believe that the decaffeination process using supercritical CO_2 can induce this effect. However, to determine whether this is a consequence of the decaffeination process, or an intrinsic characteristic of the beans forming the blend (which are different to Blend 1), further controlled experiments should be carried out.

Table 4.7: Particle tortuosity values of the coffee blends considered in this study

Blend		$\tau_{particle\ CPSM}$
1 (Ψ_E)		4.2 ± 0.4
Flaked coffee (Blend 2)		4.0 ± 0.3
3[1]	*9.0 La*	6.7
	5.5 La	6.9

[1] $\tau_{particle\ CPSM}$ was estimated from a single mercury porosimetry measurement

Generally, the tortuosity estimates obtained with the CPSM are in good agreement with the tortuosity values (between 2 and 6) typically reported for porous

particles (E.L. Cussler, 2009b). For other vegetable materials, tortuosity values using mercury hysteresis data and the CPSM were found to be considerably higher ($\tau_{particle}$ = 7.3-15.5) than those reported here (del Valle et al., 2006). The same researchers, using a fractal-texture approach, derived values of tortuosity for the same vegetable substrates between 1.6-2.0. These seem somewhat lower than the aforementioned average values for porous particles. It should be taken into consideration that the CPSM was parameterised with catalyst particles, whose microstructure may be more homogenous than that of coffee particles.

4.3.4. Conclusions of microstructure analysis

The results from the microstructure analysis of the grinds produced from Blend 1 (Ψ_A- Ψ_H), flaked coffee (Blend 2), and decaffeinated coffee roasted to different colours (Blend 3), have been presented in Sections 4.3.1, 4.3.2, and 4.3.3, and the following conclusions can be extracted from them.

Comparable values of solid density were found for all the blends with a similar roasting colour. For Blend 3, when roasted to a notably darker colour, the solid density seemed to slightly decrease. Total porosity of the particles increased for the coarser grinds. However, it was also found that for this grind a greater percentage of the total pores can be considered to be closed, i.e. isolated within the structure, and not penetrable by helium. The porosity estimate for flaked coffee resulted in a relatively low value (compared to RGC), but comparable to porosity values reported for flakes made of other vegetable substrates in the literature. This was attributed to the fact that the intense compression to which pre-ground coffee was subjected to create the flakes destroyed a great part of the cell pockets, which are the main contributors (by volume)

to the porosity of the particle. For Blend 3, although repeated measurements would be required, it was inferred that darker roasting colours (i.e. more intense thermal processing) resulted in higher total porosity values.

Pore size distribution of the particles showed two pore populations, namely 10-30 *nm* and 5-40 *μm*. The ink-bottle microstructure reported in the literature was also identified here. Its effect was shown to decrease when more intense comminution process were applied (grinding or flaking): for finer grinds, and flaked coffee, the value of the peak representing the nanopores population decreased, which was attributed to the decrease of the shielding effect.

Estimates of the particle tortuosity were obtained from the entrapped mercury fraction after intrusion-extrusion cycles, and the expression derived from the Corrugated Pore Structure Model. It was found that the estimated tortuosity increased for coarser grinds, which was consistent with the observed increase of the shielding effect for coarser grinds. For Blend 3, no apparent dependency of the estimated tortuosity with roasting colour was found. However, these values resulted being higher than the estimated values for Blend 1 (regular non-decaffeinated RGC). There is in principle no evidence to attribute this higher tortuosity values to an effect of the decaffeination process in the coffee bean structure, since the rest of the measured microstructural parameters are comparable to those of Blend 1. However, further experiments and analysis with decaffeinated coffee beans and grinds would be required to reach a clearer conclusion.

4.4. Extraction parameters

4.4.1. Initial concentration of extractable soluble solids

Values of the long time limit extraction yield ($y_0\ (\Psi_j)$) were measured at 80 $°C$ in a dilute solution of 10 $kg\ m^{-3}$ (in practice 2 g of RGC in 200 ml of water). Extraction times were 2 hours for Ψ_A, Ψ_B and Ψ_E; 4 hours for Ψ_F and Ψ_G; and 6 hours for Ψ_H. The kinetics experiments presented in Chapter 5 will show that these times are well beyond the equilibrium times of the grinds.

Figure 4.19 shows the measured long time limit extraction yields normalised by the yield of the finest grind ($y_0\ (\Psi_A)$), which was found to be the maximum amongst the assessed grinds. For a given coffee bean roasted to a certain colour, the mass of soluble species per unit mass of roast and ground coffee is independent of the particle size distribution of the grind. However, it can be observed that the long time limit extraction yield decreases for coarser grinds. Similar effects are implicit in data reported in other studies investigating coffee extraction: increasing particle size not only slowed the kinetics of extraction, but also reduced the final extraction yield after equilibrium had been reached (Nicoli et al., 1990; Voilley and Simatos, 1979; Zanoni et al., 1992). This observation suggests that some soluble species can be entrapped within the particle microstructure, and that this effect increases with particle size distribution. $y_0\ (\Psi_A)$ was found to be 31.7 ± 0.4 kg of soluble solids per 100 kg of RGC. This figure was found to be 1 % smaller than the value derived from fitting equilibrium experiments performed to derive the solid-liquid partition coefficient (see Section 4.4.6). This can be interpreted as the percentage of the total soluble solids that remain inside the grind at equilibrium in a dilute solution of 10 $kg\ m^{-3}$. Therefore the values shown in Figure 4.19 were corrected

accordingly when they were used to estimate the initial concentration of *extractable* soluble solids in the grinds (see Section 4.4.1). By *extractable* it is implied here that, although the initial amount of soluble species is the same in all the grinds regardless of their particle size distribution, only a fraction of the species is available for extraction as a consequence of the observed entrapment effect (Figure 4.19).

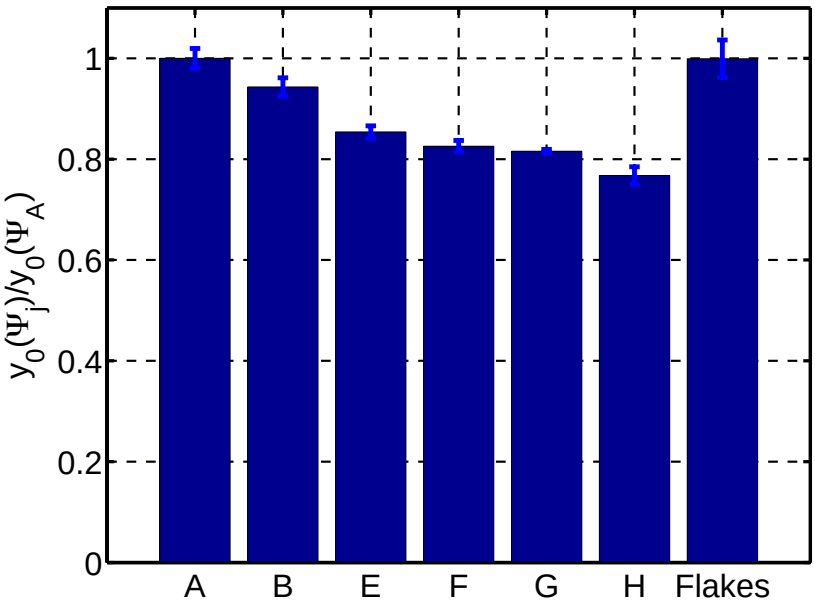

Figure 4.19: Normalised long time limit extraction yield (*y*-axis) for the considered grinds from Blend 1 and flaked coffee

Although Blend 2 and Blend 1 differ in the specific origin and roasting colour, it can be observed that flaked coffee (Blend 2) shows values of the long time limit extraction yield that are comparable to that of the finest grind (Ψ_A) of Blend 1. The long time limit extraction yield of the flaked coffee is therefore greater than that of Ψ_E, despite the comparable particle size distribution (as *dry* measured by laser diffraction) of both grinds. This reinforces the statement made from the observation of SEM pictures of flaked coffee (see Section 4.2.3): despite the apparent coarser particle size distribution measured for the flaked coffee, its behaviour in terms of extractability, and

(potentially) kinetics of extraction is determined by the thickness of the flakes, which was shown to be between 100-150 μm, and is comparable to the radius of the finer grinds Ψ_A – Ψ_B, estimated as $d_{[4,3]}/2$.

4.4.2. Relating microstructure and soluble solids entrapment

The observed entrapment effect in Figure 4.19 is expected to occur due to molecular size exclusion. The estimates of molecular sizes previously carried out in Section 3.3.8 showed that coffee soluble solids are formed by some species up to an order of magnitude bigger (from 1 to 189 *nm*) than some of the observed nanopores (10-30 *nm*, and possibly smaller) through which these species would have to diffuse in order to be extracted from within the particles to the bulk solution. As a matter of fact, in dry RGC, i.e. before extraction, it was shown (in Section 4.3.1) that some pore throats could be of such a small size scale that they may even block the penetration of small molecules like helium. Thus, the volume shielded by such pores was considered as closed porosity.

In order to relate the observed entrapment effect with the microstructure of the grinds, a percentage of entrapped material was defined. This was correlated to the value of the nano-pore peak in Figure 4.15, chosen as a relevant parameter that comparatively reflects the complexity of the microstructure of the different grinds. Mateus and Rouvet, (2007) reported that after wetting, the coffee closed porosity decreased to values near zero, and they attributed this to water plasticising effects on the coffee matrix. Although the nanopores values were measured in dry grinds, it can be assumed that the complexity of the microstructure of the wet grinds is going to be proportional to the original complexity in the dry state. As shown in Figure 4.20 the percentage of

entrapped material (*y*-axis) seems to increase exponentially with the value of the nano-pore peak (*x*-axis). An exponential equation ($\%entrapped = 0.2\ (1\text{-}e^{(-81.8 \times nano\text{-}pore\ peak)})$; $R^2 = 0.9$) was fitted to the data. This links the observed entrapment phenomenon with the microstructural characteristics of the distributions.

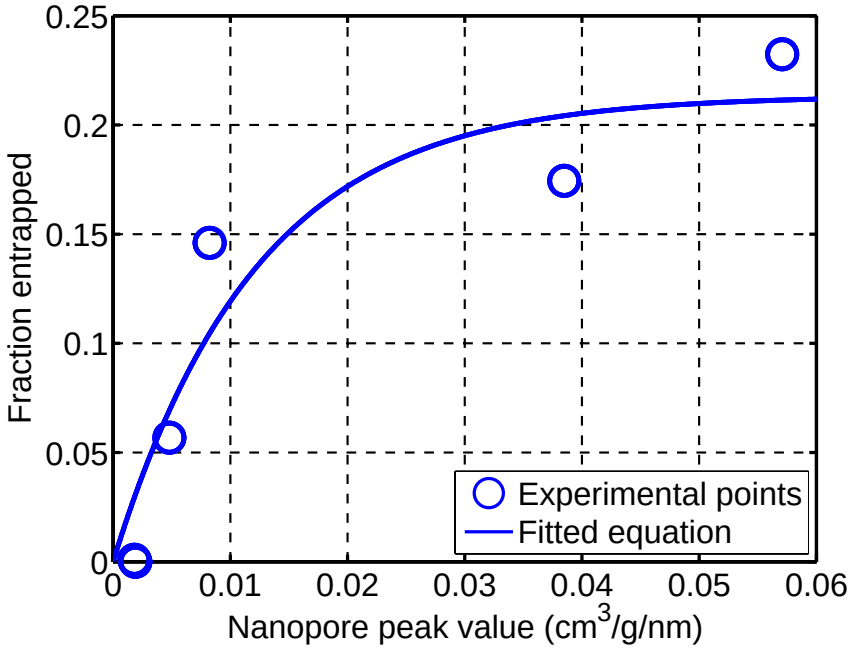

Figure 4.20: % of material entrapped with the particles (*y*-axis) vs. the measured value of the nano-pore peak in differential mercury intrusion experiments (Figure 4.15)

An interesting possibility would be to further investigate the chemical nature of the entrapped compounds in each grind, and the potential impact of the different chemical compositions on flavour. On the one hand, it has been reported that some large polymers (MW > 2000) are more likely to be entrapped within coffee particles (Schwartzberg and Chao, 1982). On the other hand, caffeine, with a molecular weight (MW) of 194.2 $g\ mol^{-1}$, and an estimated hydraulic radius (via the Stokes-Einstein equation) of 0.4 *nm*, can be almost fully extracted from whole green beans (that may present even a more restrictive, less porous microstructure than roast coffee) without the need of a previous grinding step (Heilmann, 2001).

The Dynamic Light Scattering (DLS) results presented in Section 3.3.8, showed that the modal size of the species detected from extracts obtained from grind Ψ_B was approximately 11 % bigger than the molecular size detected for the largest grind (Ψ_H). This can be explained due to the fact that, since finer grinds show a greater surface-to-volume ratio, a greater proportion of the species that suffer the molecular size exclusion inside the particles are located at the cell pockets of the surface where no restriction to mass transfer occurs.

4.4.3. Water-roast and ground coffee contact angle

The water-roast and ground coffee contact angle measurement was commissioned at the Department of Chemical Engineering of Imperial College (London, UK), and the results are reproduced here. The contact angle was estimated with the sessile drop method by circle fitting water droplets deposited on coffee packed beds. Grinds Ψ_B and Ψ_E were arbitrarily chosen to carry out the measurement. The measurement was conducted at 75 $°C$ and room temperature (not specified), and five repetitions were performed.

The water-roast and ground coffee contact angle was proven to be difficult to measure at 75 $°C$, since water wicked into the packed bed in a matter of a few seconds. Figure 4.21 shows results of measurements attempts.

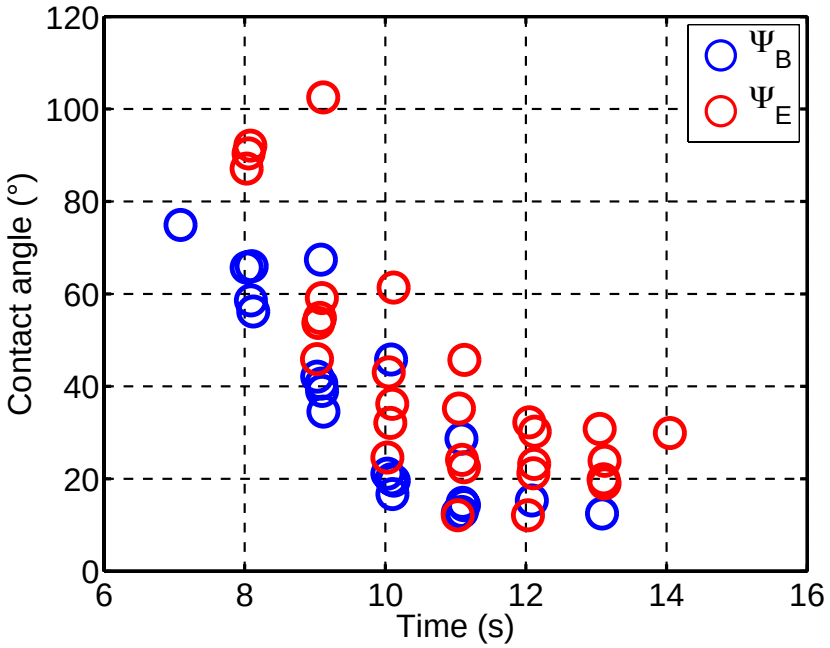

Figure 4.21: Water-roast and ground coffee contact angle (y-axis) over time (x-axis) at 75 $℃$ for Ψ_B and Ψ_E

At room temperature, Figure 4.24 shows that that contact angle decreases in a much wider time scale, as it takes longer for the water drop to penetrate into the bed as compared to 75 $℃$.

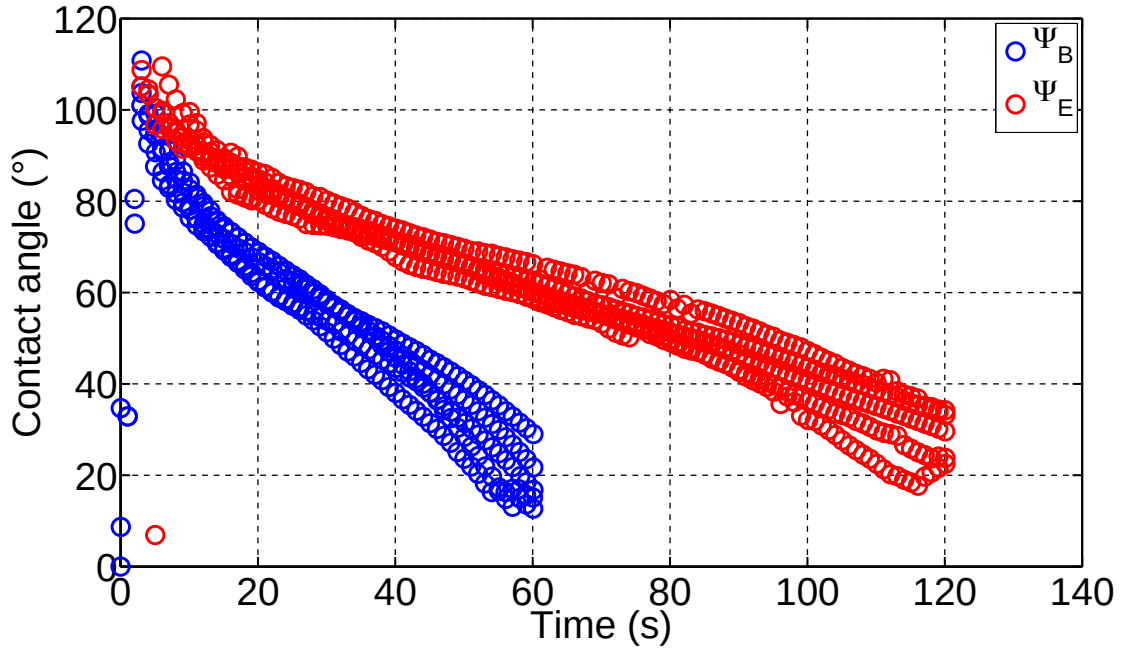

Figure 4.22: Water-roast and ground contact angle (y-axis) over time (x-axis) at room temperature for Ψ_B and Ψ_E

The penetration rate depends on the average pore size from the beds, whose values can be estimated with as follows (Hapgood et al., 2002):

$$R_{pore} = \frac{\phi d_{[3,2]} \varepsilon_{bed}}{3\left(1-\varepsilon_{bed}\right)} \qquad \text{Eq. 4.1}$$

Where Φ is the sphericity of the particles (-), $d_{[3,2]}$ is the volume-to-surface diameter (m), and ε_{bed} is the porosity of the bed (-). According to the estimates of ε_{bed} obtained in Chapter 4 using the particle microstructural information, R_{pore} for Ψ_B and Ψ_E resulted in 17.0 μm and 47.2 μm respectively. The required time for the water to penetrate a certain distance can be estimated from the short-time approximation solution for the Lucas-Washburn equation (Aguilera et al., 2004) as follows:

$$h = \sqrt{\frac{R_{pore}\gamma\cos\theta}{2\mu}t} \qquad \text{Eq. 4.2}$$

Where h is the distance penetrated by the water (m) in the time t (s), γ is the water surface tension ($N\ m^{-1}$), μ is the water viscosity ($Pa\ s$), and θ is the contact angle (°) between the water and the porous solid. Despite the fact that the required time for the water to penetrate a certain distance is inversely proportional to R_{pore}, one can see in Figure 4.22 that water seems to penetrate faster in Ψ_B. In Section 4.3.2 it was demonstrated that coffee particles possess pores with diameters in the scale of 20-40 μm and 10-30 nm. An estimate of the time required for the water to fully penetrate into the nanopores of the finest (Ψ_B) and coarsest grinds (Ψ_H) at 80 $°C$ can be obtained from Eq. 4.2 using the following parameters: R_{pore} = 10 nm; h = 236 and 3007 μm (effectively calculated from $d_{[4,3]}/2$ as *dry* measured; it was taken into account the estimated sphericity of 0.75 and the estimated tortuosity of 3.2 and 6.4 for Ψ_B and Ψ_H, respectively); representative contact-angle, θ = 50 ° (Figure 4.22); $\gamma = 6.26\times10^{-2}\ N\ m^{-1}$; $\mu = 3.57\times10^{-4}\ Pa\ s$. These times were 0.01 seconds for Ψ_B and 15.9 seconds for Ψ_H. These are upper-scale limits, since it has been assumed that all the pores of the particles are nanopores. According to this, it may be concluded that water penetration into the particles seems to occur in a much faster time scale than the extraction of the soluble solids, which will be shown in Chapter 5 to be the in the scale of several minutes.

4.4.4. Absorbed water

The volume of absorbed water per unit mass of RGC was measured in Ψ_A, Ψ_B, and Ψ_H at 80 $°C$. Water content for Ψ_A was required as it was the grind used to estimated the solid-liquid partition coefficient (Section 4.4.6). The water content of six different

samples was analysed after long-time extraction during, i.e. for 2 hours was found to be (1.3 ± 0.1) ×10^{-3} m^3 kg^{-1}.

For Ψ_B and $\Psi_{H,}$ the measurement was carried out in three different samples. Figure 4.23 shows that the water content for Ψ_B after 4 and 20 minutes is comparable, and was found to be around 1.4×10^{-3} m^3 kg^{-1}. For this same grind, the water content after 4 minutes was also measured at 20 °C, and 50 °C, and was comparable to the water content at 80 °C ((1.4 ± 0.2 ×10^{-3} m^3 kg^{-1}, and (1.5 ± 0.2) ×10^{-3} m^3 kg^{-1}, respectively). For Ψ_H, due to its size scale, another measurement at 120 minutes was carried out. It can be seen that the absorbed water increased from 3 to 20 minutes approximately by 32 %, and did not seem to increase after 120 minutes. Nevertheless, after 3 minutes, 80 % of the final water content (at 120 minutes) had already penetrated into the particles. The final water absorbed by Ψ_H was (1.7 ± 0.3) ×10^{-3} m^3 kg^{-1}.

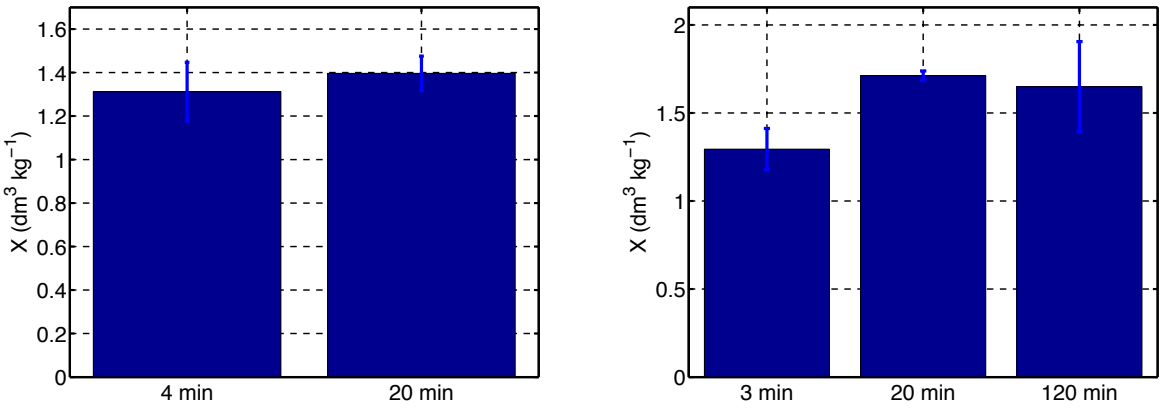

Figure 4.23: Absorbed water per unit mass of RGC (*y*-axis) over time (*x*-axis); (a) Ψ_B; (b) Ψ_H

On the one hand, the observed increment for Ψ_H is probably due to the fact that between 3 and 20 minutes, the extraction yield also increased by 24 %. It is likely that removing soluble solids increases the porosity of the particles, allowing them to hold more water. On the other hand, the swelling effect of the particles may be another

possible reason to explain the observed increment. Mateus and Rouvet, (2007) reported that, for particle sizes comparable to Ψ_H, the volume of coffee particles (as measured by laser diffraction) increased between 20-23 % after immersion in water. Spiro et al., (1989), based on microscopy observations of similar particles sizes to that of Ψ_H, reported that diameter increased by 17 % after several minutes, which means approximately a 60 % increase in volume; this is equivalent to a swelling factor (swollen volume/original volume) of 1.6. However, these observations do not agree with the findings displayed in Section 4.2.1, where it was shown that the $d_{[4,3]}$ of finer distributions than Ψ_H, either did not increase or increased its volume only by a factor of 1.04 (12 % in volume) when they were measured after having been extracted for 1,10 and 30 minutes.

In addition to the estimation based on the measurement of the particle size distribution of the extracted grinds (Section 4.2.1), the swelling factor can be also estimated from a balance to the volume of water absorbed as follows:

$$\frac{V_{aq}(m)}{m} = \left(\varepsilon_{particle} + y\left(\Psi_j\right)\left(1-\varepsilon_{particle}\right)\frac{\rho_{solid}}{\rho_{ss}} \right)\frac{V_{distribution}}{m} + \left(S-1\right)\frac{V_{distribution}}{m} \qquad \text{Eq. 4.3}$$

Where S is the swelling factor (-), V_{aq} is the absorbed volume of water (m^3) in a given mass of coffee m (kg), $\varepsilon_{particle}$ is the porosity of the grind *(-),* $y(\Psi_j)$ is the extraction yield (-), ρ_{solid} is the solid density ($kg\ m^{-3}$), ρ_{ss} is the density of the extracted soluble solids ($kg\ m^{-3}$) (assumed here to be equal to ρ_{solid}), and is the $V_{distribution}$ the volume of the grind (m^3). The term $V_{distribution}/m$ is the density of the grind, that can be expressed as $\rho_{solid}(1-\varepsilon_{particle})$. From the measured absorbed volume of water per mass of coffee for Ψ_A (previously reported in this Section), Ψ_B and Ψ_H (Figure 4.23) measured porosity of the

grinds, measured solid density, and extraction yields (0.30 for Ψ_A, 0.28 for Ψ_B, and 0.22 for Ψ_H) (Chapter 4), the swelling factor can be estimated. This resulted in S = 0.98 for Ψ_A, 1.3 for Ψ_B, and 1.05 for Ψ_H. As expected, the results for Ψ_A and Ψ_H indicate that the particles do not swell. However, for Ψ_B the particles would swell by 30 %. This does not agree with the particle size distribution measurements for extracted grinds shown in Section 4.2.1, which indicate that the $d_{[4,3]}$ of this grind does not change upon extraction. Regarding this, it must be noted that these estimates of the swelling factor are sensitive to the measurement of the absorbed water, and that could be the cause of disagreement.

To conclude, the observations reported in this Section confirm that RGC is a hydrophilic material and water penetration into the particles occurs at a faster rate in comparison to the extraction of soluble solids. Further measurements (and probably alternative methodologies to direct visual observation and laser diffraction) would be required to fully elucidate the potential swelling phenomena of the coffee polymeric matrix.

4.4.5. Hindrance factor and effective diffusion coefficient

The hindrance factor (H) is defined as the ratio between the diffusion coefficient of a given species in the bulk of a solution (D_b), and inside the porous coffee particles (D_{eff}). It is a dimensionless coefficient (typically derived from experimental extraction data) that encompasses all the restrictions imposed to diffusion by the coffee porous microstructure, i.e. surface of the pores, and their tortuous path, as well as the other described phenomena (see Section 2.3) that are involved in solid-liquid extraction (such as solvent penetration into the solid, and dissolution of molecules attached to the solid matrix). The microstructural contribution to the hindrance factor (H_m) was estimated

here as the ratio of the tortuosity ($\tau_{particle\ CPSM}$, Figure 4.18), and particle porosity (ε_{total}, Figure 4.14). The total values of particle porosity were considered (rather than the open porosity values) since, as explained in Section 4.4.2, closed porosity seems to decrease to values near zero when water penetrates into the particle, and according to the contact angle measurements shown in Section 4.4.3, this appears to occur in a very short time scales. Figure 4.24 shows that the microstructural contribution to the hindrance factor was found to be between 5 and 10, and it increases for coarser grinds. This result was expected based on previous observations in Figure 4.18 of tortuosity increasing for coarser grinds.

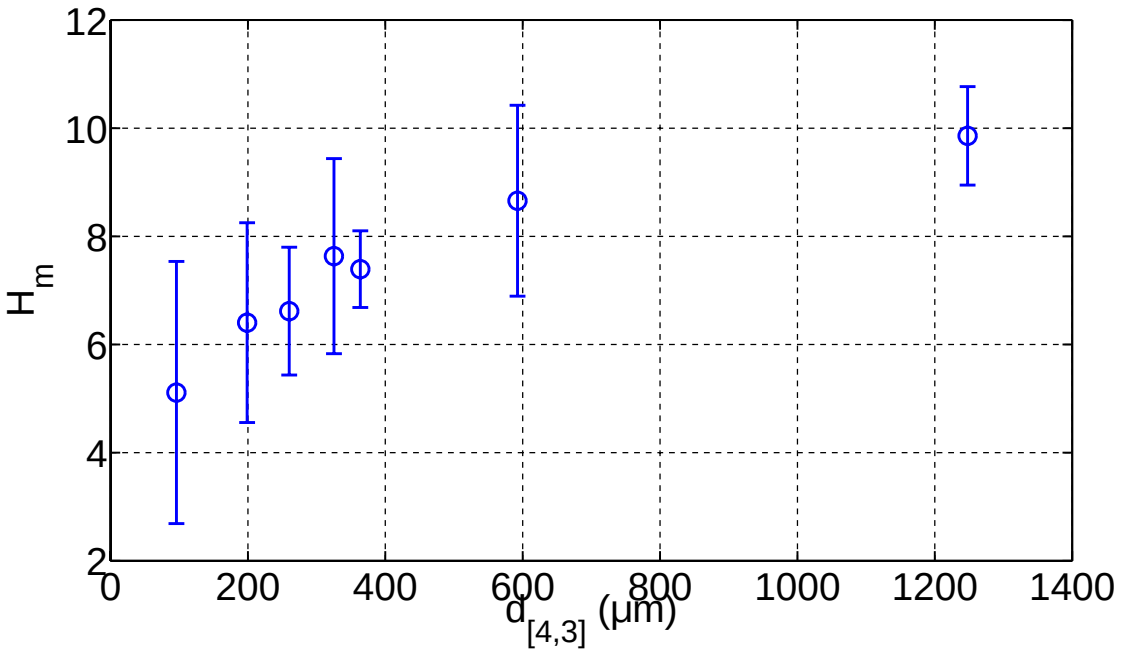

Figure 4.24: Microstructural contribution to the hindrance factor (y-axis) vs. $d_{[4,3]}$ of the particle size distributions as *dry* measured (x-axis)

Spiro et al., (1989) derived hindrance factors for caffeine by comparing the experimentally estimated D_{eff} from extraction experiments with D_b at the same temperature. At 80 $°C$, and for particles in the range of 850-1180 μm, they reported hindrance factors of approximately 10. In an attempt to unveil the contribution of each

of the aforementioned solid-liquid steps in the estimated values of the hindrance factor, they carried out extraction experiments with pre-wetted particles (conserving all the soluble solids, or conserving only the caffeine), and concluded that the combination of caffeine association to other molecules, swelling of the particles, a finite caffeine dissolution rate from the coffee matrix into the pore space of the particle, and retardation due to a counterflow of water as it penetrated into the particles, slowed down caffeine diffusion by a factor of 6. Thus, by process of elimination, coffee porous microstructure (H_m) was assumed to slow down caffeine diffusion by a factor of 4. This value is lower than the ones derived in this thesis, which resulted in values of 8-9 for particles of comparable sizes (as seen in Figure 4.24). On the one hand, based on Spiro's results and the observation that Mateus and Rouvet, (2007) reported regarding relaxation upon wetting, it might be possible that the contribution of the microstructure to the hindrance factor is overestimated when measured in *dry*, i.e. non-extracted, grinds. On the other hand, Jaganyi and Madlala, (2000), using Spiro's methodology, studied the hindrance factors for caffeine and various minerals (K^+, P, Mg^{2+}, Mn^{2+}) in coffees of six different origins. They reported H values between 11-14 for caffeine, and beweteen 18-48 for the minerals. For the same species, the estimated value of H appeared to depend on the specific coffee origin. Moreover, it is likely that the beans in their study showed different roasting colours, as it appears that they were commercially purchased. As pointed out by Spiro and Hunter (1985), roasting degree influences the coffee particle microstructure, and thus the hindrance factor. Therefore, the fact that the values of H_m estimated in this Section are higher than those in the literature, may be due to differences in the experimental methodology and to the intrinsic characteristics of the coffee beans themselves.

The microstructural contribution to the hindrance factor was also estimated for flaked coffee, and Blend 3 at the two different roasting colours, and results are shown in Table 4.8. A sample of Blend 1 with a similar $d_{[4,3]}$ to that of flaked coffee is also included for comparison purposes. It can be seen that the three considered samples showed higher values of H_m, as compared to the regular samples of RGC shown in Figure 4.24 for the same size. In the case of flaked coffee, this value is due to the comparatively low porosity as Ψ_E and the flakes showed similar values of tortuosity. In the case of Blend 3, the considered samples showed higher values of particle tortuosity. This is due to the intrinsic characteristics of Blend 3; however, it must be noted that repetitions of the measurements for the samples from Blend 3 would be required to confirm the results.

Table 4.8: Hindrance factor due to the porous microstructure (H_m) of the coffee blends considered in this study

Blend		***H_m***
1 (Ψ_E)		7.6 ± 1.8
Flaked coffee (Blend 2)		10.2 ± 1.8
*3	9.0 *La*	13.6
	5.5 *La*	12.4

* H_m was estimated from a single mercury porosimetry measurement

Estimates of the effective diffusion coefficients (D_{eff}) at 80 °*C* for the different MW categories proposed in Section 3.3.8 were obtained from the estimated bulk diffusion coefficients (D_b), and the microstructural contributions to the hindrance factor (H_m) reported in this Section (Table 4.9). The values of the low MW category (estimated assuming caffeine as the representative molecule) are comparable to D_{eff} values derived from caffeine extraction experiments (Espinoza-Perez et al., 2007; Jaganyi and Madlala, 2000; Spiro and Selwood, 1984). From the extraction of all the coffee soluble solids, Voilley and Simatos (1979) reported D_{eff} values between 8-11×10^{-11} $m^2\,s^{-1}$, which are of

the same order of magnitude as the medium MW category. However, Zanoni et al. (1992) reported values between 0.2-0.0232×10^{-11} $m^2 s^{-1}$, which are considerably lower, and comparable to the very high MW category. The difference between these two pieces of work lies in the fitting methodology used: the former fitted the experimental extraction points to the full solution of Fick's Second law, whereas the later used the steady state approximation model derived by Spiro (Eq. 2.3), and collected experimental points only after the first minute when approximately 90 % of the extraction was completed. It is thus likely that the former methodology gives more weight to the early-time points (presumably dominated by low and medium MW species), whereas the later gives more weight to longer-time points, presumably dominated by high and very high MW species.

Table 4.9: Estimated D_{eff} values at 80 °C for the proposed MW categories for coffee soluble solids. All the coefficients are expressed in $m^2 s^{-1}$ and must be multiplied by 10^{-11}

Grind	***MW category***			
	Low	***Medium***	***High***	***Very High***
A	37.0 ± 17.5	10.6 ± 5.0	3.7 ± 1.7	0.16 ± 0.075
B	29.5 ± 8.5	8.5 ± 2.5	2.9 ± 0.8	0.13 ± 0.036
C	28.6 ± 5.1	8.2 ± 1.5	2.8 ± 0.5	0.12 ± 0.022
D	24.7 ± 5.9	7.1 ± 1.7	2.5 ± 0.6	0.11 ± 0.025
E	25.6 ± 2.5	7.3 ± 0.7	2.5 ± 0.2	0.11 ± 0.011
F	21.8 ± 4.5	6.3 ± 1.3	2.2 ± 0.4	0.093 ± 0.019
H	19.2 ± 1.8	5.5 ± 0.5	1.9 ± 0.2	0.082 ± 0.0076
Flakes	18.5 ± 3.2	5.3 ± 0.9	1.8 ± 0.3	0.079 ± 0.014
9 La	13.8	4.0	1.4	0.059
5 La	15.3	4.4	1.5	0.066

In Chapter 5, D_{eff} values derived from microstructural measurements will be implemented in the extraction models shown in Chapter 3 to see how well they describe experimental data.

4.4.6. Solid-liquid partition coefficient

The partition coefficient (K) relates the equilibrium concentration of soluble solids in the bulk solution and inside the coffee particle. An estimation of K is required to solve the boundary condition of the extraction models presented in Chapter 3.

K was estimated at 20, 50 and 80 °C; Ψ_A was arbitrarily chosen to carry out the extraction experiments at the different coffee and water relations. Figure 4.25a shows equilibrium data at 80 °C plotted in the form presented in Eq. 3.17, and the data fits a straight line (R^2 = 0.99). From the intercept value of the regression, K can be obtained. Note that obtained value of K is going to depend on the chosen value of the swelling factor (S). According to the particle size distribution measurements of extracted grinds (Figure 4.8) and the swelling estimates of Section 4.4.4, it can be concluded that a swelling factor S = 1 can be adopted here.

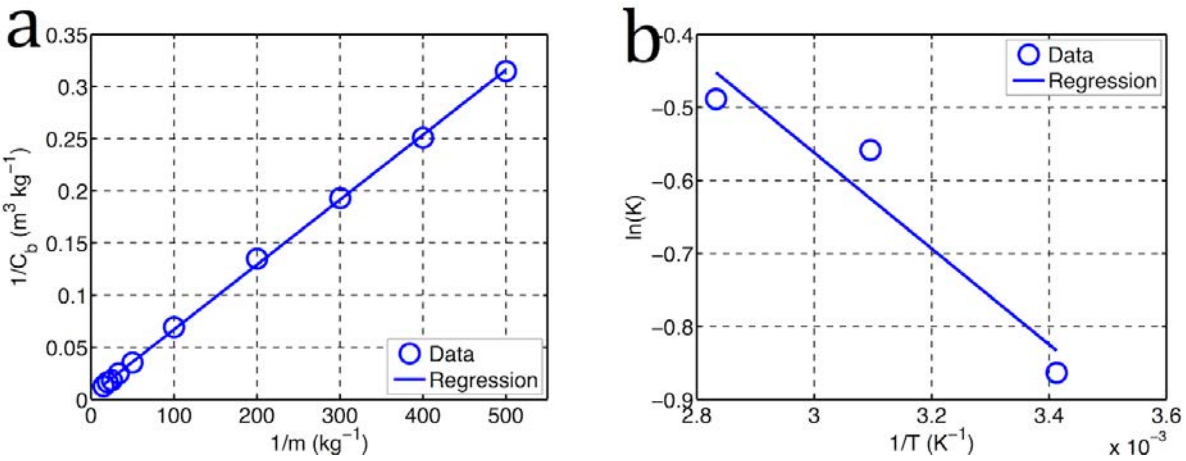

Figure 4.25: (a) Experimental data to derive the solid-liquid partition coefficient at 80 °C according to Eq. 3.17; R^2 = 0.99; (b) Arrhenius plot ($1/T$ vs. ln (K)) for K at 20, 50 and 80 °C. R^2 = 0.91. Experiments were performed in triplicate; error bars too small to be shown (relative standard deviation ~ 1 %)

Table 4.10 displays the derived values of K for a swelling factor of 1.

Table 4.10: Solid-liquid partition coefficient (K) as experimentally determined from equilibrium data under different assumptions of the swelling factor (S)

T (°C)	***S =1***
80	0.61
50	0.57
20	0.42

The values of K at 20 $°C$ are comparable to the value of 0.51 reported for caffeine by Spiro and Selwood, (1984) at 25.5 $°C$. At 80 $°C$, the values are lower to those reported for caffeine by Spiro and Selwood (circa 1.0 at 85 $°C$), and Espinoza-Perez et al., (2007) (0.98 at 90 $°C$) In addition, $y_0(\Psi_A)$ was estimated from this equilibrium data, and resulted 32.15 *kg SS* per 100 *kg* of RGC. As noted in Section 4.4.1, this value is 1 % higher that the value determined from the dilute extractions in (31.7 *kg SS* per 100 *kg* of RGC).

In Figure 4.25b, the relationship of $1/T$ vs. $ln(K)$ is showed. A linear Arrhenius behaviour is fit with R^2 = 0.91 for the three measured points for coffee soluble solids. Further work would be required to understand the origins of the dependency of the partition coefficient with temperature, e.g. association of molecules to the cell wall matrix but also possible temperature-dependent changes on the cell wall matrix itself.

4.4.7. Conclusions of the extraction parameters

The results of the extraction parameters of the grinds obtained from Blend 1 (Ψ_A-Ψ_H), flaked coffee (Blend 2), and decaffeinated coffee roasted to different colours (Blend 3), have been presented here.

It has been shown that the particle size distribution of the grinds affects their initial concentration of extractable soluble solids. This was attributed to molecular size exclusion effects of pores within the particles that were of a smaller order of magnitude than some of the species. Reducing the particle size distribution, or applying more

intense grinding processes, e.g. flaking, was shown to reduce this entrapment effect, causing an increase in the extraction yield.

Estimates of the microstructural contribution to the hindrance factor were obtained as the ratio of the particle tortuosity and porosity. They were found to be comparable to others reported in the literature, which were derived from extraction experiments. It must be noted that the hindrance factors reported in this thesis do not take into account the possible effect of other phenomena affecting coffee extraction. These values were used to estimate the effective diffusion coefficients for the four MW categories defined in Chapter 3. The solid-liquid partition coefficient was determined from experimental equilibrium data at 20, 50 and 80 $°C$, assuming a swelling factor of 1. The solid-liquid partition coefficient values at low temperature are comparable to those found for caffeine. However, at higher temperatures, the values were found to be lower than those reported for caffeine in the literature.

Chapter 5: Extraction at the Particle Scale

5.1. Introduction

The aims of this Chapter are to investigate the effect of different process variables (stirring rate, particle size distribution of the grinds, particle shape, and temperature) on the kinetics of extraction at the particle scale, and to evaluate the predictability of the corresponding mathematical model introduced in Chapter 3.

For this purpose, Section 5.2 presents a preliminary study on the required extraction time to study the kinetics of extraction. In Sections 5.3-5.8 the extraction experiments that were carried out in the batch stirred vessel set-up described in Chapter 3, are presented. Values of the effective diffusion coefficient (D_{eff}) of the extracted soluble solids were obtained by fitting the experimental data to simulation results. The obtained values were compared with the microstructural D_{eff} values derived in Chapter 4; the latter were also used to carry out simulations that were compared to the experimental data. For the sake of simplicity, the super and sub indices β and i (that were adopted in Chapter 3 to refer to *chemical species* and *size classes* of the particle size distribution, respectively) are omitted in this Chapter from the notation.

In Section 5.9, a sensitivity study of the simulations to some process parameters and assumptions of the model is also shown in this Chapter.

Section 5.10 closes the Chapter by presenting a summary of the findings and conclusions.

5.2. Estimation of the maximum extraction times at the particle scale

A preliminary step to design experiments to investigate the kinetics of extraction is determining the time required for the system to reach equilibrium, i.e. when extraction yield becomes independent of extraction time, since this determines the maximum experimental time span. For that purpose, a preliminary long-time kinetic experiment (t = 300 *min*) was carried out at stirring rate of 500 *rpm*, and a coffee-water relation of 25 $kg\,m^{-3}$ (effectively 12.5 g of RGC in 500 *ml* of water). The value of these parameters was selected to reproduce the experimental conditions that were subsequently used in the rest of the stirred vessel extraction experiments. However, the temperature was kept at 20 $°C$ and 50 $°C$ (rather than at 80 $°C$) in order to minimise possible evaporation effects over the unusually long time scale used here. Ψ_B and Ψ_H were tested in this preliminary experiment, since they are the finest and coarsest grinds used in the investigation of the kinetics of extraction at the particle scale.

Figure 5.1 shows the extraction yields achieved at the previously specified conditions (y-axis) over time (x-axis). It can be seen from Figure 5.1 that the equilibrium is reached between 20 and 40 minutes for Ψ_B, at both temperatures. In the case of Ψ_H, for the first experimental point (which was taken at 30 minutes), 92 % of the extraction is completed and equilibrium is reached between 90 and 180 minutes. For the calculation of the extraction yield, the volume of the collected aliquots for analysis (5 *ml*) was subtracted from the bulk volume (500 *ml*) of the solution. Therefore, at equilibrium, multiplying a constant bulk concentration by a decreasing bulk volume (as aliquots are taken out) results in an artificial numerical decrease of the extraction yield.

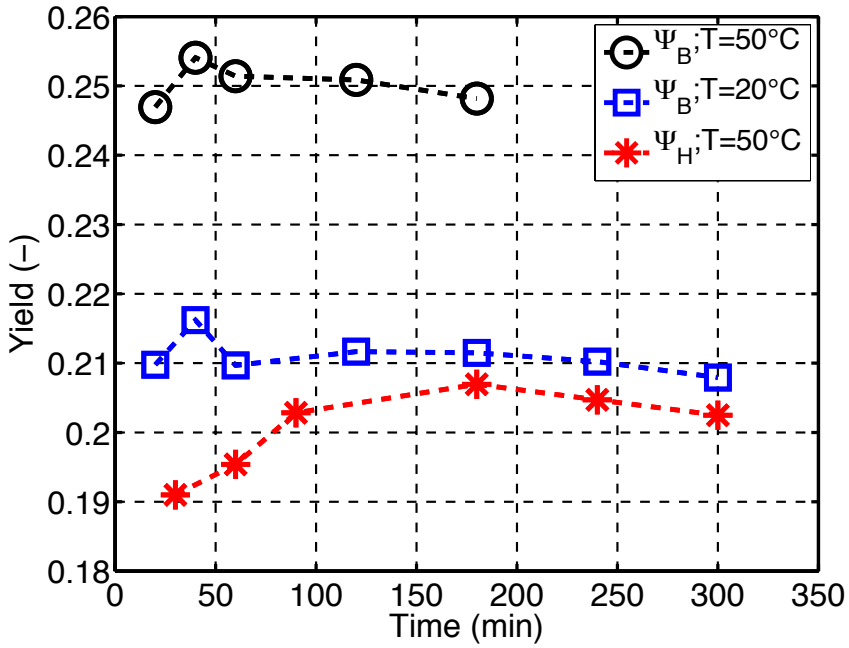

Figure 5.1: Extraction yield (y-axis) over time (x-axis) for Ψ_B at 20 and 50 °C, and Ψ_H at 50 °C. The line (----) is meant to guide the eye. Since the aim of this experiment was to obtain estimates of the equilibrium times only one repetition was carried out

The selected extraction times (2 hours for Ψ_B and 6 hours for Ψ_H) to estimate the initial soluble solids concentration of the grinds at 80 °C are beyond the equilibrium times of the coarsest grind (Ψ_H), even at the lower temperatures (50 °C) used in this preliminary experiment. Therefore, this reassures that the observed decrease in the long-time limit extraction yield for coarser grinds (Chapter 4) is in fact a molecular size exclusion effect and not a kinetic effect due to a slower extraction from the coarser grinds.

In a solid-liquid extraction process, the relaxation time of a given species being extracted from a particle is given as follows:

$$t_R = \frac{(\phi R)^2}{D_{eff}} \qquad \text{Eq. 5.1}$$

Where t_R is the relaxation time (s), R is the characteristic distance for diffusion (m), Φ is the sphericity of the particles (-), and D_{eff} the effective diffusion coefficient of the considered species ($m^2\ s^{-1}$).

In the unrealistic scenario of an infinitely diluted system, where the concentration of the extracted material in the bulk solution can be approximated to zero, t_R would be an estimate of the time required to extract all the soluble solids from the considered size class. The long-time limit extraction yield measured for Ψ_A at a coffee-water relation of 10 $kg\ m^{-3}$ (Chapter 4) was 0.99 times the value of the estimated initial concentration derived from the equilibrium experiments performed to calculate the solid-liquid partition coefficient (K) (Chapter 4). It can be concluded that an infinitely diluted system can be assumed for a coffee-water relation of 10 $kg\ m^{-3}$ with an error of approximately 1 %. The more concentrated an extraction system is, the less material is extracted from the grinds into the bulk solution. Therefore the required time to reach equilibrium is expected to decrease and consequently to differ from t_R. This parameter, however, may be still an accurate estimation of the required time to reach equilibrium in moderately concentrated systems such as the one used in this thesis (coffee-water relation of 25 $kg\ m^{-3}$).

In a particle size distribution, the largest (and hence limiting) t_R will be given by the coarsest sizes. $d_{[4,3]}$ of the particle size distributions (as *dry* measured) is assumed here as a good representation of the coarser size classes of the grinds (and their abundance in the distributions). $d_{[4,3]}$ is preferred over other alternatives, e.g. the coarse peak of the distributions, as the former incorporates information of the whole distribution, whereas the latter parameter is based on a single value. t_R for Ψ_H was estimated at 50 $°C$ for each of the four molecular weight (MW) categories in which coffee

soluble solids were classified in this thesis (Chapter 3), and the results are displayed in Table 5.1. The D_{eff} values (which were derived at 80 $°C$ from microstructural measurements were corrected to account for the effect of temperature via the Stokes-Einstein equation.

Table 5.1: Relaxation times for low, medium, high and very high MW species diffusing inside Ψ_H at 50 $°C$

Species	t_R ***(min)***
Low MW	33
Medium MW	114
High MW	330
Very High MW	7644

By comparing the estimated t_R with the observed equilibrium times, one can obtain an approximate idea of the MW of the species that have been extracted from the particles into the bulk solution, and those that remain entrapped within the particles. The equilibrium time for Ψ_H at 50 $°C$ (between 90-180 minutes, as identified from Figure 5.1), is significantly smaller than t_R for the high and very high MW species. If part of the molecules of these species present within the particles were not entrapped (and could be thus extracted), the observed equilibrium time would be in the range of their estimated relaxation times. One can think, however, that the initial amount of these species in the original coffee beans may be very small. Therefore, although their extraction process may carry on after the observed equilibrium time, such small extracted amounts may not be detected when the concentration of the collected aliquot is measured. However, in Figure 5.1 the same effect observed when the long-time limit extraction yields were measured (Chapter 4) can be appreciated: when the grind becomes finer (Ψ_H: $d_{[4,3]}$ = 1247.7 μm → Ψ_B: $d_{[4,3]}$ = 198.8 μm), the equilibrium extraction yield increases (from 0.20 for Ψ_H to 0.25 for Ψ_B). It can be then concluded that these

species are indeed present within the grain in noticeable proportions to be detected but entrapped within the particles due to molecular size exclusion.

The dependency of t_R with temperature (via D_{eff}) is given by the Stokes-Einstein equation (expressed here as a ratio of two D_{eff}):

$$\frac{t_{R_1}}{t_{R_2}} = \frac{T_1 \mu_2}{T_2 \mu_1} \qquad \text{Eq. 5.2}$$

Where t_R is the relaxation time (s), and μ_i is the water viscosity ($Pa\,s$) at the two considered temperatures T_i ($°C$).

Other potential temperature effects (which are not accounted for by the correction expressed in Eq. 5.2) have to be taken into account. On the one hand, and according to the previous observations in Figure 5.1, higher temperatures result in greater extraction yields (for Ψ_B, increasing the temperature from 20 to 50 $°C$ shifts the extraction yield from 0.21 to 0.25). It is reasonable to think that higher extraction yields may imply a greater average MW of the extracted material. Therefore, the expected higher extraction yields at a higher temperature may involve the extraction of species with lower D_{eff} than the ones extracted in this experiment, and thus longer t_R than the ones predicted from Eq. 5.2. On the other hand, possible temperature-induced relaxation effects of the coffee matrix, and an increase of the solubilisation rate from the coffee matrix to the pore space of the particle (Spiro and Chong, 1997), may increase D_{eff} and result in shorter relaxation times than the ones estimated here. Therefore, temperature produces two competing effects on the equilibrium times for coffee extraction. However, it can be observed in Figure 5.1 that, despite the higher yield achieved for Ψ_B at 50 $°C$ (1.25 times the extraction yield of Ψ_H at the same temperature) the equilibrium time is

still considerably greater for Ψ_H (~ 90-180 minutes as opposed to 20-40 minutes for Ψ_B). For these two grinds, particle size is the dominant effect over the effect of D_{eff} due to the possible increase of MW of the extracted species.

Assuming t_R at 50 $°C$ as 90 minutes for Ψ_H, and 20 minutes for Ψ_B (Figure 5.1) the estimates at 80 $°C$ according to Eq. 5.2 were 52 and 12 minutes, which are comparable to the typical extraction times in industrial soluble coffee manufacturing processes before the high temperature hydrolysis step. It must be noticed, however, that despite the fact that the general objective of this thesis is to investigate the underlying principles of coffee extraction that are common to all the processing scales, the main focus is put on consumer applications rather than industrial scale processes. Times for consumer extraction methods, which range from approximately 25 seconds for espresso coffee to circa 6 minutes for filter coffee (Gloess et al., 2013), are considerably lower than the equilibrium times estimated here. Thus, in order to optimise the experimental times, whilst allowing extraction to proceed until values close to the equilibrium, extraction times of 20 minutes were adopted for Ψ_B and Ψ_E, and 40 minutes for Ψ_F, Ψ_G, and Ψ_H.

5.3. Influence of stirring rate

Stirring rate is an important variable in the operation of batch solid-liquid extraction processes. At a macroscopic level, stirring enhances mixing in the vessel, preventing the solids from floating on the surface or settling down to the bottom. This mixing effect also homogenises the concentration of the extracted species in the bulk solution, i.e. the concentration is independent from the position in the vessel. At a microscopic level, the stirring rate may affect the extraction rate of species from the

solids, as it determines the thickness of the mass transfer boundary layer, and thus the so-called external mass transfer resistance, i.e. transport resistance from the surface of a solid particle to the bulk solution. At the industrial scale, stirring rate has to be optimised so that acceptable homogenisation of the system is achieved, and the possible effect of the external mass transfer resistance minimised whilst also minimising the power consumption of the stirrer. At the consumer scale, if the external mass transfer resistance played a relevant role in coffee extraction, it would have to be taken into account when optimising the flow rate through a coffee packed bed in applications like, for instance, espresso extraction.

The extraction model at the particle scale presented in Chapter 3 assumes a *well-stirred solution*, according to previously reported research (Spiro and Page, 1984). Therefore, the external mass transfer resistance was assumed to be negligible, and a concentration boundary condition ($C_s = C_b/K$ at $r = R$), as opposed to a boundary layer flux condition, was adopted. To validate this assumption, the influence of the stirring rate on the external mass transfer resistance was firstly estimated via the Biot number (*Bi*) (-). The Biot number is defined as the ratio of internal to external mass transfer resistance (Schwartzberg and Chao, 1982):

$$Bi = \frac{k\phi R}{D_{eff}} K \qquad \text{Eq. 5.3}$$

Where k is the external mass transfer coefficient ($m\ s^{-1}$), Φ is the particle sphericity (-), R is the representative diffusion length (m), K is the solid-liquid partition coefficient (-), and D_{eff} is the effective diffusion coefficient ($m^2\ s^{-1}$). The internal mass transfer resistance is given by the quotient of the representative diffusion length (R) and

D_{eff}. The reciprocal of the external mass transfer resistance is given by the external mass transfer coefficient (k): it represents the quotient of the boundary layer thickness (distance between the particle surface and the region in which the concentration is that of the bulk solution), and the bulk diffusion coefficient of the considered species (D_b). It can be seen that the internal mass transfer resistance decreases with finer grinds, as they show a smaller representative size value of the coarse size class ($R = d_{[4,3]}/2$). Conversely, it can be said that the relative influence of the external mass transfer resistance is higher for finer grinds. A low value of K would indicate a tendency of the considered species to remain absorbed in the coffee matrix, which would imply an extra resistance in the external mass transport.

The external mass transfer coefficient can be estimated via the Sherwood number (Sh) (-), as given for forced convection around a sphere (Cussler 2009b):

$$Sh = \frac{k\phi R}{D_b} = 2 + \left(\mathrm{Re}\right)^{1/2} \left(Sc\right)^{1/3} \qquad \text{Eq. 5.4}$$

Where Re is the Reynolds number in a stirred vessel (-), and Sc the Schmidt number (-).

It is straightforward to express the Biot number as $Sh(D_b/D_{eff})K$, where D_b/D_{eff} is the hindrance factor (H). In a hypothetical extraction scenario where no stirring is applied, i.e. $Re = 0$ and thus $Sh = 2$. For the estimated solid-liquid partition coefficient values for all the coffee soluble solids ($K = 0.61$), and microstructural contributions to the hindrance factor measured for the grinds ($H_m = 6.3\text{-}9.9$) (Chapter 4), the resulting Biot numbers are between 8 and 12 ($Bi >> 1$), which points out a dominance of the internal over the external mass transfer resistance. To confirm the validity of this estimates, the kinetics of extraction of soluble solids at different stirring rates (200, 500,

900 and 1100 *rpm*) were investigated in the stirred vessel set-up at 80 *°C*, and a coffee-water relation of 25 $kg\,m^{-3}$.Ψ_B was used since this is the finest grind used to investigate the kinetics of extraction where the relative influence of external mass transfer resistance is expected to be more noticeable

Figure 5.2 shows the extraction yield (*y*-axis) over time (*x*-axis) at the four considered stirring rates. When the stirring rate is ≥ 500 *rpm*, the extraction rate is independent of this variable. However, at the lowest stirring rate (200 *rpm*), extraction rate during the first minute seems to be lower than for the other conditions. At such a low stirring rate, it was visually observed that the system was not fully homogeneous during the first minute of the experiment. Therefore, the lower rates and bigger standard deviations are due to inconsistent sampling from an inhomogeneous system. Otherwise, the results are consistent with the estimates of Biot numbers, and experimentally validate the assumed equilibrium boundary condition stated in the extraction model.

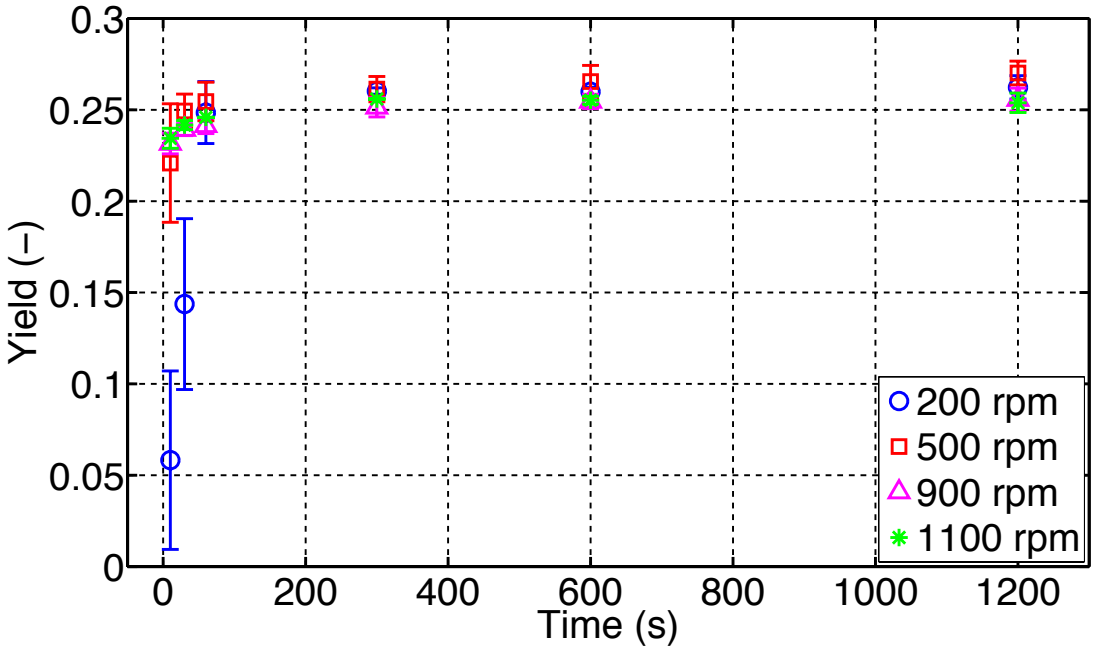

Figure 5.2: Extraction yield (y-axis) over time (x-axis) for Ψ_B at 80 °C and coffee-water relation of 25 *kg m*$^{-3}$. Stirring rate: 200 *rpm* (○); 500 *rpm* (□); 900 *rpm* (▽); 1100 *rpm* (✳)

5.4. Influence of particle size distribution

Particle size distribution of the grinds is a key parameter that affects the extraction rate, as well as the maximum amount of material that can be extracted (Nicoli et al., 1990; Voilley and Simatos, 1979; Zanoni et al., 1992), as a consequence of the reported molecular size exclusion effect (Chapter 4). At the industrial scale, whereas finer particle size distributions would be desirable to increase extraction rate (and thus reduce the size of the processing units), this would result in a greater hydraulic resistance of the packed beds formed in the industrial extraction columns. Given the size scale of this type of equipment (typically several meters), the energy requirements associated with a higher hydraulic resistance can represent a significant impact on the economics of the process. The effect of particle size distribution on the permeability of coffee packed beds is investigated and discussed in Chapter 6. At the consumer scale,

particle size distribution has been shown to significantly influence the extraction yield (and thus flavour and aroma profiles) of espresso coffees since it can lead to balanced or under- and over-extracted coffees (Andueza, De Peña, et al., 2003).

The kinetics of extraction of soluble solids from different grinds (Ψ_B, Ψ_E, Ψ_F, Ψ_G, Ψ_H, and flaked coffee) was investigated at 80 *°C*, stirring rate of 500 *rpm*, and a coffee-water relation of 25 $kg\ m^{-3}$, and the results are displayed in Figure 5.3. Note that the same normalised experimental data is shown in Figure 5.2 in a shorter dimensionless time scale, and in Figure 5.8 plotted in a logarithmic fashion.

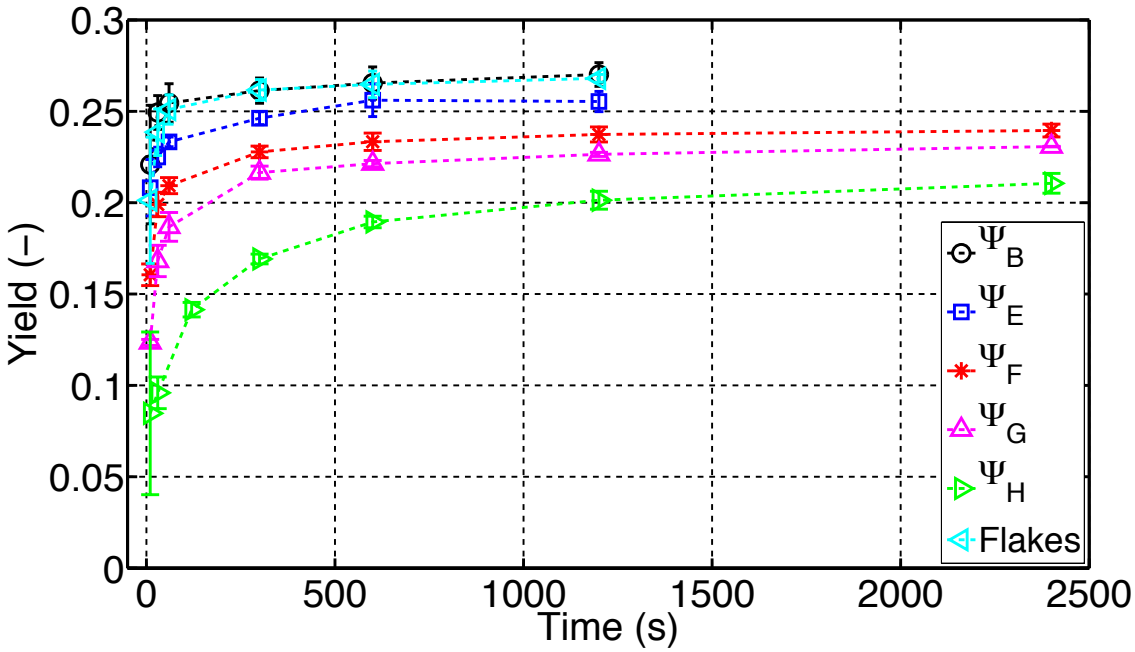

Figure 5.3: Extraction yield (*y*-axis) over time (*x*-axis) for the considered grinds at 80 *°C*, 500 *rpm*, and a coffee-water relation of 25 $kg\ m^{-3}$. The line (----) are meant to guide the eye

Finer grinds, in addition to a smaller average size of the coarse size class, also contain a higher percentage of the fine size class (d_{fine} = 40 μm for all the grinds) (Chapter 4) where the mass transfer rate is notably higher. The expected equilibrium yield for the experiments shown in Figure 5.3 was estimated from the equilibrium bulk concentration (as estimate with Eq. 3.17 with the derived K = 0.61). For all the grinds,

the measured yield at the last time point (which is either 1200 or 2400 seconds) was greater than 94 % of its estimated equilibrium value, except for the flaked coffee, which resulted to be 88 %.

Earlier extraction times are characterised by steep rise in extraction yield. This is caused by the fast extraction from the fine size class and the surface of the coarser size classes. For longer times, the extraction yield increases more gradually with time in a linear fashion towards the equilibrium yield. The linear increase, whereas in principle it can be thought to be an artefact of the experimental methodology (possible minimal evaporation occurred in the brief period in which a tiny portion of the aluminum foil was removed to take the sample), there are a number of factors to consider as to why this can be disregarded: (i) the slope of this linear increase is greater the finer the grind, despite of the fact that the total extraction time was 1200 seconds for finer grinds (Ψ_B, Ψ_E, flakes), as opposed to 2400 seconds for coarser grinds; (ii) the same effect seems to be also present at considerably smaller extraction temperatures (50 $°C$) (Section 5.8); (iii) the tendency is also present in other RGC extraction data sets obtained using different set-ups to the one used here (Voilley and Simatos, 1979; Zanoni et al., 1992). A plausible explanation (that is discussed in detail through Sections 5.5, 5.6, and 5.7) for this linear increase is the distribution of relaxation times of species that conform the coffee soluble solids. In other words, the extraction curves cannot be fit by a single effective diffusion coefficient as they represent the superposition of a number of individual extraction curves (one per each extractable chemical species present within the coffee bean and particle size forming the grind).

The measured properties of flaked coffee were compared throughout Chapter 4 to those measured for Ψ_E, based on the similar particle size distribution of both grinds as *dry* measured. It was stated, however, that the relevant size of the flakes for mass transfer was half (due to symmetry of the flake geometry) their thickness rather than the size measured by laser diffraction (which is associated to their bigger surface area). The comparison of the kinetics of extraction of flaked coffee and regular roast and ground coffee validates that affirmation: extraction from flaked coffee is faster than from Ψ_E despite the fact that the particle size distribution *dry* measured seems to be slightly coarser for the flakes ($d_{[4,3]}$ = 454.2 μm for flaked coffee, and $d_{[4,3]}$ = 363.2 μm for Ψ_E). As a matter of fact, the kinetics of extraction of the flaked coffee is virtually equal to that of Ψ_B, whose characteristic diffusion length ($R = d_{[4,3]}/2$ = 99.4 μm) is comparable to the half-thickness of the flakes (~ 75 μm) (Figure 4.11).

5.5. Normalising the effect of the particle size distribution

The extraction curves shown in Figure 5.3 were normalised for comparison purposes. The data was transformed into the following dimensionless variables: the extraction yield was normalised by the estimated extraction yield at equilibrium (estimated with Eq. 3.17) for each grind ($y^* = y/y_{eq}$); time was normalised by the relaxation time, defined as R^2/D_{eff} (Section 5.2), resulting in a dimensionless time (t^*). For the flaked coffee, the relevant transport distance was considered to be 75 μm (as half of the observed thickness in the SEM picture shown in Figure 4.11); this figure is also half the approximate separation between the rollers used to produce the flakes, which was 150 μm (Section 3.2.2). Since the objective of this normalisation is to establish a simple comparison of the effect of particle size distribution of the grinds on

extraction rate, a single arbitrary value of the effective diffusion coefficient $D_{eff} = 5 \times 10^{-11}$ $m^2 s^{-1}$, was chosen to calculate t_R. This simplification implies the assumption of the coffee soluble solids being formed by a single representative species, and all the grinds showing the same microstructural hindrance factor.

The fact that the particle size distributions contained different percentages of the fine size class (d < 100-105 μm) was also taken into account. The mass of soluble solids extracted from the fine size class was removed from the total extracted mass, and the extraction yield resulting from the coarse size class was estimated. The relaxation time for the fine size class, as estimated with the reported microstructural values of D_{eff} for Ψ_B in Chapter 4, was found to lie between 1 and 8 seconds for the low, medium, and high MW categories. The very high MW category resulted in a relaxation time of 178 seconds. Therefore, it can be safely assumed that in the first experimental data point (taken at 10 seconds) equilibrium had been reached for most part of the soluble species in the fine size class. Provided the size scale of the fine size class, molecular size exclusion is unlikely to occur. Therefore, the expected extraction yield from this size class is the maximum that can be extracted for this particular type of coffee (32.2 *kg* of soluble solids per 100 *kg* of RGC, as determined in Section 4.4.1). This value was also assumed for the flaked coffee. Thus, the yield extracted from the coarse size class (y_{coarse}) can be estimated as follows:

$$y_{coarse} = \frac{y - \left(y_o\left(\Psi_j\right)\nu_{fine}\right)}{1 - \nu_{fine}} \qquad \text{Eq. 5.5}$$

Where y is the extraction yield measured from the whole particle size distribution over time (-) (Figure 5.3), $y_0(\Psi_j)$ is the maximum extraction yield from this

particular type of coffee at 80 $^{\circ}C$ (-), and v_{fine} is the percentage of the fine size class (as *dry* measured) (-).

Figure 5.4 compares the dimensionless extraction yield for the considered grinds (y-axis) over the dimensionless time (x-axis) considering the whole particle size distribution, and just the coarse size class.

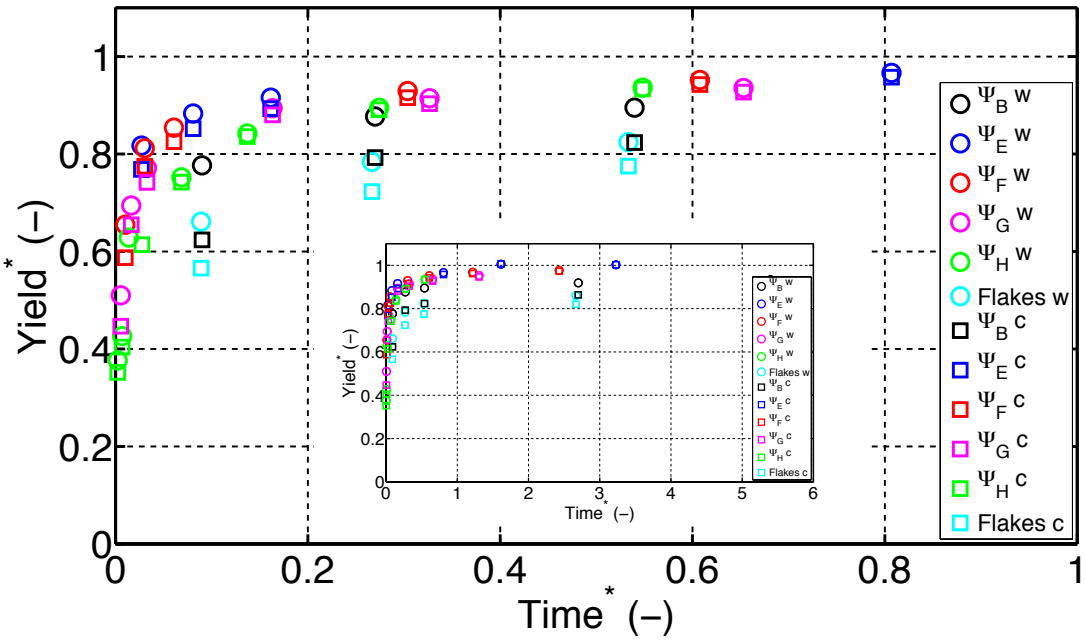

Figure 5.4: Dimensionless extraction yield (y-axis) over dimensionless time (x-axis) for the considered grinds at 80 $^{\circ}C$, 500 *rpm*, and a coffee-water relation of 25 $kg\ m^{-3}$. Whole distribution (w) (○); only the coarse size class (c) (□). The smaller figure shows the same data in a longer time scale

At earlier times, the normalised extraction curves collapse well when the whole particle size distribution is considered, except for the case of flaked coffee. This difference may be explained due to the fact that more than just one observation (Figure 4.11) would be required to obtain a more representative value of the thickness of the flakes. Note that considering a slightly bigger average thickness, e.g. 200 μm as opposed to 150 μm, would involve displacing the normalised extraction curve leftwards, resulting in an agreement of the behavior of flaked coffee with the other grinds at earlier

dimensionless times. As expected, the extraction rate when the whole particle size distribution is considered is much faster than that of the coarse size class. This is especially true in the first experimental point and for finer grinds. According to the estimated relaxation times, most part of the material is extracted from the fine size class in the time scale in which the first experimental point was taken, i.e. 5 seconds. However, upon removal of the contribution of the fine size class, although Ψ_H lies slightly below the general trend, the curves for the coarse size class still coincide. In the case of Ψ_B and flaked coffee, the curves lie considerably below the general trend. This suggests that, in dimensionless units, i.e. when the effect of particle size distribution has been normalised across the grinds, the extraction rate is lower for the finest grind and flaked coffee.

On the one hand, the estimated equilibrium yields by which the kinetic data sets were normalised are different for each grind, as their initial concentration of *extractable* soluble solids was shown to decrease with particle size distribution due to the reported molecular size exclusion effect (Chapter 4). For example, the equilibrium concentration of Ψ_B and flaked coffee resulted to be 18 % and 35 % (respectively) greater than that of Ψ_H. Extracting more material may imply the diffusion of species with a bigger molecular weight, and thus smaller values of D_{eff}. From the definition of the relaxation time, it can be seen that the assumption of smaller D_{eff} values would imply bigger relaxation times, which would effectively displace the curves leftwards. In Chapter 4 D_{eff} for the range of the considered MW were estimated and it was shown that these values differ by several orders of magnitude.

On the other hand, the distribution of the coarser sizes ($d \geq$ 100-105 μm) seems to be wider the finer the grind (Figure 4.1). This may suggest that $d_{[4,3]}$ (from which R was calculated) is a better representation of the average size of the coarse size class of the particle size distributions for coarser grinds. Additionally, the considered $d_{[4,3]}$ is for the whole particle size distribution and thus the value includes the contribution of the fine size class. In the finest grind, the volume percentage of the fine size class is 35.9 % and this may result in a lower $d_{[4,3]}$ that slightly underestimates the effect of the coarser sizes of the distribution. If the upper-extreme values of the tails (557.8 μm for Ψ_B as opposed to its $d_{[4,3]}$ = 189.6 μm, and 1740 μm for Ψ_H as opposed to its $d_{[4,3]}$ = 1247.7 μm) were considered, t_R values would result to be bigger than those calculated from $d_{[4,3]}$ by 8-fold and 2-fold factors for Ψ_B and Ψ_H, respectively. The effect of considering a greater R to calculate t_R would be equivalent to considering smaller D_{eff} i.e, displacing the extraction curve leftwards, and thus a better agreement of Ψ_B with the behaviour of the other grinds. However, the assumed values are the upper-extremes and the volume percentage of particles of that size is extremely low (approximately 2 %). Furthermore, due to the differences of order of magnitude in the D_{eff} of the different species considered, this appears to be the dominant factor over the particle size effect.

5.6. Modelling coffee extraction with a single effective diffusion coefficient

The distribution of species forming the coffee soluble solids (simplified in this thesis to four MW categories) (Chapter 3) and the distribution of sizes forming the grinds (Chapter 4) make modelling of coffee extraction a complex task. However, it may

be relevant (and undoubtedly convenient for practical applications) to perform a baseline modelling analysis of coffee extraction in which all the coffee soluble solids are lumped as a single pseudo-compound (sp = 1), thus characterised by a single D_{eff} representing their global behaviour. This analysis may assist to decide whether this baseline case is a *simple but not an oversimplified* representation of the system, or, in turn, further level of refinement is required in order to tailor the model to various applications, e.g. product development, industrial-scale process design, etcetera.

For the baseline analysis, the continuously bimodal particle size distributions were simplified to two particle size classes, namely the fine (d <100-105 μm with an average size of d_{fine} = 40 μm) and coarse size class (rest of the particles with an average size of $d_{coarse} = d_{[4,3]}$ of the distribution). As shown in Chapter 4 the only difference in the fine size classes of the different grinds is their volume percentage, i.e. they have the same maximum yield as they have the same size. Therefore, once the extracted material from the fine size class is removed from the experimental extraction data the differences appreciated in the extraction curves can be assumed to be due to the characteristics of the coarse size class.

In Section 5.5, it was postulated that the lower extraction rate observed for the coarse size class of Ψ_B and the flaked coffee was due their higher maximum extraction yields involving the diffusion of higher MW species with lower D_{eff}. It must be taken into account, however, that the rate of extraction from the coarse size class is also influenced by the concentration gradient between the surface of the particle and the bulk solution. For a given value of dimensionless time (t^*), and due to the higher percentage of their fine size class, the coarse size class from these finer grinds would be extracted in a

solution with a higher bulk concentration, as compared to coarser grinds. This would effectively result in a lower concentration gradient and the consequent decreasing extraction rate, as compared to coarser grinds. Therefore, in order to assess to what extent this effect is reflected in the estimated extraction data from the coarse size class, extraction from Ψ_B ($d_{[4,3]}$ = 198.8 μm) was simulated with the model at the particle scale (Chapter 3) for its real measured percentage of the fine size class (v_{fine} = 35.9 %), and was compared with the simulation of a hypothetical situation in which the fine size class was removed (v_{fine} = 0 %) and thus only the coarse size class (effectively a single particle represented by the $d_{[4,3]}$ of the particle size distribution) was considered. The model was numerically solved for both cases for a coffee-water relation of 25 $kg\,m^{-3}$ (as used in the experiments), K = 0.61, and the results expressed into dimensionless variables (y^*, t^*), as detailed in Section 5.5.

Figure 5.5 presents the simulated dimensionless yield (y-axis) over the dimensionless time (x-axis) for the coarse size class of Ψ_B. One can see that although as expected, the extraction rate from the coarse size class is slightly higher in the case where the fine size class is not present (small plot), but there is virtually no difference (average relative error = 0.2 %) between both scenarios. It can be then concluded that the effect of the higher bulk concentration (due to a bigger volume percentage of the fine size class in finer grinds) on the extraction rate from the coarse size class is minimum at this particular coffee-water relation and can be neglected for this analysis. This effect, however, is expected to become more noticeable as the extraction system becomes more concentrated, i.e. coffee-water relation increases.

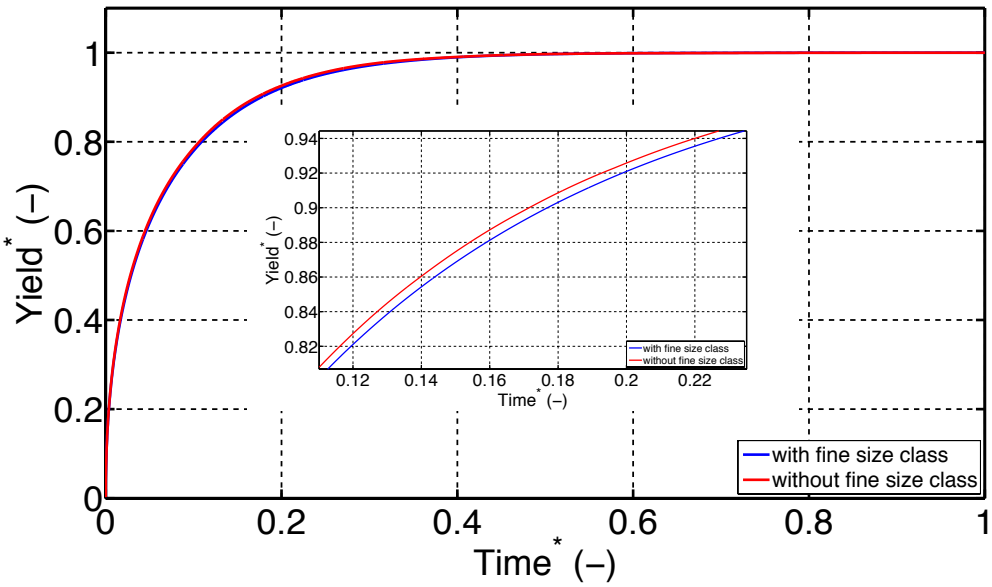

Figure 5.5: Simulation of the dimensionless extraction yield (y-axis) over dimensionless time (x-axis) for the coarse size class of Ψ_B at a coffee-water relation of 25 $kg\ m^{-3}$, 80 $°C$, and K = 0.61 in the presence of the real percentage of the fine size class (v_{fine} = 35.9 %) and a hypothetical situation of v_{fine} = 0 %. The small plot is a zoom where the difference in the extraction rate for both situations can be appreciated

As reviewed in Chapter 2 if D_{eff} is to be derived from the experimental extraction data, the chosen fitting strategy seems to provide values that can differ in orders of magnitude. In an analysis of the sensitivity of the simulations to the number of mesh elements (Section 3.5.2) it is shown that the considered number of terms in the Fourier series solution to Fick's second law determines the early time convergence of the solution. In order to capture the early time behaviour of the system, Voilley and Simatos (1979) fitted data using six terms of the Fourier series solution. On the other hand, Stapley (2002) and Zanoni et al. (1992) used only one term of the Fourier series in their analysis of extraction and this was shown to predominately capture the long time behaviour of the system. Both alternatives (*early time* approach (Section 5.6.1) and *long time* approach (Section 5.6.2)) are implemented here.

5.6.1. The early time approach

The *early time* approach fits experimental extraction data to the numerical solution of Fick's second law trying to capture the early time behaviour of the system. This approach was implemented here as follows:

I. Based on the estimates of the effective diffusion coefficient shown in Chapter 4, a range of D_{eff} values between 0.05-35.0×10^{-11} $m^2 s^{-1}$ (a total of 34951 values; step size of 0.001×10^{-11} $m^2 s^{-1}$) were selected.

II. For each of these values, the corresponding relaxation time for each grind was calculated. As per usual in this Chapter, $d_{[4,3]}$ was adopted to calculate R. However, an additional fit was carried out assuming the coarse peak value (see Figure 4.1) to calculate R in order to assess the differences between both assumptions. In the case of flaked coffee, half of the thickness, i.e. 75 μm, as observed in Figure 4.11 was considered as the relevant dimension of the particle to estimate the relaxation time.

III. The experimental extraction time was then normalised by each of the relaxation times obtaining one set of experimental dimensionless times for each of considered effective diffusion coefficients.

IV. The model at the particle scale was solved for a single particle and the result transformed into dimensionless variables (t^* and y^*).

V. For each set of the generated experimental dimensionless time, the experimental dimensionless extraction yield was compared to that predicted by the model at the same values of dimensionless time. The criterion to select the optimal set of experimental dimensionless time (and thus the D_{eff} value that best fits the data) was the minimisation of the residual $\Sigma\,[y^*_{mod}\,(t^*) - y^*_{exp}\,(t^*)]^2$.

The optimisation with this approach was carried out in two different ways: (i) fitting a single D_{eff} for all the data sets; and (ii) fitting a D_{eff} for each individual data set from a given grind. Since, as already observed in Figure 5.4, the extraction rate of Ψ_B and the flaked coffee considerably differed from the rest of the grinds, they were left out from the determination of a single coefficient for all the coarse size classes.

The extraction model at the particle scale for a flake is equivalent to that presented in Chapter 3 for roast and ground coffee, but considering a cylindrical geometry for the flakes (as opposed to spherical). The diameter of the flakes was considered to be equal to the $d_{[4,3]}$ of the distribution (as *dry* measured) (454.2 μm) corrected with a measured sphericity of 0.79 (Table 4.3), and a height of twice the observed thickness (75 μm) (Figure 4.11). Given the dimensions of the flakes, mass transport is assumed to occur only in the direction of the thickness (axial direction of the cylinder).

Figure 5.6 shows the simulated dimensionless extraction yield (y-axis) over the dimensionless time (x-axis), and the comparison with the experimental data as normalised with the fitted D_{eff} values (reported in Chapter 4).

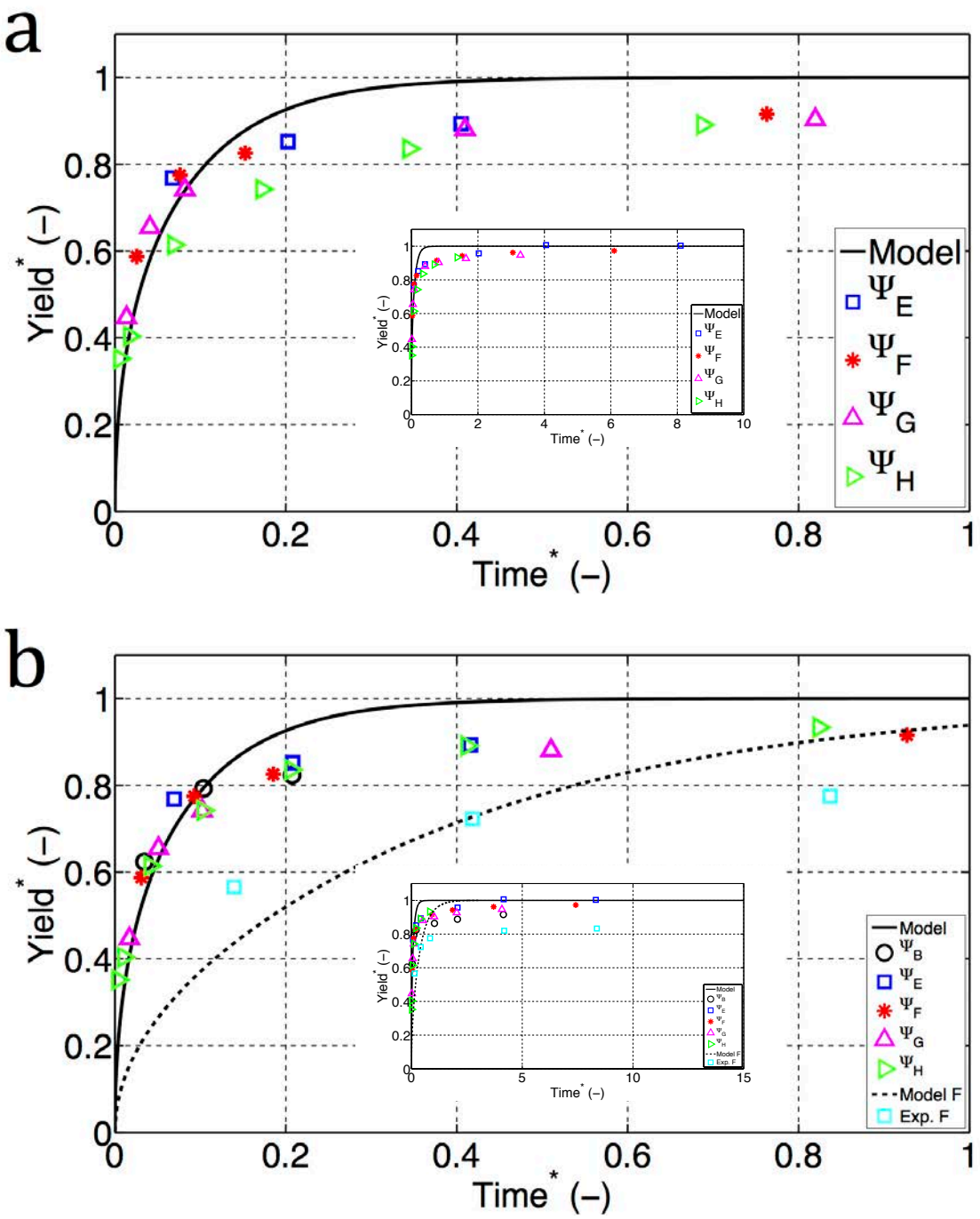

Figure 5.6: Dimensionless extraction yield (*y*-axis) over dimensionless time (*x*-axis) for the coarse size class of the considered grinds at a coffee-water relation of 25 $kg\ m^{-3}$, 80 °C, and $K = 0.61$. D_{eff} was fitted according to the *early times* approach using $d_{[4,3]}$; (a) single value for all coarse size classes; (b) a value for each individual coarse size classes. Model (—); Model for the flakes (----); Experiments (Points). The smaller figures show the same data in a longer time scale

Table 5.2: Fitted D_{eff} ($m^2\ s^{-1}$) for the coarse size class of the considered grind and all the soluble solids, according to the *early time* approach

Grind	***D_{eff} all grinds ($\times10^{-11}$) ($d_{[4,3]}$) ($m^2\ s^{-1}$)***	***D_{eff} individual grinds ($d_{[4,3]}$) ($\times10^{-11}$) ($m^2\ s^{-1}$)***	***D_{eff} individual grinds (coarse peak) ($\times10^{-11}$) ($m^2\ s^{-1}$)***
Ψ_B	—	1.9	5.3
Ψ_E		12.9	21.4
Ψ_F	12.6	15.3	18.8
Ψ_G		15.6	21.0
Ψ_H		7.5	12.3
Flakes		7.9	—

Table 5.2 shows the fitted D_{eff} for the individual coarse size class when $d_{[4,3]}$ or the coarse peak of the distribution are considered. It can be seen that, while the values derived for both assumptions differ, they still have the same order of magnitude. In both cases D_{eff} follows an increasing trend with grind size (except for Ψ_H). In addition to the aforementioned effect of the low MW species being more noticeable due to the lower extraction rate, the average MW of the extracted species may decrease for coarser grinds due to the reported molecular size exclusion effect (Section 4.4.2). Thus, not surprisingly, and as expected from Figure 5.4, Ψ_B showed a considerably lower D_{eff} than the rest of the distributions for both assumptions of particle sizes ($d_{[4,3]}$ and coarse peak). When the fitting was carried out for all the grinds (except from Ψ_B and flaked coffee), the obtained value ($12.6\times10^{-11}\ m^2\ s^{-1}$) is close to the average value ($12.8\times10^{-11}\ m^2\ s^{-1}$ for $d_{[4,3]}$) of the values when the fitting was performed for the individual coarse size classes (Table 5.2).

A single D_{eff}, despite of resulting in reasonable values of Mean Percentage Error (*MPE* less than 15 % for regular RGC) between the experimental and predicted values (Table 5.3), is unable to predict the whole extraction curve: the model tends to underestimate earlier time points (approximately t^* less than 0.1), and overestimate

longer time points (approximately t^* greater than 0.1), which corresponds to approximately $y^* = 0.8$.

Table 5.3: *MPE* between the simulation and the experimental points with D_{eff} fitted according to the *early times* approach and $d_{[4,3]}$

Grind	***MPE all grinds (%)***	***MPE individual grinds (%)***
Ψ_B	—	10.6
Ψ_E	5.8	5.8
Ψ_F	7.6	6.4
Ψ_G	9.3	8.1
Ψ_H	14.6	14.8
Flakes	—	16.7

This can be more clearly seen in the analysis of the relative error over time between the model predictions and the experimental points as presented in Figure 5.7.

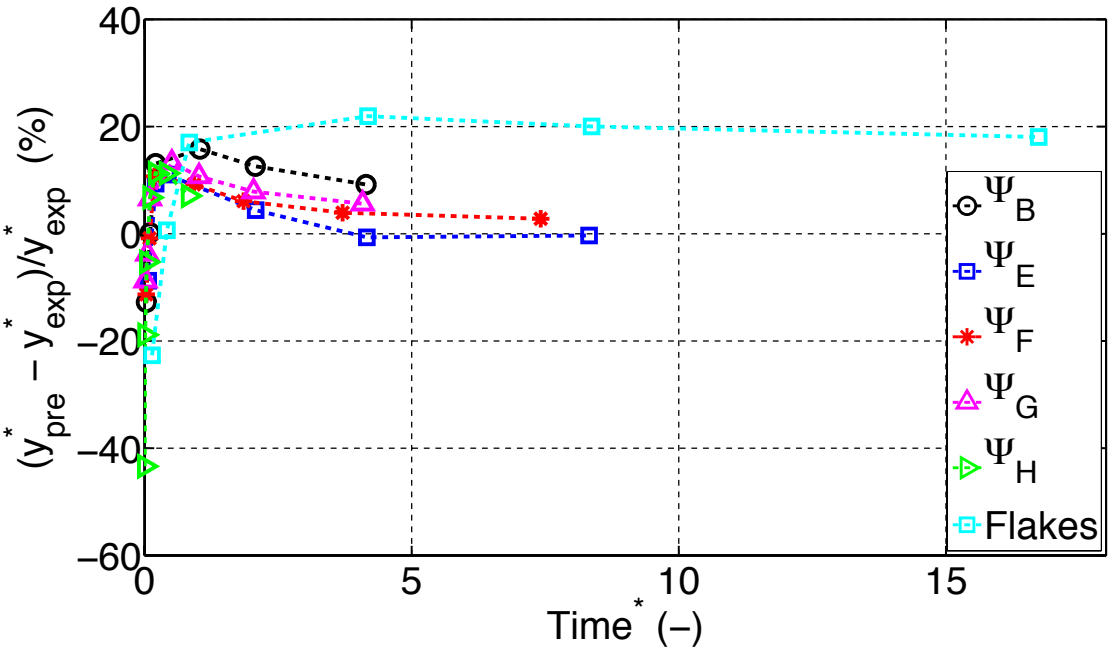

Figure 5.7: Evolution of the relative error between the model simulation and the experimental points (y-axis) over dimensionless time (x-axis) for D_{eff} fitted for the individual coarse size classes and $d_{[4,3]}$ according to the *early time* approach

The negative error in Figure 5.7 indicates under-prediction while the positive error indicates over-prediction. In general, excluding Ψ_B, the *MPE* increases for coarser

grinds. This seems to suggest that the adoption of a single D_{eff} to model extraction of all the soluble solids becomes more inaccurate for coarser grinds. On the one hand, because extraction rates are lower in coarser grinds, the collected experimental data offer a more complete representation of the extraction curve. For example, the first experimental point, i.e. after 10 seconds, for Ψ_B and Ψ_E represents 62 and 77 % of the total extracted material, respectively, whereas it represents 38 % for Ψ_H (Figure 5.6). Therefore, the presence of low MW species (that diffuse considerably faster than the bigger species) is more noticeable in the experimental data obtained for coarser grinds. On the other hand, as detailed in the model development (Chapter 3), the porous microstructure of coffee particles is assumed to be an homogenous medium characterised by an average particle porosity and tortuosity. Pore size distribution measurements (Section 4.3.2) performed on the considered grinds suggested that for higher grinding levels, the microstructure of the grinds is more homogeneous, i.e. the ink-bottle effect is reduced. Therefore, for a given species, the difference in the extraction rate depending on its initial position in the particle, i.e. cell pockets of the surface or inside the particle, may become bigger for coarser grinds.

The simulated dimensionless transport in the flaked coffee (cylindrical geometry) is significantly slower than in regular RGC (sphere geometry). For the same transport distance, a spherical geometry shows a lower volume/surface ratio than a cylinder. The showed simulation for flaked coffee is not fully dimensionless though, as it applies only to cylinders of the same radius/length ratio as the one considered here. The D_{eff} for the flaked coffee resulted in a relatively high value as compared to Ψ_B. This difference may be a consequence of the last experimental point (considering only the coarse particles) representing only 85 % of the total extraction whereas that value represents 92 % for

Ψ_B. Additionally, assuming a value of the thickness based on a single observation, introduces uncertainty to the fitting. A more detailed study (and possibly methodology) would be required in order to obtain statistically significant values.

5.6.2. The long time approach

The model for multiple size classes and a concentrated system has no analytical solution. The concentration boundary condition at the surface of a given size class is dependent on the transport in the other size classes, and thus Fick's second law has to be solved in each size class simultaneously using a numerical scheme. However, since the analysis presented here is considering only the coarse size class, it is possible to use the analytical solution of Fick's second law for a concentrated system (Stapley, 2002) to derive D_{eff} values for the grinds.

When a large number of terms of the summation, i.e. n = 500, is implemented in the general solution to second Fick's law (expressed as a infinite Fourier series), and plotted in its logarithmic form (rather than the exponential form), it can be seen that the concentration at earlier times increases exponentially (Stapley, 2002). As time elapses, this exponential trend flattens until the relationship gradually becomes linear. The equation of this linear region may be obtained from the full analytical solution when only the first element of the summation i.e. n = 1 of the series is considered. The resulting expression (Stapley, 2002) (in its logarithmic form) takes the form of a first-order equation similar to Spiro's steady-state model (Spiro and Selwood, 1984) (Section 2.3.1):

$$\ln\left(\frac{C_{eq}}{C_{eq}-C_b}\right)=\ln\left(\frac{F^2\alpha_2^2+9F+9}{6F\left(1+F\right)}\right)+\frac{\alpha_1^2 D_{eff}}{R^2}t \qquad \text{Eq. 5.6}$$

Where C_b and C_{eq} ($kg\ m^{-3}$) are the concentration in the bulk solution at any time and at equilibrium, respectively, F (-) is given by $K(V_{bulk}/V_{coffee})$ and represents the volume ratio of the bulk aqueous and solid phase corrected by the solid-liquid partition coefficient, and R (m) the representative diffusion length of the particle (assumed here to be $d_{[4,3]}/2$). The group ($\alpha^2 D_{eff}/R^2$) is typically referred to as the observed kinetics constant of the model (k_{obs}) (s^{-1}), where αn is the n-root of Eq. 5.7:

$$\tan\alpha=\frac{3\alpha}{3+F\alpha^2} \qquad \text{Eq. 5.7}$$

Note that for the case of the flaked coffee, Eq. 5.6 and Eq. 5.7 were considered for a slab geometry, as the equations for this geometry were readily available in Stapley (2002). This approximation is considered to be valid, since the geometry of the flakes is not perfectly defined.

The considered grinds showed a range of particle porosities of 0.50-0.65 (Figure 4.14). For a K = 0.61, F was estimated to be between 11-16 and thus α_1 was found to be 3.3 and 3.4, respectively. It is worth mentioning that for the somewhat unrealistic scenario of an infinite dilute system where C_b can be approached to 0 at any time (no external mass transfer resistance), $\alpha_1 = \pi$.

Figure 5.8 shows the extraction data from Figure 5.6 plotted in the form of Eq. 5.6 (i.e. logarithmic form). One can see that the data, rather than linear, appears to be exponential not only at earlier times. As a matter of fact, in the theoretical plot obtained from the full solution of Fick's second law, linearity of the curve starts when the

concentration in the bulk solution is approximately 35 % of its equilibrium value (Stapley, 2002). Figure 5.3 showed that even the first experimental points are generally well beyond this point. Thus, this progressive reduction in the slope (k_{obs}) is correlated to the observed linear increase at longer times in Figure 5.3 and may be caused by the two possible sources of variation of t_R, i.e. different particle sizes (R) and different species (D_{eff}). As detailed in Section 5.5, the effect of the range of D_{eff} values for the different species seems to be the dominant factor.

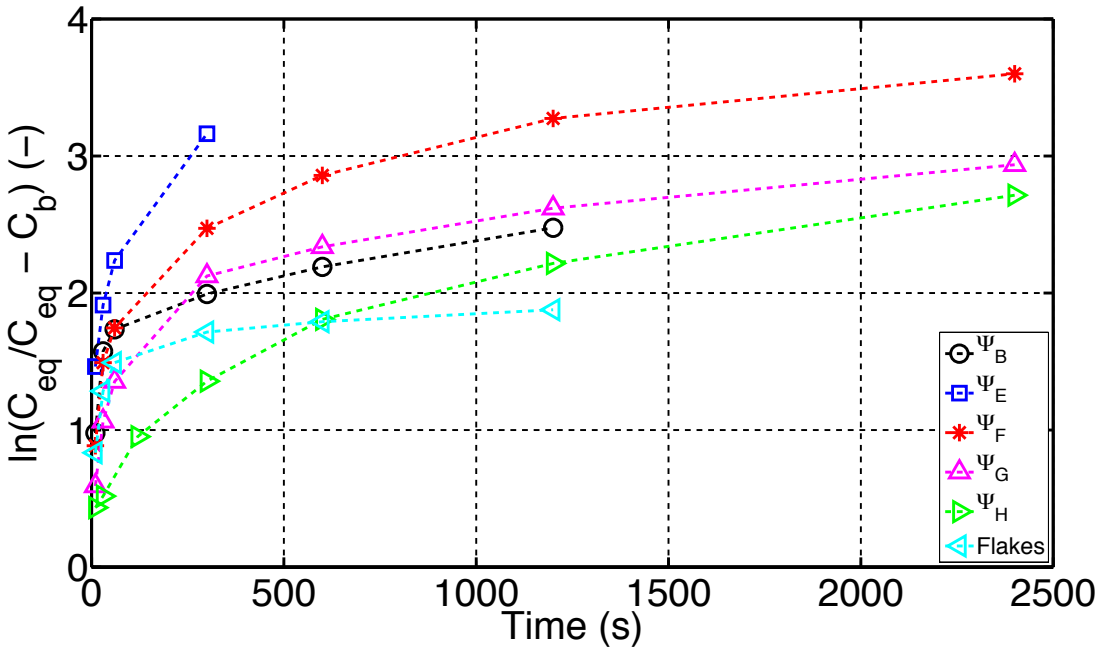

Figure 5.8: Logarithm of the evolution of the concentration in the bulk solution (y-axis) over time (x-axis). The line (----) is meant to guide the eye

In order to derive the value of D_{eff} from k_{obs}, linear regressions of the data presented in Figure 5.8 were carried out. According to Figure 5.6, disagreement between the predicted and the experimental points for the *early time* approach started after 80 % of the extraction had been completed. Therefore, only points beyond this limit (last three or four points) were considered for the linear regression. The derived effective diffusion coefficients (Table 5.4) were found to be between 0.03 and 0.7×10^{-11} $m^2\,s^{-1}$.

These values are significantly smaller (an order of magnitude) than the ones reported from the *early time* approach (Table 5.2).

Table 5.4: Fitted D_{eff} for the coarse size class of the considered grind according to the *long time approximation* approach

Grind	***D_{eff} ($\times 10^{-11}$) ($m^2\ s^{-1}$)***	***R^2***
Ψ_B	0.03	0.97
Ψ_E	0.8	0.98
Ψ_F	0.3	0.83
Ψ_G	0.4	0.96
Ψ_H	1.1	0.98
Flakes	0.04	0.98

It can be seen that, because of the logarithmic transformation carried out to express the data in the form of Eq. 5.6, the error of the long-time points is amplified as compared to the error in the *early time* approach. For example, in the *early time* approach an absolute error of 0.01 for long time points, e.g. y_{exp} = 0.98 and y_{mod} = 0.99, is amplified through the logarithmic transformation of the data to 0.69, i.e. 70-fold difference. Conversely, at earlier times, the same error of 0.01, e.g. y_{exp} = 0.10 and y_{mod} = 0.11, is only amplified by a factor of 1.12. Thus, in a least square minimisation of the logarithmic data, the long-time points (presumably dominated by higher MW species) have more weight than those at earlier times. Comparison of the fitted and microstructural effective diffusion coefficients

Two methodologies, namely microstructural (Chapter 4) and fitted values from experimental data (Section 5.6), have been used in this thesis to derive values of D_{eff} of coffee soluble solids, and the aim of this Section is to compare both sets of results.

Figure 5.9 shows the microstructural (M) and fitted (F) D_{eff} values (y-axis) for the $d_{[4,3]}$ of the particle size distribution (as *dry* measured) of the considered grinds (x-axis). Excluding Ψ_B ($d_{[4,3]}$ = 198.8 μm), it can be seen that the values fitted with the *early time* approach (ET) lie between the values derived from microstructural measurements for the low and medium MW categories. For the case of the *long time* approach (LT), the fitted values lie between those derived from microstructural measurements for the high and very high MW categories. As explained in Section 5.6.2, the LT approach gives more weight to the long time points, which are presumably dominated by higher MW species. One can also observe that the microstructural values decrease with particle size as the estimated hindrance factor (H_m) of the particles increases. Despite this fact, the fitted values seem to follow a general increasing trend with particle size, and this can be due (as discussed in Section 5.6.1) to a potential lower MW of the extracted species.

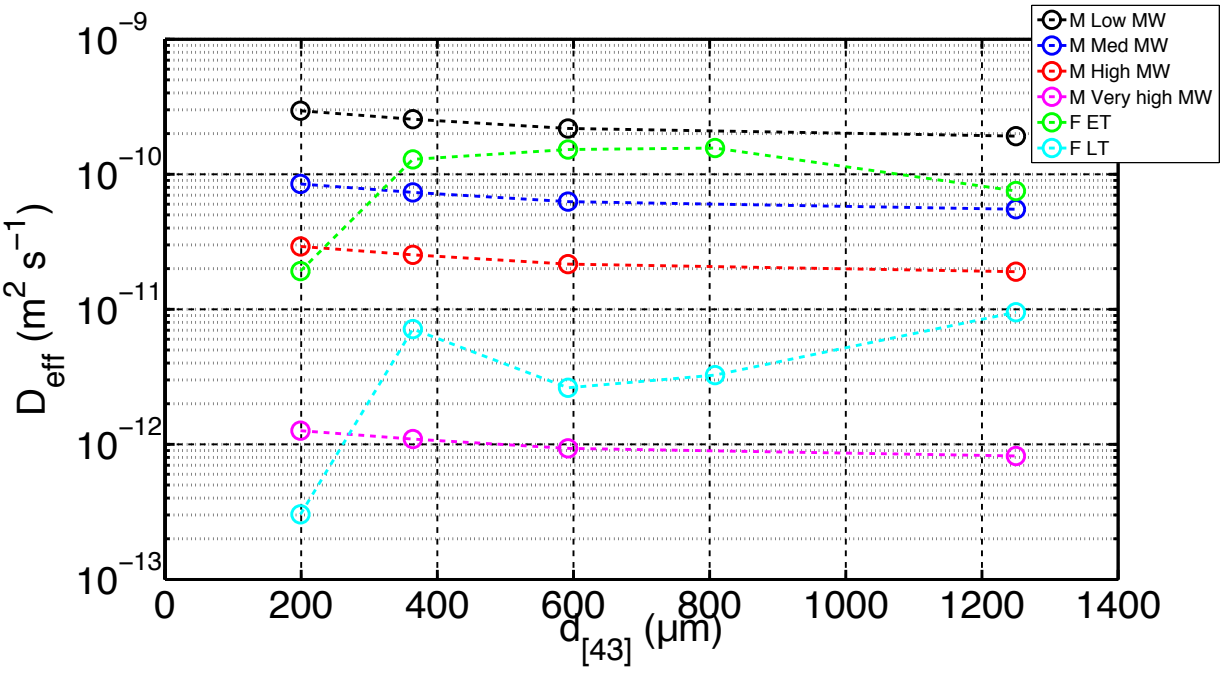

Figure 5.9: Microstructural and fitted D_{eff} (y-axis) vs. $d_{[4,3]}$ (x-axis) of the particle size distributions of the considered grinds. The line (----) is meant to guide the eye. M: values derived from microstructural measurements; F: values fitted from experimental data; ET: Early time; LT: long time

The microstructural estimation of D_{eff} was carried out from the bulk diffusion coefficient of four species (that cover the whole MW spectrum of coffee soluble solids), and the particle microstructural characteristics ($\varepsilon_{particle}$, $\tau_{particle\ CPSM}$) as per Chapter 4. On the one hand, the main advantage of this approach is that it provides estimates of D_{eff} from first principles, and thus there is not the imperative need of experimental data to derive the coefficients. Moreover, it avoids some of the problems encountered when fitting a single representative D_{eff} to a distribution of diffusing species (Section 5.6) and offers a more complete description of the system as it incorporates average information of the porous nature of the solid to the model. On the other hand, the disadvantage of the approach is the required knowledge of the chemical nature of the coffee soluble solids and the experimental effort to estimate the microstructural parameters. In this respect, whereas measuring the porosity of the particles is relatively easy with typical measurement techniques, such as mercury porosimetry, estimating the tortuosity may not be straightforward as accurate models of the pore structure of the solid are required.

The two methodologies introduced in Section 5.6 consist of the typical fitting of extraction data to the numerical or analytical solution of the relevant equation describing the dynamics of the system. The main advantage of this approach is that it provides optimal coefficients for at least a part of the extraction curve. However, on the other hand, in addition to the need of experimental data itself being a potential limiting factor in certain situations, fitting a D_{eff} in such a complex system without some pre-acquired knowledge may hide some of its relevant features, e.g. extraction rate of different species.

It can be then concluded that the fact that the microstructural estimates lie within the values fitted numerically with the *early time* approach (weight given to early time points) and the *long time* approach (weight given to longer time points) indicate that the considered range of MW covers well the whole spectrum of coffee soluble solids, and the fitted values may represent an average of the species that are diffusing at early and long time scales.

5.7. Using the microstructural D_{eff} values in the model at the particle scale

In the previous Section, comparing the fitted and the microstructural D_{eff} values seemed to indicate that the microstructural values are sensible estimates of the real behaviour of the extraction system. For instance, the fitted values with the *early time* approach (describing earlier time extraction) are virtually an average value of the microstructural values for low and medium MW species. The same argument holds true for the fitted values with the *long time* approach and the high and very high MW microstructural values.

It is the aim of this Section to assess the performance of the microstructural effective diffusion coefficients in the model. For that purpose, the model at the particle scale was solved for the multiparticle baseline case. The continuously bimodal particle size distribution was divided into a bimodal discrete distribution with a fine size class (d <100-105 μm and R_{fine} = 20 μm) and coarse size class (R_{coarse}= $d_{[4,3]}$/2). According to the SEM pictures of the flaked coffee, the coarse and fine size classes were modelled as a cylinder and a sphere, respectively. The rest of the conditions were those typically used

in the experiments presented so far in this Chapter, i.e. T = 80 °C, K = 0.61 and coffee-water relation of 25 $kg\ m^{-3}$.

5.7.1. A single D_{eff}

Figure 5.10 shows the comparison between the simulated and experimental extraction yield (y-axis) over time (x-axis) for each of the estimated microstructural D_{eff} values. As already seen in Figure 5.6 and Figure 5.8, the use of a single D_{eff} is unable to describe the whole extraction curve. One can see how as time elapses the experimental points spread towards the curves simulated with the smaller effective diffusion coefficients. In general, D_{eff} for the low MW species predict well the experimental points before 60 seconds, whereas the coefficients for the high MW species predict well long time points. The coefficients for the medium MW species seem to slightly under-predict at earlier times and over predict at longer times. However, from the qualitative point of view, the later seems to be the most sensible option for the majority of the grinds if the behaviour of the system over a long time span is to be represented with a single D_{eff}.

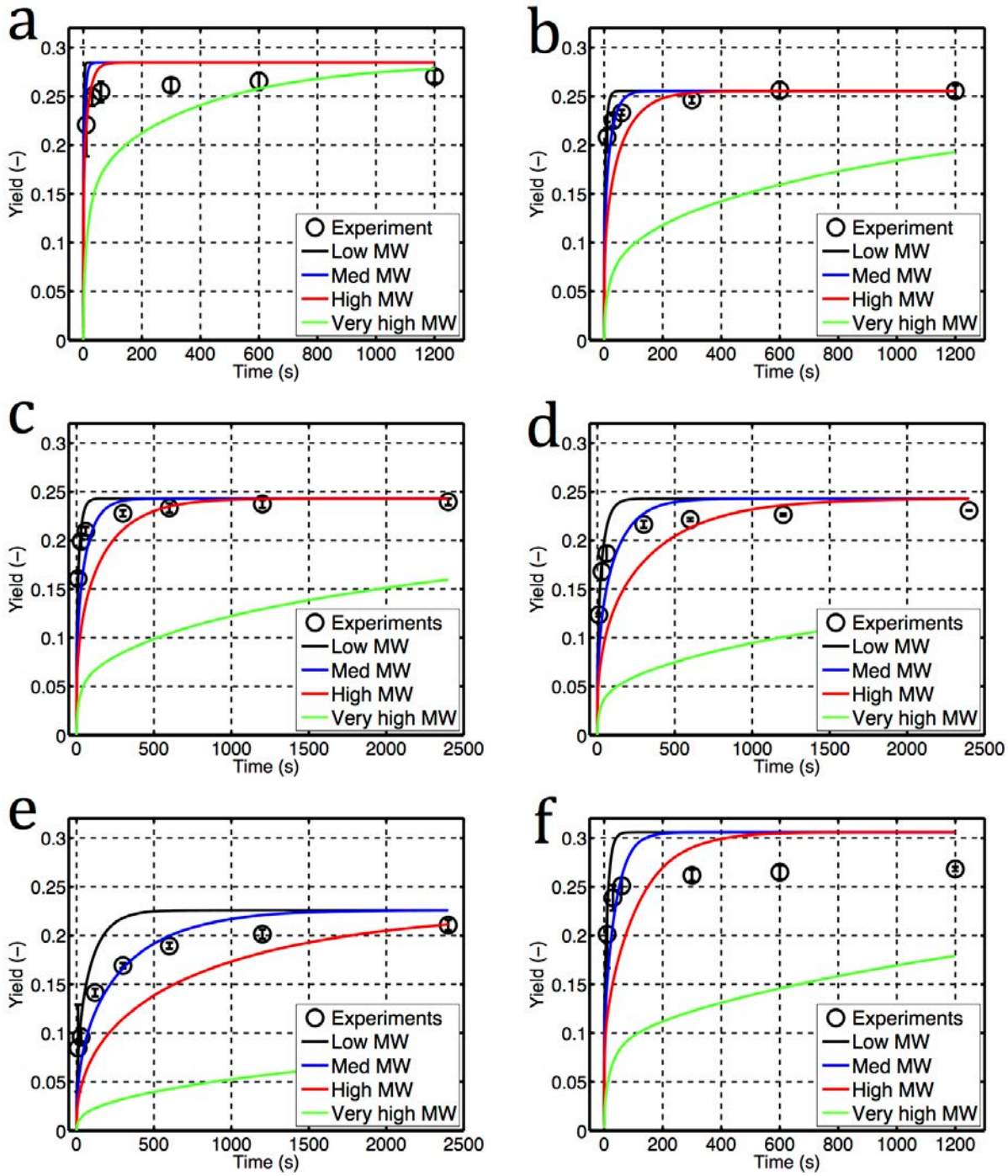

Figure 5.10: Extraction yield (y-axis) over time (x-axis) at coffee-water relation of 25 $kg\ m^{-3}$, 80 $°C$, and K = 0.61 for the D_{eff} derived from microstructural measurements for each grind. The model was solved for two size classes (fine and coarse); (a) Ψ_B; (b) Ψ_E; (C) Ψ_F; (d) Ψ_G; (e) Ψ_H; (f) Flakes. Model (—); Experiments (Points)

The Mean Percentage Error (*MPE*) between the experimental data for the grinds and the simulations for the four MW categories was calculated and is shown in Figure 5.11. As can be seen from the simulations, considering all the soluble solids, as high or

very high MW species does not offer good agreement with the experimental data. Average *MPE* values of 11 and 13 % were obtained when the D_{eff} for the low and medium MW species were used. Given the variability of D_{eff} for the different species, and that no fitted parameters were used in these simulations, the values can be considered as acceptable. Despite the smaller average *MPE* value for the low MW category, it should be noticed that, proportionally, more experimental points were collected in the region where the D_{eff} for the low MW species performs better (t < 60 s). Therefore, also from the quantitative point of view, if a single D_{eff} is to be used, the best option for most grinds to represent extraction over a wide time span (up to 1200 or 2400 seconds), seems to be the estimates for the medium MW species. However, if the objective of the simulations is the evolution of the system at earlier times, the microstructural estimates for low MW species or the fitted coefficient from the *early time* approach may offer a better agreement.

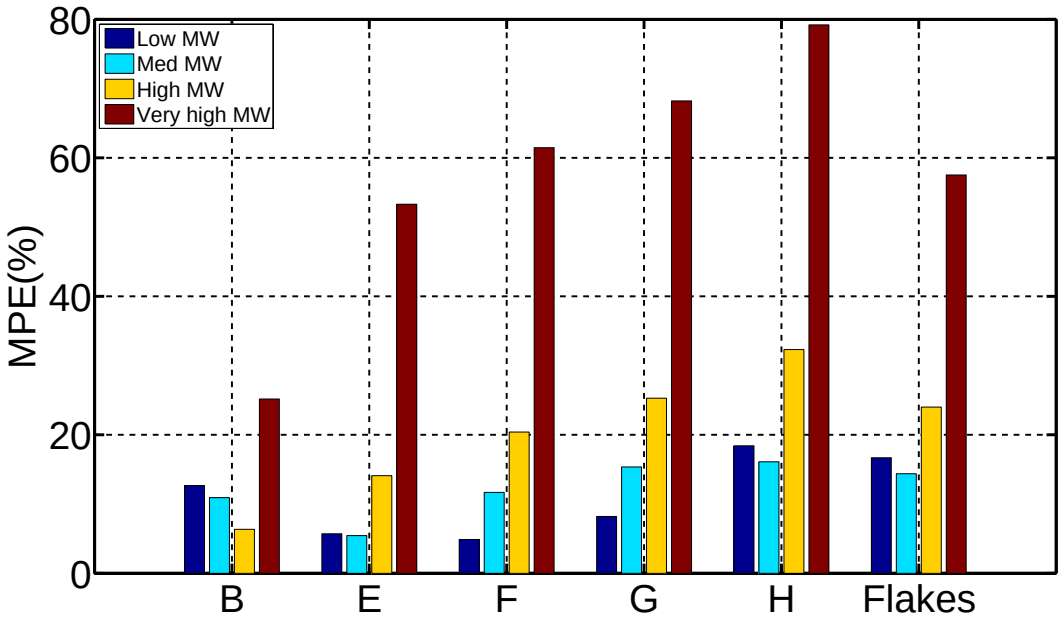

Figure 5.11: Mean Percentage Error (*MPE*) between the model simulations and the experimental data showed in Figure 5.10

5.7.2. Multiple D_{eff}

For all the analysis and simulations that have been carried out so far in this Chapter, a single D_{eff} to model the extraction has been considered, i.e. all the coffee soluble solids were assumed to be a pseudo-component. However, the significant difference in the values of D_{eff} provokes that, when a single value is used (and the model is solved considering two size classes), only part of the experimental extraction curve is well represented (Figure 5.10).

If the diffusion of a given species inside the solid is assumed to be independent of other molecules, the extraction yield can be estimated as the sum of the simulated curves shown in Figure 5.10 weighted by a mass percentage of the considered species:

$$y_{pre} = \sum_{\beta=1}^{sp} y_{pre}^{\beta} \omega^{\beta} \qquad \text{Eq. 5.8}$$

Where y_{pre} the predicted extraction yield (-), y^{β}_{pre} is the predicted extraction yield assuming all the soluble solids as being the species β (-), and ω^{β} is the mass fraction of the soluble solids represented by the species β (-).

The weight of each of the four MW categories consiered in this thesis were estimated from the literature. Bekedam et al. (2006) isolated high MW and low MW fractions from coffee brews with an extraction yield of 20 % using a dialysis membrane (cut-off value 12-14 *kDa*) and diafiltration (cut-off value 3 *kDa*) and the percentages obtained are reported in Table 5.5.

Table 5.5: Percentages of low and high MW of coffee fractions (Bekedam et al., 2006)

Technique	***High MW***	***Low MW***
Dialysis	31.7 %	68.3 %
Diafiltration	15.5 %	84.5 %

The simulated curves showed in Figure 5.10 (obtained for the estimated microstructural D_{eff} for each of the four MW categories and two size classes) were rescaled with the weights showed in Table 5.5. The percentage of high MW species was divided in three equal parts and assigned to the medium, high and very high MW categories.

Figure 5.12 compares the experimental extraction data and the simulated yield assuming three different scenarios: best single D_{eff} (typically the one estimated for the medium MW category except for the case of Ψ_B), and the weights reported from dialysis (multiple $D_{eff}1$) and diafiltration (multiple $D_{eff}2$).

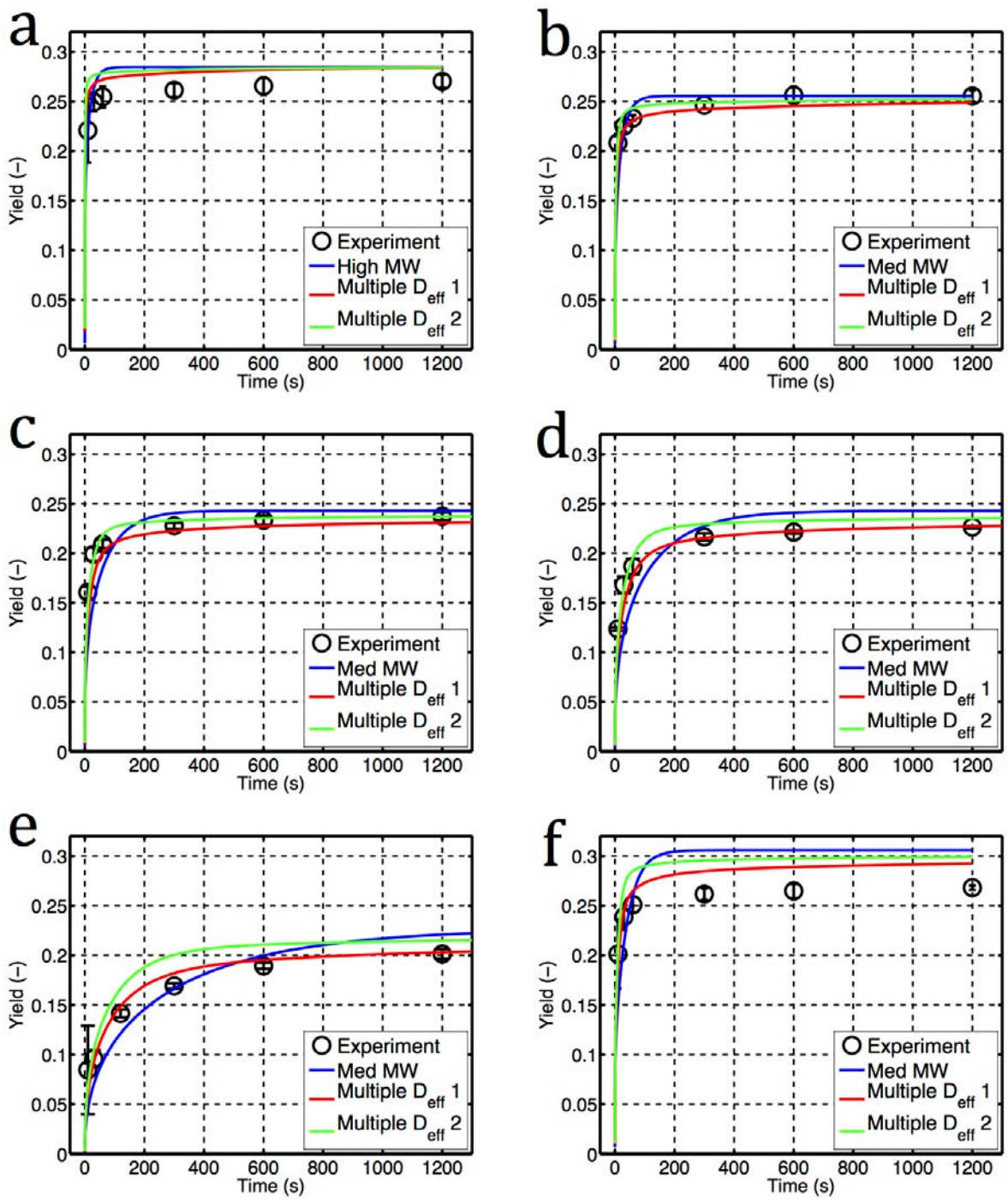

Figure 5.12: Extraction yield (y-axis) over time (x-axis) at a coffee-water relation of 25 $kg\ m^{-3}$, 80 $°C$, and K = 0.61 for multiple D_{eff} derived from microstructural measurements for each grind. The individual extraction curves showed in Figure 5.10 were rescaled with weights of the different fractions obtained from literature values (Table 5.5); (a) Ψ_B; (b) Ψ_E; (C) Ψ_F; (d) Ψ_G; (e) Ψ_H; (f) Flakes. Model (—); Experiments (Points)

From the qualitative point of view, it can be seen that when the effect of the different D_{eff} is taken into account, the simulated curve mimics the shape of the

experimental data. Assigning different weights to the curves obtained with the range of D_{eff} results in a global curve that reflects well the early time rise seen in the experimental extraction yield and its long time linear increase. From the quantitative point of view, in Figure 5.13 it can be seen how the calculated *MPE* values for the chosen weights considerably decrease (by approximately 50 %) with respect to the values obtained in the best D_{eff} case scenario.

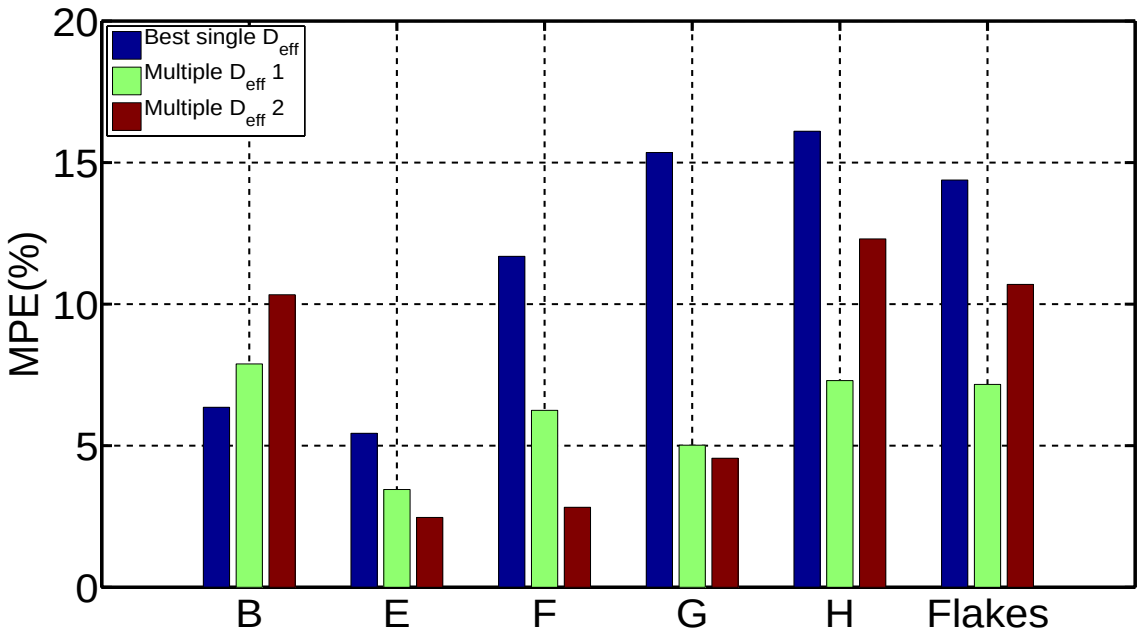

Figure 5.13: Mean Percentage Error (*MPE*) between the model simulations and the experimental data showed in Figure 5.12

Ψ_B and flaked coffee, showed a considerably greater maximum extraction yield as compared to the rest of the grinds. Due to their microstructure they may allow extracting higher quantities of the high and very high MW species. Consequently, it can be seen in Figure 5.12a and f, that using the same weights (that were measured in an extract with an extraction yield of 20 %) to rescale the curves as for the other grinds, it still results in poorer predictability of the long time points. As a matter of fact, in the case of Ψ_B better agreements were obtained when a single effective diffusion coefficient

(as estimated for the high MW species was considered). The maximum yield of Ψ_B and the flaked coffee resulted 23 % and 30 % higher respectively than that of Ψ_H. Therefore, with the aim of improving the agreement between the model and the experimental data, the weight assigned to the low MW category for these grinds was arbitrarily reduced by 23 % and 30 %, and the difference was added to the very high MW category. Figure 5.14 shows how adapting the percentage of the low and very high MW categories dramatically improves the agreement between the model and the experimental data. *MPE* of 3.2 and 4.5 % and 7.8 and 4.8% were obtained, which implies an approximate further 50 % reduction as compared to the use of a single D_{eff}.

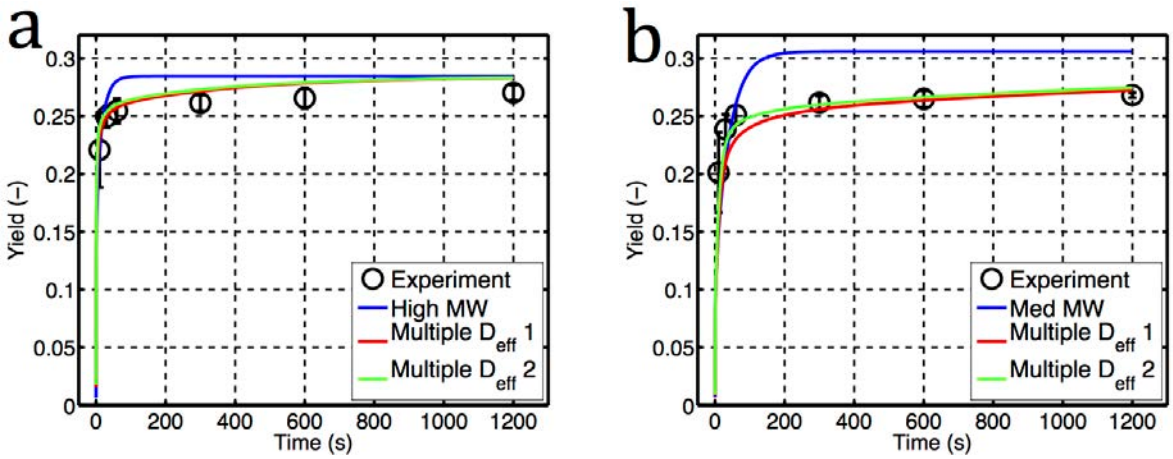

Figure 5.14: Extraction yield (y-axis) over time (x-axis) for the same conditions as in Figure 5.10 but with the following weights for the fractions: (a) Ψ_B: Multiple D_{eff}1: low MW = 55.5 %; Med and high MW: 10.6 %; Very high MW: 23.3 %; Multiple D_{eff}2: low MW = 68.7 %; med and high MW: 5.2 %; very high MW: 21.0 %; (b) Flakes: Multiple D_{eff}1: low MW = 52.5 %; Med and high MW: 10.6 %; Very high MW: 26.3 %; Multiple D_{eff} 2: low MW = 65.0 %; med and high MW: 5.2 %; very high MW: 24.7 %; Model (—); Experiments (Points)

5.8. Effect of temperature

Temperature is a relevant variable for coffee extraction as it modifies the solubility of the species, and their extraction rate through its effect on the effective diffusion coefficient of the species. At the consumer scale, the energy efficiency of the extraction methods, e.g. espresso, filter coffee, French press, is not a major concern and

thus the optimal extraction temperatures are decided based on the optimal sensory profile in the cup. However, at the industrial scale, the desired sensory profile of the extract is also coupled to the maximisation of the extraction yield whilst energy consumption is kept to a minimum, due to both economic and environmental reasons.

Therefore, to investigate the influence of temperature on extraction rate, experiments were carried out at 20, 50 and 80 $°C$ for Ψ_B and a coffee-water relation of $25\ kg\ m^{-3}$. D_{eff} values were derived with the *early time* approach as described in Section 5.6.1. From the results shown in Section 5.2 for the long-time extraction of Ψ_B at 20 and 50 $°C$, the system was assumed to have reached equilibrium by t = 1200 seconds (20 minutes). It must be also noticed that the experimental data used here represent the extraction yield coming only from the coarse size class. Note that if the relaxation times estimated for the fine size class estimated in Section 5.2 (1-8 seconds) are corrected to account for the effect of temperature (20 and 50 $°C$), with the Stokes-Einstein equation, at the first experimental point, i.e. t = 10 seconds, the fine size class was not extracted to equilibrium and thus the point was removed from this analysis. At 20 $°C$, the second point was removed as well. The considered maximum extraction yield for this coffee at 20 $°C$ (29.2 kg of soluble solids per 100 kg of RGC) and 50 $°C$ (31.6 kg of soluble solids per 100 kg of RGC) to be subtracted as the fine size class contribution and to calculate the contribution of the coarse size class was taken from the experiments used to estimated the partition coefficients (Chapter 4).

Figure 5.15 shows the simulated dimensionless extraction yield (y-axis) over the dimensionless time (x-axis) and the comparison with the experimental data, as normalised with the derived optimal D_{eff} values (Table 5.6). One can see that, in

dimensionless variables, and for the considered coffee-water relation of 25 $kg\ m^{-3}$, there is virtually no difference between the model predictions obtained with different partition coefficients (K *(80 °C)* = 0.61*; K (50°C)* = 0.57*; K (20 °C)* = 0.42) corresponding to the considered different temperatures.

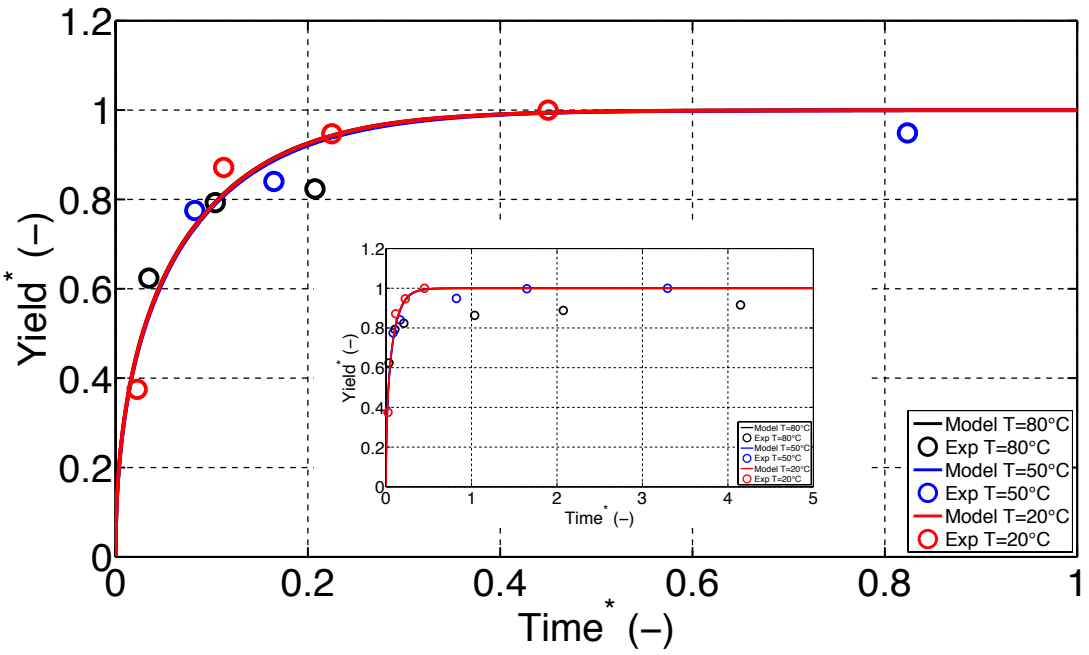

Figure 5.15: Dimensionless extraction yield (y-axis) over dimensionless time (x-axis) for the coarse size class of Ψ_B at 20, 50, and 80 °*C* and a coffee-water relation of 25 $kg\ m^{-3}$; K (80 °*C*) = 0.61; K (50 °*C*) = 0.57; K (20 °*C*) = 0.42. D_{eff} was fitted according to the early time approach; Model (—); Experiments (Points)

Table 5.6 also shows the ratios of D_{eff} at two temperatures calculated from the actual fitted value, and the theoretical as estimated from the Stokes-Einstein equation. When the temperature is increased from 50 to 80 °*C*, D_{eff} is expected to increase by a factor of 1.7, but experimentally it increased by a factor of 1.3. Increasing the temperature results in a increment of the extraction yield which in practice means the extraction of slower species and thus a smaller than expected D_{eff}. However, in the case of 80 and 20°*C* the experimental ratio is 2.7 times greater than the theoretical one. This

effectively means that the fitted coefficient at 20 °*C* is smaller than it would have been expected from a simple decrease due to a slower diffusion rate at lower temperatures.

Table 5.6: Fitted D_{eff} ($m^2\ s^{-1}$) at 20, 50 and 80 °*C*, comparative ratios and *MPE*

T (°C)	***D_{eff} (×10^{-11})***	***D_{eff} (80 °C)/ D_{eff} (T) fitted***	***D_{eff} (80 °C)/ D_{eff} (T) theoretical***	***MPE (%)***
80	1.9	1.00	1.0	10.6
50	1.3	1.3	1.7	3.3
20	0.21	9.3	3.5	2.1

Spiro and Chong, (1997) reported similar observations for caffeine extraction from RGC as they found hindrance values (*H*) of 11.1 at 80 °*C* and 29.7 at 25.5 °*C* (which is a comparable ratio to the one found here). Diffusion within the porous solid matrix is typically the limiting step in solid-liquid extraction processes (Aguilera, 2003). However, at lower temperatures (well below the usual temperatures used in coffee extraction), the rate of other steps may also become significant. Spiro attributed the increment of *H* at lower temperatures to a major tendency of caffeine to form complexes (thus bigger molecules) with, for example, chlorogenic acids, and the finite rate of detachment of caffeine from the bean matrix, i.e. dissolution and the greater tendency to be reabsorbed onto the matrix. Currently, the effect of temperature on the possible association between the coffee soluble solids is unknown. However, the latter effect is pointed out by the lower value of the solid-liquid partition coefficient derived for all the soluble solids, which was found to be in this work 0.61 at 80 °*C* as opposed to 0.42 at 20 °*C*. Additionally, the relaxation of the matrix structure, i.e. swelling, due to glass transition effects, was pointed out by Spiro as another potential factor contributing to this observed behaviour Spiro and Chong, (1997). However, according to Geiger et al., (2002), the phase transition from the glass to the rubbery state in coffee beans occurs at

ambient temperature, i.e. 20-25 $°C$, for a moisture content of approximately 20 g per 100 g of dry coffee. The measured moisture content measured at 20 $°C$ and 50 $°C$ ((1.4 ± 0.2) $\times 10^{-3}\ m^3\ kg^{-1}$, and (1.5 ± 0.2) $\times 10^{-3}\ m^3\ kg^{-1}$, respectively) (Chapter 4) is greater than 20 % (and comparable to the measured moisture at 80 $°C$). The phase transition can be expected to have also occurred in the kinetic experiments at 20° C.

5.9. Sensitivity study of the extraction model at the particle scale

The tested parameters for this sensitivity study are the number of considered size classes, the percentage of the fine size class, the effect of assessing the particle size distribution according to the *dry* or *wet* method, the coffee-water relation, and the solid-liquid partition coefficient.

5.9.1. Number of considered sizes

It is the objective of this Section to analyse the sensitivity of the simulations to the number of considered size classes. For that purpose, extraction simulations were carried out using the finest grind (Ψ_B)(T = 80 $°C$, K = 0.61, and D_{eff} = $8.4\times10^{-11}\ m^2\ s^{-1}$), assuming different numbers of the discrete size class to represent the whole particle size distribution. Ψ_B was chosen as its coarse size class is wider than that in coarser grinds (Chapter 4). In addition, the maximum effect of the fine size class on the $d_{[4,3]}$ of the distribution is expected on this particular grind, as the volume percentage of the fine class is maximum. When the grind was characterised by a single size class, the average parameters of the distributions ($d_{[3,2]}$, X_{50}, and $d_{[4,3]}$) were considered. For the multi-particle cases, since the transport in a fine size class of d = 40 μm was shown to be

remarkably fast, it was not subdivided in more size classes. The coarse size class was represented by either one particle size ($d_{[4,3]}$ or the value of the coarse peak) or more multiple particles. For the latter case, starting at the border delimiting the fine and the coarse regions (d = 100-105 μm), increments of approximately 300, 200 and 100 μm were considered. This resulted into the coarse size region divided in two (105-430 and 430-730 μm), three (105-300, 300-510, and 510-730 μm), and six intervals (150-210, 210-300, 300-430, 430-510, 510-610 and 610-730 μm), respectively. The size classes were considered to be represented by the mean of the considered intervals (Table 5.7).

Table 5.7: Discretisation of the continuously bimodal particle size distribution of the grinds into different number of size classes

Run	***Number of size classes (i)***	***Characterised by***	
		Size	***Percentage***
1	1	$d_{[3,2]}$ = 79.7 μm	100 %
2	1	X_{50} = 189.6 μm	100 %
3	1	$d_{[4,3]}$ = 198.8 μm	100 %
4	2	Fines	35.9 %
		$d_{[4,3]}$ = 198.8 μm	64.1 %
5	2	Fines	35.9 %
		Coarse peak (328.6 μm)	64.1 %
		Fines	35.9 %
6	3	*267.5 μm*	58.1 %
		580 μm	5.9 %
		Fines	35.9 %
7	4	202.5 μm	37.9 %
		405 μm	24.6 %
		620 μm	1.6 %
		Fines	35.9 %
		157.5 μm	18.1 %
		255 μm	19.8 %
8	7	365 μm	20.3 %
		470 μm	4.4 %
		560 μm	1.5 %
		670 μm	0.7 %

Figure 5.16 shows the simulations for the scenarios considered in Table 5.7. Using a single particle size ($d_{[3,2]}$, $d_{[4,3]}$ or X_{50}) to characterise the whole distribution results in notable differences in the evolution of extraction yield with time. $d_{[3,2]}$, which gives more weight to the finer sizes of the distribution, results in a faster predicted extraction as compared to $d_{[4,3]}$ or X_{50}. This emphasises the need for considering the different scales within the distribution in the model by including (at least) two size classes. For the runs where two size classes were considered, one can see that when the coarse size class is represented by the $d_{[4,3]}$ of the distribution, the resulting simulation

lies between the upper and lower cases of the one size class simulation: there is an early time rise of the extraction yield that flattens towards the equilibrium. When the coarse size class is approximated with the coarse peak, although one can see that the simulations also show the early time rise, it starts to flatten out before as compared to the $d_{[4,3]}$ case. One can see that, as a greater number of size classes are considered in the model (3, 4 and 7), the results of the simulations tend towards the case of two size classes with $d_{[4,3]}$ representing the coarse size class (baseline multi-particle case). The advantage of considering the $d_{[4,3]}$ (and not other parameter representative of the coarse size region, such as the value of the coarse peak) is that this parameter encompasses information of all the sizes forming the distribution. The disadvantage is that the $d_{[4,3]}$ of the distribution also contains information of the fine size class, which was accounted for independently. If more size classes were considered, the intervals would become smaller and, that would reduce the mean particle size representing the size class. The simulations would be then closer to the simulated curve with the baseline multiparticle case considering $d_{[4,3]}$. However, for the model accuracy that has been adopted in this Thesis (0.66 mesh elements per μm, generating an approximate error of 1 %), the computational time increased dramatically (40-fold) for the case of 7 size classes, which is certainly inconvenient from the practical point of view.

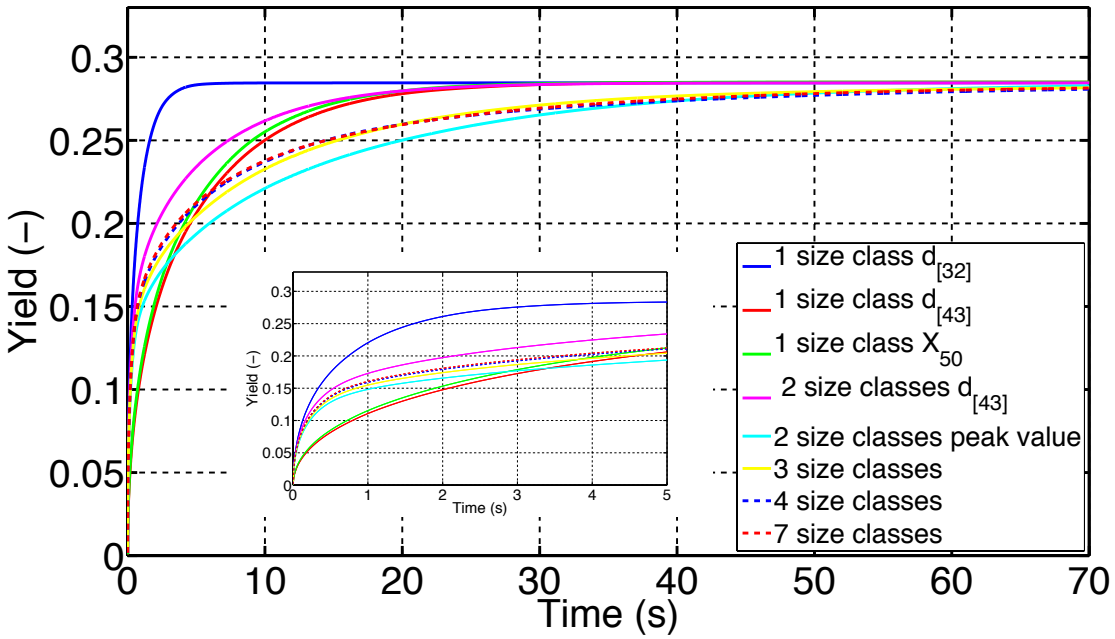

Figure 5.16: Sensitivity of the simulated extraction yield (y-axis) over time (x-axis) (coffee-water relation of 25 $kg\ m^{-3}$, 80 °C, and K = 0.61) to number of size classes considered in the model

5.9.2. The fine size class

Due to its size scale (d_{fine} = 40 μm), mass transfer in the fine size class is remarkably fast. Its abundance, at the cost of higher pressures in the packed beds (see Chapter 6), determines to a great extent the extraction yield at earlier times. This parameter is therefore of paramount importance in extraction techniques where the extraction time is considerably short, e.g. espresso coffee are typically prepared in a time scale of 10-30 seconds.

Extraction from Ψ_E (T = 80 °C, K = 0.61, and α = 25 $kg\,m^{-3}$, considering a fine and coarse size class parametrised from *dry* measurements) was simulated but modifying its original percentage of the fine size class (from 0 to 100 %). The value of D_{eff} used here was 7.3×10^{-11} $m^2\,s^{-1}$ as determined for Ψ_E from the microstructural measurements for

the medium molecular weight range. Ψ_E was chosen as its particle size distribution is typically used in espresso coffee extraction.

The impact of the fine size class can be appreciated in Figure 5.17. When 100 % of the fine size class is considered, i.e. monomodal distribution of particles with a d_{fine} = 40 μm, extraction yield reaches 0.25 in a matter of 1-2 seconds (green dotted line); when 0 % of the fine size class is considered, i.e. monomodal distribution of particles with a $d_{fine} = d_{[4,3]}$ of the distribution, extraction yield is only 0.05-0.06 at the same time point.

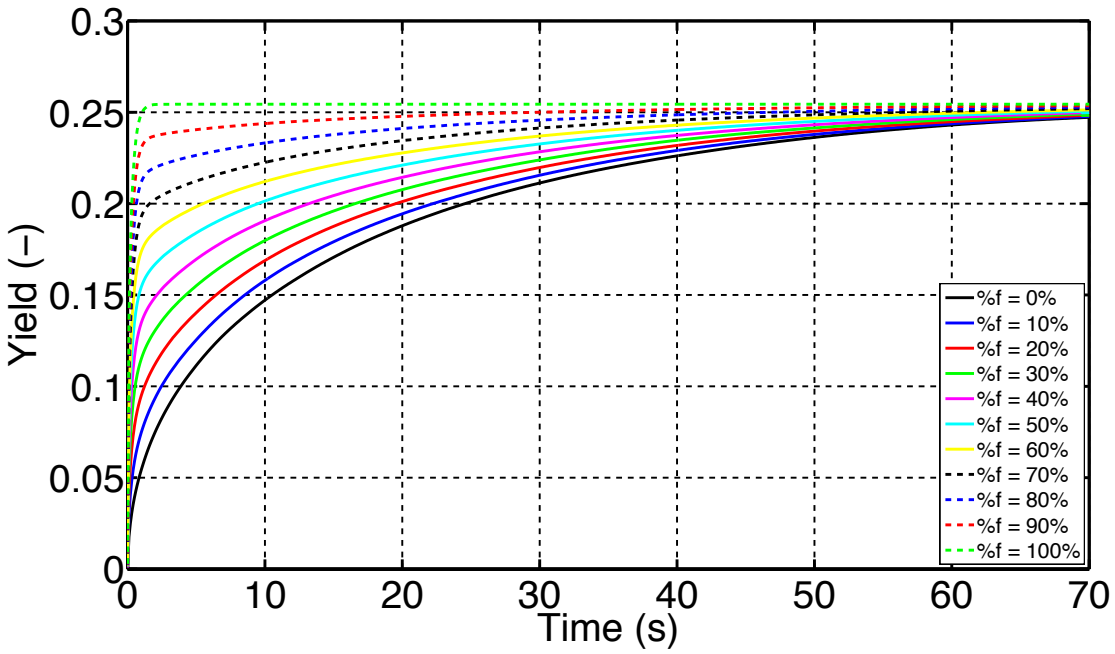

Figure 5.17: Effect of the % fine size class on extraction yield (y-axis) over time (x-axis). The simulations were performed for Ψ_E (T = 80 °C, K= 0.61, D_{eff}= 7.3×10^{-11} m^2 s^{-1} and a coffee-water relation of 25 kg m^{-3}) under the assumption of different % of the fine size class

For a coffee bean of certain mechanical properties, the relationship between the % of the fine size class and the value of the $d_{[4,3]}$ of the obtained particle size distribution depends on the design of the used grinder. For example, for Ψ_E (obtained with a disc grinder), its $d_{[4,3]}$ = 363.6 μm (*dry*) or 384.2 μm (*wet*), correspond to a percentage of the fine size class of 16.7 % and 29.7 %, respectively. With other types of grinder typically

used in the coffee industry, e.g. roller grinders, it may be possible to obtain similar $d_{[4,3]}$ values with a smaller percentage of fines. However, due to the heterogeneous coffee microstructure (formed by cells and cell walls), it is challenging to obtain radically different distributions, e.g. monomodal distributions, or distributions with a relatively coarse size class but higher percentage of the fine size class.

5.9.3. Particle size distribution measurement method

In Chapter 4, it was shown that the results provided by the *dry* and *wet* particle size distribution measurement methods notably differed in the case of $d_{[3,2]}$ and percentage of the fine size class, and, to a lesser extend in the case of $d_{[4,3]}$. The percentage of the fine size class (when *wet* measured) was found to be between 1.4 and 1.8 times the *dry* measured value. The sensitivity of the simulations due to the variation of this parameter and the $d_{[4,3]}$ is investigated here. The model at the particle scale was solved for Ψ_B and Ψ_E, the *dry* and *wet* set of parameters, and the usual set of conditions (T = 80 $°C$, K = 0.61, and a coffee-water relation of 25 $kg\,m^{-3}$); D_{eff} for the medium and high MW species were considered in the simulations. As expected, Figure 5.18 shows that when the *wet* values are considered, the simulation provides higher values of extraction yield due to the higher percentage of the fine size class. The effect of the *dry* and *wet* parameters (effectively considering a higher percentage of the fine size class) is sensitive to the value of the D_{eff}: at a given time, a higher percentage of the fine size class allows extracting a greater percentage of slow diffusing species. Therefore, to simulate extraction at the particle scale, the choice of the *dry* or *wet* method to parametrise the particle size distribution may be only relevant to the prediction of the high and very high MW species.

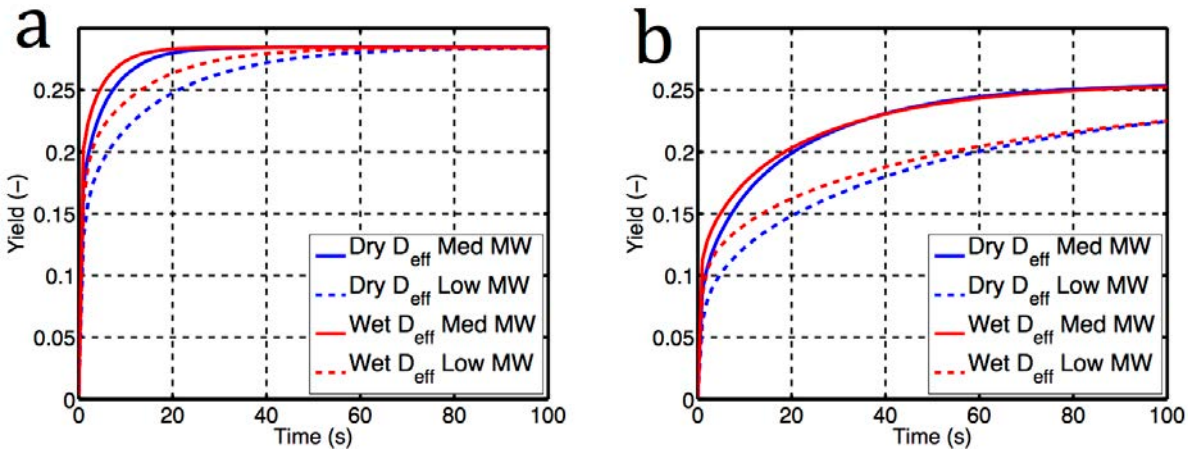

Figure 5.18: Simulation of the extraction yield (y-axis) over time (x-axis) with the distribution parameters ($d_{[4,3]}$ and % fines) as *dry* and *wet* measured. T = 80 °C, K= 0.61, and a coffee-water relation of 25 $kg\ m^{-3}$; (a) Ψ_B with D_{eff} = $8.5\times10^{-11}\ m^2\ s^{-1}$ (—) and D_{eff}= $2.9\times10^{-11}\ m^2\ s^{-1}$ (----); (b) Ψ_E with D_{eff} = 7.3×10^{-11} $m^2\ s^{-1}$ (—) and D_{eff} = $2.5\times10^{-11}\ m^2\ s^{-1}$ (----)

5.9.4. Coffee-water relation and partition coefficient

In the conducted stirred vessel experiments, a coffee-to-water relation of α = 25 $kg\ m^{-3}$ has been used in order to allow extraction proceeding until values closed to the maximum extraction yield, whilst keeping a not very concentrated system in order to measure the concentration of the samples accurately.

From the operational point of view, working with highly concentrated systems at the laboratory scale can be challenging. Some of the main experienced difficulties when working with more concentrated systems (α > 50 $kg\ m^{-3}$), lie, for example in magnetic stirring the system to achieve quick homogenisation, or developing a quick sampling method from the bulk solution to measure the concentration of the extract, due to constant syringe blockages.

Regarding the solid-liquid partition coefficient, a value of 0.61 has been used in all the simulations. This value, which represents an average of all the extractable soluble solids, was derived from the equilibrium experiments (Chapter 4) under the assumption

of non-swelling particles. However, due to the wide variety of MW, and the different chemical nature of the species forming the soluble solids, a distribution of solid-liquid partition coefficients is expected. Deriving the values for each of these individual species may be a challenging task: the variety of species is enormous and a great number of chemical analysis would be required; additionally, knowledge about the nature of some them (carbohydrates, melanoidins) is still very limited.

It is the aim of this Section to investigate the effect of the coffee-to-water relation and solid-liquid partition coefficients. For that purpose, extraction was simulated for Ψ_B and the D_{eff} for the medium MW as estimated from microstructural measurements. α values ranging from 10 $kg\,m^{-3}$ to 500 $kg\,m^{-3}$ were considered; these two limits represent a very diluted and a very concentrated system. In practice these ratios, translated to the stirred vessel set up used in this thesis, would mean extracting 5 g and 250 g in 500 ml, respectively. Note that it was taken into account in the simulations that part of the water originally in the bulk solution is absorbed by the coffee particles; this value was found to be 1.4×10^{-3} $kg\,m^{-3}$ for Ψ_B (Section 4.4.4). For the solid-liquid partition coefficient a range from 0.10 to infinite, i.e. no material remains inside the solid, was considered.

Figure 5.19 shows an example of the effect of the coffee-to-water ratio (α) on the kinetics of extraction, and the extraction yield achieved at equilibrium. For a coffee-water relation of 10 $kg\,m^{-3}$, one can see that the extraction yield eventually approaches the value of the maximum yield measured for Ψ_B (30.3 kg of soluble solids per 100 kg of RGC). For the range of α = 200-500 $kg\,m^{-3}$, it can be seen that the equilibrium is reached much faster as compared to smaller α. In the most concentrated case, i.e. a coffee-water

relation of 500 $kg\ m^{-3}$, the equilibrium is reached within 10-20 seconds after the extraction process commenced.

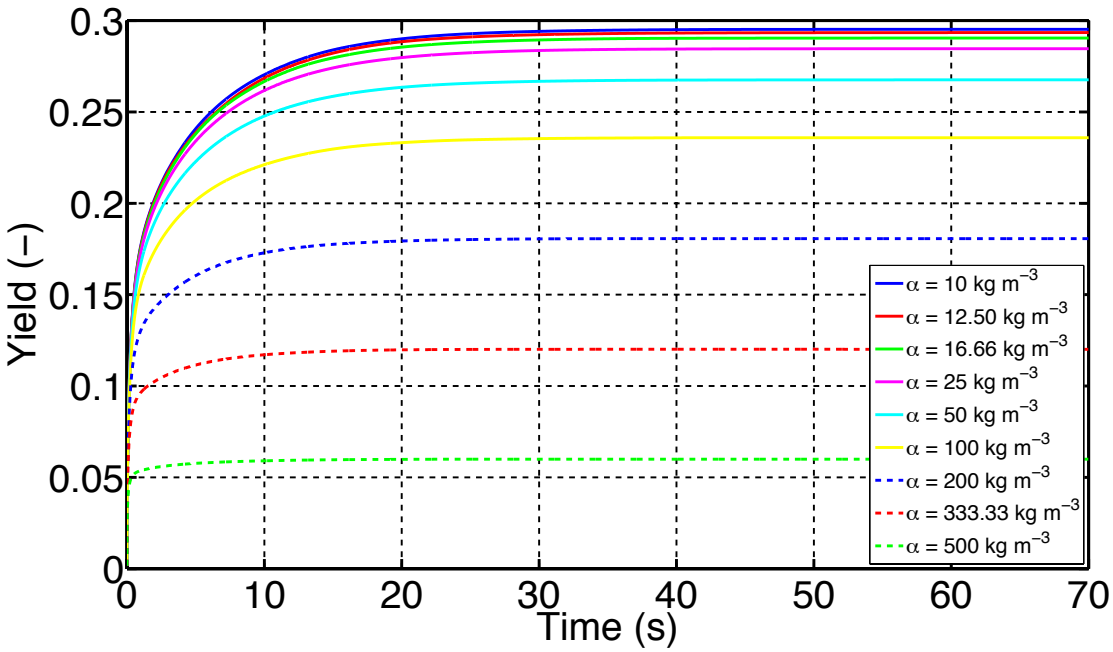

Figure 5.19: Effect of the coffee-to-water ratio (α) on the kinetics of extraction and the achieved equilibrium yield. The simulations were carried out for Ψ_B with the distribution parameters ($d_{[4,3]}$ and % fines) as dry measured, T = 80 °C, K = 0.61, and $D_{eff} = 8.5\times10^{-11}\ m^2\ s^{-1}$

Figure 5.20 shows the cumulative extracted mass normalised by the final extracted mass (at t = 70 seconds) (y-axis) over time (x-axis) for the fine and coarse size classes. The transport in the fine and coarse classes is coupled through their common bulk concentration boundary condition, and an effect of this coupling can be seen here: as expected from the estimated relaxation time for the medium molecular weight species (2.7 seconds), extraction in the fine size is remarkably fast. After the cumulative extracted mass from this size class reaches its maximum value, it starts decreasing until it reaches a plateau. Consequently, the peak value in the y-axis (M/M_{eq}) is greater than 1. This seems to indicate that the partial equilibrium reached by the fine size class with the bulk solution after 2-3 seconds after the beginning of extraction is shifted, and a portion

of the extracted mass is reabsorbed on these particles. This occurs because the transport in the coarse size class is considerably slower than in the fine size class. Thus, the concentration gradient between the surface of these particles and the bulk solution still allows material to be extracted (Figure 5.20b), consequently increasing the concentration of the bulk solution above the concentration at which the fine size class is partially equilibrated at that time. This effect is more pronounced for greater coffee-to-water ratio.

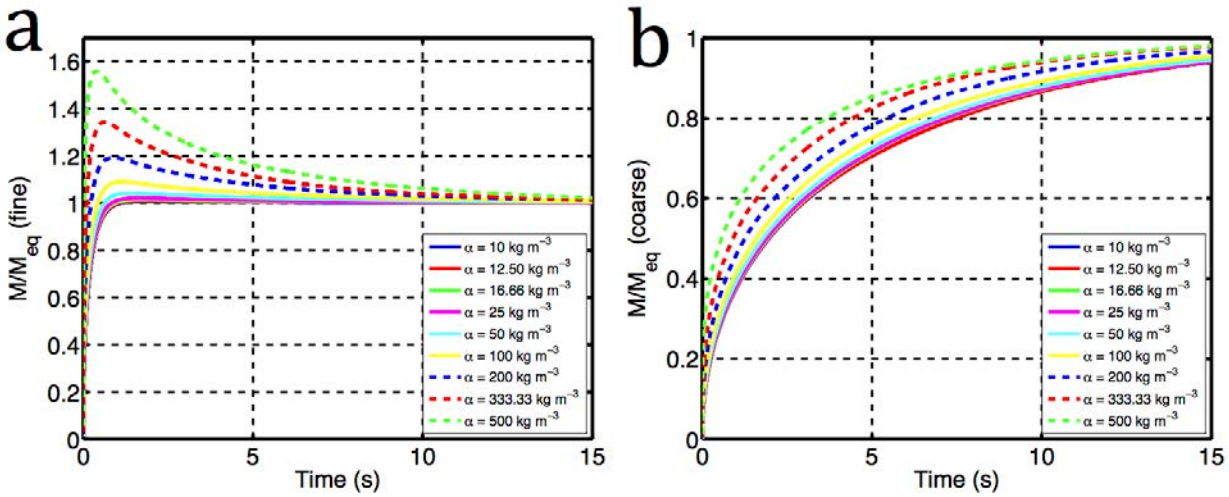

Figure 5.20: Cumulative extracted mass normalised by the final extracted mass (at t = 70 seconds) (y-axis) over time (x-axis) at different coffee-to-water ratios (α). The simulations were carried out for ΨB with the distribution parameters ($d_{[4,3]}$ and % fines) as dry measured, T = 80 °C, K = 0.61, and D_{eff}= 8.4×10^{-11} m^2 s^{-1}; (a) fine size class; (b) coarse size class

It was also noticed that for very high coffee-to-water relations i.e. 333.3 and 500 $kg\ m^{-3}$, the simulation of the extracted mass from the fine size class seems to be less accurate at earlier times for the number of mesh elements used in the simulations (0.66 per μm). At t = 0 the predicted cumulative extracted mass (which should be close to 0 %) resulted to be 2.9 % and 5.8 % for the aforementioned ratios. For more diluted systems, i.e. coffee-water relations of 10 and 25 $kg\ m^{-3}$, the value resulted to be around 1 %. This figure compares well with the average error estimated by comparing the analytical and numerical solution (obtained with 0.66 mesh elements per μm) for an infinite diluted

system (α = 0 $kg\,m^{-3}$) from the study of the optimal mesh size (Chapter 3). Refining the mesh in the fine size class to 1.22 and 1.98 elements per μm was shown not to be beneficial, as the cumulative extracted mass at t = 0 increased. However, it must be noticed that, although an independent study of the optimal mesh should be carried out to model very concentrated systems, the impact of this observation on the actual relevant outcome of the simulations (extraction yield) is attenuated as the cumulative mass extracted from each size class is multiplied by its volume percentage.

Figure 5.21 shows the extraction simulations at a coffee-to-water relation of 25 $kg\ m^{-3}$ and a range of different solid-liquid partition coefficient values from 0.10 to infinite. An infinite solid-liquid partition coefficient (no material remains inside the solid) effectively implies an infinite diluted system, as it generates a zero concentration at the boundary. One can see that, at the selected coffee-to-water relation, the extraction profile considerably differs for very low partition coefficients (K = 0.1, 0.2). However, as it increases, the difference between the profiles decreases. Thus, it can be considered that the approximation of considering an average partition coefficient of 0.61 is a good approximation for most species, except for those with very low partition coefficients.

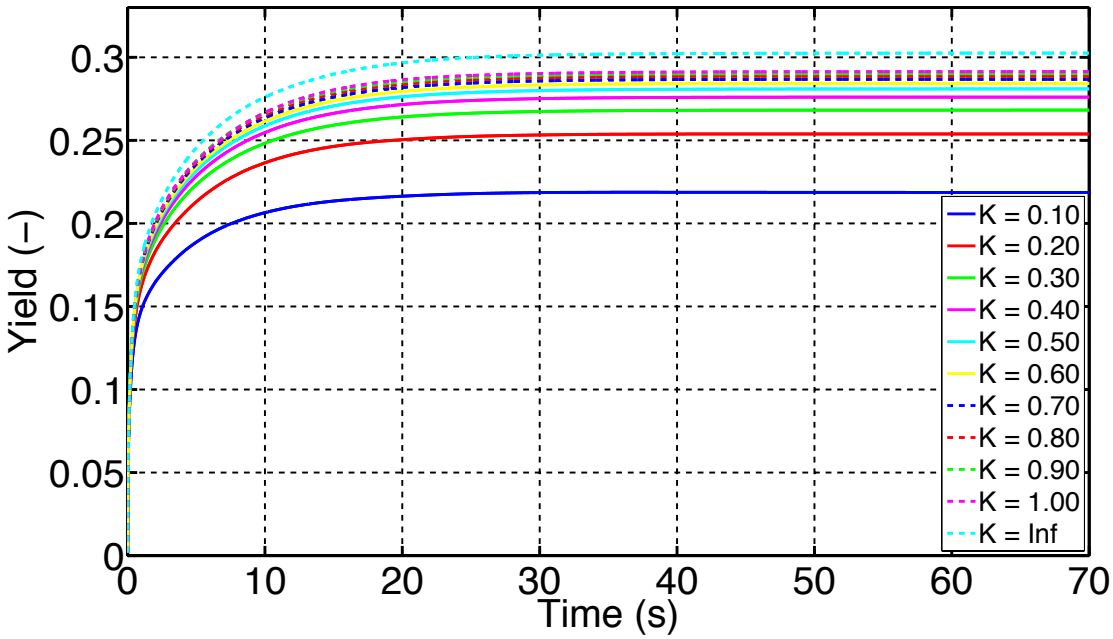

Figure 5.21: Effect of the partition coefficient (K) on the kinetics of extraction and the achieved equilibrium yield. The simulations were carried out for Ψ_B with the distribution parameters ($d_{[4,3]}$ and % fines) as *dry* measured, T = 80 $°C$, α = 25 $kg\ m^{-3}$, and D_{eff}= 8.5×10^{-11} $m^2\ s^{-1}$

In Chapter 4 the dependency of the estimated solid-liquid partition coefficient for all the soluble solids on temperature was studied. However, different dependencies for each individual species are expected. Despite the challenge that represents studying the solid-liquid partition coefficients of the individual species, it can be beneficial in various ways. For example, for coffee beans from different origins subjected to different roasting conditions, a more specific understanding of the thermodynamic behaviour of the species may assist in the determination of the extraction temperature profile to obtain optimal organoleptic profiles.

5.10. Conclusions

The kinetics of extraction of coffee soluble solids at the particle scale has been investigated in this Chapter for a variety of process parameters, using a combination of experimental and modelling approaches.

D_{eff} values were derived from the experimental kinetic data according to two different approaches: the *early time* approach and *long time* approach. The former was shown to provide values that were between the microstructural values estimated for the low and medium MW species (that are extracted at earlier times), whereas the latter provided D_{eff} values between the high and very high MW species. Simulations were obtained with the extraction model at the particle scale, considering two size classes (fine and coarse), and the derived microstructural D_{eff}. Comparison with the experimental data showed that, as it had seen before when fitting D_{eff} from the experimental data, the extraction curve of the soluble solids can not be fully described using a single effective diffusion coefficient. However, based on the simulation provided by the effective diffusion coefficient as estimated for the medium MW species (slight under and over-prediction at earlier and longer times, respectively), this option was considered to be the most appropriate for most of the grinds to model extraction using a single effective diffusion coefficient. To simulate the extraction of multiple species, weight values were assigned to the four MW categories defined and the individual simulated curves rescaled for all the grinds according to the literature. Excellent agreement was shown between the resulting curves (combination of the four individual ones) and the experimental data, if it is taken into account that no parameters were fitted in these simulations.

Chapter 6: Hydrodynamics of Coffee Packed Beds

6.1. Introduction

The most popular coffee extraction methods (espresso coffee, On-Demand systems, or soluble coffee production at the industrial scale) require a pressure gradient to drive hot water through a packed bed of roast and ground coffee (RGC). Therefore, the aim of this Chapter is to investigate the hydrodynamics of coffee packed beds.

Section 6.2 investigates the permeability at the steady state (flow rate and pressure drop are independent of time) of RGC packed beds typically used in espresso coffee extraction. The usual process parameters (particle size distribution, bed density, particle shape, temperature, and bed aspect ratio) are considered in the study. The steady state permeability is evaluated with a new measurement methodology developed using the custom extraction rig described in Chapter 3.

Section 6.3 compares the derived experimental steady state permeability values with the predictions obtained with the permeability models proposed Chapter 3. The parameters for the models ($d_{[3,2]}$ and bed porosity) were estimated from the experimental measurements presented in Chapter 4. After an analysis of the performance of the models, routes to improve their predictability are proposed.

Section 6.4 presents a brief analysis of the non-steady state and hypothesis to explain the observed behaviours are proposed.

Lastly, Section 6.5 closes the Chapter by presenting a summary of the findings and conclusions.

6.2. Steady state permeability

This Section investigates the effect of process parameters on the measured steady state permeability of RGC packed beds typically used in espresso extraction.

In order to reach the steady state, the beds were hydrated for 10 minutes at 80 $°C$ using a brewing chamber with an aspect ratio (diameter-length) of 2:1. After this time, it was observed that the RGC was virtually fully extracted: the extract showed a very light yellow colour (almost transparent), which indeed indicated the presence of soluble solids, but in a very low concentration. Thus, the measured permeability values in steady state correspond to that of extracted beds. This observation of soluble solids still being extracted after 10 minutes is in good agreement with the observed subtle linear increase in the extraction curves obtained in the stirred vessel set-up (Chapter 5).

Preliminary experiments showed that, upon the application of flow, the beds consolidated, i.e. their length decreased over time. The consolidation degree of the bed determines the value of the length that was used to calculate the steady state permeability values. Therefore, in spite of consolidation being a non-steady state process, consolidation results are reported and discussed in this Section.

6.2.1. Packed bed consolidation

The consolidation degree ($\Delta L/L_{initial}$) of the beds was measured at different time points with a caliper by gently disassembling the extraction cell of the rig as shown in Figure 3.9. The measurement was carried out at 80 $°C$ and in the diameter-length brewing chamber 2:1; both conditions are representative of typical espresso extraction.

The same hydrodynamic conditions used to hydrate the beds in order to achieve steady state conditions were used to study the consolidation of the beds.

Figure 6.1a-d show the estimates of the consolidation degree (*y*-axis) over time (*x*-axis) for beds made of Ψ_B -Ψ_E at the initial ρ_{bed} = 360 $kg\ m^{-3}$, 400 $kg\ m^{-3}$, and 480 $kg\ m^{-3}$. Consolidation degree was found to increase over time, but occurred predominately within approximately the first 20-30 seconds of applied flow. Consolidation has been reported to be dependent on the applied hydrodynamic conditions (Sivetz and Desrosier, 1979c). As a matter of fact, from preliminary hydration experiments it was observed that the application of higher hydrodynamic forces on unconsolidated, i.e. dry, beds could result in macroscopic cracks and holes in their structure. As reported by Hekmat et al. (2011), consolidation in beds typically used in chromatography results in a bed porosity decrease. This may be one of the underlying reasons to explain the reported flow rate-pressure dependency in espresso beds by Petracco (2005). In this work, it was observed that the average flow rate across the bed increased as the applied pressure was increased from 3 to 5 *bar*, but decreased when the pressure head was increased to 7 *bar*. This observation can be attributed to the consolidation of the bed.

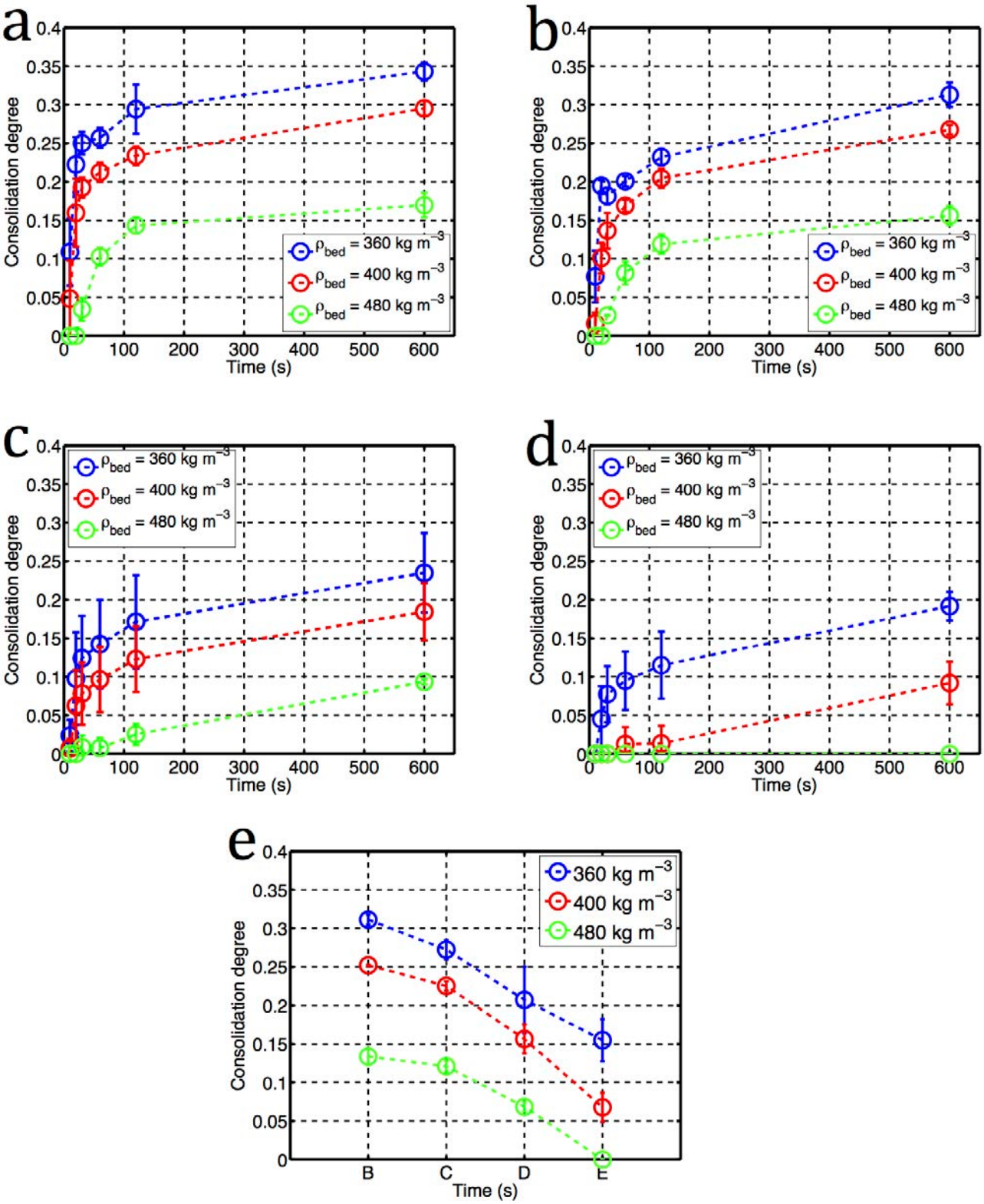

Figure 6.1: Consolidation degree (y-axis), as calculated with Eq. 3.22 over time (x-axis) for: (a) Ψ_B; (b) Ψ_C; (c) Ψ_D; (d) Ψ_E; hydrostatic pressures in the tank: $2.5\times10^5\,Pa$ for initial ρ_{bed} = 360 $kg\,m^{-3}$, $3.0\times10^5\,Pa$ for initial ρ_{bed} = 400 $kg\,m^{-3}$, and $4.5\times10^5\,Pa$ for initial ρ_{bed} = 480 $kg\,m^{-3}$, respectively; (e) steady state consolidation degree after 600 seconds as calculated with Eq. 3.24, at the initial ρ_{bed} = 360 $kg\,m^{-3}$, 400 $kg\,m^{-3}$, and 480 $kg\,m^{-3}$. The lines (----) are meant to guide the eye

The hydrostatic pressure used for beds of initial ρ_{bed} = 360 and 400 $kg\,m^{-3}$ was 2.5 and 3.0×10^5 Pa, respectively. Since the maximum hydrostatic pressure used in the collection of the steady state data is 4.5×10^5 Pa, an additional measurement of the length of these beds was taken after a minute at this hydrostatic pressure. It was observed that the length did not further decrease. Thus, at this point the beds were fully consolidated (steady state) for the tested range of hydrodynamic conditions.

Figure 6.1e displays the estimated steady state consolidation degree (y-axis) for the considered grinds (x-axis). It was found to vary from 0 % (Ψ_E with an initial ρ_{bed} = 480 $kg\,m^{-3}$) to 31 % (Ψ_B with an initial ρ_{bed} = 360 $kg\,m^{-3}$). It was also noticed that the consolidation degree, as measured directly from the length of the bed after 600 seconds resulted in lower values (between 1.2 and 2.3 fold) than those measured from the reduction of the length of the bed (see Figure 3.9). A more accurate methodology to measure consolidation rate and steady state consolidation degree may require the performance of flow experiments in a graduated cylinder.

From Figure 6.1e can be seen that coarser grinds were subjected to less consolidation under flow. This is consistent with the observations reported by Sivetz and Desrosier, (1979c), who stated that finer coffee grinds are intrinsically weaker and less resistant to compression. However, as later illustrated in Figure 6.4, the greater hydraulic resistance of beds made from finer grinds resulted in considerably greater hydrodynamic forces exerted on these beds. Therefore, in order to test this affirmation, an independent axial compression test was carried out with beds made out of the considered grinds. Figure 6.2 displays the achieved dry bed density (y-axis) as a function of the applied axial force (x-axis). The results are consistent with the observed

behaviour under flow: for the same applied force, coarser grinds compacted considerably less than finer grinds. Moreover, the measured forces in Figure 6.2 were found to be comparable to the range of 'few kilos' to 20 *kgf* (~196 *N*) typically applied on beds for espresso extraction, as reported by Petracco, (2005).

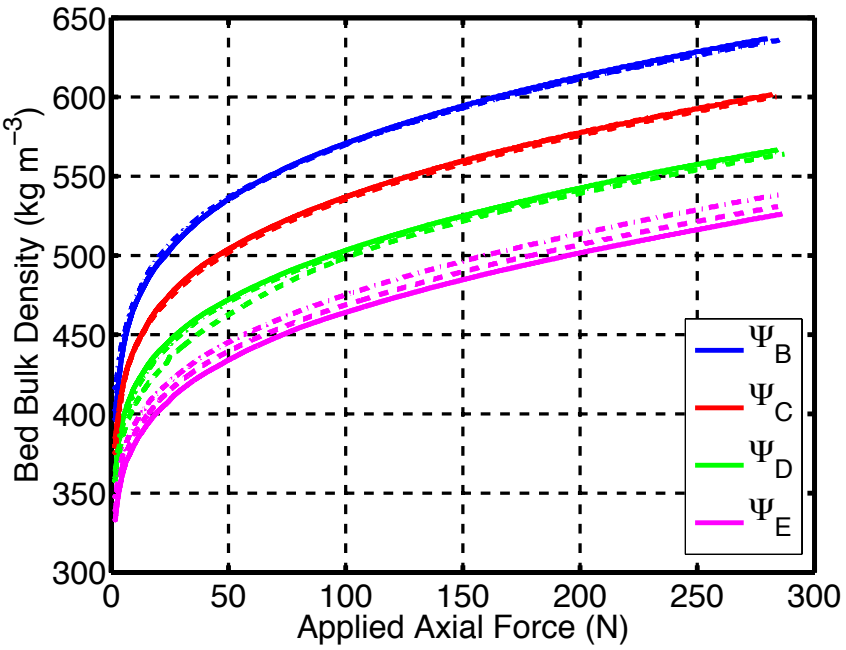

Figure 6.2: Bed density evolution (*y*-axis) as a function of the applied axial force on the beds (*x*-axis) for the considered grinds. The measurement on three independent samples is shown

Assuming a pressure drop across the bed equal to the maximum hydrostatic pressure in the tank (4.5×10^5 *Pa*), and for the used 2:1 diameter-length brewing chamber (cross-section area of $A = 1.1\times10^{-3}$ m^2), the maximum hydrodynamic force exerted on the beds was estimated to be 492 *N*. As it can be observed from Figure 6.2, this force was higher than the forces applied to pack the dry beds to the stated initial bed densities. Although the compressibility properties of dry and wet beds may differ, the application of hydrodynamic forces of this magnitude can be one of the causes leading to the observed consolidation.

The fact that the application of higher axial forces when packing RGC results in beds that are more stable under flow is something that is well-known by espresso coffee *aficionados* and professional *baristas*: an inappropriate (weak, uneven) tamping of bed can lead to undesired effects, such as channels (Petracco, 2005b). Also, it has been reported in the literature that the hardness of the used water plays a role in the consolidation degree of the bed. Fond (1995) found that both the required time to produce an espresso coffee (volume of 40 *ml*) and pressure increased from 27.5 to 42 seconds and from 6.4 to 12.8 *bar,* respectively, when tap water or softened water was used. All the aforementioned observations exemplify how poor control of the factors that determine the mechanical strength of the bed may result in non-optimal (higher or lower) flow rates. This can considerably impact the final quality of the beverage, as it is known that short and long times lead to under and over-extracted brews.

6.2.2. Influence of particle size distribution and bed bulk density

The effect of the particle size distribution on the steady state permeability of the bed was investigated at 80 $°C$ with RGC grinds typically used in espresso extraction (Ψ_B, Ψ_C, Ψ_D, and Ψ_E). In order to estimate the effect of the bed density, 7.2, 8.0 or 9.5 g of these grinds were packed in the 2:1 diameter-length brewing chamber ($V_{chamber}$ = 20 cm^3) to generate beds with initial ρ_{bed} = 360, 400 and 480 $kg\,m^3$, respectively.

The permeability of three independent samples of each grind was assessed, and the results subsequently averaged. Figure 6.3 shows an example of the best fit lines of the experimental steady state flow rate-pressure drop across the bed to Darcy's equation, i.e. Eq. 3.20 with Q as the independent variable; this particular case

corresponds to the three samples of Ψ_B packed at ρ_{bed} = 360 $kg\ m^{-3}$. All the linear regressions showed a goodness of fit (R^2) greater than 0.97. Each individual experimental point shown in Figure 6.3 corresponds to the average of the flow rate-pressure drop points of the last 30 seconds of each experiment, which in total lasted 60 seconds (see Figure 3.8). Consolidation of the bed (investigated in Section 6.2.1) was taken into account to calculate the steady state length of the bed used to derive the permeability.

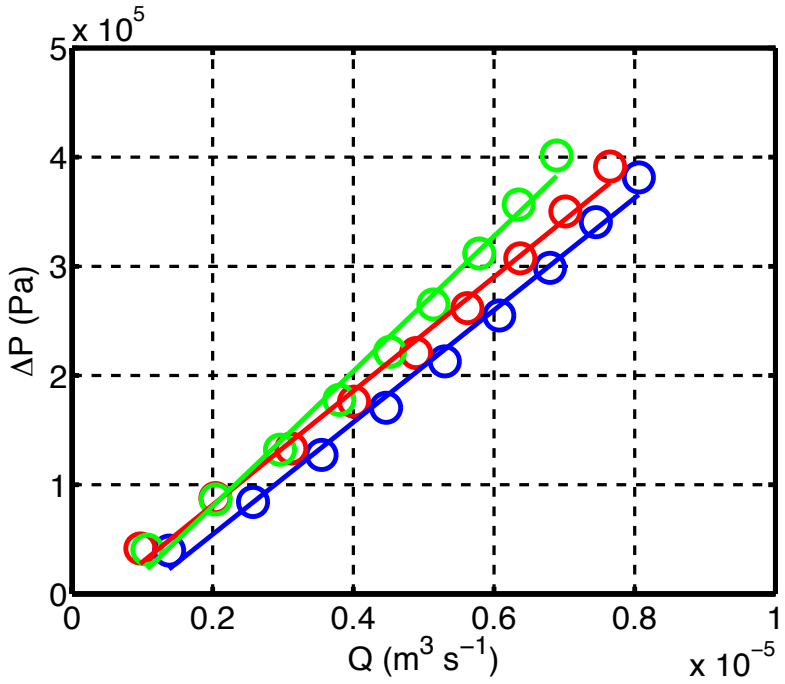

Figure 6.3: Flow rate (x-axis)–pressure drop (y-axis) for three independent samples of Ψ_B at the starting ρ_{bed} =360 $kg\ m^{-3}$. The solid lines (—) represent the best-fit lines (R^2 > 0.97 for all cases) from the data to Eq. 3.20, rearranged to make Q the independent variable. Permeability values were derived from each of the data set and subsequently averaged

For the sake of clarity, the experimental collected steady state flow rate-pressure drop is shown in Figure 6.4 as averages rather than as three individual data sets. One can see that the main source of variability in the data comes from the flow rate. Despite the applied standard packing procedure for the beds the resulting structure is intrinsically variable and heterogeneous. From the practical point of view, this results in

variable required times to produce a given volume of drink. For example, Andueza et al. (2007) reported times between 18 and 24 seconds to obtain 40 *ml* of beverage.

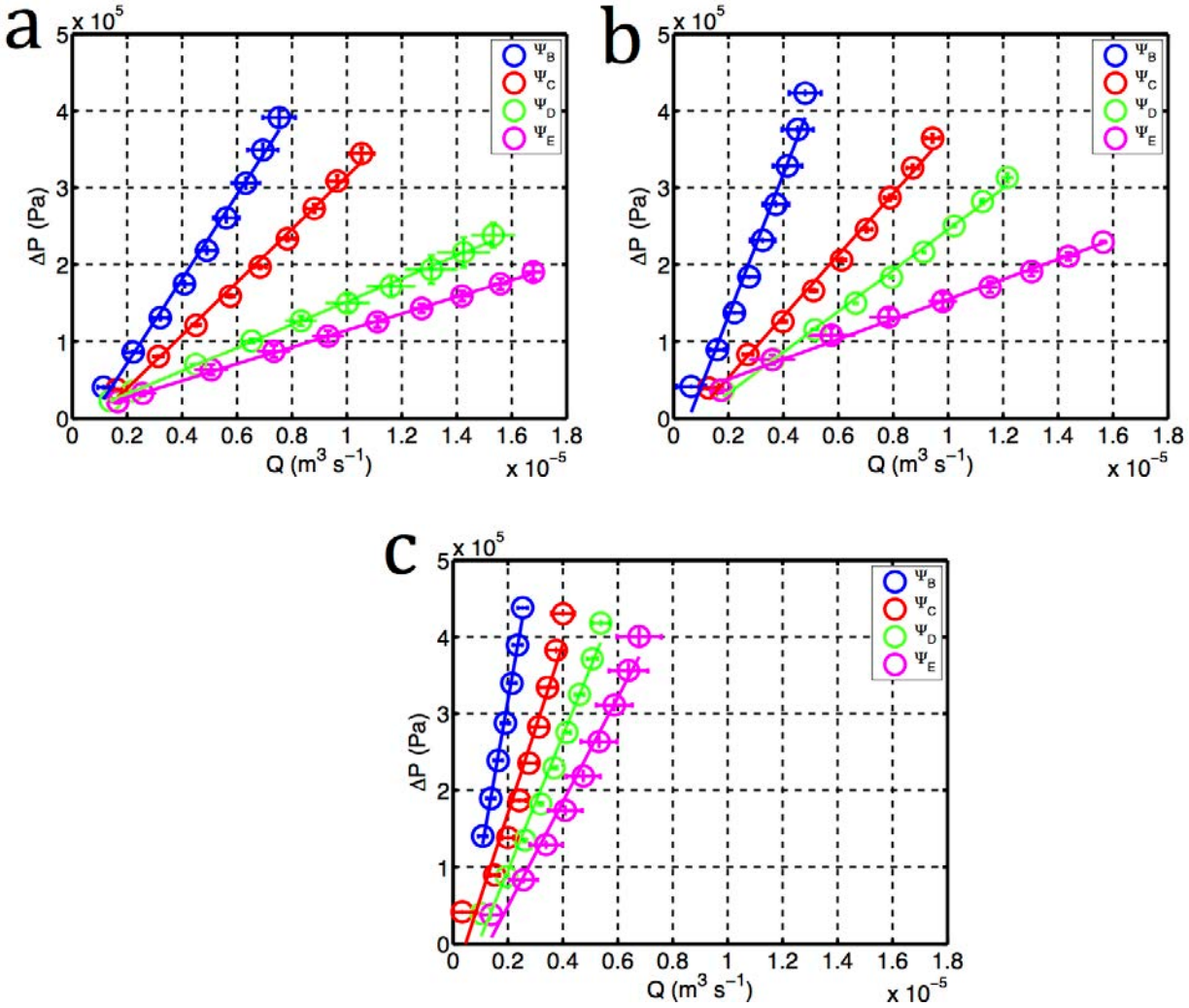

Figure 6.4: Average flow rate (*x*-axis) – pressure drop (*y*-axis) data at the initial ρ_{bed} = (a) 360 $kg\ m^{-3}$; (b) 400 $kg\ m^{-3}$; and (c) 480 $kg\ m^{-3}$

The Reynolds number of the beds (Re_p) was computed for the average flow rates shown in Figure 6.4. The relevant length scale of the beds to estimate Re_p is the diameter of the pores in the bed, which was estimated according to Eq. 6.1. The velocity of the fluid in a pore was calculated as the superficial velocity (Q/A) divided by the steady state porosity of the bed ($\varepsilon_{bed\ ss}$):

$$R_{pore} = \frac{\phi d_{[3,2]} \varepsilon_{bedss}}{3\left(1-\varepsilon_{bedss}\right)} \quad \text{Eq. 6.1}$$

Where R_{pore} is the radius of the pores of a given bed (m), Φ the measured sphericity of the particles (-), and $\varepsilon_{bed\,ss}$ the porosity of the bed corrected to account for consolidation (-); the values of the latter are given in Section 6.3.1. Re_p resulted to lie between 0.04 and 4. This confirms that, as already observed from the linearity of the experimental flow rate-pressure drop data (Figure 6.3, Figure 6.4), the flow is in the laminar regime ($Re_p \leq 10$) (Rhodes, 2008). Therefore, the inertial effects ($\Delta P_{bed} \propto Q^2$) can be neglected and the permeability of the beds can be derived from Darcy's law.

The derived permeability values (Table 6.1) were found to lie between 3.4×10^{-13} and 2.6×10^{-14} m^2, and are in good agreement with literature values (4.00×10^{-13} - 7.00×10^{-14} m^2 reported by King (2008) and Navarini et al. (2009)). As acknowledged by Navarini et al., the permeability value reported by Gianino, (2007) (2.3×10^{-12} m^2) seem to be underestimated, as it is one or two order or magnitude lower than values derived for similar systems.

Table 6.1: Experimental permeability estimated from Darcy's equation and the collected flow rate – pressure drop data

Grind	ρ_{bed} ***= 360 kg m^{-3}***	ρ_{bed} ***= 400 kg m^{-3}***	ρ_{bed} ***= 480 kg m^{-3}***
Ψ_B	$7.7 \pm 0.8 \times10^{-14}$ (a,b)	$4.9 \pm 0.3 \times10^{-14}$ (c)	$2.6 \pm 0.3 \times10^{-14}$ (d)
Ψ_C	$1.4 \pm 0.1 \times10^{-13}$ (e)	$1.2 \pm 0.1 \times10^{-13}$ (e)	$4.9 \pm 0.1 \times10^{-14}$ (c)
Ψ_D	$2.4 \pm 0.3 \times10^{-13}$ (f)	$1.9 \pm 0.1 \times10^{-13}$ (f)	$6.4 \pm 0.4 \times10^{-14}$ (b)
Ψ_E	$3.4 \pm 0.4 \times10^{-13}$ (h)	$4.4 \pm 0.4 \times10^{-13}$ (g)	$9.00 \pm 0.8 \times10^{-14}$ (a)

* Different letters indicate significant differences for different grinds and ρ_{bed}

An analysis of variance (ANOVA) was performed where the sources of variation were the grinds and the ρ_{bed}. A Tukey T-test was subsequently performed (risk level, α = 0.05). The statistical analysis was conducted in JMP 11®. As one can see from Table 6.1,

the estimated permeability values are overall significantly different across the tested grinds and bed density values. However, for Ψ_C and Ψ_D there is no signficant difference at the intial ρ_{bed} = 360 $kg\ m^{-3}$ and 400 $kg\ m^{-3}$. This may be due to the bed consolidation (Section 6.2.1) resulting in beds of a very similar structure at the steady state.

Across the whole range of data, the greatest to the smallest permeability ratio is 13. For a fixed pressure drop, the flow rate (and hence the water residence time and required extraction time to obtain a given volume of drink) would vary according to the permeability of the bed. Conversely, to achieve a given flow rate, the permeability determines the resulting pressure drop across the bed, and hence the pressure head that should be provided by the pumping device. This is of paramount importance for the design of brewers and industrial processes. Moreover, given the size scale of the industrial extraction columns used in soluble coffee manufacturing processes (typically several metres), the permeability of the beds may contribute significantly to the overall economic viability of the process.

The data also confirms the extreme sensitivity of permeability to bed density. An increment in the initial ρ_{bed} of approximately 30 % (360 to 480 $kg\ m^{-3}$), achieved by packing a bed with 2.3 extra grams, caused the permeability of the bed to decrease between 3 and 4 fold. The particle size distribution of the grinds has a much bigger effect on permeability when the initial ρ_{bed} was 360 and 400 $kg\ m^{-3}$ as compared to the 480 $kg\ m^{-3}$ case. For an initial ρ_{bed} = 360 $kg\ m^{-3}$, the permeability of the coarsest grind (Ψ_E) is 4.4 times that of the fine one (Ψ_B), whereas this ratio is reduced to 3.4 when it comes to initial ρ_{bed} = 480 $kg\ m^{-3}$. This becomes more obvious if the permeability values are plotted against $d_{[3,2]}$ (Figure 6.5).

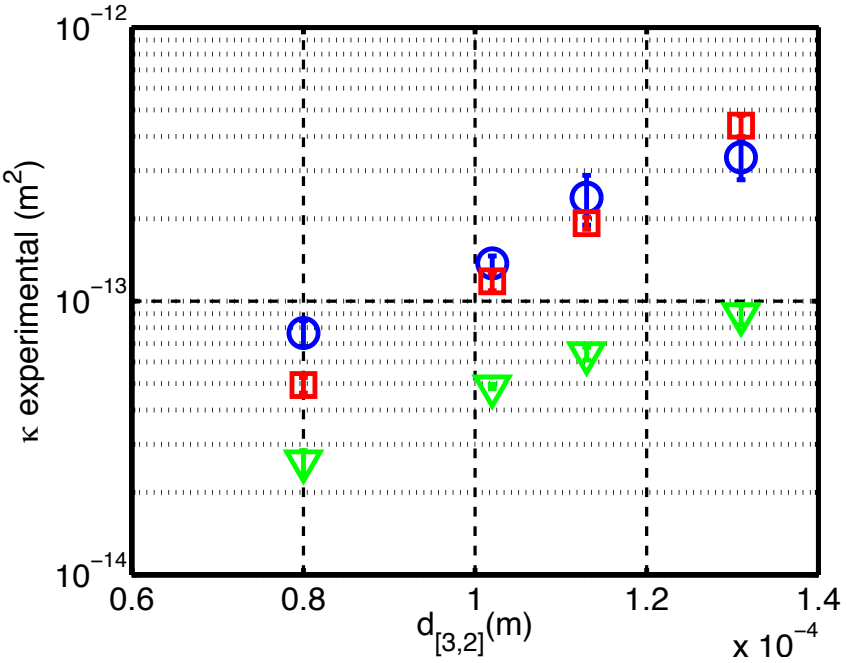

Figure 6.5: Dependency of experimental permeability (logarithmic *y*-axis) on $d_{[3,2]}$ (*dry* measured) (*x*-axis) for the initial ρ_{bed} = 360 (○), 400 (□), and 480 $kg\ m^{-3}$ (▽)

It is observed that the κ-$d_{[3,2]}$ dependency is different in the case of initial ρ_{bed} = 480 $kg\ m^{-3}$, and this becomes more obvious for coarser grinds. It has to be noted that, as shown in Figure 6.2, higher forces (especially for coarser grinds) were applied to obtain an initial ρ_{bed} = 480 $kg\ m^{-3}$, as compared to lower bed densities. Therefore, the different dependency may be explained due to a more dramatic modification of the initial dry packing structure of the bed caused by such forces.

6.2.3. Influence of particle shape: permeability of flaked coffee

The influence of particle shape on the steady state permeability of the bed was investigated at 80 $°C$ with flaked coffee (Blend 2). This grind was packed at initial ρ_{bed} = 400 and 480 $kg\ m^{-3}$ in the 2:1 diameter-length brewing chamber, and the permeability of these beds measured following the usual methodology.

Figure 6.6 compares the derived permeability values of flaked coffee (y-axis) to those obtained for RGC packed at the same initial ρ_{bed}. One can see that the experimental permeability for the flaked coffee resulted to lie between that estimated for Ψ_B and Ψ_C (Section 6.2.1). The $d_{[3,2]}$ of Ψ_B and the flaked coffee are of a comparable magnitude ($d_{[3,2]}$ = 79.7 μm for Ψ_B and $d_{[3,2]}$ = 83.6 μm for flaked coffee, as *dry* measured). Therefore, the reason for the greater permeability values of the former may be found in a greater porosity of the beds. For instance, for the beds packed at initial ρ_{bed} = 480 $kg\ m^{-3}$, the estimated initial bed porosity (before consolidation) resulted to be 0.41 for the flaked coffee and 0.28 for Ψ_B. In addition to this, less acute consolidation under flow was observed for the beds made of flaked coffee (8 % and 0 % for flaked coffee at 400 and 480 $kg\ m^{-3}$, respectively as compared to 25 and 13 % for Ψ_B).

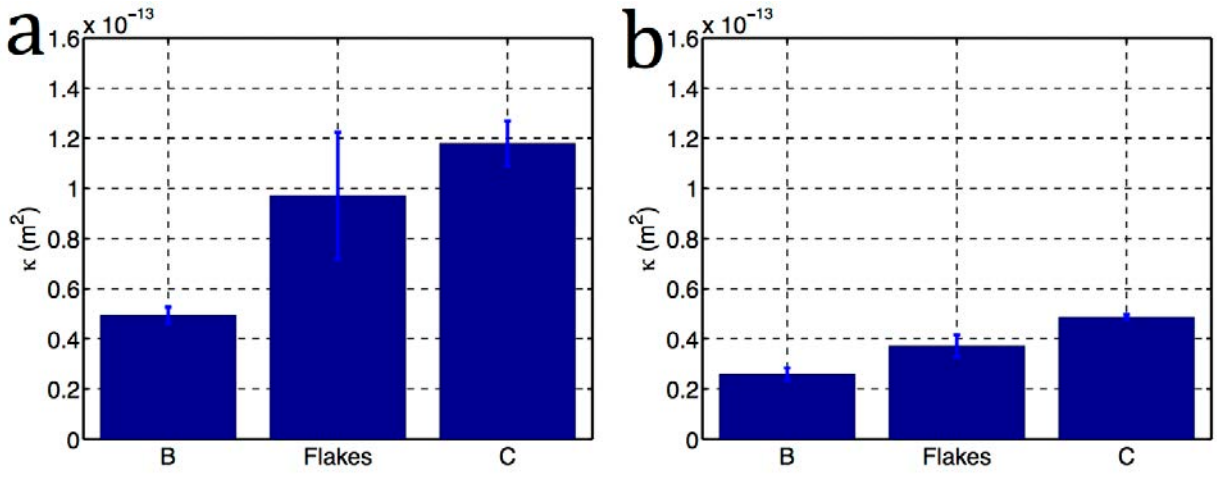

Figure 6.6: Experimental permeability (y-axis) for Ψ_B, Ψ_C, and flaked coffee; (a) initial ρ_{bed} = 400 $kg\ m^{-3}$; (b) initial ρ_{bed} = 480 $kg\ m^{-3}$

The observed behaviour for flaked coffee in this thesis may be summarised at this point as follows. From the kinetic point of view, their extraction rate was found to be comparable to that observed for the finest grind (Ψ_B) (Section 5.2). From the hydrodynamic point of view, flaked coffee resulted in beds of a greater permeability as

compared to that derived for finest grind. It can be then concluded that the use of flakes allows fast extraction, whilst potentially some of the typical difficulties (poor flow, high pressure requirements from the pumps) encountered when finer coffee grinds are used.

6.2.4. Influence of temperature

In order to investigate the influence of temperature, the permeability of Ψ_B at initial ρ_{bed} = 400 $kg\ m^{-3}$ was investigated at 15 $°C$. The measurement was carried out with the developed methodology. However, the beds were hydrated for 15 instead of 10 minutes, in order to ensure that steady state was achieved at this colder temperature. This time was chosen based on preliminary visual observations of the evolution of the flow rate over time at this temperature (Figure 6.24).

The derived permeability values at 15 and 80 $°C$ are displayed in Figure 6.7. The permeability at 15 $°C$ was greater as compared to 80 $°C$. This may be due to a more porous bed as a consequence of the observed lower bed consolidation degree (16 % at 15 $°C$ as compared to 25 % at 80 $°C$). It can be observed from Figure 6.7, that the experimental ratio between the permeability estimated at 15 $°C$ and 80 $°C$ is approximately 6. In order to check this hypothesis, the ratio was also estimated theoretically from Kozeny-Carman equation. The initial porosity of the bed was 0.36 as estimated from Eq. 3.19, ρ_{bed} = 400 $kg\ m^{-3}$, and a particle porosity of 0.53. Note that the actual measured particle porosity for Ψ_B was 0.50, and 0.53 represents the average of the measured porosity values for Ψ_B – Ψ_E. As will be shown in Figure 6.11, the average value seems to be more representative for the grinds than the actual measured individual values. Upon correction to account for the reported consolidation, the steady

state bed porosities resulted to be 0.15 (80 *°C*) and 0.24 (15 *°C*). This resulted in a theoretical ratio of 5.3, which compares well with the experimental ratio.

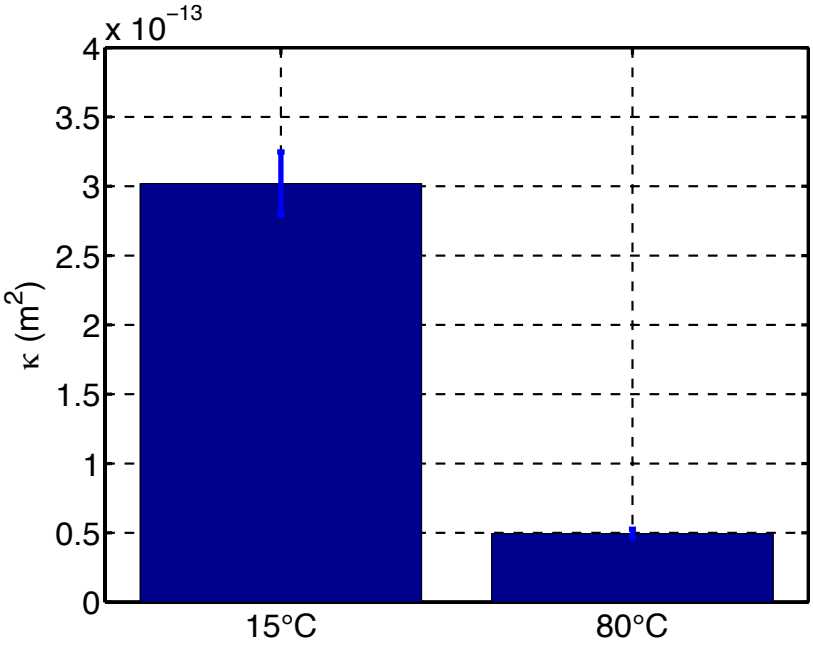

Figure 6.7: Experimental permeability (*y*-axis) for Ψ_B at the initial ρ_{bed} = 400 $kg\ m^{-3}$, and 15 *°C* or 80 *°C*

This difference in consolidation may stem from the intrinsic dependency of the mechanical properties of RGC on temperature. The extraction behaviour of roast and ground coffee at cold temperatures i.e. 20 *°C*, is shown in Chapter 5. It is observed there that the extraction rate, maximum extractable material, and solid-liquid partition coefficient considerable decreased at 20 *°C* as compared to 80 *°C*. In the case of extraction rate, the Stokes-Einstein equation predicts a decrease in the diffusion coefficient of a given species with temperature. However, the fitted effective diffusion coefficient at 20 *°C* was found to be lower than the theoretical value predicted by this equation. Amongst other causes (such as different physical-chemical interactions of the species at lower temperatures), this phenomenon has been attributed to the intrinsic dependency of the mechanical properties of RGC on temperature (that also results in less consolidation): grinds extracted at higher temperatures, i.e. 80 *°C*, swell thus

relaxing their microstructure and thus easing diffusion of the species (Spiro and Chong, 1997) .

The mechanical properties of the bed may also depend on the chemical composition of the partially extracted grinds, and this is also temperature-dependent. This dependency was pointed out by the observed decrease in extraction yield and partition coefficient with temperature. At 15 $°C$, the less soluble high and very high MW species (mainly carbohydrates polymers and melanoidins) are less likely to be extracted. Due to their considerably large size, these species (although not the most abundant in the grinds) surely contribute significantly to the mechanical strength of the particles. Conversely, since at higher temperatures these species are likely to be removed from the grinds, a decrease in the mechanical strength of the particles would be expected, contributing this to the observed greater consolidation degree. Along these lines, Sivetz and Desrosier, (1979) acknowledged that grinds extracted at atmospheric pressure to 20-25 % yield were more resistant to compression than grinds with an extraction yield (after a hydrolysis step) of 37 %. Furthermore, for the same extraction yield, they found that grinds that had been hydrolysed at higher temperatures were 'softer'.

6.2.5. Influence of bed aspect ratio

All the experimental permeability results presented so far have been derived using a 2:1 diameter-length brewing chamber. Therefore, in order to test the influence of the aspect ratio of the bed, the permeability of Ψ_B and Ψ_E at the initial ρ_{bed} = 480 $kg\ m^{-3}$ was investigated at 80 $°C$ using a diameter-length brewing chamber of 6:1. The volume of this chamber was the same as the 2:1 one, i.e. $V_{chamber}$ = 20 cm^3.

The measurement was carried out with the developed methodology to estimate the steady state permeability. However, the beds were hydrated in this case using a hydrostatic pressure in the tank of $1.5\times10^5\,Pa$, (as opposed to the $4.5\times10^5\,Pa$) in order to obtain similar flow rates. After the hydration step, the same range of hydrostatic pressures (4.5 - $1.5\times10^5\,Pa$) was selected in the tank. Since the only diffence between both extraction cells was just the brewing chamber, no calibration was carried out for the 6:1 brewing chamber and the one previously derived for the 2:1 brewing chamber (Chapter 3) was also used here.

The obtained average steady state flow rate-pressure drop across the bed data for Ψ_B and Ψ_E in the 2:1 and 6:1 brewing chambers is displayed in Figure 6.8. As expected, the slope of the flow rate-pressure drop is significantly greater in both cases when a 2:1 brewing chamber was used. The hydraulic resistance of the 2:1 beds is greater as their cross-section area is smaller and their length longer as compared to the 6:1 case.

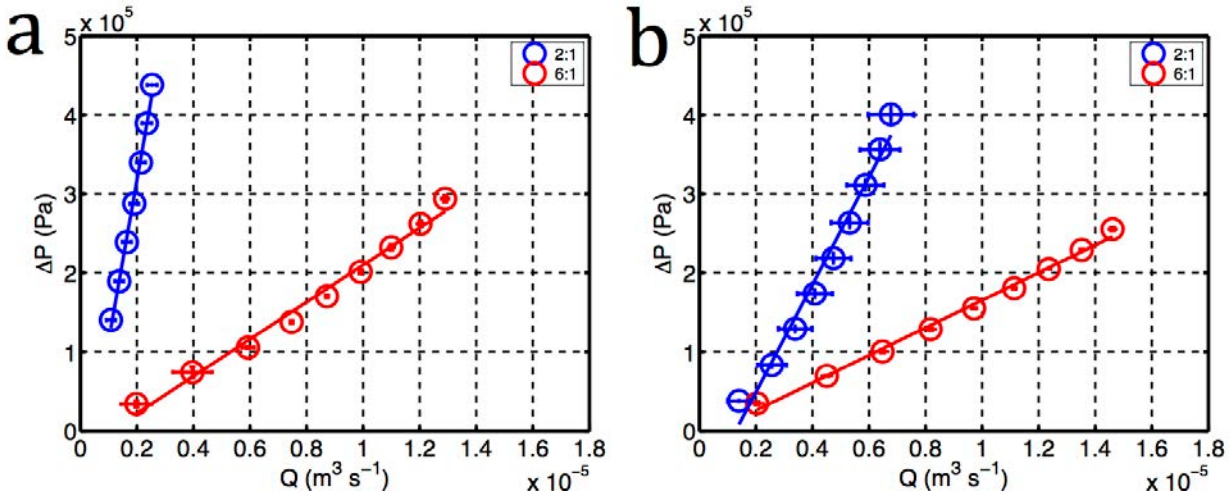

Figure 6.8: Average flow rate (x-axis) – pressure drop (y-axis) data at the initial ρ_{bed} = 480 $kg\ m^{-3}$ in 2:1 and 6:1 brewing chamber; (a) Ψ_B; (b) Ψ_E

Figure 6.9 shows the experimental permeability (y-axis) for the considered grinds as measured in the 2:1 and 6:1 brewing chambers. It can be seen that, whereas the permeability measured for Ψ_B resulted to be greater in the 6:1 brewing chamber, for Ψ_E the values are comparable. No bed consolidation was observed for any of the brewing chambers in the case of Ψ_E. However, for Ψ_B, the bed was observed to consolidate 13 % when a 2:1 brewing chamber was used (Figure 6.1b), but no consolidation was observed in the 6:1 case. The absence of consolidation in the case of Ψ_E is consistent with the greater stability provided by the required higher axial forces to pack the beds (Figure 6.2) and the lower hydrodynamic forces exerted on the coarser grinds. In the case of Ψ_B, the reduction in consolidation when moving from a 2:1 to a 6:1 brewing chamber is consistent with the lower hydrodynamic forces exerted on the bed for the latter case (Figure 6.8a). As mentioned in Section 6.2.1, consolidation is sensitive to the magnitude of the applied hydrodynamic forces; in turn, these are dependent on the geometric characteristics of the bed. In this case, it can be observed from Figure 6.9, that the experimental ratio between the permeability for Ψ_B in the 6:1 and 2:1 brewing chambers is approximately 3. However, applying the same methodology explained in Section 6.2.4, the theoretical ratio resulted to be 10.6. A hypothetical consolidation value of 8 % (as opposed to the observed 0 %) for Ψ_B in the 6:1 brewing chamber is required to match the observed experimental ratio of 3.

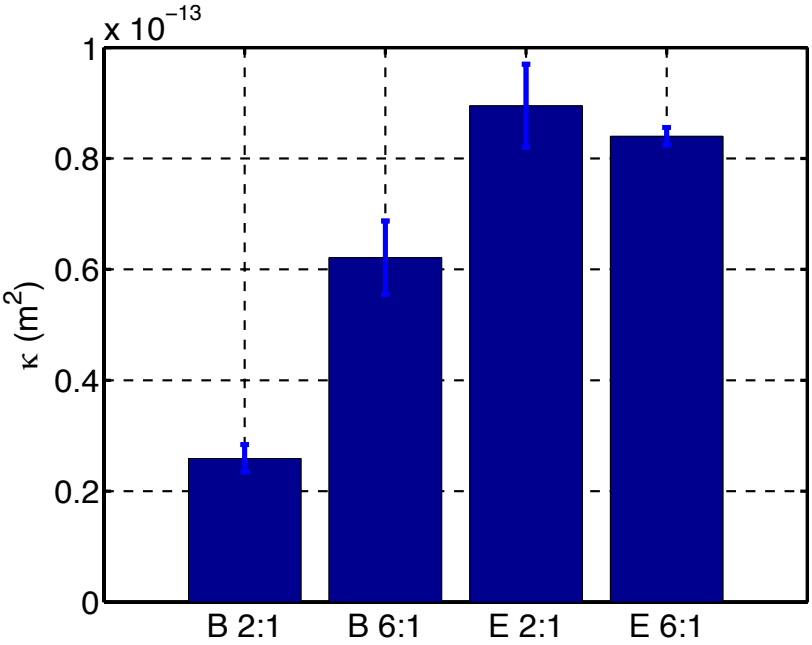

Figure 6.9: Experimental permeability (y-axis) for Ψ_B and Ψ_E at the initial ρ_{bed} = 480 $kg\ m^{-3}$, as measured in a 2:1 or 6:1 diameter-length brewing chamber

This illustrates that the design of the brewing chamber is a relevant parameter to extraction performance. Using brewing chambers of higher aspect ratio not only reduces the hydraulic resistance of the beds because of its greater and lower cross-section area and length, respectively, but also through the milder effect of the generated hydrodynamic forces on the bed packing structure (and thus on its permeability). Therefore, by adjusting the aspect ratio, beds of a lower permeability (finer grinds and/or greater bed densities) could be then used to obtain benefits provided by such beds (higher extraction rates and mechanical stability) whilst avoiding the associated hydrodynamic problems.

In this respect, it may be convenient from a practical point of view to derive the relationship between the pressure drops produced by a grind (packed at a given bed density) and the aspect ratios of the beds in which it is packed. Thus, for a given flow rate through a bed of permeability κ, the relationship between the pressure drop (ΔP_{bed})

produced when RGC is packed in two beds (*1* and *2*) of the same volume but different aspect ratios can be expressed from Darcy's law as follows:

$$\frac{\Delta P_{bed1}}{\Delta P_{bed2}} = \frac{L_1}{L_2}\frac{A_2}{A_1} \qquad \text{Eq. 6.2}$$

Where L is the length of the bed (m) and A its cross-section area (m^2). When the brewing chamber is fully filled with coffee, the length of the bed equals the length of the brewing chamber. The length of the bed can be thus expressed as a function of the diameter-length ratio of the chamber ($\alpha_{chamber}$); applying this to Eq. 6.2 results in:

$$\frac{\Delta P_{bed1}}{\Delta P_{bed2}} = \frac{\alpha_{chamber2}}{\alpha_{chamber1}}\frac{R_2}{R_1} \qquad \text{Eq. 6.3}$$

Where R is the radius of the brewing chamber (m). If it is now imposed that the volume of the brewing chambers must be the same, the following relationship is obtained:

$$\frac{R_2}{R_1} = \left(\frac{\alpha_{chamber2}}{\alpha_{chamber1}}\right)^{1/3} \qquad \text{Eq. 6.4}$$

Substituting Eq. 6.4 into Eq. 6.3, the relationship between the pressure drops for beds of and the diameter-length ratios of the beds with the same volume is given as follows:

$$\frac{\Delta P_{bed1}}{\Delta P_{bed2}} = \left(\frac{\alpha_{chamber2}}{\alpha_{chamber1}}\right)^{4/3} \qquad \text{Eq. 6.5}$$

Eq. 6.5 was plotted for a range of $\alpha_{chamber\,2}/\alpha_{chamber\,1}$ and the results are shown in Figure 6.10. For the actual experimental case investigated here ($\alpha_{chamber\,2}/\ \alpha_{chamber\,1}$ = 3), one can see that the predicted ratio of pressure drops is 4.3. The experimental pressure drop ratio may be obtained by multiplying Eq. 6.5 by the derived experimental permeability of the beds (κ_2/κ_1). The ratio resulted 10.37 for the case of Ψ_B and 4.06 for Ψ_E. It can be noted from Ψ_E, that in the absence of bed consolidation, the observed experimental value is comparable to that predicted by Eq. 6.5. However, when the use of different brewing chamber results in different consolidation degrees (Ψ_B), Eq. 6.5 underpredicts the experimental value.

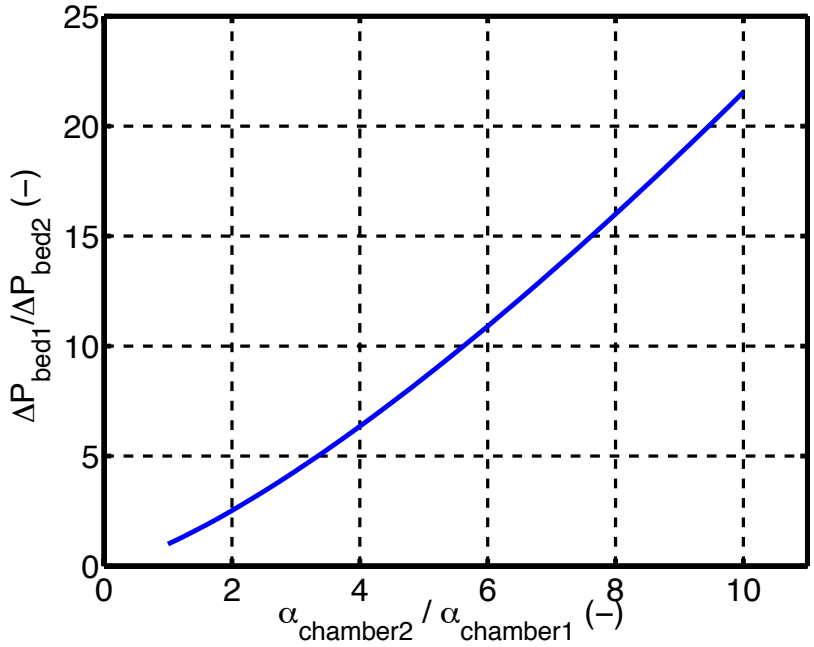

Figure 6.10: Ratio of pressure drops in two packed beds of equal permeability (y-axis) as a function of their diameter-length aspect ratios of the brewing chamber (x-axis)

6.3. Comparison of the predicted and experimental permeability

The aim of this Section to investigate how the theoretical permeability models proposed in Chapter 3 can predict the experimental values (Table 6.1) derived for the grinds produced from Blend 1 (Ψ_B - Ψ_E). Model 1 corresponds to the well-known Kozeny-Carman equation; Model 2 is an extension of Model 1 that includes an empirical dependency of bed tortuosity on bed porosity.

6.3.1. Parametrisation of the permeability models: bed porosity and $d_{[3,2]}$

In the theoretical permeability models, the packing structure of the bed is accounted for by the bed porosity and particle size. From the hydrodynamic point of view, the relevant average size parameter of the particle size distribution of the grinds is $d_{[3,2]}$. The particle size distribution was assessed according to the *dry* and *wet* methods described in Section 3.3.2, and significant differences in the $d_{[3,2]}$ values were found; the discussion of this results can be found in Section 4.2.1. Values of $d_{[3,2]}$ obtained with both methodologies will be implemented in the permeability models and the resulting predictions compared.

The corresponding bed porosity for each bed density was estimated from Eq. 3.19 with the experimentally determined intrinsic density (Section 4.3.1), and particle porosity values for each grind of Blend 1 (Section 4.3.1). The steady state bed porosity was obtained by correcting the estimated bed porosity as per Eq. 3.25 in order to account for a reduction due the observed bed consolidation (Figure 6.1e).

Figure 6.11a shows the estimated steady state bed porosity (*y*-axis) as a function of the $d_{[3,2]}$ (*dry* measured) of the grinds. It can be seen that the results obtained for Ψ_B (estimated $\varepsilon_{particle}$ = 0.50) and Ψ_E (estimated $\varepsilon_{particle}$ = 0.57) are quite comparable; the results for Ψ_C (estimated $\varepsilon_{particle}$ = 0.57) and Ψ_D (estimated $\varepsilon_{particle}$ = 0.50) are (in comparison) considerably lower and greater, respectively. It can be deduced from this that the derived steady state bed porosity is quite sensitive to the estimated values of particle porosity. The general trend of the particle porosity values for the 8 grinds produced from Blend 1 (see Figure 4.14) is considered now. According to the observed tendency, either the values of Ψ_B and Ψ_D are lower, or conversely the values of Ψ_C and Ψ_E are greater than expected. Steady state bed porosity was therefore also estimated using the average particle porosity of the four considered grinds, i.e. 0.53, and the results are displayed in Figure 6.11b. It can be seen that the steady state bed porosity follows now an increasing tendency with $d_{[3,2]}$ since coarser grinds experienced less consolidation under flow (Figure 6.1). Both sets of porosity values will be implemented in the permeability models to evaluate the resulting predictions.

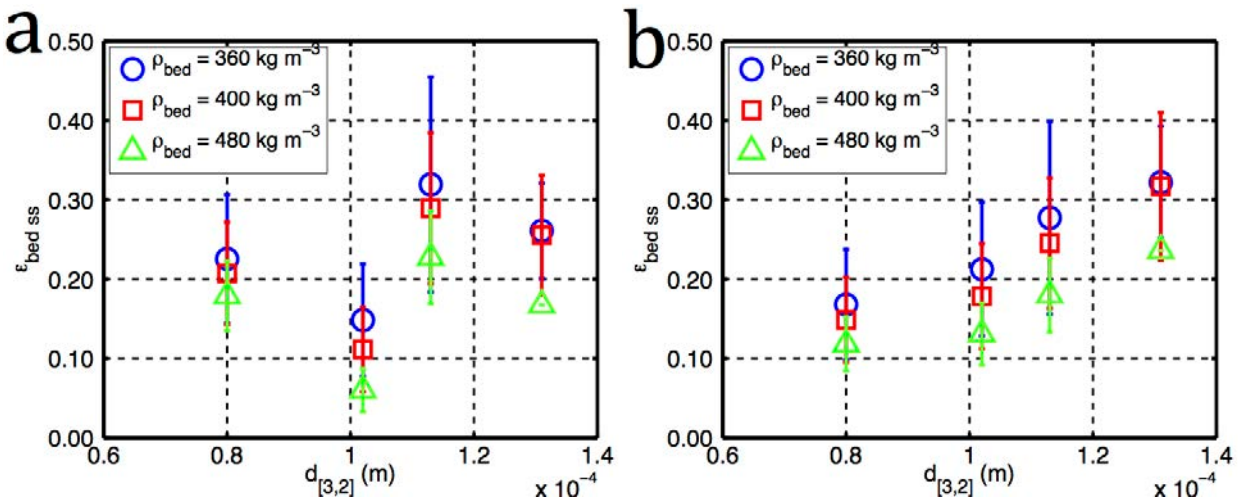

Figure 6.11: Steady state bed porosity (*y*-axis) vs. $d_{[3,2]}$ (*dry* measured) of the considered grinds; (a) as determined from the estimated particle porosity values (Figure 4.14); (b) as determined from the average of the particle porosity values (0.53)

In Section 4.2.4, estimates of bed porosity (packed at the tapped density) were obtained from the results of the linear mixing model applied to two log-normal distributions of equal standard deviation (Yu and Standish, 1993) (Table 4.4). The values were found to be 0.24 to 0.26, and followed an increasing tendency with grind size. The estimates qualitatively agree with the observed tendency of the tapped density (see Figure 4.12). However, from the quantitative point of view, they are lower than those estimated from particle porosity measurements (Figure 6.11). If the values derived with the linear mixing model were corrected for the actual density at which the beds were packed (greater than tapped density) and bed consolidation some of the resulting steady state porosity values would be negative. The limitations of this model applied to coffee grinds were discussed in Section 4.2.4

6.3.2. Steady state permeability predictions with $d_{[3,2]}$ *dry* measured

The *dry* measured $d_{[3,2]}$ values were firstly implemented in Model 1 and Model 2 (with a tortuosity exponent n = 0.5) with both steady state bed porosity data sets (Figure 6.11a and b).

Figure 6.12 shows the comparison of the theoretical permeability (y-axis) and the experimentally measured values (x-axis) (Table 6.1). Regarding the influence of the chosen steady state bed porosity, when the values estimated from the actual measured particle porosity (Figure 6.11a) are implemented, both models underestimate the permeability of Ψ_C significantly (Figure 6.12a and c). However, in the case of the steady state bed porosity values estimated with the average particle porosity (Figure 6.11a b),

Model 1 overestimates all the permeability values, whereas Model 2 underestimates for Ψ_B and Ψ_C, and overestimates for Ψ_D and Ψ_E. In the latter case, the agreement between the experimental and theoretical values considerably improves and Ψ_C does not appear to be an outlier (Figure 6.12b and d). Based on these observations, the latter the steady state porosity values (Figure 6.11a b) will be adopted for the rest of the predictions unless otherwise stated. Thus, only Figure 6.12b and d will be further discussed.

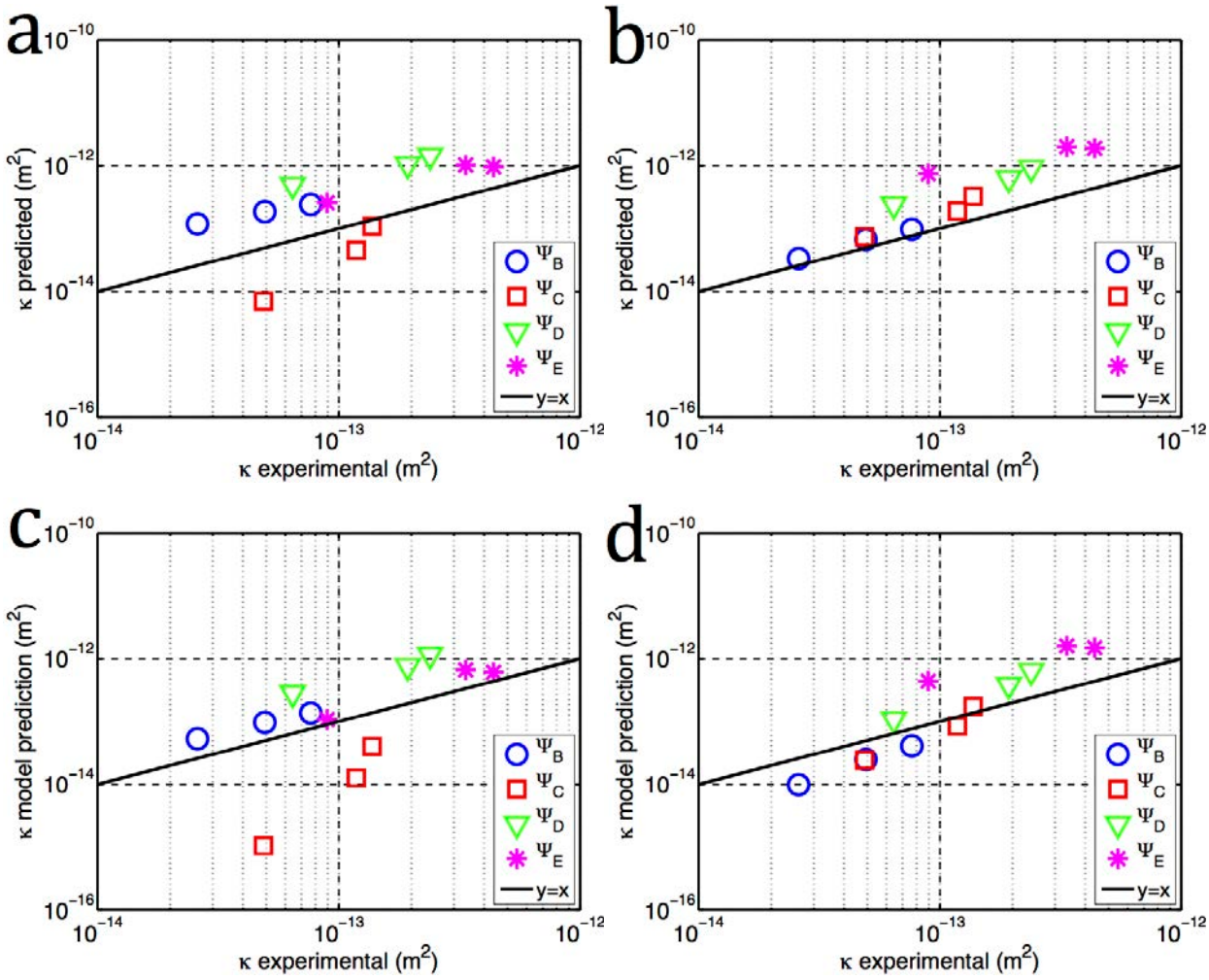

Figure 6.12: Comparison between the theoretical (y-axis) and experimental steady state permeability for Ψ_B (○), Ψ_C (□), Ψ_D (▽), and Ψ_E (✳) at the initial ρ_{bed} = 360, 400 and 480 $kg\ m^{-3}$. The predictions were obtained with: (a) Model 1 and $\varepsilon_{bed\ ss}$ from Figure 6.11a; (b) Model 1 and $\varepsilon_{bed\ ss}$ from Figure 6.11b; (c) Model 2 and $\varepsilon_{bed\ ss}$ fromFigure 6.11a; (d) Model 2 and $\varepsilon_{bed\ ss}$ from Figure 6.11b. The solid line (—) represents $y=x$

Regarding the performance of the models, when Model 1 is used (Figure 6.12b) there is a strong disagreement between the predictions and experimental data. The error, normalised to the experimental data, increases with grind size (30 % for Ψ_B as opposed to 520 % for Ψ_E); in the case of the coarser grinds is comparable to that reported by Macdonald et al. (1979) for other consolidated beds. This is not surprising, since the particle size distributions were shown to be continuously bimodal (Section 4.2.1), and Model 1, i.e. Kozeny-Carman equation, was developed for a single particle size. Furthermore, it seems unlikely that axial compression and consolidation of the bed can be taken into account just as a mere decrease in bed porosity. The dependency of tortuosity on porosity is now considered (Model 2 with n = 0.5, as found by Dias et al. (2006) for a random close packed bed of discrete bimodal spheres). Figure 6.12d shows that, despite of the notable effect on the agreement of the coarser grinds (relative error of 340 % for Ψ_E as opposed to 520 % found with Model 1), the prediction for these grinds is still poor.

Therefore, the tortuosity exponent (n) in Model 2 was varied in an attempt to fit the experimental data with a single value of n applied to each grind over the considered range of initial bed densities. Figure 6.13 shows the comparison of the theoretical permeability (y-axis) (as derived with Model 2 and the fitted n) and the experimentally measured values (x-axis) (Table 6.1).

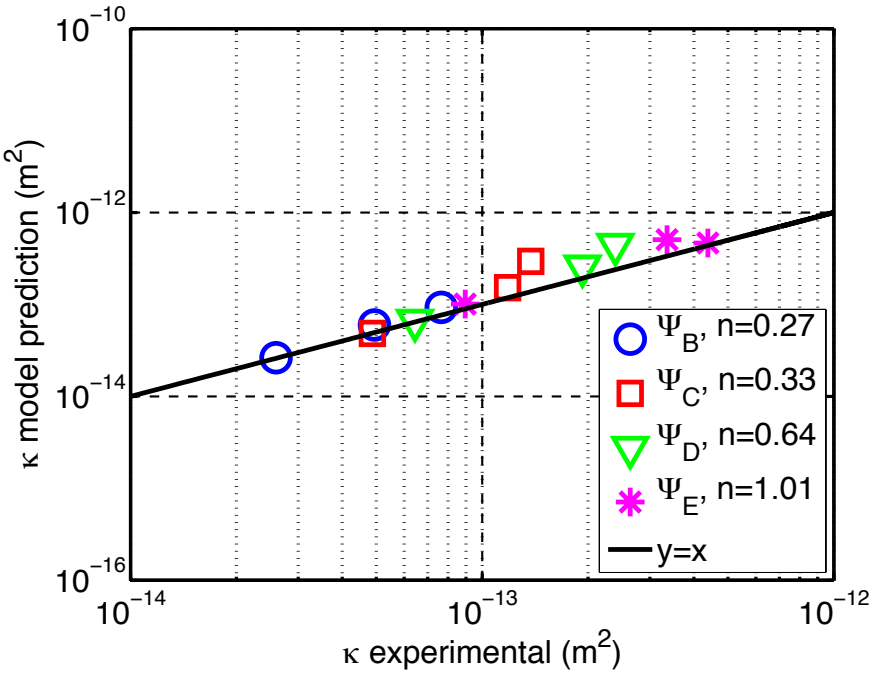

Figure 6.13: Comparison between the theoretical (*y*-axis) and experimental steady state permeability for Ψ_B (○), Ψ_C (□), Ψ_D (▽), and Ψ_E (✳) at the initial ρ_{bed} = 360, 400 and 480 $kg\ m^{-3}$. The predictions were obtained with Model 2 and the fitted values of the parameter *n* for each grind. The solid line (—) represents $y = x$

The fitted parameter (with a goodness of fit (R^2) between 0.81-0.98) was found to lie between 0.27 and 1.01, and it was found to increase the coarser the grind. The Kozeny-Carman pre-factors (180 in Kozeny-Carman equation) calculated with this fitted *n* parameter were between 189 and 1330. The values are in good agreement with the reported pre-factors for other consolidated beds (Macdonald et al., 1979), and beds made up of other non-spherical packing materials (Nemec and Levec, 2005).

The tortuosity exponent (*n*) is intended to account for the method used to pack the bed. Values of 0.4 and 0.5 have been reported for beds of discrete bimodal glass spheres, which were loosely or densely randomly packed, respectively (Dias et al., 2006). However, glass is an uncompressible material and thus the beds were not subjected to either axial compaction during the packing operation, or hydrodynamic consolidation. In this regard, in the beds in which the applied axial compaction force was

lower (Ψ_B, Ψ_C), the value of *n* tends to the reported 0.4; in the other beds (Ψ_D, Ψ_E), the value of *n* is greater than the reported 0.5. However, this tendency is not consistent with the fact that the beds with the lower fitted *n* values are those that underwent greater hydrodynamic consolidation. It should be then considered that, in addition to the packing method of the dry beds, the fitted *n* values for RGC beds may also encompass the evolution of the beds until steady state was reached.

The lower *n* values obtained here for finer grinds may compensate the possible underestimation of the model parameters. Firstly, as observed in Section 4.2.1, some of the solid particles initially packed in the (dry) bed are lumps of soluble material that dissolve in hot water. Dissolution of these may cause the overall porosity of the bed to increase. Conversely, this effect may also contribute to the observed higher consolidation for finer grinds (Section 6.2.1), as the bed structure may collapse upon removal of particles. Secondly, it was observed in subsequent packed bed extraction experiments (Chapter 7), that during approximately the first 5-10 seconds of the operation, some insoluble solid particles were removed from the bed. This effect was not quantified here, but it has been estimated (based on the typical solid residue measured for espresso coffees) that these particles may represent between 1 and 3 % of the original mass of coffee (Andueza et al., 2007; Petracco, 2005c). In addition to a possible increase in the bed porosity, this effect could also cause the $d_{[3,2]}$ of the particle size distribution to increase, provided the removed particles belonged to the fine size class. Lastly, preliminary observations with a newly built device that allows flow visualisation through a bed with transparent walls, showed that upon consolidation of the bed a head space of water was created and some of the particles were floating in it.

Since these free particles would not be contributing to the surface area of the bed, this would effectively increase the $d_{[3,2]}$ of the particle size distribution in the bed.

The greater percentage of the fine size class, and less mechanical consistency of the beds, make finer grinds more sensitive to the described effects that may affect the estimated bed porosity. However, these effects may be considerably smaller as compared to the uncertainty previously discussed in the determination of the particle porosity (Section 6.3.1).

The larger than expected values of n for Ψ_D, Ψ_E are consistent with the fact that higher axial forces were applied to these coarser grinds to pack the beds (Figure 6.2). The original packing structure of the dry beds may be more affected than in the case or finer grinds. However, it is challenging to unveil the physical significance of the higher obtained n values, as the exact effects of the applied axial forces to pack the beds on the grinds and the packing structure are largely unknown. Various events that would justify a greater n value are likely to occur: (i) the application of an axial force on a bed formed by compressible spherical-like material (Figure 4.11a) may produce elongation of the particles, resulting into flaked-like material (Figure 4.11c). If this flaked-like material were relatively ordered in the bed (mostly as parallel horizontal plates), this would substantially increase the bed tortuosity. Permeability of beds made from flaked coffee resulted to be greater than that for RGC (Section 6.2.3), but it must be taken into account that these beds were randomly packed; (ii) the application of an axial force may fracture the brittle dry grinds. The used $d_{[3,2]}$ in the models do not acknowledge this possible particle size reduction and thus a greater n value would compensate for it; (iii) the formation of regions with very dense lumps of material where the local bed porosity is

near 0: it was shown in Section 4.2.4 that when packing bimodal particle size distributions, segregation (regions of the bed where the concentration of the finer or the coarser is higher than the average) appear. According to the estimates from the linear mixing model (Section 4.2.4), bed porosity increases with grind size. Although, as acknowledged in Section 6.3.1, these bed porosity values may be underestimated, from the qualitative point of view this increase seems to indicate that segregation occurs in the coarser grinds.

6.3.3. Comparison of the permeability predictions for *dry* and *wet* $d_{[3,2]}$

It is the aim of this Section to establish a comparison of the experimental data with the predictions obtained with Model 2, when the model is parametrised with either the *dry* (Table 4.1) or *wet* $d_{[3,2]}$ (Table 4.2). The *wet* $d_{[3,2]}$ of the extracted grinds (Figure 4.5) was also considered here.

Figure 6.14 shows the comparison of the theoretical permeability (*y*-axis) (as derived with Model 2, $n = 0.5$) obtained with the *dry* and *wet* $d_{[3,2]}$ and the experimentally measured values (*x*-axis). Whereas the *dry* parameters overestimate the experimental results, the *wet* parameters considerably and underestimate them. Using the $d_{[3,2]}$ values of the extracted grinds (as *wet* measured) for Ψ_B and Ψ_E shows to improve the agreement, especially in the case of Ψ_E.

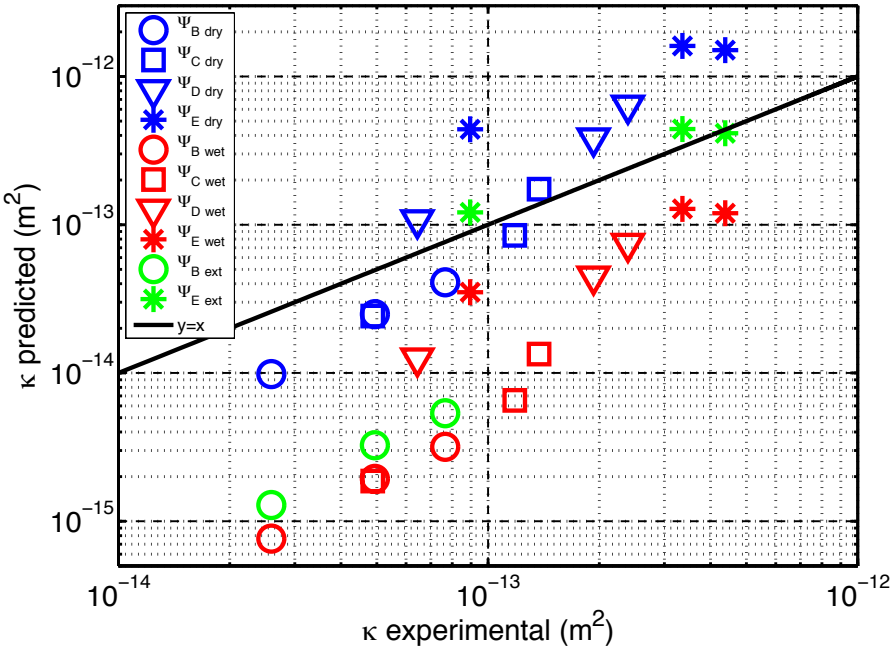

Figure 6.14: Comparison between the theoretical (*y*-axis) and experimental steady state permeability for Ψ_B (○), Ψ_C (□), Ψ_D (▽), and Ψ_E (✳) at the starting ρ_{bed} = 360, 400 and 480 *kg m*$^{-3}$. The predictions were obtained with Model 2 (n = 0.5), *dry* $d_{[3,2]}$ (blue symbols), *wet* $d_{[3,2]}$ (red symbols) and *wet* $d_{[3,2]}$ of the extracted grinds (green symbols). The solid line (—) represents *y=x*

In principle, it would be expected that the finer grind (Ψ_B) contained higher quantity of the lumps of material that dissolve upon extraction as compared to a coarser grind (Ψ_E). In this case, the $d_{[3,2]}$ of the extracted Ψ_B should increase by a greater factor than that by which the $d_{[3,2]}$ of the extracted Ψ_E does. Nevertheless, the experimental observation, (1.3 and 1.9-fold for Ψ_B and Ψ_E, respectively) is in contradiction with this affirmation. As noted in Section 4.2.1, when the particle size distribution of the grinds is assessed with the *wet* method, extracted oil droplets may be also measured. The amount of extracted oil scales with the surface area per unit volume of the grinds, and Ψ_B presents a greater one as compared to Ψ_E. Therefore, it is likely that the presumably higher amount of oil droplets in the case of Ψ_B hides to some extent the increase of $d_{[3,2]}$ when the lumps are dissolved.

6.3.4. Potential routes to improve the parametrisation of the permeability models

In the previous Sections, some of the challenges found when deriving a model to estimate the permeability of coffee beds have been pointed out. Thus, the aim of this Section is to propose routes to potentially improve the predictability of the permeability models.

Regarding the $d_{[3,2]}$:

- Investigate the particle size measurement methodologies in order to: (i) quantify to what extend the *dry* $d_{[3,2]}$ may be overestimated as the finer insoluble particles are not detected; (ii) quantify to what extend oil droplets and soluble lumps may be underestimating the *wet* $d_{[3,2]}$.

- Evaluate the effect on $d_{[3,2]}$ caused by the removal of insoluble particles from the bed.

- Quantify the effect on particle shape (elongation) and size of the grinds (breakage) of the axial forces applied to pack the beds.

Regarding the steady state porosity:

- Investigate more accurate methodologies to estimate the porosity of the particles.

- Develop accurate methodologies for direct quantification of the bed porosity, as opposed to the use of estimates from indirect measurements.

- Evaluate to what extend the bed porosity may increase upon wetting of the bed due to dissolution of soluble lumps.

- Investigate whether the consolidation effect can be fully attributed to a compression effect (affecting bed porosity), or in turn part is due to a mere decrease of the bed length due to reshuffle as particles are dissolved/removed.

6.4. Non-steady state

It is the aim of this Section to investigate the non-steady state observed during the earlier times of extraction. A typical example of the flow rate and pressure drop across the bed profiles over 600 seconds is displayed in Figure 6.15.

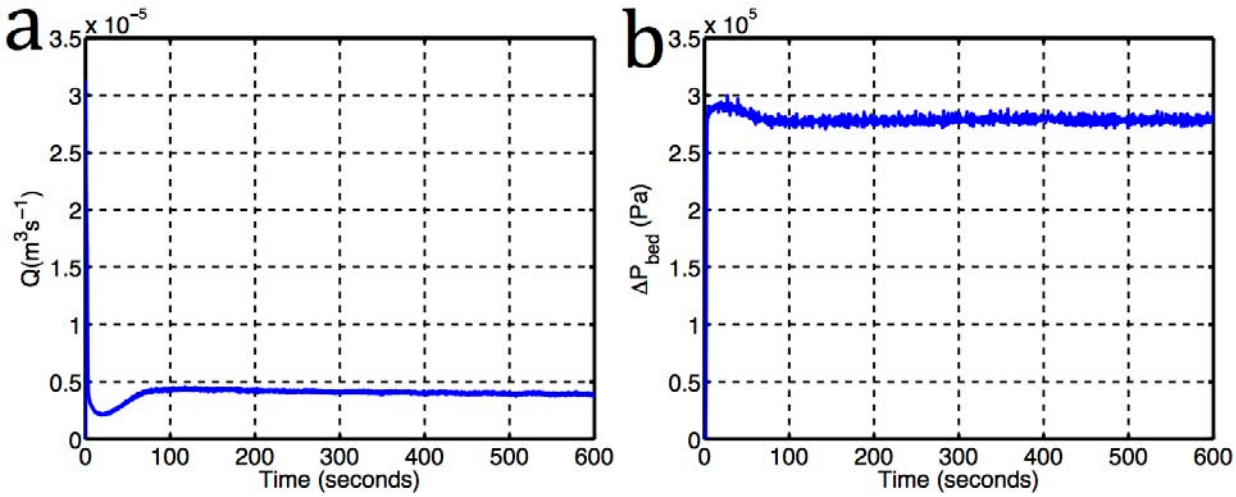

Figure 6.15: Observed time profiles during the hydration of Ψ_B at 80 °C and initial ρ_{bed} = 400 $kg\ m^{-3}$; (a) flow rate; (b) pressure drop across the bed

The observed flow rate evolution here may be described as follows: (i) at the beginning of the operation, the flow reaches a maximum value almost instantaneously. This corresponds to the low resistance hydraulic circuit before the extraction cell being filled. The same effect was observed each time that the flow was restarted to collect the steady state data. Then, flow rate decreases over the first 20-30 seconds until a

minimum value is reached; (ii) between approximately 30 and 80 seconds the flow rate increases; and (iii) over the next 500 seconds, the flow rate is stable and only decreases in a very mild fashion. The pressure drop across the bed follows the opposite tendency to that observed for the flow rate. The change in its magnitude, however, is not that as dramatic. This can be more clearly appreciated in Figure 6.16, which displays the flow rate (*x*-axis) vs. pressure drop across the bed (*y*-axis) data shown in Figure 6.15: whereas the flow rate increases from 2.5 to 4.5×10^{-6} $m^3\ s^{-1}$, the pressure drop decreases from 2.9 to 2.7×10^{5} *Pa*.

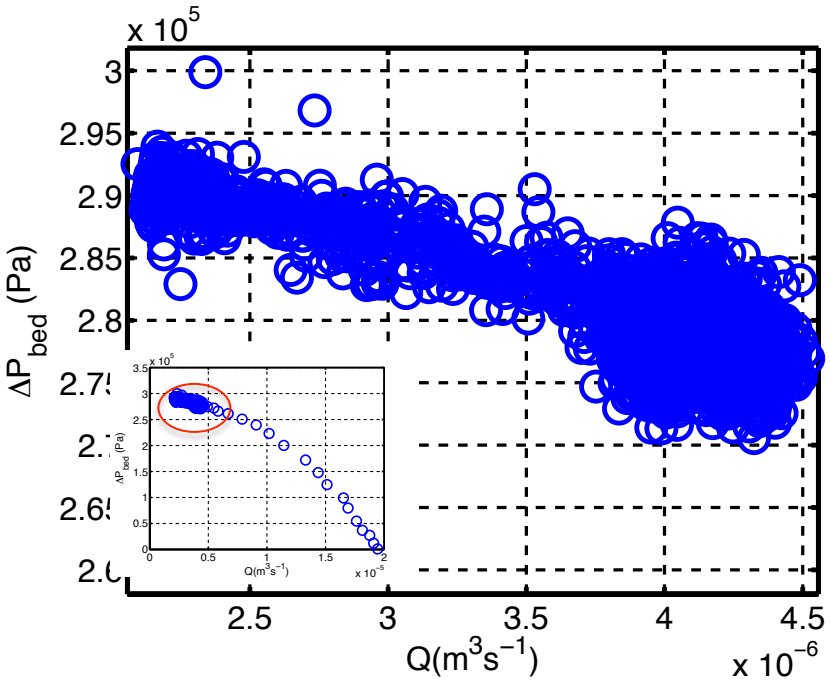

Figure 6.16: Flow rate (*x*-axis) vs. pressure drop across the bed (*y*-axis) during the hydration of Ψ_B at 80 °*C* and initial ρ_{bed} = 400 $kg\ m^{-3}$. The small plot shows the whole data set whereas the big plot is a magnification of the circled points

Qualitatively, the observed flow rate profile agrees with that reported by Petracco (2005). The observed behaviour was attributed to a time-dependent geometry of the coffee bed. In this case, the maximum flow rate was achieved within 2 seconds and that can be due to the characteristic curve of the pump used in their experiments. Since

they reported data only for the 12 first seconds, none of the effects observed here after this time was reported.

The non-steady state regime of the beds for which the steady state permeability was measured in Section 6.2 is now considered. Their flow rate profile (*y*-axis) over time (*x*-axis) is displayed in Figure 6.17 for the first 60 seconds of extraction.

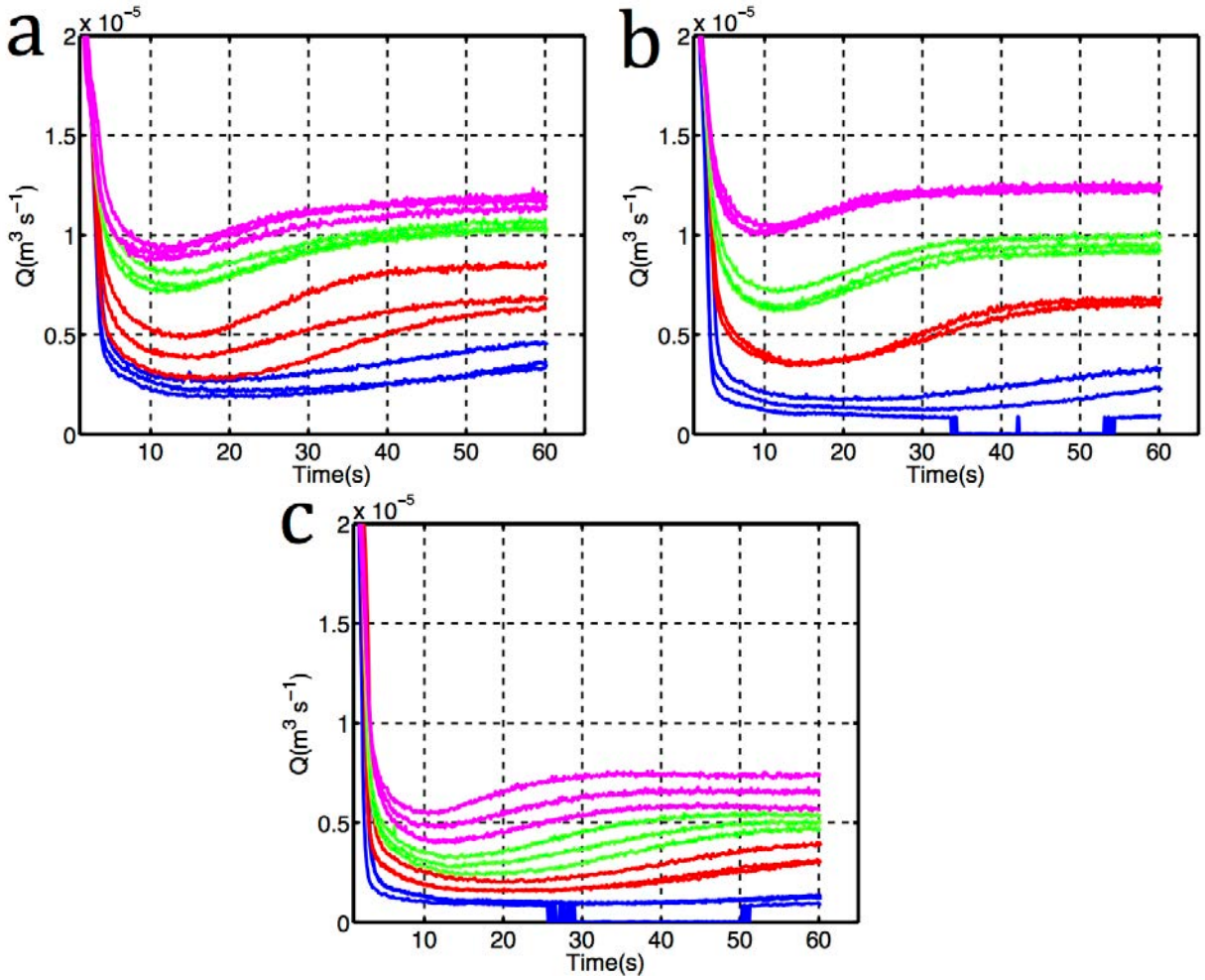

Figure 6.17: Flow rate profile for: (a) Initial ρ_{bed} = 360 *kg m*$^{-3}$; (b) Initial ρ_{bed} = 400 *kg m*$^{-3}$ Ψ_C; (c) Initial ρ_{bed} = 480 *kg m*$^{-3}$; Ψ_B (—); Ψ_C (—); Ψ_D; (—); Ψ_E (—). Three repetitions are shown for each grind (two in the case of Ψ_C at Initial ρ_{bed} = 400 *kg m*$^{-3}$)

All the profiles follow the same tendency observed in Figure 6.15. The selection of the same hydrostatic pressure in the tank for a given initial ρ_{bed} resulted in greater flow rates for coarser grinds. In some of the experiments conducted with the finest grind

(Ψ_B) at initial ρ_{bed} = 400 and 480 $kg\,m^{-3}$, it can be observed that the resistance of the bed increased and could not be overcome by the available pressure energy. Thus, the recorded flow rate decreased to 0, but after approximately 20 seconds it was reestablished. In practice, what was observed in these situations was a very low dripping flow rate that went back to a continuous regular flow.

For each of the considered grinds, the calculated hydraulic resistance ($\Delta P_{bed}/Q$) (y-axis) over time (x-axis) is displayed in Figure 6.18 for the first 60 seconds of extraction. The hydraulic resistance of the bed is given by extraction cell geometry (area, length), permeability of the medium, and viscosity of the fluid.

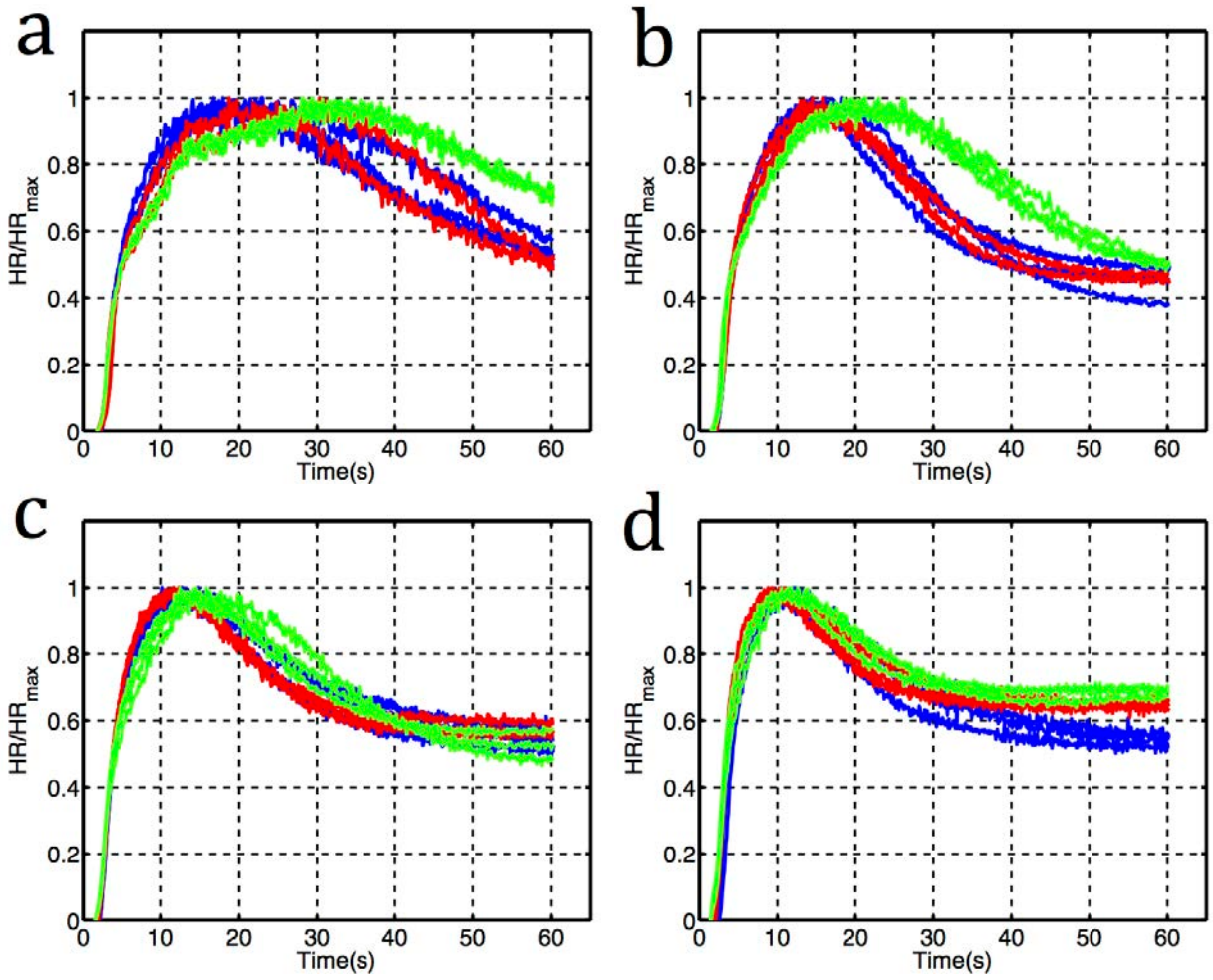

Figure 6.18: Hydraulic resistance / maximum hydraulic resistance for: (a) Ψ_B; (b) Ψ_C; (c) Ψ_D; (d) Ψ_E; Initial ρ_{bed} = 360 $kg\ m^{-3}$ (—); Initial ρ_{bed} = 400 $kg\ m^{-3}$ (—); Initial ρ_{bed} = 480 $kg\ m^{-3}$ (—). Typically three repetitions are shown for each initial ρ_{bed}

As expected from the observations of Figure 6.18, the hydraulic resistance of the beds is time-dependent and follows the opposite trend to that observed for the flow rate. One can see that for the finer grinds (Figure 6.18a and b), the profiles seem to evolve more slowly as compared to coarser grinds (Figure 6.18c and d): the maximum hydraulic resistance (peak of the profiles) is reached later in time and is maintained in the system for longer. The observed profiles for initial ρ_{bed} = 480 $kg\ m^{-3}$ differ from the profiles at the lower initial ρ_{bed}, which were similar between themselves. This difference, however, becomes less significant as grind size increases.

Although the average hydration steady state temperature was 80 *°C*, the actual thermal profiles through the beds were found to differ. Typical temperatures at the inlet of the bed were found to be between 70 and 80 *°C* after 3 seconds. It was assumed that within this range, the influence of temperature (that affects viscosity of the extract, consolidation of the bed and CO_2 solubility in water) on the observed hydraulic resistances is not significant.

The non-steady state flow rate and hydraulic resistance profiles have been introduced and described in this Section. The underlying phenomena that may be give rise to the observed behaviour of the system are discussed in the next Sections.

6.4.1. Phenomena that do not modify the permeability of the bed

- Wetting moving front

At the steady state, the pressure gradient across the bed ($\Delta P_{bed}/L$) is constant with time. However, in the non-steady state, the term should be written as $\partial P/\partial x$, which represents the variation of pressure (P) across the axial direction of the bed (x). Until the bed is fully penetrated by the wetting moving front, i.e. extract starts coming out of the bed, the distance travelled by the fluid increases with time ($L(t)$); consequently so does the hydraulic resistance. From observations of the first extract coming out of the bed, this effect has been estimated to occur in a time scale of 2-4 seconds. Also, dry coffee has the ability to absorb a given amount of water (Section 4.4.4). Since the displayed flow rates profiles in Figure 6.17 are measured at the inlet of the extraction cell, this effect cannot be appreciated here.

- Viscosity of the extract

The second phenomenon to be taken into account is related with the effect caused by the mass transferred of soluble solids from within the grinds to the pore space of the bed.

It has been reported that due to the effect of the dissolved solids, the viscosity of espresso coffees is twice that of water at the same temperature (Petracco, 2005c). However, at the earlier stages of extraction, the concentration of the fluid in the pore space of the bed can be considerably higher than that obtained in the final espresso beverage. Navarini et al., (2004) measured relative viscosities ranging from 9 to 2 for extracted volumes varying between less than 10 *ml* up to approximately 40 *ml*. The temperature at which the viscosities were measured, were not specified; it is assumed here that coffee and water have the same temperature-viscosity dependency. The viscosity of the extract vs. extracted volume values were cross-checked with the concentration vs. extracted volume values, both provided in the aforementioned publication. This allowed correlating the extract concentration (*x*-axis) to the relative viscosity (*y*-axis) (Figure 6.19). The data was fits well (R^2 = 0.96) to a straight line; the intercept was imposed to be 1 so that when the concentration of the extract is 0 (pure water), the relative viscosity is 1.

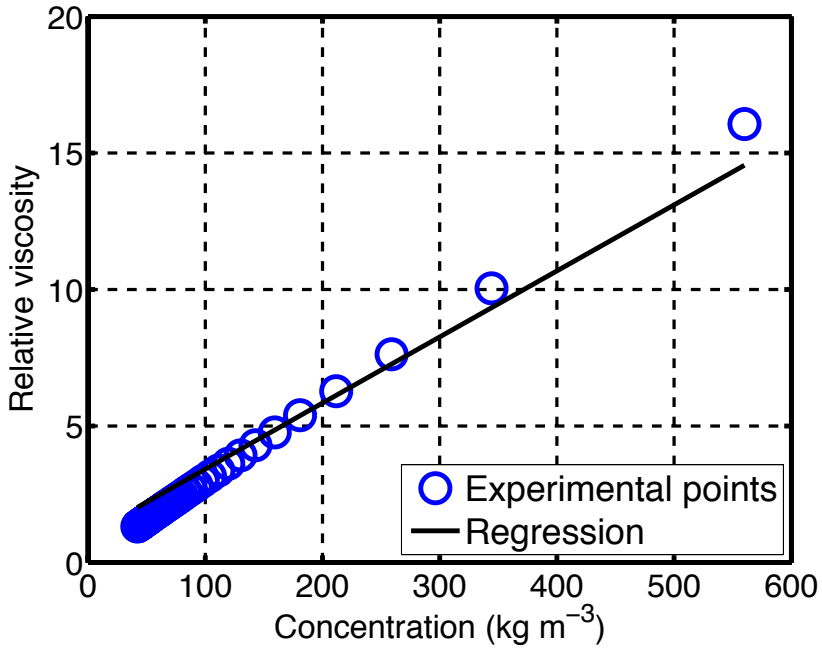

Figure 6.19: Relative viscosity (*y*-axis) vs. concentration (*x*-axis) for a (espresso) coffee extract*; Relative viscosity* = 0.02· *Concentration* +1; R^2 = 0.96

In order to elucidate the possible effect of viscosity in the observed hydraulic resistance profiles, packed bed extraction data from Ψ_B (Chapter 7) (initial ρ_{bed} = 480 $kg\ m^{-3}$; Q = 1.2×10^{-6} $m^3\ s^{-1}$; T = 72 $°C$) is used here. In this extraction experiment, the extract was fractionated into 8 aliquots (collected for 10 seconds) and their soluble solid concentration measured. The viscosity was calculated with the derived concentration-viscosity correlation in Figure 6.19. Figure 6.20 shows the estimated hydraulic resistance and viscosity (normalised by the maximum values) (*y*-axis) over time (*x*-axis). The maximum viscosity values were found to be between 3.3 and 3.6 $Pa\ s$. Ψ_B is the finest grind and it was extracted at a typical espresso flow rate (Q = 1.2×10^{-6} $m^3\ s^{-1}$). Therefore, the concentration values measured from this experiment were the maximum across the range of experimental conditions. The reported extract viscosity values set the upper limits expected for the considered grinds.

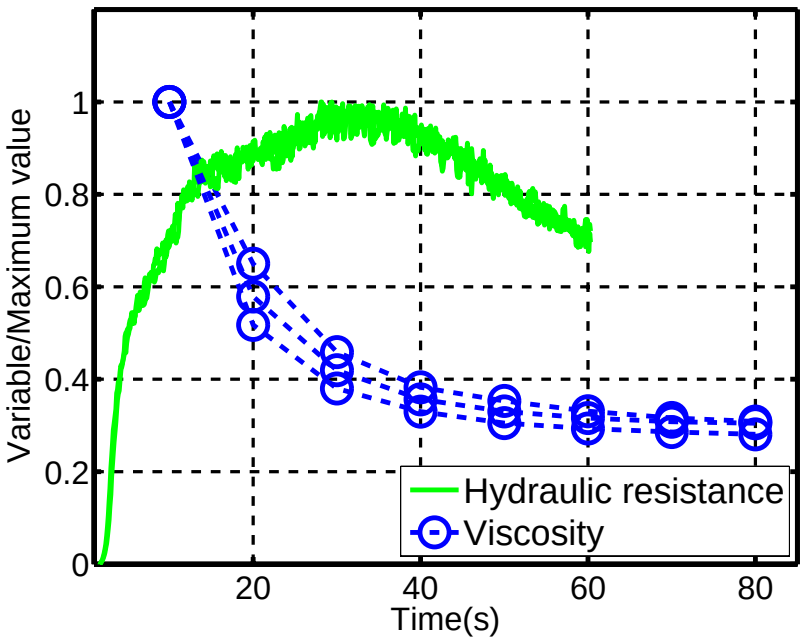

Figure 6.20: Hydraulic resistance profiles for Ψ_B at initial ρ_{bed} = 480 $kg\ m^{-3}$ and average flow rate of $2.1\times10^{-6}\ m^3\ s^{-1}$; viscosity profiles for Ψ_B at initial ρ_{bed} = 480 $kg\ m^{-3}$ and average flow rate of $1.2\times10^{-6}\ m^3\ s^{-1}$

It can be seen from Figure 6.20 that the time scale for the hydraulic resistance of the beds to start decreasing is much longer than that at which the viscosity does. This indicates that although viscosity certainly influences the non-steady state profiles, it appears not to be the most significant factor. As a matter of fact, as shown in Figure 6.17 the beds made from Ψ_C-Ψ_E were hydrated at flow rates that are several times greater than those used in typical espresso extraction, i.e. 1 $ml\ s^{-1}$; this is especially true for the cases of initial ρ_{bed} = 360 and 400 $kg\ m^{-3}$. Due to the resulting low residence times in the bed, the concentration of the pore space is expected to be very diluted in these cases. Therefore, viscosity values lower than the ones reported before for Ψ_B can be assumed. Nevertheless, profiles of hydraulic resistance with similar shapes (increase-decrease) are still observed.

- Gas in the pore space of the bed

Gas presence in the bed can be straightforwardly corroborated from the recognisable foam layer on top of espresso coffees. The mechanisms of foam formation involve a mixing process at the outlet of the bed between the extracted soluble solids and a gas (Petracco, 2005c). In a dry bed, the pore space is occupied by air. Additionally, part of the CO_2 produced during the roasting stage remains entrapped into the microstructure of the coffee particles, and is extracted to the pore space of the bed as water penetrates into the particles. Some studies (Anderson et al., 2003; Wang and Lim, 2014) have been published regarding the degassing kinetics of roast and ground coffee in air. They showed that the initial amount of CO_2 in the grinds increases with roasting degree. After grinding, it was shown that the roast and ground coffee can still conserve between 4.5 and 12 $mg\ g^{-1}$ of CO_2. Characteristic degassing times of roast and ground coffee in air were reported to be in the order of 10 hours at 20 $°C$. The beans used in this work were roasted a medium-dark roasting degree, and they were ground just before each experiment was carried out. Therefore, it is expected that noticeable amounts of gas were still entrapped in the particles.

The incorporation of gas bubbles to the pore space of the bed effectively results in a multiphase flow between the extract and the gas. In a porous medium where two or more immiscible phases coexist, Darcy's equation for each phase (p) can be written as follows:

$$v_p = -\frac{\kappa_{r,p}\kappa}{\mu_p}\frac{\partial P_p}{\partial x} \qquad \text{Eq. 6.6}$$

Where v is the fluid velocity ($m\ s^{-1}$), μ is the viscosity ($Pa\ s$), $\partial P/\partial x$ is the pressure gradient ($Pa\ m^{-1}$), κ is the permeability of the bed (m^2) and κ_r is the relative permeability. The latter has been defined as a non-linear function of the saturation of the bed, i.e. volume percentage of a given phase in the pore space (Weerts et al., 2005); its value is 0 when no water is present and 1 when the system is fully saturated with water. Thus, from Eq. 6.6 one can see that the presence of gas in the system reduces the permeability of the bed.

The volume (V) occupied by the typical reported amounts of CO_2 at the extraction conditions used in this work, can be estimated assuming the ideal gas behaviour:

$$PV = nRT \qquad \text{Eq. 6.7}$$

Where P (atm) is the absolute pressure in a given point of the bed during extraction (assumed here to be the maximum possible pressure drop plus the atmospheric pressure, $5.5\times10^5\ Pa = 5.4\ atm$), n is the number of moles (mol), R the ideal gas constant ($0.082\ atm\ dm^3\ mol^{-1}K^{-1}$) and T the temperature (K) (assumed here to be 80 $°C$, i.e. 353 K). The estimated occupied volumes for the three tested coffee weights 7.2, 8.0 and 9.5 g), as well as the initial volume of the pore space (before consolidation, and assuming a particle porosity of 0.53) are reported in Table 6.2.

Table 6.2: Estimated maximum and minimum volumes of CO_2 released from the coffee grinds

Amount of CO2 **(*mg g^{-1}*)**	***Mass of coffee in the bed*** **(*g*)**	***Volume of CO_2 in the bed*** **(*cm^3*)**	***Volume of pore space*** **(*cm^3*)**
	7.2	10.6	8.5
12	8.0	11.6	7.3
	9.5	13.8	4.7
	7.2	3.9	8.5
4.5	8.0	4.4	7.3
	9.5	5.2	4.7

It can be seen from Table 6.2 that for the maximum CO_2 content (12 *mg g^{-1}*), its estimated volume (according to the assumed thermodynamic conditions) is between 1.2 and 3 times the pore space volume of the bed. These figures are reduced to 0.5 and 1.1 when the minimum amount of CO_2 (4.5 *mg g^{-1}*) is considered. Based on the measured mass of gas, it should remain pressurised inside the coffee structure (Anderson et al., 2003). It must also be taken into account that, as gas bubbles travel through the bed, the thermodynamic conditions change. Pressure decreases due to the pressure drop across the bed and temperature decreases until thermal equilibrium is achieved. This variation generates competing effects that affect the water saturation of the system: pressure decrease causes the gas to expand, whereas compression of the gas results from a temperature decrease. Additionally, the latter also increase the solubility of the gas in the water phase, thus occupying less volume in the pore space.

In order to promote the required mixing to produce foam, espresso machines and On-Demand systems typically incorporate a nozzle at the outlet of the bed (Navarini et al., 2008). However, in the case of the packed bed extraction rig used in the experiments conducted in this Thesis, no nozzle was used and the outlet of the bed was connected to a transparent plastic pipe. The lack of the nozzle resulted in the creation of a negligible

amount of foam, and this allowed the visualisation of the gas bubbles coming out of the bed. An example is displayed in Figure 6.21.

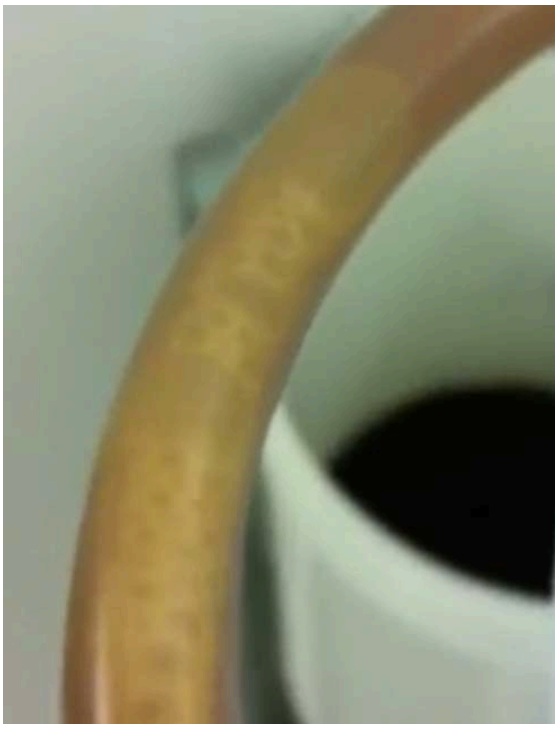

Figure 6.21: Gas bubbles coming out of the bed during the earlier times of a typical extraction experiment

The time scale in which it was observed that bubbles were coming out of the bed (60-80 seconds) agrees well with the time scale in which the hydraulic resistance of the bed was observed to increase (Figure 6.18).

In a porous medium the ability of a liquid to displace a gas depends on the capillary number (Ca) (-), which represents the ratio of viscous to the capillary forces at the interface of the fluids and is given as follows (Leal, 2010):

$$Ca = \frac{\mu v}{\gamma} \qquad \text{Eq. 6.8}$$

Where μ is the liquid viscosity ($Pa\ s$), v is the fluid velocity (given as Q/A) ($m\ s^{-1}$), and γ is the liquid-gas surface tension ($N\ m^{-1}$).

As a rule of thumb, values of the capillary number greater than 10^{-5} indicate that viscous forces dominate the system, whereas smaller values indicate that capillary forces are the dominant ones (Armstrong et al., 2014). At earlier extraction times, the capillary number is time-dependent, as the system is at the non-steady state. However, a limiting case considering the minimum viscosity (water) and velocity (that corresponding to the minimum observed flow rate, i.e. approximately 10^{-6} $m^3\,s^{-1}$ (Figure 6.17) can be considered to test if the system could be possibly dominated by capillary forces. Under the proposed scenario, the capillary number resulted to be 5.3×10^{-6}, which would indicate a dominance of capillary forces. However, as explained before with Figure 6.19, the viscosity of the extract is on average twice that of water viscosity. Additionally, it must be noted that: (i) as reported by Navarini et al. (2004), the espresso coffee-air surface tension values are remarkably lower than the water-air values at the same temperature, and (ii) the hydration flow rates used in the beds are considerably higher than the minimum flow rate considered for this calculation.

Greater values of the capillary number may help displace the gas out of the bed more quickly. Thus, the resulting greater flow rates during the hydration of beds in the case of the coarser grinds may explain the sooner decrease in their hydraulic resistance (Figure 6.18). In order to test this hypothesis, a bed made from the coarsest grind (Ψ_E) and packed at initial ρ_{bed} = 400 $kg\,m^{-3}$ was hydrated at an average flow rate of 2.09×10^{-6} $m^3\,s^{-1}$ (approximately 6 times lower than that observed in Figure 6.17b). The hydraulic resistance results for the beds hydrated at these two average flow rates are displayed in Figure 6.22.

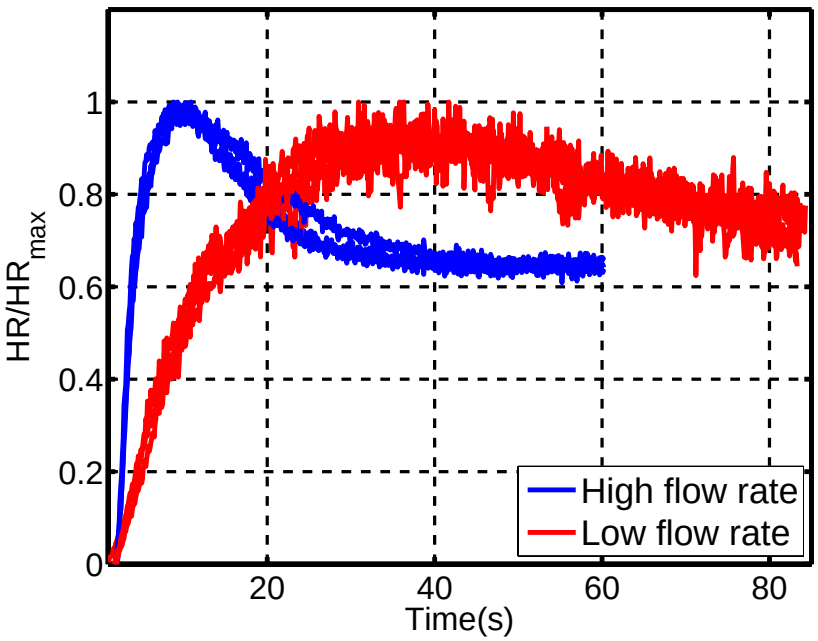

Figure 6.22: Hydraulic resistance / maximum hydraulic resistance for Ψ_E at the initial ρ_{bed} = 400 $kg\ m^{-3}$ at average flow rates of 12.2×10^{-6} and 2.1×10^{-6} $m^3\ s^{-1}$. Three repetitions are shown for each flow rate

It can be observed that when the hydration flow rate is decreased, the non-steady state regime evolves more slowly towards a steady state. This may confirm the aforementioned effect of the capillary number on the removal of the gas from the bed.

6.4.2. Phenomena that modify the permeability of the bed

The phenomena that modify the permeability of the bed are now analysed. During the time scale in which the hydraulic resistance increases (10-30 seconds), it has been observed that the greatest consolidation of the beds occurred (Section 6.2.1). Although beyond this point it was observed that the beds still consolidated, the decrease in the hydraulic resistance, as CO_2 is expulsed from the bed appears to be the dominant effect. Swelling of the particles could also contribute to the reduction of the porosity. However, it must be taken into account that: (i) no swelling was observed in this work (see Chapter 4) when it was attempted to reproduce the experiments reported by

Mateus and Rouvet (2007); (ii) the reported observations were measured in a stirred vessel-like system and it is unclear what the effect of the applied axial and hydrodynamic forces on swelling would be.

Regarding the decrease in hydraulic resistance, it is unknown whether upon consolidation of the bed, further structural reshuffle (that may result in channelling) occurs. Also the removal of some particles from the bed into the cup and the possible increase in porosity due to the dissolution of the chunks of soluble material can play a role in the observed behaviour. However, the characteristic time scales of these observations (few seconds) are far earlier than with the times in which the hydraulic resistance of the system was observed to occur.

6.4.3. Effect of temperature on the non-steady state hydraulic resistance

The factors that contribute to modifying the hydraulic resistance of the bed (with or without modifying its permeability) depend on temperature. In order to investigate this dependency, the observed flow rate and pressure drop across the bed profiles for Ψ_B at the initial ρ_{bed} = 400 $kg\ m^{-3}$ at 15 and 80 $°C$ are displayed in Figure 6.23.

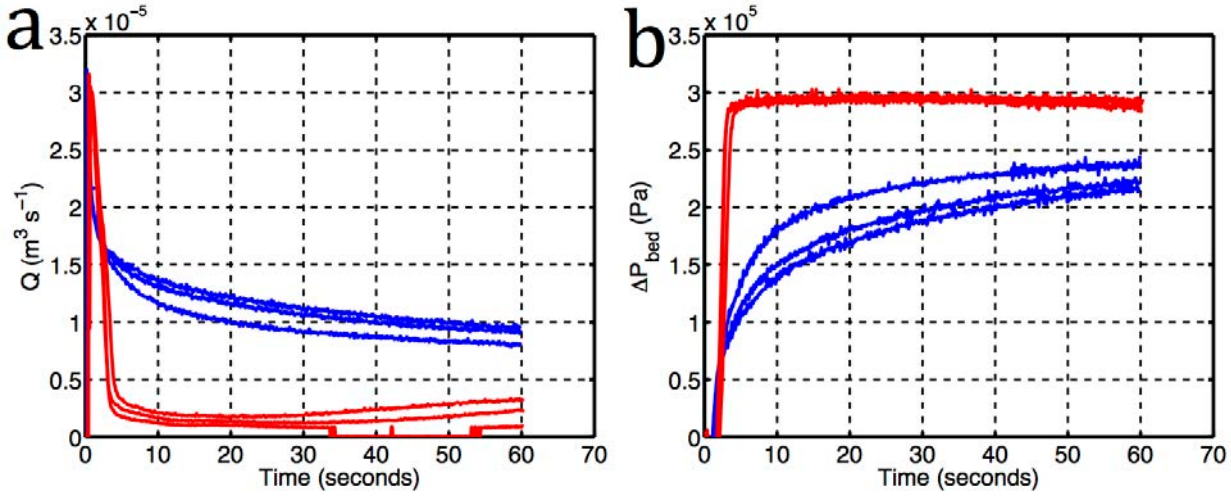

Figure 6.23: Observed time profiles during the hydration of Ψ_B at the initial ρ_{bed} = 400 $kg\ m^{-3}$ at 80 $°C$ (—) or 15 $°C$ (—); (a) flow rate; (b) pressure drop across the bed. Three repetitions are displayed

Due to the low extraction rate observed at 20 $°C$ in a stirred tank (Chapter 5) the viscosity of the extract at 15 $°C$ can be approximated to that of water. Despite of the higher water viscosity at 15 $°C$ (approximately 3.2-fold), it can be seen that the hydraulic resistance of the beds is considerably lower. This behaviour holds even after the viscosity at 80 $°C$ decreases as concentration of extracted solids decreases over time (Figure 6.20). The observation indicates that there are other factors (consolidation, CO_2) that seem to play a more relevant role in the dynamics of the system than fluid viscosity. These observations are in good agreement with Petracco (2005), who observed that the

non-steady state flow rate across the bed in an espresso machine was significantly higher at 4 ℃ as compared to 90 ℃.

Figure 6.24 shows one of the cold flow rate profiles displayed before but in a longer time scale.

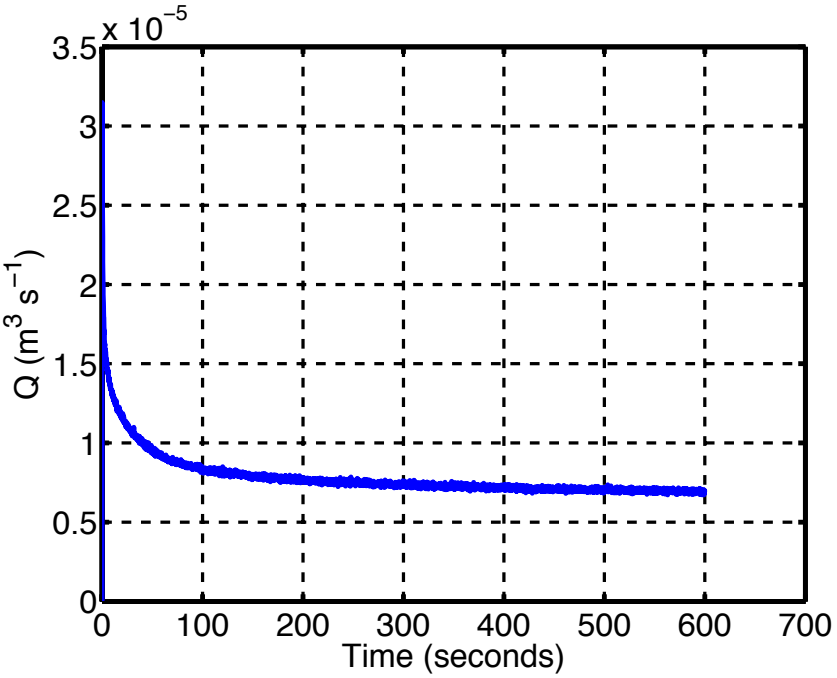

Figure 6.24: Observed flow rate profile during the hydration of Ψ_B at the starting ρ_{bed} = 400 $kg\ m^{-3}$ at 15 ℃

The flow rate decreases over a much longer time scale at colder temperatures. This corroborates that the wetting-moving front through the bed is not the main phenomena responsible for this behaviour either. Also, the fact that no flow rate increase is observed at colder temperatures seems to indicate that the influence of the insoluble particles extracted from the bed on the observed profiles is minimum. Therefore, the flow rate increase produced between the approximately 30 and 80 seconds of the profile may correspond to CO_2 bubbles leaving the bed (Figure 6.21). At colder temperatures the solubility of CO_2 in water increases exponentially as temperature decreases, and the gas occupies less volume in the pore space at the same

pressure. It is then entirely possible this explains the lower observed hydraulic resistance of the bed at colder temperatures. This would explain why the flow rate increase reported at greater temperatures (Figure 6.17) is not appreciated here.

From experiments presented in Section 6.2.4, it can be seen that the resulting beds at steady state are essentially different, as indicated by the greater permeability value (~ 6-fold) derived for the cold bed. This was attributed to the different consolidation degrees and the underlying causes were discussed. Since temperature would minimise the effect of the gas in the bed, the observed profiles in Figure 6.23 may be due to a more slowly consolidation rate.

It can be then concluded from the analysis of the system at a cold and hot temperature, that the factors that seem to dominate the observed non-steady state behaviour of the system are bed consolidation and the effect of CO_2 bubbles in the bed.

6.5. Conclusions

The hydrodynamics of coffee packed beds typically used in espresso practice has been investigated at the steady and non steady state.

At the steady state, permeability of the beds has been studied as a function of particle size distribution, bed density, particle shape, temperature and bed aspect ratio. A combination of experimental and modelling approaches have been employed. From the experimental standpoint, the developed measurement technique has been shown to provide steady state permeability values that were comparable to those reported in the literature. Finer grinds and higher density beds resulted in lower permeability values. A contribution to these low values is that greater consolidation under flow was observed

for these beds. In the case of beds made of coarser grinds, the derived values at the highest tested bed density appeared to be lower than expected according to the observed tendency at the lower bed densities. This was attributed to the effect of the higher axial forces required to pack the beds to the selected density. It was proposed that this could result in a substantially modification of the original bed structure, i.e. particle shape and thus bed tortuosity, and particle breakage. The effect of particle shape was evaluated with flaked coffee (Blend 2). It was found that the permeability of these beds was higher than that of the finest grind (Ψ_B), despite of the similar obtained $d_{[3,2]}$ values (as *dry* measured). Even though temperature and aspect ratio of the bed do not explicitly appear in the permeability models (but influence the hydraulic resistance of the beds), they were shown to influence the derived permeability values through their effect on the packing structure of the beds. A colder temperature and a higher aspect ratio bed resulted in greater permeability values, and this was attributed to the less observed consolidation. In the case of temperature, a possible milder swelling effect of the particles (even though in the experiments showed in Section 4.2.1 no evidence of swelling was obtained) could contribute to greater bed porosity, thus increasing its permeability.

From the modelling standpoint, the permeability models proposed in Chapter 3 were used to test how well they predict the experimentally measured values. It has been shown that variability in the measured particle porosity is propagated to the estimates of bed porosity and this had a notable effect on the predicted permeability. A similar effect has been found regarding the variability in $d_{[3,2]}$, when the particle size distribution is *dry* or *wet* measured. Regarding the proposed permeability models, Model 1 (Kozeny-Carman equation) has been shown to considerably overpredict the

experimental results. This was not surprising if the assumptions of this model (bed of mono-sized spheres) are taken into account. The introduction of a bed porosity-dependent tortuosity factor improved the agreement to some extend, but still resulted into considerably disagreement (especially for coarser grinds). Fitting the coefficient (n) of the tortuosity expression was found to provide greater values for the coarser grinds than those found for the discrete bimodal distribution of spheres (0.4-0.5), and this was attributed to various possible effects of the higher applied axial forces to pack these beds.

Overall, it was shown that the two main challenges to obtain reliable models to estimate the permeability of coffee packed beds at the steady state is the great sensitivity of the results to the parameters and that bed structure and particle size are process-history dependent. Therefore, potential routes to improve the parametrisation of the permeability models were proposed and discussed.

At the non-steady state, the hydraulic resistance of the beds was observed to increase and decrease in a time scale of approximately 80 seconds. The potential factors giving rise to the time-dependent hydraulic resistance were analysed and discussed. Bed consolidation and the presence of CO_2 in the bed appeared to be the main phenomena driving the behavior of the system during this time scale. A detailed experimental and modelling study of all the phenomena occurring in the non-steady state was beyond the scope of this thesis. Thus, the objective of this Section was to establish the preliminary fundamental understanding to set a baseline for future work.

Chapter 7: Extraction at the Bed Scale

7.1. Introduction

The aims of this Chapter are to investigate the kinetics of extraction at the bed scale in roast and ground coffee (RGC) typically used in espresso coffee extraction, as a function of the usual process parameters (particle size distribution, flow rate and bed density), and to evaluate the predictive capability of the corresponding mathematical model presented in Chapter 3.

Section 7.2 investigates the observed responses of the process parameters (flow rate and temperature) during the non-steady state regime and proposes alternatives as to how to incorporate their effect in the extraction model.

Section 7.3 presents the extraction experiments carried out in the packed bed extraction rig set-up described in Chapter 3. The microstructural effective diffusion coefficients (derived in Chapter 4 and tested in Chapter 5 for a slurry system) were used here to see how well the simulations obtained with the model compared to the experimental data.

Section 7.4 presents a sensitivity analysis study of the kinetics of extraction to some of the assumptions adopted in the model. The effect of a constant or time-dependent flow rate, temperature, particle porosity and bed porosity are considered.

Section 7.5 compiles the experimentally measured values of extraction yield and drink strength for an extracted volume of 45 ± 7 *ml* (range of espresso coffee). The influence of process parameters on the final attributes of the drinks is discussed in this Section.

Section 7.6 illustrates a practical case study where the proposed extraction model is used to simulate the extraction profiles reported in the literature of various low molecular weight species, as obtained from a real On-Demand brewer (*Hyper Espresso*® by *Illy*) and traditional espresso machines.

Lastly, Section 7.7 closes the Chapter by presenting a summary of the findings and conclusions.

7.2. Experimental responses of the variables in the extraction rig

Flow rate and temperature are non-steady state variables at earlier extraction times (Chapter 6). It is the aim of this Section to study the observed responses of these variables during the extraction experiments in order to propose alternatives as to how to incorporate their effect in the extraction model at the bed scale.

7.2.1. Flow rate response

In the extraction model at the bed scale, flow rate sets the convective mass transport rate through the porous space of the bed and eventually into the cup. The influence of flow rate on the kinetics of extraction was investigated here by conducting extraction experiments in two regimens, which cover the typical flow rates reported in espresso extraction (Romani et al., 2004): a high flow rate regime (HF), with an average flow rate value of circa 3.5×10^{-6} $m^3 s^{-1}$, and a low flow rate regime (LF), with an average value of circa 1×10^{-6} $m^3 s^{-1}$. These were selected by adjusting the hydrostatic pressure in the tank of the extraction rig (Figure 3.1) according to the particle size distribution of the grinds and bed density (400 or 480 $kg\ m^{-3}$).

At the earlier stages of extraction, the magnitude of the inlet flow rate measured by the flow meter of the extraction rig differed from the outlet flow rate of the bed: the hydraulic circuit prior to the bed fills up and RCG absorbs a certain amount of water. Therefore, the experimental cumulative volume of extract ($V_{cum\ exp}$) was measured at the outlet of the bed by weighing the collected aliquots. A time-dependent flow rate at the outlet of the bed (Q_{exp}) was then estimated as the collected volume in each aliquot divided by the sampling time (5 and 10 seconds for HF and LF, respectively). The density of the extract was assumed to be circa that of water (~ 1000 $kg\ m^{-3}$) at the same temperature (Navarini et al., 2004). Depending on the concentration of the extract, this assumption entails an error between 1-3 %.

Table 7.1a shows a typical example of the experimental outlet flow rate at HF and LF regimes at the two considered bed densities (400 and 480 $kg\ m^{-3}$) for the particular case of grind Ψ_E. The flow rate decays exponentially at earlier extraction times, and then slightly increases.

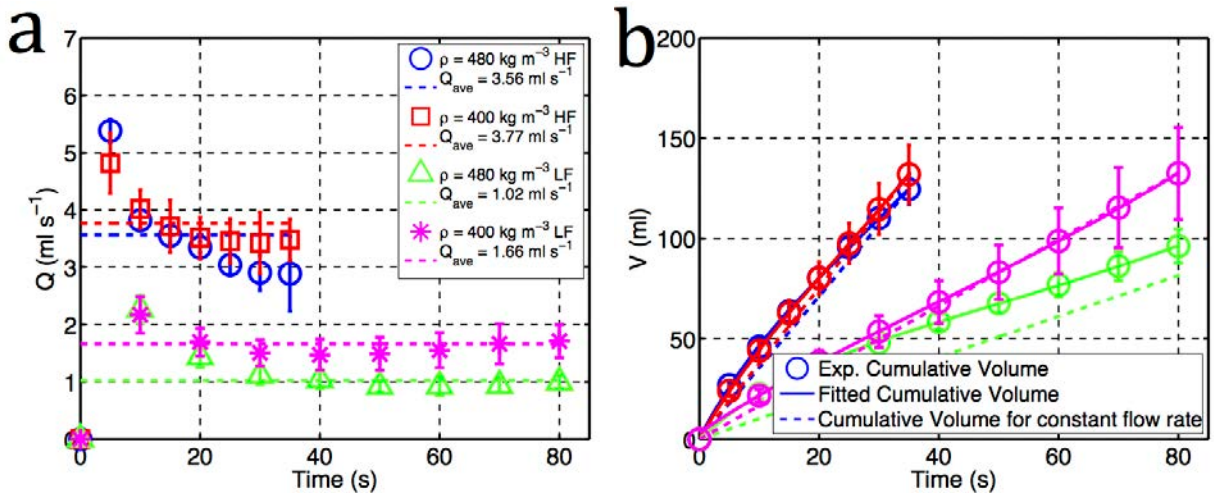

Figure 7.1: (a) Measured time-dependent flow rate (points) and average flow rate (----); (b) measured cumulative volume (points), fitted cumulative volume (—) and cumulative volume calculated from the average flow rate (----). The data corresponds to Ψ_E

From the modelling perspective, three different approaches can be adopted with respect to the non-steady state flow rate: (i) the most straightforward alternative from the practical stand point is to calculate an average representative value of the flow rate profile (shown as dotted lines in Table 7.1a); (ii) a more refined option in order to better capture the dynamics of the system is to fit the observed flow rate behaviour to an *ad hoc* analytical function; and lastly (iii) building a physical-based model that incorporates the phenomena driving the observed non-steady state. Given the number of phenomena that are shown to contribute to the observed non-steady state regime (Chapter 6), and their intrinsic complexity, option (iii) is beyond the scope of this thesis and is regarded as future work. Thus, for the purpose of this investigation, options (i) and (ii) were further considered.

The fitted analytical expressions to the measured cumulative volume were of the form of Eq. 7.1.

$$V_{cumfitted} = ae^{(bt)} + ce^{(dt)} \qquad \text{Eq. 7.1}$$

Where $V_{cum\,fitted}$ is the cumulative volume (ml), t is the time (s), and a, b, c and d are constants. The resulting equations are displayed in Table 7.1. All the fittings exhibited a goodness of fit (R^2) of 0.99. The time-dependent flow rate, i.e. $Q(t)$, was introduced in the extraction model at the bed scale (Chapter 3) as the time derivative of $V_{cum\ fitted}$. Fitting an analytical expression to the measured cumulative volume was chosen (alternatively to fitting and expression to the estimated flow rate). Accuracy in the determination of the cumulative volume was preferred since this is the relevant parameter for drink strength and yield calculations (Chapter 3).

Table 7.1: Average flow rate and derived *ad hoc* expressions for the cumulative volume

Ψ_j	ρ_{bed} (kg m^{-3})	Exp	$Q_{ave}\times10^{-6}$ (m^3 s^{-1})	$V_{cum\ fitted}\times10^{-6}$ (m^3)
	480	1	1.2 ± 0.3	*22.99·exp·(0.01943·t) + (-23.03·exp·(-0.06238·t))*
B	400	2	3.1 ± 0.6	*69.45·exp·(0.02337·t) + (-69.69·exp·(-0.007841·t))*
		3	01.0 ± 0.2	*26.27·exp·(0.01406·t) + (-26.22·exp·(-0.04151·t))*
	480	4	3.3 ± 0.7	*26.64·exp·(0.04238·t) + (-26.60·exp·(-0.09211·t))*
C		5	1.3 ± 0.3	*27.43·exp·(0.01703·t) + (-27.61·exp·(-0.05930·t))*
	400	6	3.1 ± 0.6	*29.16·exp·(0.03706·t) + (-29.27·exp·(-0.1195*t))*
		7	1.2 ± 0.2	*30.51·exp·(0.01292·t) + (-30.42·exp·(-0.03923·t))*
	480	8	3.7 ± 0.7	*32.95·exp·(0.03908·t) + (-32.92·exp·(-0.1224·t))*
D		9	1.3 ± 0.3	*36.50·exp·(0.01275·t) + (-36.45·exp·(-0.05043·t))*
	400	10	3.9 ± 0.6	*52.08·exp·(0.02824·t) + (-52.06·exp·(-0.08380·t))*
		11	1.5 ± 0.2	*40.73·exp·(0.01331·t) + (-40.60·exp·(-0.03698·t))*
	480	12	3.6 ± 0.9	*64.86·exp·(0.02005·t) + (-64.49·exp·(-0.06799·t))*
E		13	1.0 ±0.5	*40.93·exp·(0.01078·t) + (-40.75·exp·(-0.05488·t))*
	400	14	3.8 ± 0.5	*65.73·exp·(0.02190·t) + (-65.59·exp·(-0.05585·t))*
		15	1.7 ±0.2	*51.20·exp·(0.01236·t) + (-47.97·exp·(-0.02838·t))*

Table 7.1a shows the average flow rate (Q_{ave}) for the measured time-dependent flow rate at the outlet of the bed (Q_{exp}). The calculated Q_{ave} for the rest of the experimental conditions are reported in Table 7.1. All of them were found to be around the initially proposed average values of the time-dependent HF and LF regimes Table 7.1b shows the experimentally measured cumulative volume ($V_{cum\ exp}$), and how it compares with the predicted cumulative volume using the fitted *ad hoc* analytical expression (Eq. 7.1), and the cumulative volume ($V_{cum\ ave}$) from the average flow rate (Q_{ave}). The cumulative volume calculated from the average flow rate (Q_{ave}) lies below the measured cumulative volume ($V_{cum,\ exp}$), but the observed discrepancy between them decreases over time. All the simulations performed in this Chapter were carried out implementing a time-dependent flow rate, unless otherwise stated. However, since it is straightforward to estimate an average flow rate, and this is the reported parameter in

all the reviewed studies of coffee extraction techniques (Section 2.3.2), the sensitivity of the simulations to the choice of a constant or time-dependent flow rate is presented in Section 7.4.1.

7.2.2. Temperature response

Temperature in the extraction rig was measured before and after the extraction cell. Figure 7.2 shows an example of the inlet, outlet and inlet-outlet average temperature profile in a typical extraction experiment (Experiment number 12 in Table 7.1 and Table 7.2). Temperature is a non-steady state variable during extraction due to the thermal mass of the system and heat losses to the surroundings. It can be observed that for this particular case, the inlet temperature remains between 80-90 $°C$, whereas the outlet temperature quickly increases to 70-75 $°C$. In general, after 5-10 seconds, differences of around 5-15 $°C$ were found between inlet and the outlet temperature for all the experiments.

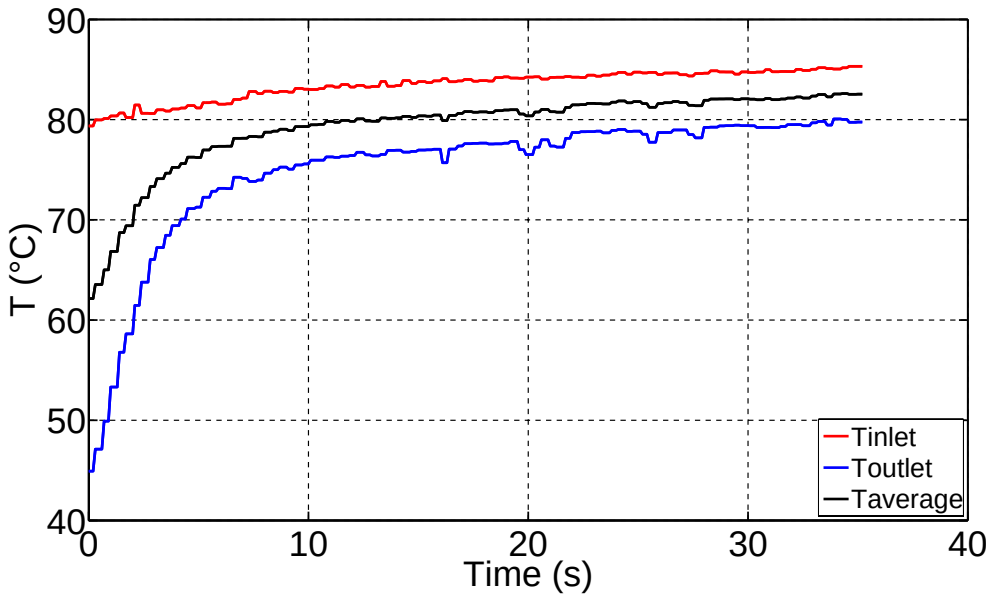

Figure 7.2: Typical inlet, outlet and average temperature profile of Ψ_E at HF and ρ_{bed} = 480 $kg\ m^{-3}$

This scenario may well reflect the real situation in espresso coffee machines. For example, Masella et al. (2014) reported water inlet temperatures of 80 ± 5 $°C$ and temperatures of the beverage in the cup of around 67-77 $°C$. Beyond the first 5 seconds (after the water has heated the bed), the average inlet-outlet profile (black line) tends to the characteristic steady state plateau. From the modelling point of view, extraction was assumed to occur at the average temperature value of the inlet-outlet average profile. The extraction temperature of the experiments was in the range of 75-85 $°C$ (Table 7.2), with the exception of Experiment 1 and 13 in which the average temperature was 72 $°C$.

The representative solid-liquid partition coefficient of coffee soluble solids and the microstructural effective diffusion coefficients were derived at 80 $°C$ (Chapter 4). The values were corrected for the calculated average temperature values and the results are reported in Table 7.2. The sensitivity of the simulations to the observed range of average temperatures as well as to the simplification of the temperature profile to a single representative temperature value is presented in Section 7.4.2.

Table 7.2: Average extraction temperatures and extraction parameters

Ψ_j	*Exp*	T_{ave} (°C)	[1]K	$^2D_{eff\,low} \times 10^{-11}$ ($m^2\,s^{-1}$)	$^2D_{eff\,med} \times 10^{-11}$ ($m^2\,s^{-1}$)	$^2D_{eff\,high} \times 10^{-11}$ ($m^2\,s^{-1}$)
	1	72.0 ± 3.2	0.61	25.9	7.4	2.6
B	2	80.1 ± 2.4	0.64	29.6	8.5	2.9
	3	75.8 ± 0.7	0.62	27.6	7.9	2.7
	4	77.9 ± 3.2	0.63	27.6	7.9	2.7
C	5	76.0 ± 1.3	0.63	27.8	7.7	2.7
	6	82.4 ± 0.6	0.64	29.6	8.5	2.9
	7	74.6 ± 2.6	0.62	26.2	7.5	2.6
	8	82.8 ± 1.0	0.65	25.9	7.4	2.6
D	9	77.3 ± 0.6	0.63	23.7	6.8	2.4
	10	83.1 ± 0.6	0.65	26.0	7.4	2.6
	11	79.9 ± 1.2	0.64	24.7	7.1	2.5
	12	80.3 ± 1.1	0.64	25.7	7.4	2.5
E	13	72.3 ± 2.7	0.61	22.5	6.5	2.2
	14	85.4 ± 0.8	0.65	27.8	8.0	2.8
	15	80.2 ±2.6	0.64	25.6	7.4	2.5

*[1]: Estimated from ln (K) = -657 (1/T) + 1.4 derived in Chapter 4 (*Figure 4.25*)*
[2]: Corrected with the Stokes-Einstein equation

7.3. Experimental results and model simulations

The aim of this Section is to present the results from the extraction experiments at the bed scale and compare them with the simulations provided by the extraction model.

7.3.1. General considerations

In addition to the parameters reported in Table 7.1 and Table 7.2, the following considerations were taken into account to perform the simulations.

- The initial concentration of extractable soluble solids in the grinds was estimated from Eq. 3.12. The maximum extraction yield for grinds Ψ_C and Ψ_D was not measured. From Figure 4.19, it can be seen that their maximum extraction yield

should lie between those measured for the finest (Ψ_B) and coarsest (Ψ_E) grinds used in this experiments. Thus, values of 0.28 and 0.29 were assumed for Ψ_C and Ψ_D, respectively.

- Due to the short time scale of these extraction experiments (35 and 80 seconds), the effective diffusion coefficient derived for the very high MW species (in the order of 10^{-12} m^2 s^{-1}) will not be considered in the simulations. From the relaxation time, it can be estimated that in 80 seconds a molecule with an estimated effective diffusion coefficient of 10^{-12} m^2 s^{-1} would have only diffused approximately 9 μm.

- Despite the varying particle porosity values derived for grinds Ψ_B - Ψ_E, it was found out in Chapter 6 that an average value of 0.53 was sensible to derive permeability estimates. This value is also assumed here for the simulations. Under these circumstances, the porosity of the beds resulted to be 0.36 and 0.24 for the lower (400 kg m^{-3}) and higher (480 kg m^{-3}) bed density, respectively.

- The effective diffusion coefficients derived from the microstructural measurements with the original measured porosity of the particle, were not corrected for the average particle porosity value of 0.53. In the case of a measured particle porosity of 0.50, considering a porosity of 0.53 would increase the effective difusion coefficient by 6 %. In the case of a measured particle of 0.57, considering a porosity of 0.53 would decrease the effective diffusion coefficient by 8 %. Simulations comparing both values (Section 7.4.3) show that there is virtually no difference in the profiles when this variability is considered.

- It was reported in Chapter 6 that, upon the application of a hydrodynamic load, the beds may consolidate. Consolidation was not observed in these experiments (except for Experiment 2) and this may be due to the considerably lower applied pressures, i.e. flow rates. The sensitivy of the simulations to consolidation through its effect on bed porosity and the volume of the packed bed is presented in Section 7.4.3.

7.3.2. Using the microstructural D_{eff} values in the model at the bed scale

The effect of particle size distribution (Ψ_B – Ψ_E) and the chosen effective diffusion coefficients (as derived from microstructural measurements) (Table 7.2) on the simulations is illustrated in this Section. Figure 7.3 shows the experimental and simulated extraction yield (*y*-axis) vs. extraction time (*x*-axis) for the four considered grinds at ρ_{bed} = 480 $kg\ m^{-3}$ and time-dependent LF regime (Table 7.1). These simulations were carried out with the extraction model reported Chapter 3 considering two size classes: fine and coarse particles (represented by the $d_{[4,3]}$ of the particle size distribution, as *dry* measured). Analogous results were obtained for the rest of the experimental conditions.

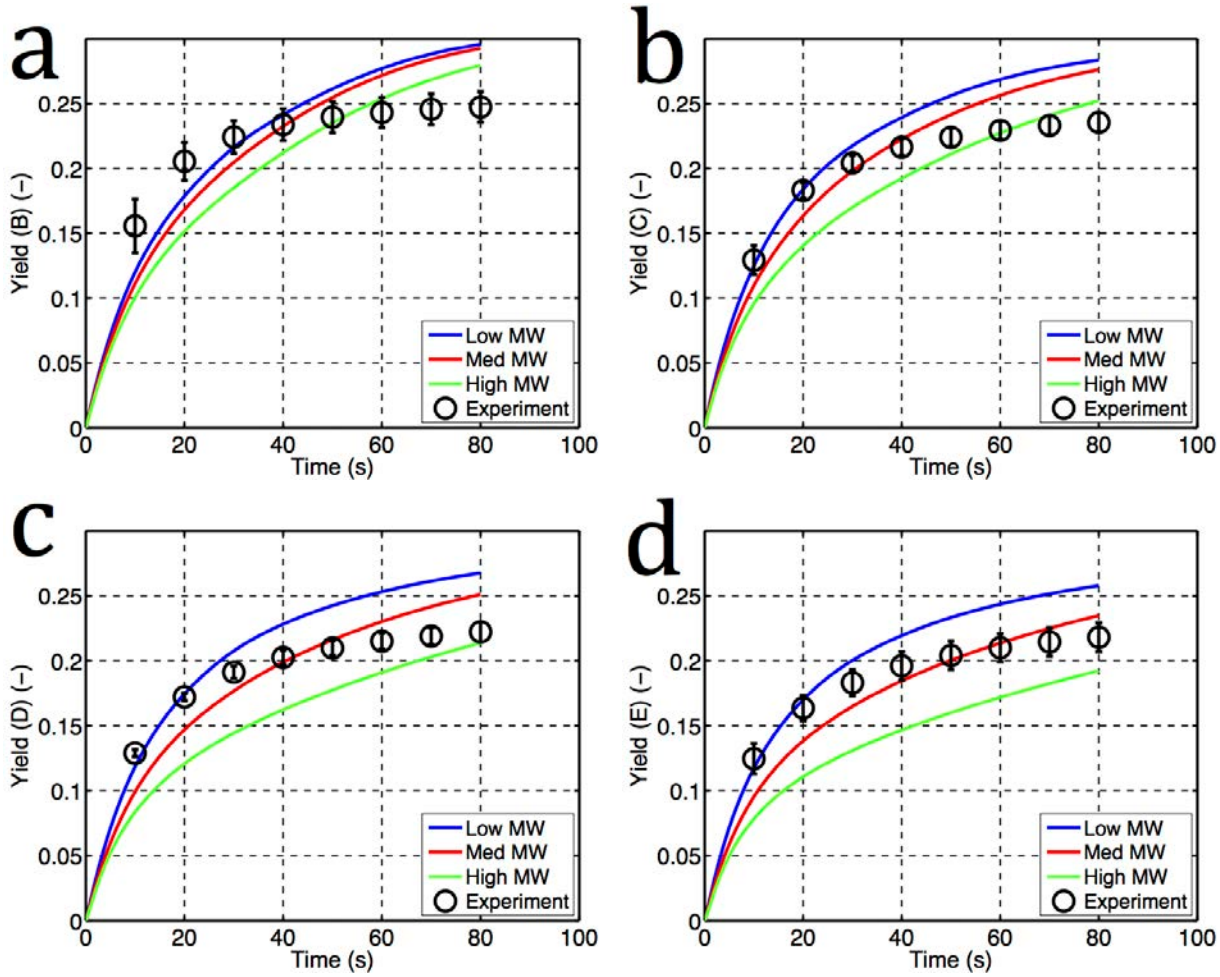

Figure 7.3: Extraction yield (y-axis) vs. time (x-axis). Simulation sensitivity to D_{eff} at ρ_{bed} = 480 $kg\ m^{-3}$ and LF; Experimental points (○), model (—). (a) Ψ_B (Experiment 1) ;(b) Ψ_C (Experiment 5); (c) Ψ_D (Experiment 9); (d) Ψ_E (Experiment 13)

The sensititivy of the simulations to the selection of an effective diffusion coefficient increases with grind size: the simulations obtained for the finest grind (Ψ_B) with the three considered effective diffusion coefficients differ less than in the case of the coarsest grind size (Ψ_E). The reason is the intrinsic increase of mass transfer resistance within coffee grinds with size. As expected from the simulations carried out throughtout Chapter 5, the effective diffusion coefficient for the low MW species tends to predict well the earlier time points of the extraction curve. However, as time elapses, effective diffusion coefficients for larger species predict the curves better. The effective diffusion coefficient for the medium MW species provides simulations that compare well

with the measured experimental data in the espresso coffee extraction regime, i.e. 30-40 *ml* extracted in 10-40 seconds. As can be seen in Figure 7.4, these effective diffusion coefficients provided the overall better MPE values (9-14 %) for all the tested experimental conditions reported in Table 7.1 and Table 7.2. This can be considered as acceptable to predict the extraction yield in espresso coffees if it is taken into account that no parameters were fitted to the experimental results.

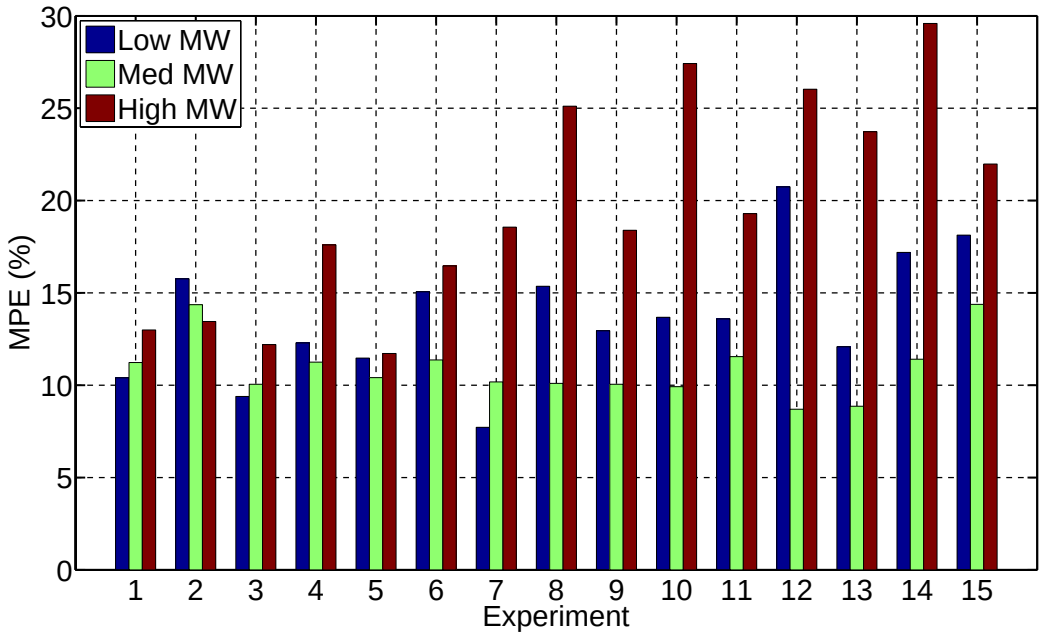

Figure 7.4: Medium percentage error (MPE) of the experiments reported in Table 7.1 and Table 7.2

Figure 7.5 displays the experimental and simulated drink strength (*y*-axis) vs. extraction time (*x*-axis). From the qualitative point of view, the trend is similar to that reported by Navarini et al. (2004), who fitted the experimental data to a power law. Comparing Figure 7.3 and Figure 7.5, one can see that longer extraction times result in higher extraction yields but lower drink strengths as the extracted volume increases. Thus, one can see that the natural solution to obtain acceptable extraction yields, in

relatively small volumes (high strength) is to use finer grind sizes at the cost of a greater pressure drop across the bed.

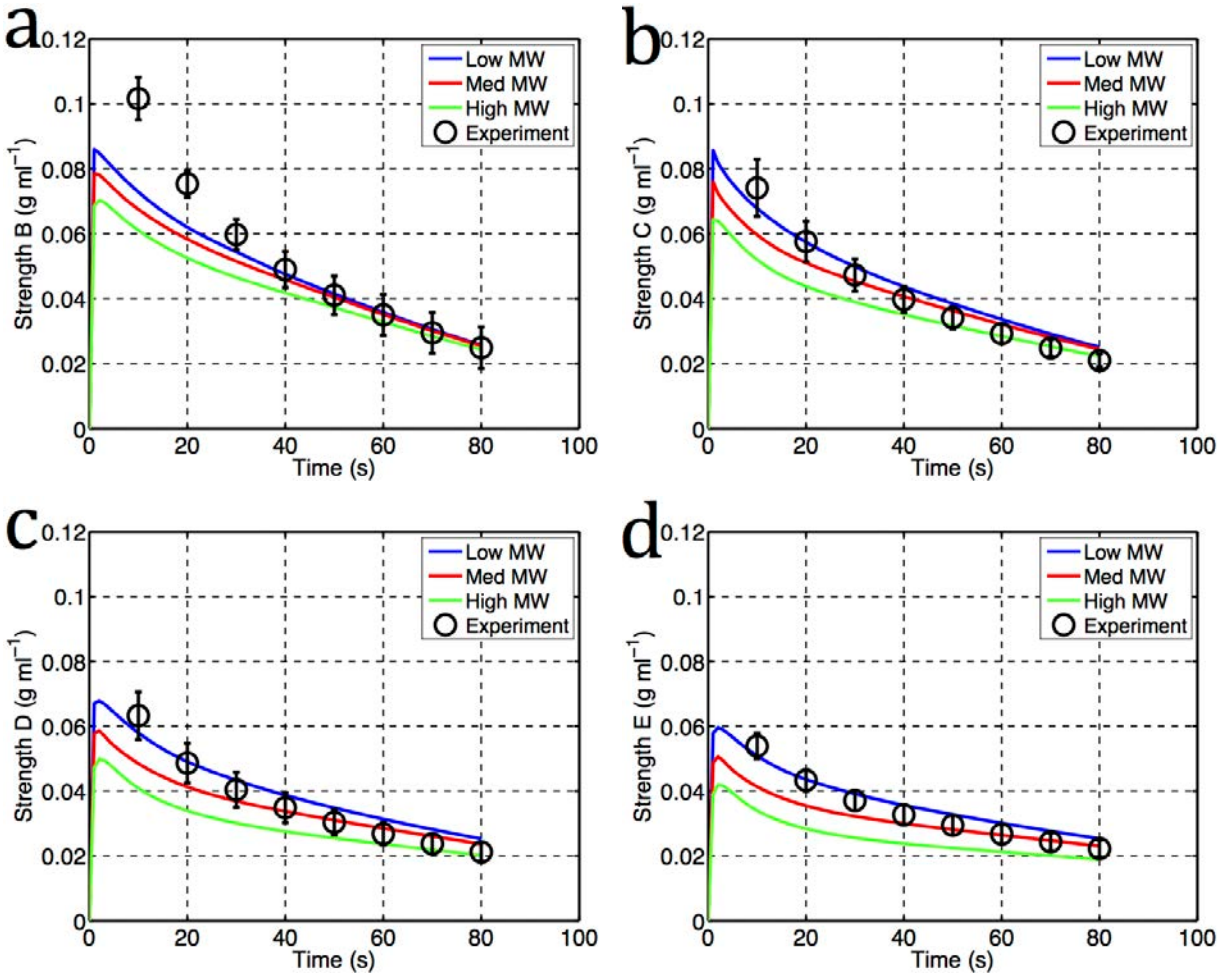

Figure 7.5: Drink strength (y-axis) vs. time (x-axis) at ρ_{bed} = 480 $kg\ m^{-3}$ and LF; Experimental points (○), model (—). (a) Ψ_B (Experiment 1) ;(b) Ψ_C (Experiment 5); (c) Ψ_D (Experiment 9); (d) Ψ_E (Experiment 13)

7.3.3. Multiple Deff and effect of the solid-liquid partition coefficient (K)

Figure 7.3 and Figure 7.5 showed that the experimental points beyond the espresso regime are over-predicted by the model for finer grinds (Ψ_B – Ψ_D). This effect was also observed in Chapter 5. The equilibrium yield achieved in the stirred vessel was preceded by gradual increase of the yield over time (between 60 and 1200 seconds for

the fine grinds and 300 and 2400 seconds for coarser grinds), not predicted by the model with a single effective diffusion coefficient. The time scale in which the model starts to over-predict coincides with that observed in the slurry vessel. In the latter case, generating an extraction curve that accounted for the multiple effective diffusion coefficients was shown to fit the experimental data well. The same strategy was implemented here: according to the results of Chapter 5 (Section 5.7.2), a low MW species fraction of 84.5 % or 68.3 % was assumed for the grinds. Equal percentages for the medium and high MW species were assumed. Note that due to the much shorter time scale of the packed bed experiments, the percentages assumed here for the medium and high MW species are lower than those assumed in Chapter 5 for the finest grind (Ψ_B). The curves shown in Figure 7.3 were re-scaled according to the aforementioned percentages and the results, as well as the simulation provided by the effective diffusion coefficient obtained for the low and medium MW species, are shown in Figure 7.6.

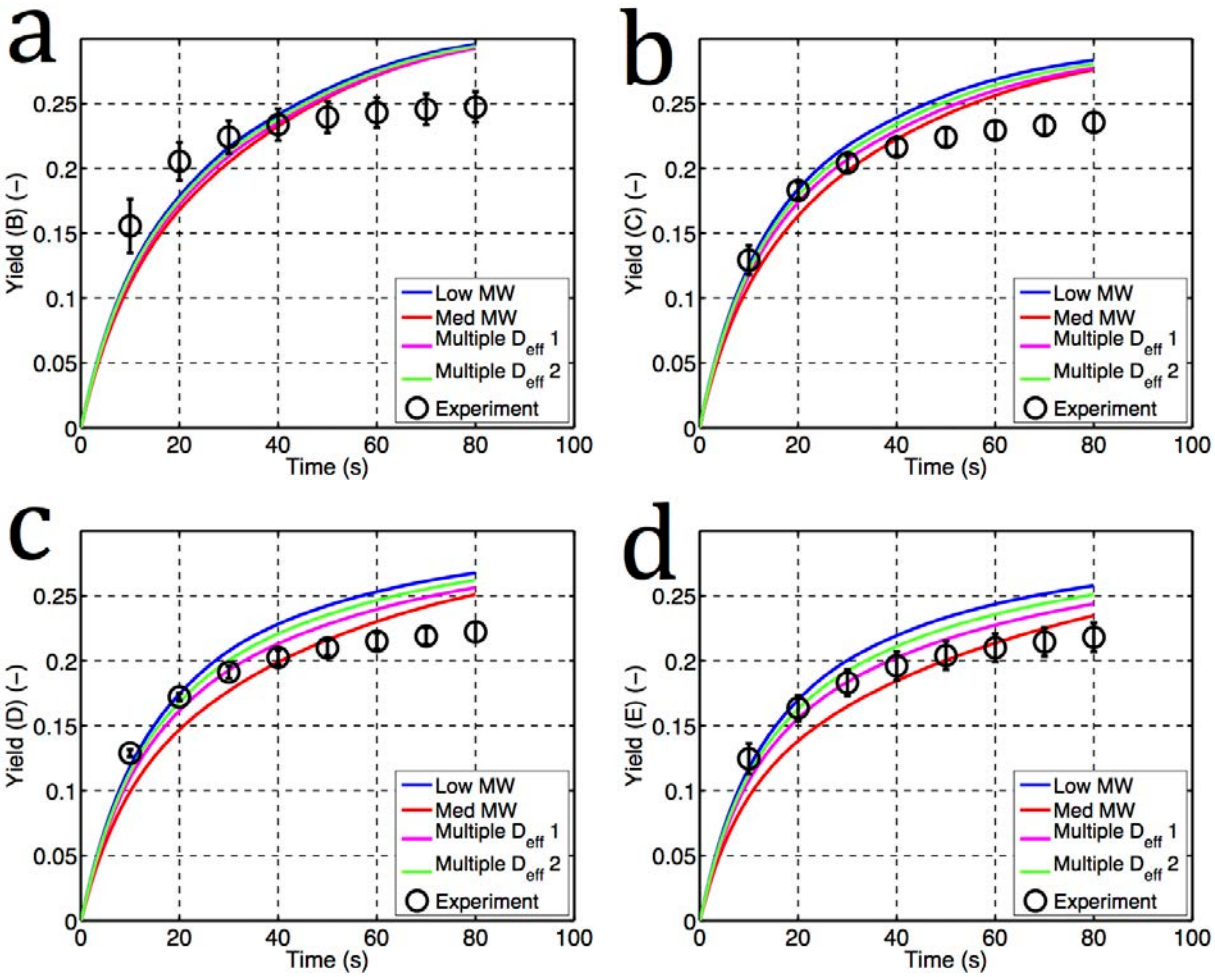

Figure 7.6: Re-scaling of the individual extraction curves shown in Figure 7.3 by assuming a percentage of the low MW of 68.3 % ($D_{eff}1$) or 84.5 % (D_{eff} 2) and equal percentage of the medium and high MW species. ρ_{bed} = 480 $kg\ m^{-3}$ and LF; Experimental points (○), model (—). (a) Ψ_B (Experiment 1) ;(b) Ψ_C (Experiment 5); (c) Ψ_D (Experiment 9); (d) Ψ_E (Experiment 13)

Unlike the case of the slurry vessel, the improvement when the different effective diffusion coefficients are incorporated into a single extraction curve is not as significant, especially for the case of finer grinds (Ψ_B – Ψ_C). This points out that, in addition to the effect of the different diffusing species, there may be further effects that have not been considered so far. The simulations were carried out with a single representative value of the solid-liquid partition coefficient (Table 7.2). As shown in the sensitivity analysis performed Chapter 5, this constitutes a fair approximation in very diluted regimens. In the slurry vessel experiments, the maximum concentration of soluble solids can be

estimated to be 0.7 g per 100 g of solution (as estimated from 12.5 g of RGC in 500 *ml* of water with an extraction yield of 0.28). However, in espresso-style extraction concentrated extracts are generated, especially during the first seconds of the operation. This is especially true for the case of lower flow rates (longer extraction and residence times) and finer grinds. For instance, the concentration of the first two aliquots taken in Experiment 1 (Ψ_B) was 10 and 4 g per 100 g, respectively; this resulted to be 5 and 3 g per 100 g in the case of Experiment 13 (Ψ_E). In such a concentrated regime, accounting for the different values of the solid-liquid partition coefficient of the species may be relevant. However, deriving individual solid-liquid partition coefficients is a tedious task, as it would require equilibrium experiments (at least three temperatures) similar to the ones shown in Section 3.3.13, and measuring the concentration of each individual species. Thus, in order to illustrate the effect of the solid-liquid partition coefficient on the extraction curves in a packed bed, values for the different species were assumed: according to Spiro and Page (1984), the partition coefficient of caffeine is circa 1 at 85 $°C$ and this value was assumed here. Smaller values of the partition coefficient (0.5 and 0.1) were arbitrarily assumed for the medium and high MW species, respectively, as solubility is expected to decrease for larger molecules. The comparison between the simulations with a single or multiple solid-liquid partition coefficients are shown in Figure 7.7 considering multiple diffusing species (percentage of low MW species = 68.3 %).

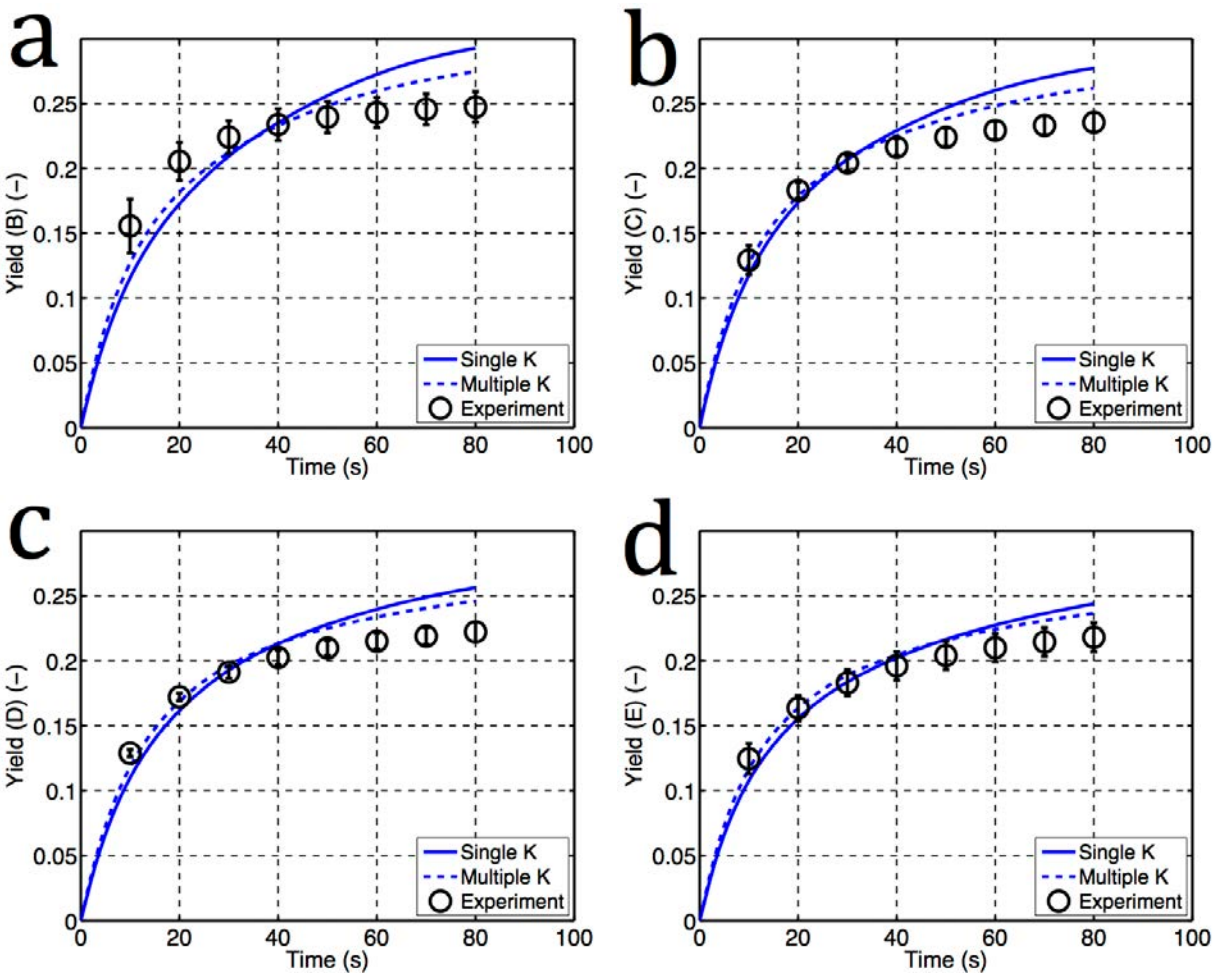

Figure 7.7: Extraction yield (y-axis) vs. time (x-axis) for multiple diffusion species (low MW species percentage of 68.3 %) and multiple partition coefficients (K = 1 for low MW species, 0.5 for medium MW species, and 0.1 for large MW species); ρ_{bed} = 480 $kg\ m^{-3}$ and LF; Experimental points (○), model (—). (a) Ψ_B (Experiment 1) ;(b) Ψ_C (Experiment 5); (c) Ψ_D (Experiment 9); (d) Ψ_E (Experiment 13)

The shape of the extraction curve in a packed bed can be more accurately mimicked when different values of the partition coefficients are considered. It can be seen that in the case of the finer grinds (precisely where the extracts are more concentrated) the over-prediction at longer times becomes less dramatic. This illustrates the relevance of the solid-liquid partition coefficients in extraction from packed beds. However, since the values of the partition coefficients were arbitrarily assumed and thus their dependency with temperature is unknown, this approach will not be further considered in the next simulations.

In addition to the effect of the value of the parameters of the model, there are other potential factors that are intrinsic to the nature of packed beds that may contribute to the observed over-prediction of the model. Segregation and axial compaction of the beds (Section 6.2.1) may create plugged regions of agglomerated material through which the local flow may be very slow. This results in a low concentration gradient between the surface of the particle and the pore space of the bed thus decreasing the mass transfer rate. Extraction yield reduction for fine particle sizes has been previously reported in the supercritical extraction literature and was attributed to agglomeration (del Valle et al., 2008; Eggers et al., 2000).

7.3.4. Effect of flow rate

The effect of flow rate on extraction from a packed bed was experimentally evaluated by conducting extraction experiments HF and LF regimes, and the results were compared to model simulations. Figure 7.8 shows the experimental and simulated extraction yield (*y*-axis) vs. drink volume (*x*-axis) for Ψ_B (at ρ_{bed} = 400 $kg \cdot m^{-3}$) and Ψ_E (at ρ_{bed} = 480 $kg \cdot m^{-3}$) and multiple effective diffusion coefficients (low MW percentage of 68.5 %) at the corresponding HF and LF time-dependent flow rate regimes, respectively. The simulations overall match the experimental points except for the aforementioned effect in Section 7.3.2 at longer extraction times/ greater volumes.

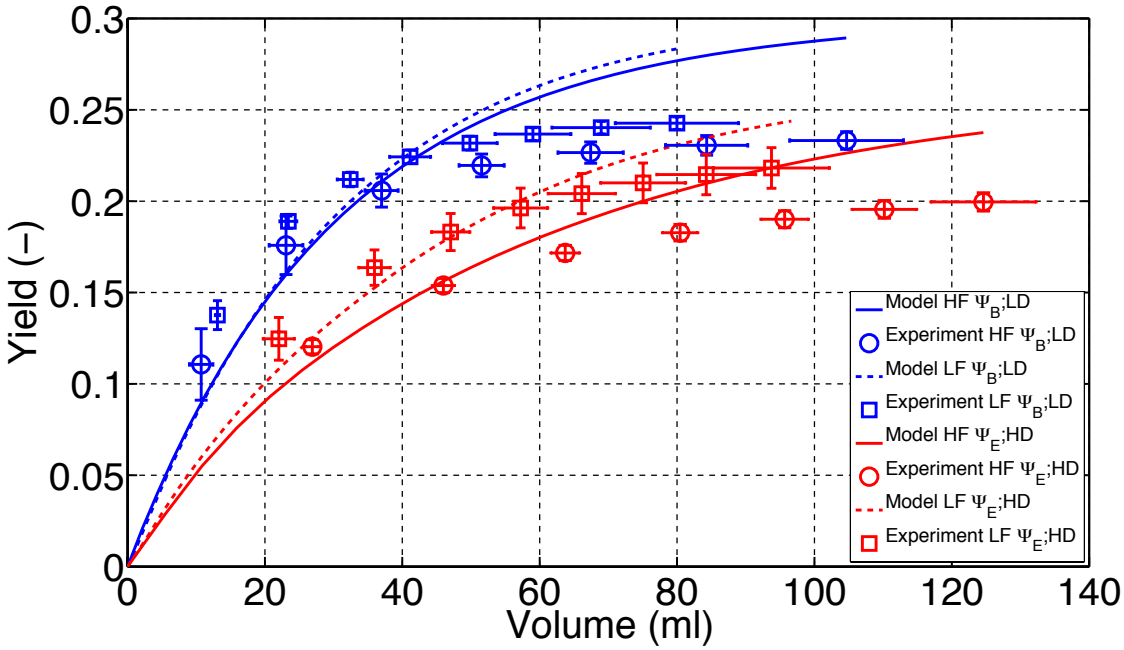

Figure 7.8: Extraction yield (y-axis) vs. volume (x-axis) for Ψ_B at ρ_{bed} = 400 $kg\ m^{-3}$ (LD) and HF (Experiment 2) and LF (Experiment 3) and Ψ_E at ρ_{bed} = 480 $kg{\cdot}m^{-3}$ (HD) and HF (Experiment 12) and LF (Experiment 13). Multiple diffusion species (low MW species percentage of 68.3 %); Experimental points (○), model (—)

The effect of flow rate is twofold: it fixes the extraction time, defined as the time required to produce a given drink volume ($t_{extraction} = V_{drink}/Q_{ave}$), and water residence time, defined as the time spent by the water inside the bed ($t_{residence} = (V_{bed}\,\varepsilon_{bed})/Q_{ave}$). Regarding extraction time, one can see that to produce 40 *ml* of drink approximately 40 seconds are required at LF versus 11.4 seconds at HF. Longer extraction times imply that more material from the grinds will be extracted. Figure 7.8 illustrates that the effect on extraction yield of using a LF regime is more accute the coarser the particle size distribution of the grinds is, and this is well captured by the model. As pointed out in Chapter 5, the characteristic extraction time from the grinds ($t_R = R^2/D_{eff}$) scales as the square of their size. Thus, increasing $t_{extraction}$ balances the slower internal mass transfer rate in coarser grinds. Also, for Ψ_E the average extraction temperature at the HF was 80 $°C$ whereas it was 72 $°C$ for the LF. The greater extraction yield for the case of LF

points out that, in this temperature range, extraction time (as set by the flow rate) may dominate over temperature effects.

The effect of the water residence time is a more subtle one. The mass transfer driving force is the concentration gradient at the surface of the particle and its value depends not only on how fast species are transported within the grain to the surface (as estimated by their relaxation time), but also on how fast species are removed from the pore space of the bed to the cup ($t_{residence}$). For LF regimes, the effect of longer extraction times on extraction yield may be partially counteracted by the effect of a reduced mass transfer rate given by the low concentration gradients. In order to investigate this effect, the total transported mass (M) from both fine and coarse size classes to the bed pore space was defined as follows:

$$M = \int_0^{t_{exp}} \sum_{i=1}^{sc} \frac{3\left(1-\varepsilon_{bed}\right)}{\varepsilon_{bed} R_i} \upsilon_i J_i dt \qquad \text{Eq. 7.2}$$

Where ε_{bed} is the porosity of the bed (-), R_i (m) is the average size of the size classes, v is the volume percentage of the size classes (-) and J is the diffusive flux coming out of each size class($kg\ m^{-2}\ s^{-1}$).

Figure 7.9 displays the simulated transported mass from the particles to the bed pore space for Ψ_B at 480 $kg\ m^{-3}$ and 80 $°C$ at three different constant flow rates, 5×10^{-6}, 1.0×10^{-6} and 0.5×10^{-6} $m^3\ s^{-1}$.

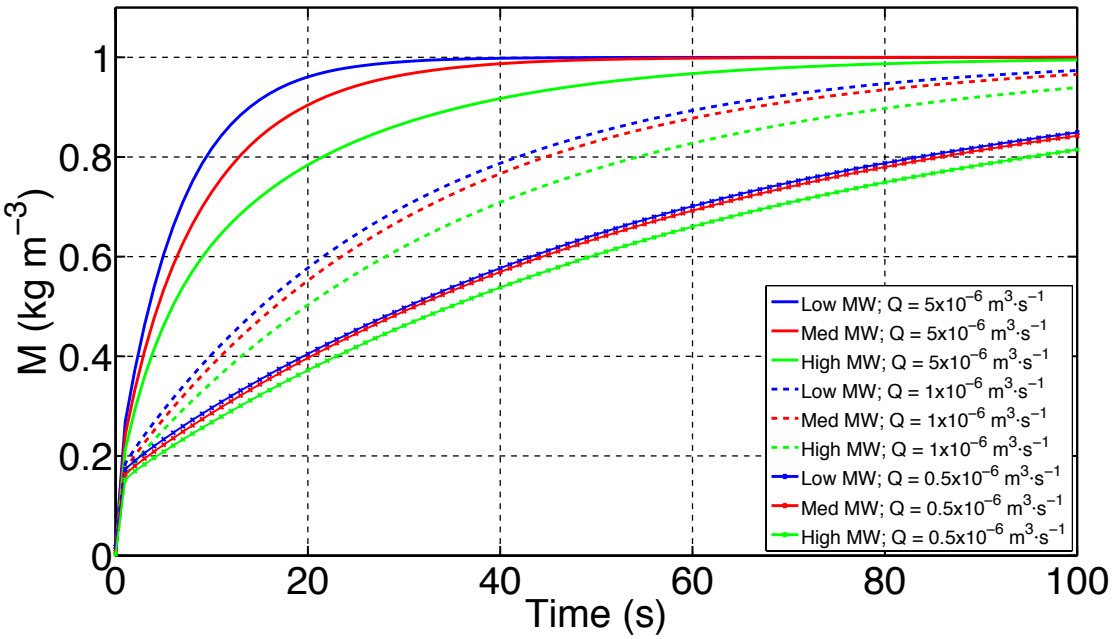

Figure 7.9 Particle-pore space of the bed mass transfer rate of the low, medium and high MW species in Ψ_B at 480 $kg\ m^{-3}$ and 80 °C; $Q = 5\times10^{-6}\ m^3\ s^{-1}$ (—); $Q = 1.0\times10^{-6}\ m^3\ s^{-1}$ (----); $Q = 0.5\times10^{-6}\ m^3\ s^{-1}$ (-x-)

As flow rate decreases, the particle-pore space of the bed mass transfer (M) is considerably lower for the considered species. This effect is caused by the pore space concentration of the bed building up at lower flow rates due to the longer resisdence times achieved. The concentration of the molecules with the highest effective diffusion coefficient would build faster in the pore space of the bed, and thus a more pronounced reduction in its particle-bed pore space extraction rate is observed. Additionally, although it has not been accounted for in this simulation, these species presumably have the highest solid-liquid partition coefficient, and that would contribute even more dramatically to the observed effect.

Figure 7.10 shows the contribution of the fine size class of Ψ_B to the particle-bed pore space transport at the three considered flow rates. At higher flow rates, the three considered species are extracted from the particles at a similar rate, despite their notably different effective diffusion coefficient. However, when lower flow rates are

considered, the species with the lowest diffusion coefficients are extracted faster. The slower transport inside the particle, due to a lower effective diffusion coefficient, allows maintaining a higher driving force as compared to species with higher effective diffusion coefficients Additionally, a negative slope is observed at early times at the lower flow rates in the particle-bed pore space extraction. This suggests that there is a mass flux from the pore space of the bed into the fine particles. The driving force in fine particles decreases very quickly since extraction procceds rapidly, and the driving force in coarser particles decreaes more slowly and it may still allow extraction from this particles to occur. This would increase the concentration in the pore space of the bed above that at the surface of the finer particles creating the negative driving force.

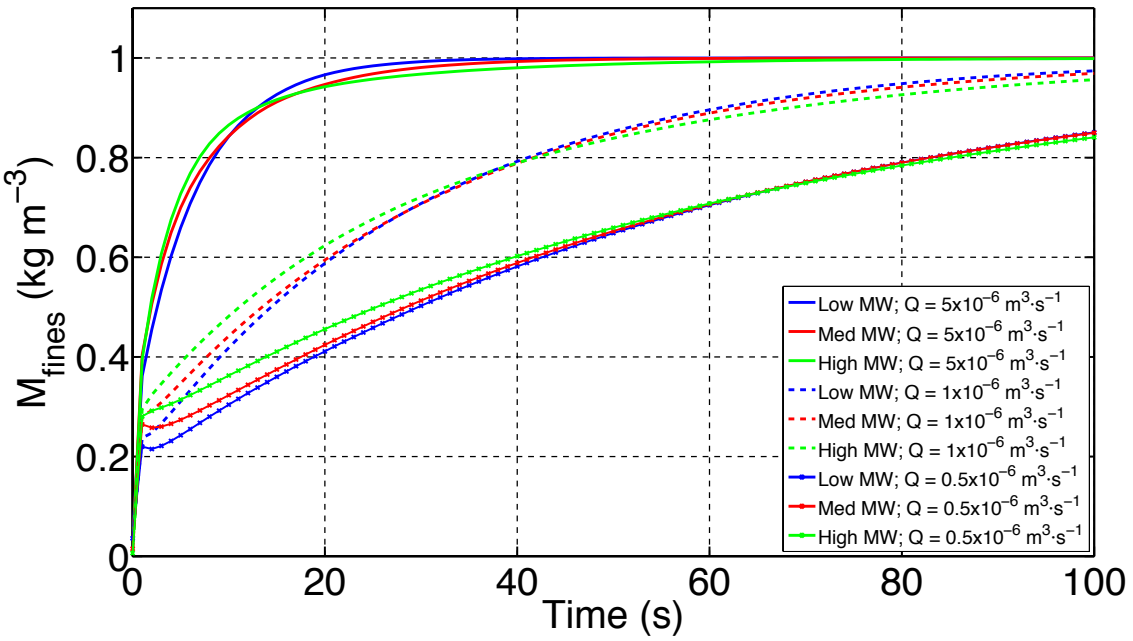

Figure 7.10: Particle-pore space of the bed mass transfer rate of the three considered species in the fine size class of Ψ_B at 480 $kg\ m^{-3}$ and 80 °C; Q = 5×10-6 $m^3\ s^{-1}$ (—); Q = 1.0×10-6 $m^3\ s^{-1}$ (----); Q = 0.5×10^{-6} $m^3\ s^{-1}$ (-x-)

In Figure 7.11 the influence of the bed density on the particle-pore space of the bed mass transfer is illustrated. The simulation was carried out with the same

parameters as in Figure 7.9 at two bed densities (400 and 480 $kg\ m^{-3}$) and the lowest flow rate (Q = 0.5 $m^3\ s^{-1}$). The influence of flow rate becomes more noticiable at the higher bed densities (and hence lower bed porosity) as the concentration in the bed pore space would build up faster due to the smaller pore space volume available.

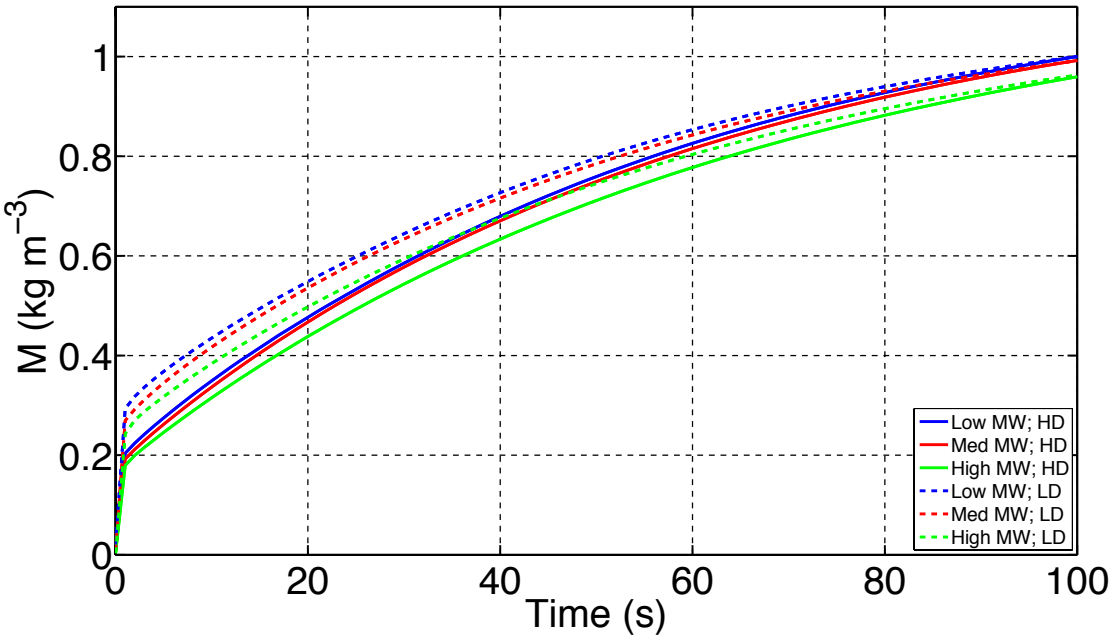

Figure 7.11 Particle-pore space of the bed mass transfer rate of the three considered species in Ψ_B at 80 °C and 0.5 $m^3\ s^{-1}$; ρ_{bed} = 480 $kg\ m^{-3}$ (HD) and ε_{bed} = 0.24 (—); ρ_{bed} = 400 $kg\ m^{-3}$ (LD) and ε_{bed} = 0.36

Both reported flow rate effects (extraction time and residence time) are thus competing effects. On the one hand, a slower flow rate provides a longer brewing time and thus higher extraction yields for a given drink volume. On the other hand, a slow flow rate also provides longer water residence times that can decrease particle-bed pore space mass transfer rate as the driving force is reduced as the concentration in the bed builds up. Table 7.3 displays the required times to produce 40 *ml* (typical in espresso coffee) and the simulated extraction yield of the considered species for the three considered flow rates. One can see that the extraction time effect is the dominant effect: although at higher flow rates the particle-bed pore space mass transfer rate is higher,

the effect of a shorter extraction time results in lower extraction yields. Morever, it can be seen that for lower yields, the relative proportion of smaller MW species in the drink is higher.

Table 7.3: Required extraction times and obtained extraction yields for the three considered flow rates

Q (ml·s⁻¹)	***Extraction time (s)***	***Extraction yield low MW***	***Extraction yield med MW***	***Extraction yield high MW***
0.5	80	0.24	0.24	0.23
1	40	0.24	0.23	0.21
5	8	0.23	0.20	0.17

7.3.5. Effect of pressure drop

The pressure drops across the beds studied in this Chapter using the experimental conditions detailed in Table 7.1 are shown in Figure 7.12.

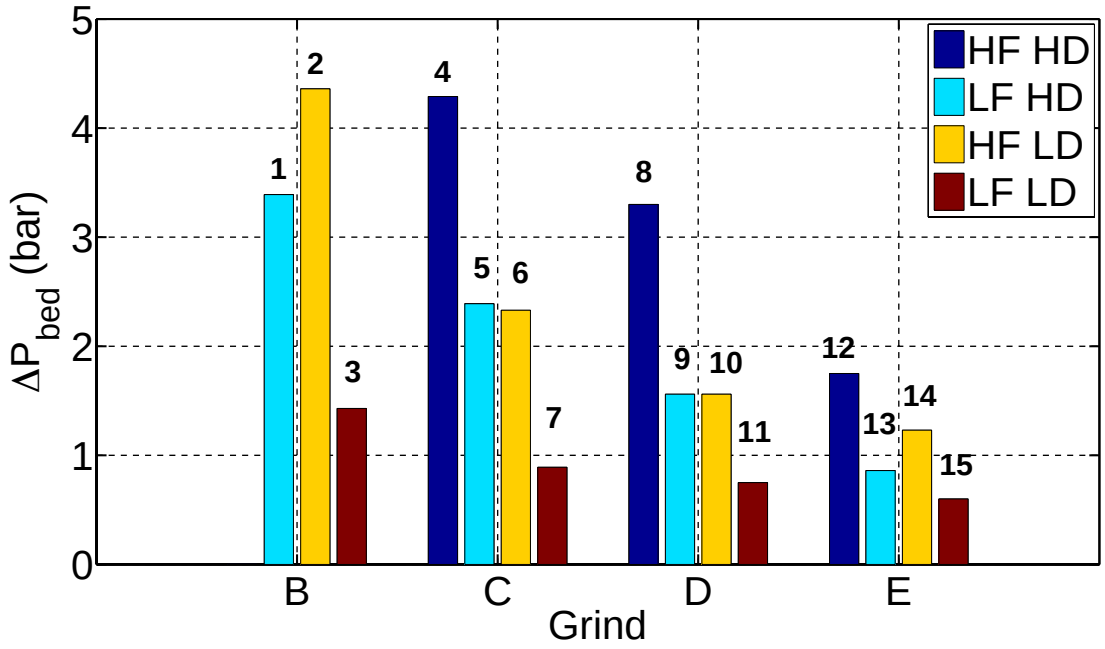

Figure 7.12: Pressure drop across the bed resulting for the considered grinds in the experimental conditions detailed in Table 7.1.The numbers identify the experimental conditions to which the pressure drop is referred. Relative standard deviation < 3 % in all the cases

The pressure drop across the beds made from the finest grind (Ψ_B), significanlty differ for HF and LF regimens at 400 $kg\ m^{-3}$ (ΔP_{bed} = 4.4 and 1.4 *bar*, respectively). However the extraction profiles, as shown in Figure 7.8, are virtually identical. It is thus clear that using a quite different *extraction pressure* (as typically referred in the literature) had no relevant effect neither on the kinetics of extraction or on the total extracted amount. As illustrated here (and throughout Chapter 6), the role of *extraction pressure* was limited to set the desired flow rate for a given hydraulic resistance of the beds, or more generally, the system, if the nozzles typically located at the outlet of espresso machines to create foam are considered. In the case of the coarsest grind (Ψ_E) at 480 $kg\ m^{-3}$, the pressure drop across the beds was certainly more similar (1.8 and 0.9 *bar*, respectively) than in the case of Ψ_B. However, the extraction profiles are somewhat different. Furthermore, it can be seen in this case that the selection of a lower *extraction pressure* results in a higher extraction yield (and thus brew strength) due to the longer extraction times.

As shown before in Section 7.3.4, flow rate is the variable that may really influence the beverage properties and pressure drop is a consequence of the desired flow rate. In commercial brewers, the way to adjust the flow rate to a desired value is by increasing the hydraulic resistance of the bed via decreasing grind size and increasing bed density by increasing the mass of coffee and/or tamping the bed harder. These operations increase the pump working pressure and consequently the pressure drop across the bed. The higher yields obtained as a consequence of the lower flow rates, i.e. longer extraction times and higher residence times, and smaller particle size distributions (as seen in Figure 7.8) can be wrongly attributed to this observed change in pressure. It is then likely that the distinctive characteristics attributed to the effect of

different *extraction pressure* in commercial systems (Andueza et al., 2002; Caprioli et al., 2012, 2014) may be due to other factors, such as, for example, the aforementioned modification of residence times in the bed.

7.3.6. Effect of coffee mass

The effect of coffee mass was investigated by conducting extraction experiments with beds made with either 8.0 or 9.5 g (400 or 480 $kg\ m^{-3}$). Figure 7.13a shows the simulated and experimental extraction yield (y-axis) vs. drink volume (x-axis) for Ψ_B and Ψ_E for LF, multiple effective diffusion coefficients (low MW percentage of 68.5 %) and ρ_{bed} = 480 and 400 $kg\ m^3$. One can see that in a packed bed (unlike the case of extraction in a stirred vessel investigated in Chapter 5), the achieved extraction yield does not depend on the amount of RGC being processed, but only on the size of the grind and extraction time. The model predicts fairly accurately the virtually equal experimental extraction yield for both bed densities in both grinds.

Figure 7.13b displays the simulated and experimental drink strength (y-axis) vs. volume (x-axis) for the same conditions. One can see that drink strength notably increases as bed density increases. It can be concluded that for a given grind and flow rate regime, drinks produced with different coffee masses will have similar extraction yields, but different sensory properties based on the different drink strengths. These findings agree with Andueza et al (2007), who found that increasing the mass of RGC from 6.5 to 8.5 g resulted in an increment of brew strength from 3.4 to 4.2% but did not show any effect on extraction yield.

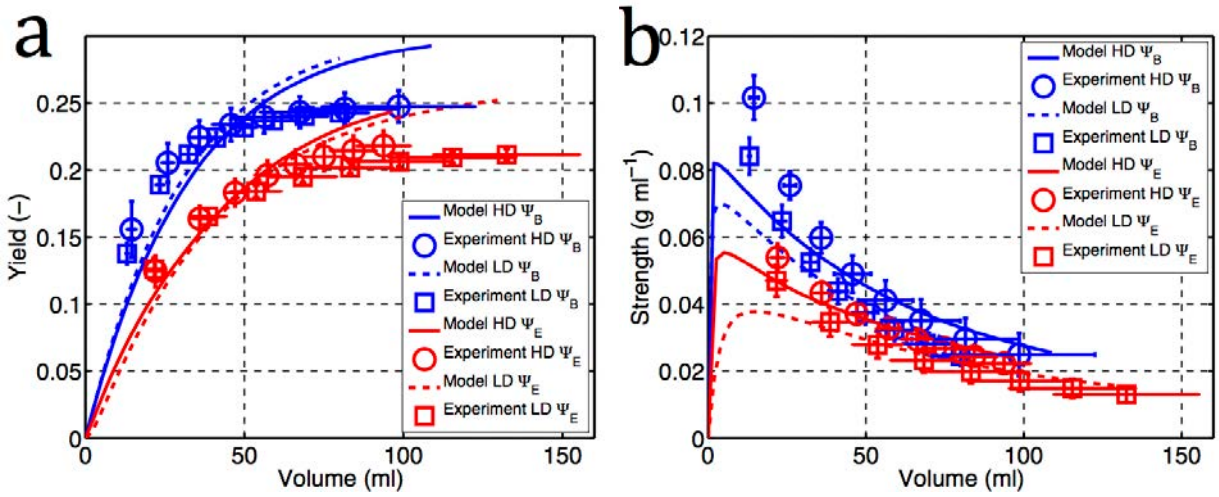

Figure 7.13: Simulated and experimental extraction for Ψ_B and Ψ_E at LF and ρ_{bed} = 480 $kg\ m^{-3}$ (HD) Multiple diffusion species (low MW species percentage of 68.3 %); Model (—), Experiment (○); ρ_{bed} = 400 $kg\ m^{-3}$ (LD): Model (----), Experiment (□); (a) Yield; (b) Drink strength

7.4. Sensitivity study of the extraction model at the bed scale

The aim of this Section is to carry out a sensitivity study to test the implications of some of the assumptions that have been adopted in the extraction model at the bed scale. The considerer parameters are selection of a constant or time-dependent flow rate, temperature, and particle and bed porosity.

7.4.1. Flow rate selection

The model sensitivity to the adoption of a time-dependent or the assumption of a constant flow rate was evaluated by comparing the simulations resulting from both choices via the relative difference in the simulations. To illustrate this, the model was solved at 80 $°C$ for the four considered grinds at bed density of 480 $kg\ m^{-3}$, the LF regime, and the effective diffusion coefficient for the medium MW species (Chapter 4).

Figure 7.14a and b show the simulated extraction yield and drink strength (y-axis) vs. time (x-axis). The observed under estimation of the cumulative volume when a

constant flow rate was considered results in lower simulated extraction yields but higher drink strengths.

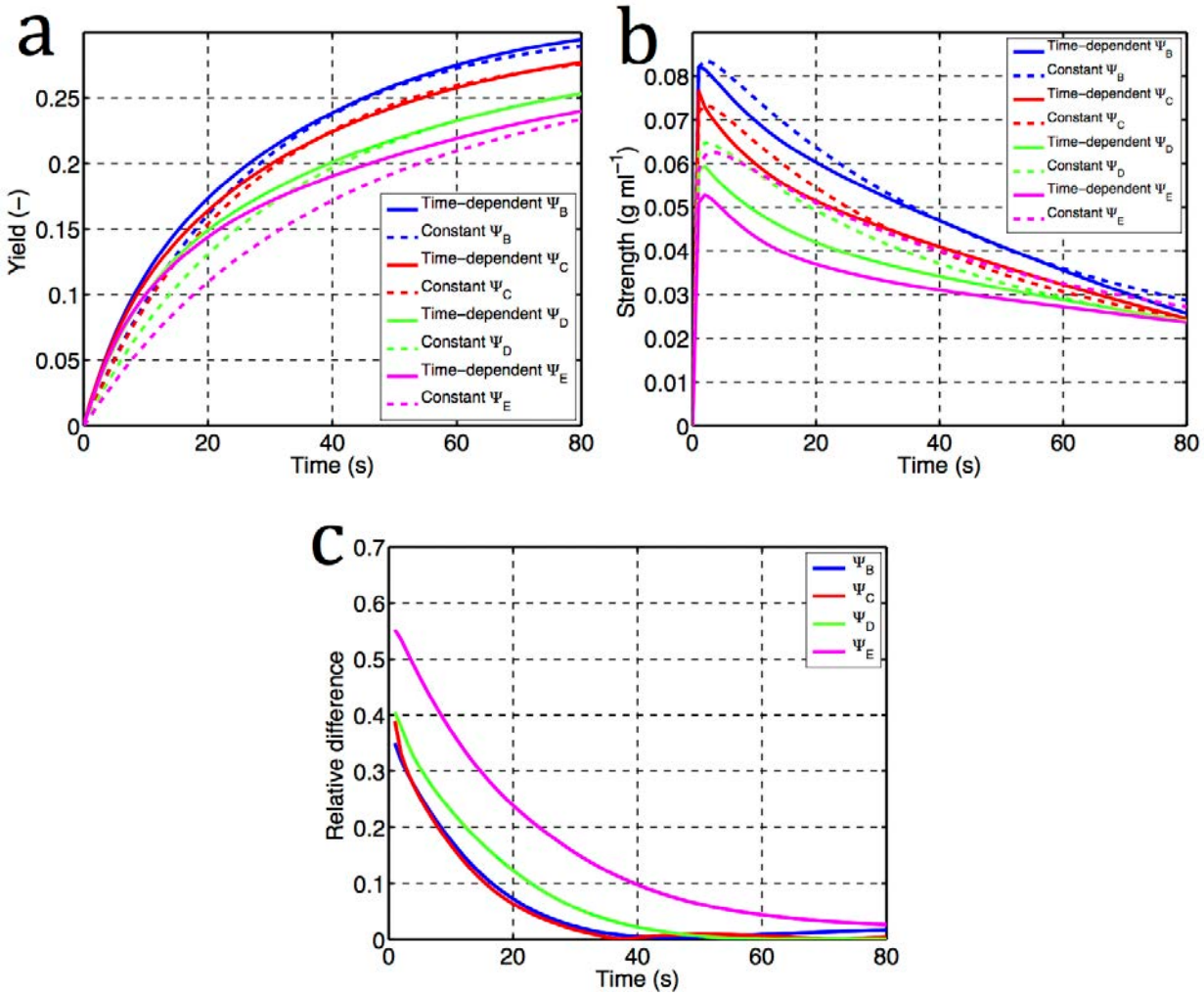

Figure 7.14: Extraction simulation of the four considered grinds for ρ_{bed} = 480 $kg\ m^{-3}$, LF and the effective diffusion coefficient of the medium MW species at 80 °C; Time-dependent flow rate (—); constant flow rate (----); (a) Extraction yield vs. time; (b) Strength vs. time; (c) Relative difference between the simulations

Figure 7.14c shows the relative difference between the time-dependent and constant flow rate simulations. Note that the relative difference decreases and approaches zero as time elapses. Therefore, depending on the purpose of the simulation, e.g. estimating final extraction yield or drink strength in an espresso coffee, an average flow rate may provide a similar estimation to the one provided by the real time-dependent flow rate profile. This conclusion is certainly useful from the practical point

of view, since the relevant parameter for product development is the final result in the cup rather than the dynamics of the system. Implementing in the model an average flow rate avoids having to characterise the non-steady state flow rate through the system.

7.4.2. Temperature

Temperature influences the solubility of coffee soluble solids via the solid-liquid partition coefficient, and the rate at which they are extracted via the effective diffusion coefficient. The effect of the different values of the solid-liquid partition coefficient for the considered species was analysed in Section 7.2.2. In order to assess the sensitivity of the simulations, a range of temperatures from 60 to 90 $°C$ was considered. Ψ_E was chosen since the sensitivity to model parameters selection increases with grind size. A ρ_{bed} = 480 $kg\ m^{-3}$, LF, and effective diffusion coefficient for the medium MW species (Chapter 4) were selected to carry out the simulation. The solid-liquid partition coefficient and effective diffusion coefficient (for medium MW species) at 80 $°C$ were corrected to account for the temperature difference (Table 7.4).

Table 7.4: Parameters for the analysis of the sensitivity of the simulations to temperature

T (°C)	***D_{eff}×10^{-11}(m^2 s^{-1})***	***K***
60	5.2	0.57
65	5.7	0.59
70	6.2	0.60
75	6.8	0.62
80	7.3	0.64
85	7.9	0.65
90	8.6	0.67

Figure 7.15 shows the simulated extraction yield (y-axis) vs. time (x-axis) for the conditions reported in Table 7.4. As expected, extraction rate increase with temperature.

The simulations are less sensitive to temperature as temperature increases: this is, the difference between the profiles at 60 and 65 °*C* is greater as compared to the case of 85 and 90 °*C*.

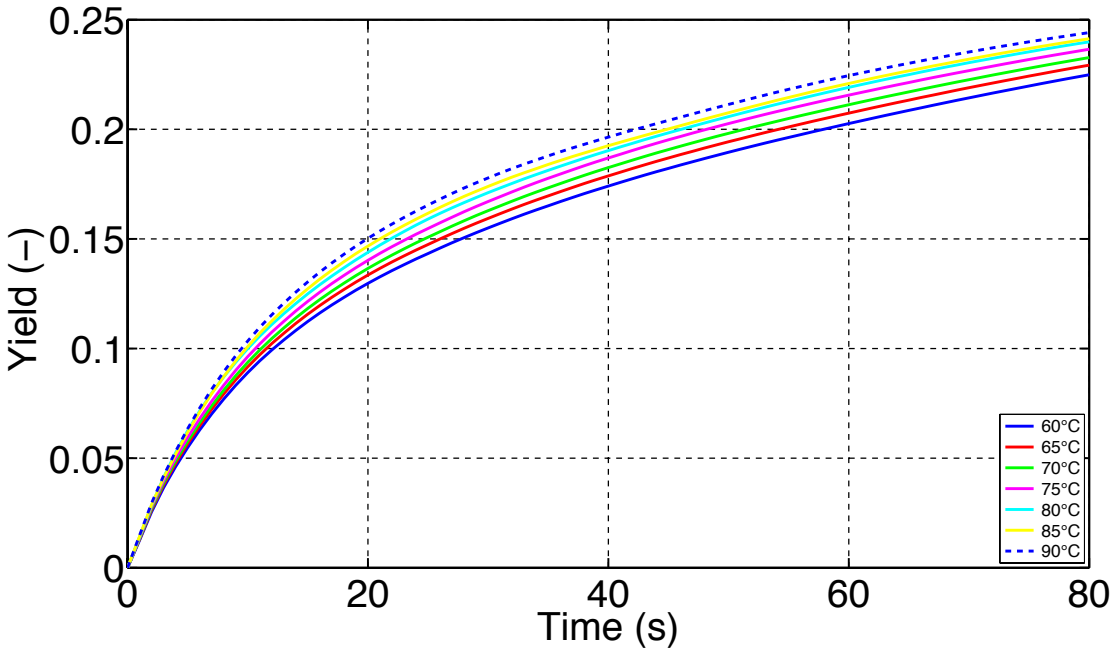

Figure 7.15: Extraction yield (*y*-axis) vs. time (*x*-axis). Model sensitivity to temperature; ΨE, ρ_{bed} = 480 $kg\ m^{-3}$, effective diffusion coefficient for the medium MW species and LF

Overall, the maximum and minimum temperatures observed at the inlet and outlet of the rig were 90 and 60 °*C*. The maximum and minimum average temperatures in the experiments were 85 and 72 °*C*. Thus, Figure 7.16 shows the difference between the simulations at 60 and 90 °*C* and 70 and 85 °*C*, both relative to the higher temperature. The relative difference decreases over time. For the greatest temperature difference (which never occurred in the experiments), the relative difference in the espresso regime is around 12 %. For the experimental average temperatures, the difference in the espresso regime is around 5 %. These differences are in the range of those found by Andueza et al. (2003) (14 % difference when the temperature was increased from 88 to 98 °*C*).

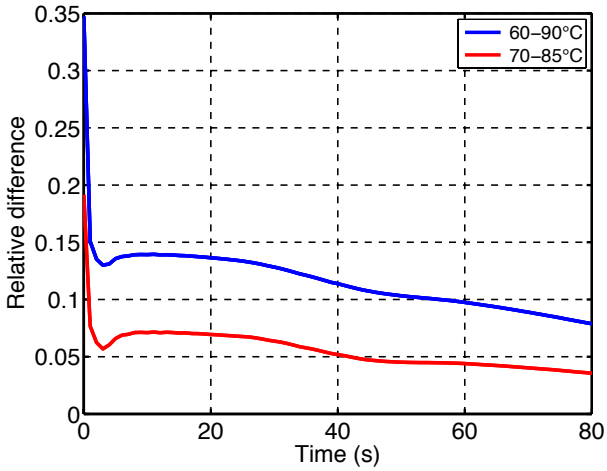

Figure 7.16: Relative difference (y-axis) vs. time (x-axis) for the extraction yield simulated at 90 and 60 $℃$ and 85 and 70 $℃$

7.4.3. Porosity of the bed

The sensitivity of the simulations to the selected value of particle porosity and bed porosity is analysed in this Section. As determined from Chapter 6, an average particle porosity of 0.53 was selected to estimate the porosity of the bed, but the effective diffusion coefficients derived from microstructural measurements were not corrected, as the effect on the outcome of the simulations was minimal. This is illustrated in Figure 7.17 with Ψ_E at 80 $℃$, ρ_{bed} = 480 $kg\ m^{-3}$ (bed porosity of 0.24, as estimated from the average particle porosity of 0.53) and LF for the effective diffusion coefficients as estimated from the measured particle porosity or corrected for an average porosity of 0.53.

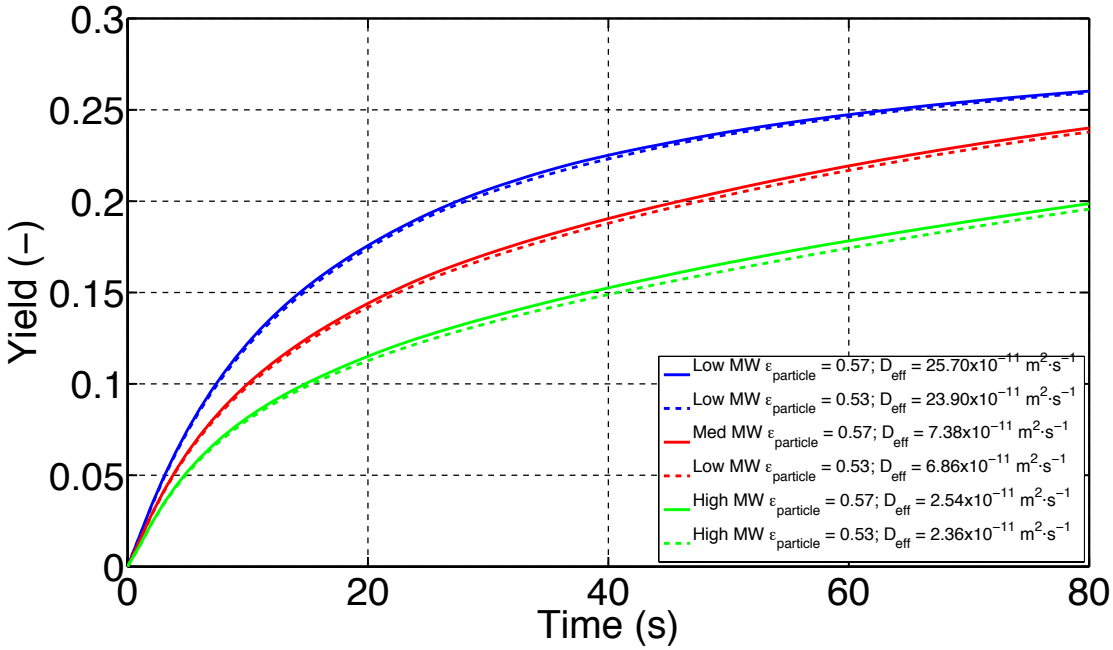

Figure 7.17: Simulated extraction yield (y-axis) vs. time (x-axis) for Ψ_E at 80 °C, ρ_{bed} = 480 $kg\ m^{-3}$ and LF and the effective diffusion coefficients estimated from microstructural measurements and the actual measured particle porosity ($\varepsilon_{particle}$ = 0.57) (—) or the assumed average particle porosity ($\varepsilon_{particle}$ = 0.53) (- - -)

The measured porosity particle values for the considered grinds were found to lie between 0.50 and 0.57. In order to test the sensitivity of the simulations to the resulting bed porosity as a function of the considered particle porosity, particle porosity values between 0.50 – 0.60 were considered and extraction was simulated for the same conditions reported in Figure I-4, and the resulting bed porosity values (0.29 – 0.10) for a bed density of 480 $kg\ m^{-3}$. The results for these simulations are displayed in Figure 7.18 and it can be appreciated that there is virtually no difference in the simulated extraction yield.

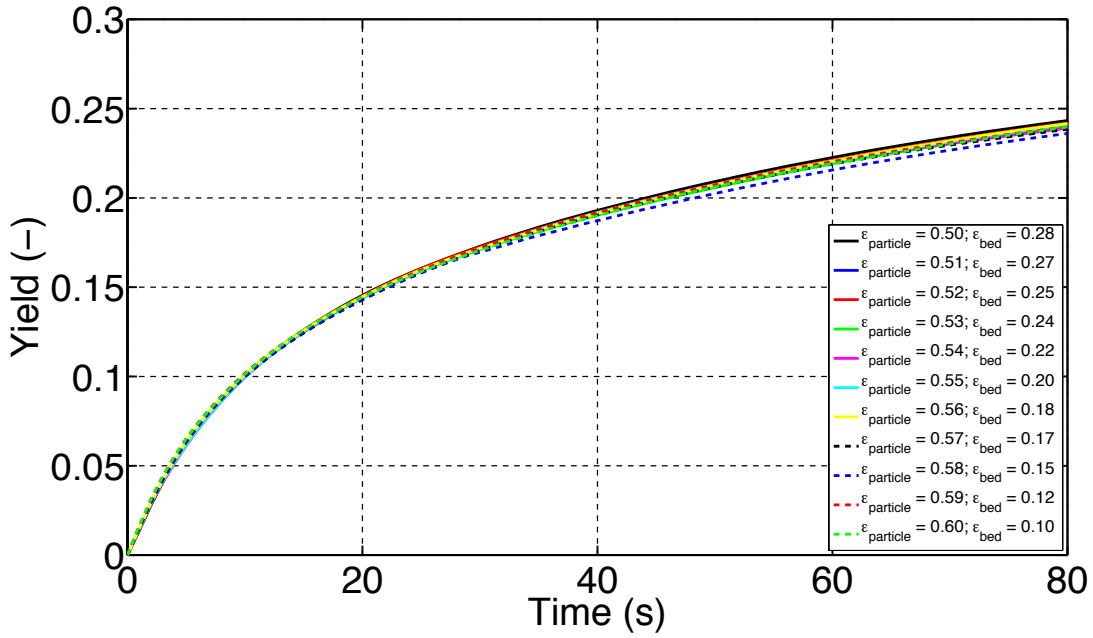

Figure 7.18: Simulated extraction yield (y-axis) vs. time (x-axis) for Ψ_E at 80 °C, ρ_{bed} = 480 $kg\ m^{-3}$ and LF, the effective diffusion coefficients for the medium MW species. Particle porosity values between 0.50 and 0.60 were assumed and the bed porosity calculated accordingly

Another source of variability for the bed porosity is due to bed consolidation. Across all the experimental conditions, consolidation was observed only in Experiment 2. The sensitivity of the simulations to bed consolidation was studied by assuming values of consolidation between 0 and 30 % for Ψ_B at ρ_{bed} = 400 $kg\ m^{-3}$, HF and 80 °C .The porosity of the bed was recalculated for these consolidation degrees as detailed in Chapter 3. The decrease in the volume of the bed was also accounted for. Figure 7.19 displays the simulated extraction yield (y-axis) vs. time (x-axis) for the considered consolidation degrees. In the espresso regime at the HF (around approximately 11-12 seconds), the relative difference between a bed consolidated by 30 % and a non-consolidated bed is 11 %.

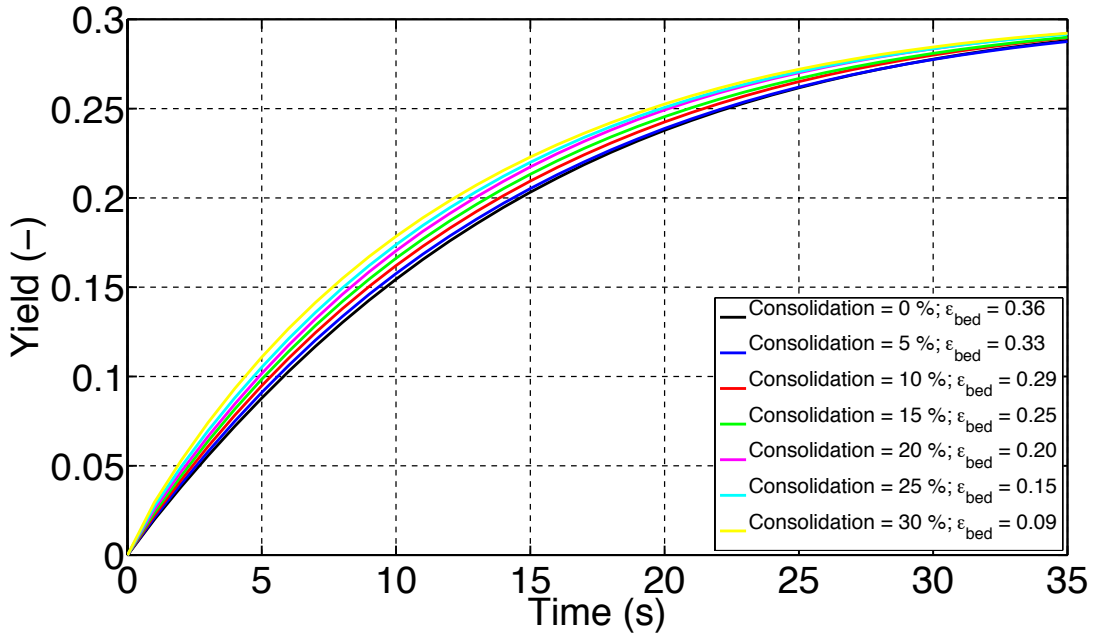

Figure 7.19: Simulated extraction yield (y-axis) vs. time (x-axis) for Ψ_B at 80 °C, ρ_{bed} = 400 $kg\ m^{-3}$ and HF, the effective diffusion coefficients for the medium MW species. Bed consolidation values between 0 – 30 % were assumed and the bed volume and bed porosity recalculated accordingly

7.5. Espresso coffee

It has been mentioned and discussed throughout this thesis that non-optimal *espresso* coffees are typically associated to the over-extraction and under-extraction phenomena. Although taste and flavour are a question of personal preference, research has suggested that the optimal extraction yield region for espresso coffee lies between 0.18 and 0.22 (18 – 22 %) (Navarini et al., 2009). The latter percentages may vary depending on the coffee beans that are being extracted (origin, roasting degree).

From the product development point of view, e.g. new capsules for On-Demand systems, it is useful to understand the relationship between the process variables (particle size distribution of the grinds, flow rate, bed density) and the attributes of the cup of coffee. For that purpose, Figure 7.20 presents the extraction yield (y-axis) vs. drink strength (x-axis) for all the experimental conditions reported in Table 7.1 and

Table 7.2 and for a drink volume of 45 ± 5 *ml*. An over-extracted, optimal and under-extracted region has been defined according to the aforementioned extraction yield values of 0.18 and 0.22.

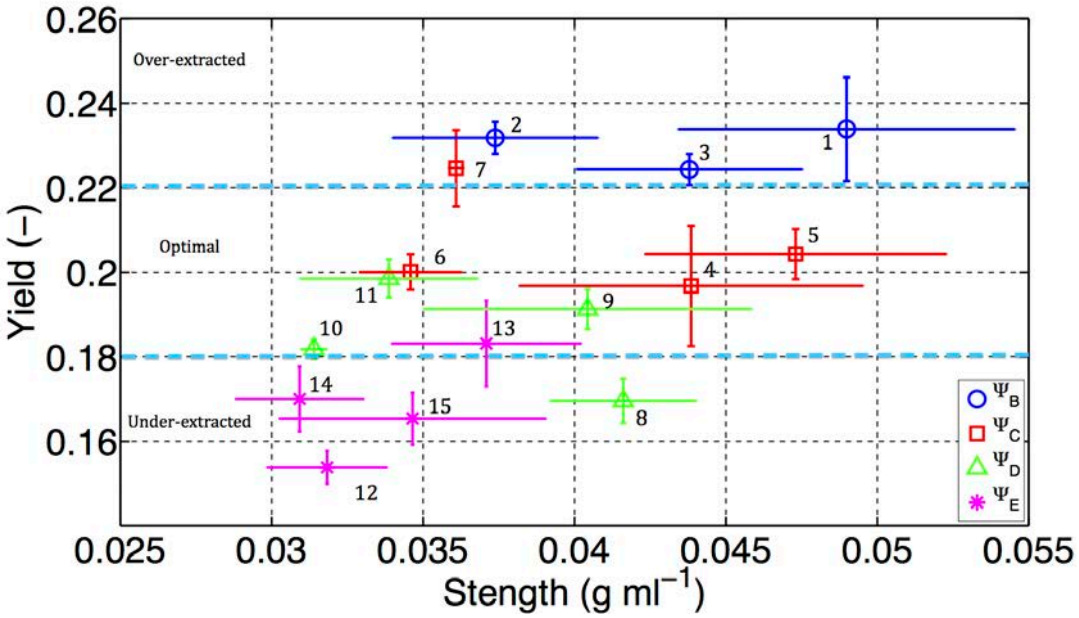

Figure 7.20: Extraction yield (*y*-axis) and strength (*x*-axis) of 45 ± 7 *ml* of coffee drinks. The numbers correspond to the experimental conditions reported in Table 7.1 and Table 7.2

It can be seen that due to the higher mass transfer rate from smaller grains, the finest grind (Ψ_B) led to over-extracted espresso coffees (1,2,3) whereas the opposite holds true for the coarsest grind (Ψ_E) (12,14,15) except for the case of 13. As discussed in Section 7.3.4, an inappropriate flow rate through the bed can also be the cause of non-optimal drinks. For example, in the case of Ψ_C, at the lower bed density, the combination of a slow flow rate (long extraction times) and high mass transfer rate from the grains results in an over-extracted drink (7). However, for the same conditions, a higher flow rate (shorter extraction time) results in a smaller extraction yield and the drink falls into the defined optimal zone (6). The opposite case can be seen for coarser grinds (Ψ_D, Ψ_E):

whereas higher flow rates produce under-extracted espressos (8,12), decreasing the flow rate results in the drinks being in the optimal zone (13, 9).

It can be concluded that for a given coffee bean, grind size and extraction time determine the value of the extraction yield, whereas coffee weight determines the strength of the drink. It should be taken into account that, since the temperature profiles during extraction are not identical from experiment to experiment, normalisation of the temperature would result in an increase in the extraction yield and strength of those points obtained at lower temperatures (or vice versa for those points obtained at higher temperatures). Nevertheless, for the experimental temperature range (72-85 $°C$), it can be seen that the effect of the particle size distribution of the grinds dominates over temperature. For example, the finest grind (Ψ_B) extracted at 72 $°C$ (Experiment 1) still resulted in the highest extraction yield overall. Also, it must be noticed that although lower pressures than the ones typically reported for espresso brewing (7-11 *bar*) have been used here, extraction yield and drink strength values compare well with those typically reported in the literature (see Table 2.3).

7.6. A practical case: application of the extraction models to commercial coffee machines

In order to illustrate how the developed extraction model can be applied to the optimisation of real systems, the experimental extraction profiles of certain species obtained from a commercial On-Demand extraction system and a traditional espresso machines were compared to model simulations.

The considered On-Demand system was *Hyper espresso*®, one of *Illy*'s systems especially tailored to produce espresso coffees. In 2008, *Illy* published a research paper (Navarini et al., 2008) in which the performance of the *Hyper espresso*® system was compared with the performance of a traditional espresso coffee machine. For that purpose, amongst other analyses, the extraction profiles of caffeine, trigonelline, and chlorogenic acids (obtained with both methods) were measured and compared.

The technical characteristics of the *Hyper espresso*® machine reported in the aforementioned paper are summarised in Table 7.5. Further to this, it must be noted that: (i) as pointed out in Section 7.2.1, the flow rate across the bed during extraction is a non-steady state variable. Since the flow rate profile with time was not reported, the reported average profile was input in the simulations. This has been shown in Section 7.4.1 to provide similar predicted yields to the time-dependent flow rate profile in the espresso regime; (ii) particle size distribution of the grinds was not specified. However, the capsules are commercially available and were purchased from Amazon UK (*www.amazon.co.uk*). The particle size distribution of the grinds was measured with the *dry* method described in Section 3.3.2, and the results are shown in Table 7.5; (iii) the effective diffusion coefficient derived for the low MW species and grind Ψ_E is assumed here; (iv) since the microstructural characteristics of this grind were not measured, the average of the measured particle porosities (0.53) is assumed; (v) a single partition solid-liquid partition coefficient of 1 for all the species is assumed for the simulations, as the reported extraction profiles are for low MW species.

As quoted by Petracco, the caffeine yield in an espresso extraction varies between 75 – 85 % of the total caffeine (Petracco, 2005b). Thus, in order to calculate the initial concentration of the species in the grains, for the experiments in which the total

extracted volume was around 40 – 42 *ml*, the cumulative extracted mass was assumed to correspond to 85 % of their initial concentration in the grinds. For experiments in which the total extracted volume was 57 *ml*, the cumulative mass was assumed to correspond to 95 % of the initial concentration in the grinds.

Table 7.5: Parameters used in the simulation of the *Hyper espresso*® On-Demand system

Parameter	Value	Source
Mass (g)	6.6 ± 0.2	(Navarini et al., 2008)
Water T (°C) (assumed to be at the inlet)	93 ± 3	(Navarini et al., 2008)
Assumed extraction temperature (°C)	85	—
Flow rate (ml·s^{-1})	1.2 ± 0.1	(Navarini et al., 2008)
Capsule height (cm)	1.6	Measured
Capsule diameter (cm)	3.3	Measured
Capsule volume (cm^3)	14.0	Measured
d[4,3] (μm)	386.8 ± 2.6	Measured
% fines	20.0 ± 0.1	Measured
Particle porosity	0.53	Measured
Bed porosity	0.25	This work
D_{eff} (m^2 s^{-1}) at 85 °C	25.7×10^{-11}	This work

For the traditional espresso machines, in addition to the data obtained from the *Hyper espresso*® study (Navarini et al., 2008), caffeine, trigonelline and nicotinic acid kinetic data was extracted from Caprioli et al. (2014). Both articles reported the typical flow rate used in espresso extraction, i.e. 25-30 *ml* in 25-35 seconds. The former work reported a mass of RGC of 6.5 ± 1.5 *g* (virtually the same mass of RGC used in the *Hyper espresso*® capsule) whereas the in the latter 7.5 *g* were used. Both works reported similar flow rates comparable to that for the On-Demand system (~ 1 *ml s^{-1}*). The particle size distribution of the grinds used in the traditional espresso machines was not reported, so it was assumed to be the same as that measured for the On-Demand machine. To calculate the volume of the bed for the simulation of the data showed in Caprioli et al. (2014), the same bed density as the one measured in the On-Demand

system (typical for espresso extraction), was assumed. For 7.5 *g* the volume of the bed resulted to be 15.9 cm^3.

Figure 7.21 compares the dimensionless extraction yield (*y*-axis) over time (*x*-axis) simulated with the extraction model and the parameters reported in Table 7.5 for beds made of 6.6 and 7.5 *g*, and the experimentally measured extraction yield of the species.

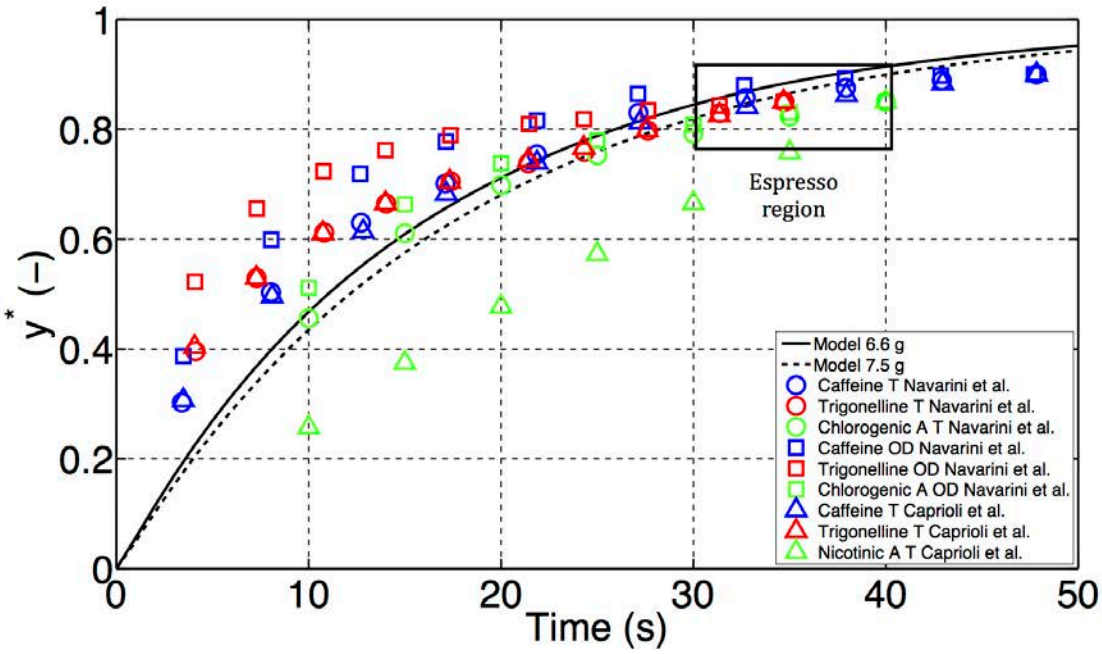

Figure 7.21: Simulated and experimental dimensionless yield (y-axis) vs. time (x-axis) for various species in commercial coffee extraction systems; T: traditional espresso machine; OD: On-Demand machine. (—) Model for 6.6. *g*; (----) Model for 7.5 *g*

It can be noted that, as also observed in Section 7.3.4, the use of an average flow rate (as opposed to a time-dependent flow rate set by the characteristic curve of the pump and the hydraulic resistance of the system), under-predicts the experimental data at earlier times but provides comparable results in the espresso regime. The cumulative extraction curve of most of the considered species displayed the characteristic shape of a first order kinetic profile, similar to that observed for the total soluble solids (Figure

7.3) However, in the case of nicotinic acid, one can see that the extraction profile is a straight line, not predicted by the model. If the assumption of 85 % of its total mass being extracted after 40 seconds was true, this profile would indicate that the extraction of this compound is driven by a different mechanism to the one assumed here. Similar profiles were observed in the extraction of low polarity aroma compounds from RGC (Mestdagh et al., 2014). If the extracted mass corresponds to a smaller percentage than 85 % of its total mass, the observed profile would indicate that the release of this compound is very slow despite of showing a molecular weight (123 $g\ mol^{-1}$) comparable to that of caffeine (194 $g\ mol^{-1}$).

Overall, the model predicts accurately the extraction profile of a range of species. The simulation could be more finely tuned to the experimental data if the initial concentrations of the species and, in the case of the traditional espresso machines, the volume of the coffee bed (after tamping) were known. Nevertheless, this example clearly illustrates the potential of the model to delve into the extraction mechanisms of relevant species and to assist the development and optimisation of commercial extraction systems.

7.7. Conclusions

The kinetics of extraction of coffee soluble solids at the bed scale has been investigated in this Chapter for a variety of process parameters typically used in espresso extraction, using a combination of experimental and modelling approaches.

It has been illustrated that for shorter extraction times (as compared to those used in the stirred vessel experiments in Chapter 5), the extraction profile cannot be

described with a single effective diffusion coefficient. The best choice of a single effective diffusion coefficient was shown to be that derived for the medium MW species. Accounting for the different diffusing species did not significantly improve the agreement between the simulations and the experimental data as in the case of the stirred vessel. However, it was shown here that due to the considerably higher concentrations achieved in the pore space of the bed, the assumption of different solid-liquid partition coefficients for the species (as opposed to the average value derived from equilibrium experiments) mimicked the extraction curve better.

Regarding the hydrodynamic variables, the extraction flow rate was shown two have two effects: on the one hand, for a given volume of drink, a lower flow rate increased the extraction time and that was shown to increase extraction yield. On the other hand, lower flow rates also increase the water residence time in the bed. Simulations illustrated that this effect decreased the extraction rate as the concentration gradient between the particle surface and the bed pore space decrease. The former effect was shown to be the dominant one in the espresso regime. The pressure drop across the bed was not correlated to extraction and, as anticipated in Chapter 6, it was shown to be a consequence of the desired flow rate through the bed and its hydraulic resistance.

Coffee mass was shown to control the drink strength, but it had virtually no effect on extraction yield. Increasing the coffee weight effectively resulted in beds of higher density, and thus a lower value of porosity, i.e. higher hydraulic resistance.

Lastly, the extraction model at the bed scale was used to simulate the extraction profile of various species in real commercial traditional espresso machines and in an On-

Demand system (*Hyper espresso*® by *Illy*). The simulations compared favourably with the experimental data for various species. This points out the potential of the developed extraction model to be applied for future product development and investigation of the variability of On-Demand systems.

Chapter 8: Conclusions and Future Work

The rise of On-Demand coffee systems, and the need for more efficient soluble coffee processes (since stress on energy and water resources is constantly increasing) demand more robust design and optimisation routines for coffee extraction than mere empirical evidence. Therefore, advancing the fundamental engineering understanding of coffee extraction was the main objective of this Engineering Doctorate thesis.

In order to achieve this objective, a mathematical model coupling the extraction of coffee soluble solids at the particle ($\sim\mu m$) and bed scale ($\sim cm$), and bed permeability models were proposed. The macrostructure, microstructure and extraction parameters (including effective diffusion coefficients) of coffee grinds with different processing histories were measured or estimated by applying a wide variety of analytical and experimental techniques. Relevant extraction and hydrodynamic experiments were conducted over range of conditions. The proposed mathematical models constituted the foundation to interpret the experimental data and analyse the sensitivity of the studied systems to the experimental conditions. Additionally, the models were also applied to study features of the systems that were not straightforward to measure experimentally. An advantage of deriving all the model parameters experimentally is that extraction simulations can be run without the need of experimental data to fit the parameters.

8.1. Main conclusions

In this Section, the main conclusions of this thesis are summarised.

8.1.1. Particle fundamental characterisation

1. There is a strong dependency of the measured particle size distribution on the employed laser diffraction method (*dry* or *wet*). The latter was shown to detect a higher percentage of fine particles, presumably due to a more efficient dispersion system whereby fine particles would detach from the surface or cell pockets of the coarser particles. This resulted into lower $d_{[3,2]}$ values, as compared to the *dry* method. However, the measured percentage of fine particles in non-extracted grinds was shown to be higher as compared to that found in grinds extracted at 80 *°C*. This pointed out that some of the measured fine particles in non-extracted grinds are soluble material that dissolves during extraction.

2. The effective diffusion coefficients derived from microstructural estimates, i.e. porosity and tortuosity of the grinds, for low, medium, high and very high molecular weight species were shown to be comparable to those previously reported in the literature from fitting experimental data to extraction models.

3. The previously reported ink-bottle microstructure of coffee grains (cell pockets and nanopores connecting one cell pocket to another) was also identified in this thesis. A simpler microstructure was correlated to the increment in the maximum amount of material that can be extracted upon finer grinding. In fact, Dynamic Light Scattering data showed that there were species in the coffee soluble solids that were considerably larger (diameter = 170–190 *nm*) than the measured nanopores (diameter = 10-15 *nm*), and these species could only be extracted upon more finely grinding.

8.1.2. Extraction at the particle scale

1. At the typical extraction temperatures, i.e. 80 °*C*, the limiting mechanism of extraction of coffee soluble solids is the internal diffusion of the solutes.

2. The effective diffusion coefficients derived from fitting experimental data to the numerical solution of the extraction model were comparable to the values previously reported in the literature and were found to lie between the estimated coefficients for low and medium molecular weight species derived from microstructural measurements. The extraction curve could not be described with a single effective diffusion coefficient. This resulted in Mean Percentage Errors between 10 and 15 %. These values can be considered as reasonable, if it is taken into account that a system formed by multiple species whose hydraulic radius varies in a range of 2-3 orders of magnitude, was modelled with a single effective diffusion coefficient.

3. The four individual extraction curves (obtained with the effective diffusion coefficients derived from microstructural measurements and assumptions regarding the chemistry of the species) were re-scaled by a mass percentage for each group. The resulting single extraction curves incorporating the effect of the different species resulted in a considerably better agreement with the experimental data (Mean Percentage Errors reduced by 50 %).

8.1.3. Hydrodynamics of coffee packed beds

1. A new method to estimate the permeability of coffee packed beds at the steady state was developed. The method was shown to provide values of permeability that are

comparable to those reported in the literature. Across the tested grinds and bed densities (typical of espresso extraction), a maximum-minimum permeability ratio of 13 was identified.

2. The proposed permeability models (Kozeny-Carman and Kozeny-Carman modified with an expression to account for the variability of the tortuosity of the bed with porosity) were used to obtain theoretical predictions that were compared to the measured values. It was shown that the predictions did not compared satisfactorily with the measured values and, in an attempt to obtain a better fit, the coefficient of the tortuosity expression was fitted to experimental data.

8.1.4. Extraction at the bed scale

1. The extraction curves cannot be fully described with a single effective diffusion coefficient. Accounting for the effect of the different diffusing species did not significantly improve the agreement. Nevertheless the values of the Mean Percentage Error for the effective diffusion coefficient for the medium molecular weight species were found to be reasonable (9 – 14 %) provide that no parameters were fitted, but estimated from experimental measurements. It was illustrated that accounting for different values of the solid-liquid partition coefficient in the concentrated espresso regime could mimic the shape of the extraction curves.

2. In the espresso regime, the particle size distribution and the extraction time were shown to be the dominant effects over the temperature (in a range of 85 ± 5 $^{\circ}C$). For the finest grind size, the resulting espresso coffees were over-extracted regardless of

the extraction time. However, for the other grinds, the selection of flow rate resulted in over-extracted coffees (finer grinds at low flow rates) or under-extracted coffees (coarser grinds at high flow rates).

3. The extraction model provided simulations that compared favourably in the espresso regime with the experimentally measured extraction profiles from low molecular weight species profiles obtained molecular weight species from real On-Demand systems and traditional espresso machines. This illustrates the potential of the model to be used in real extraction scenarios.

8.2. Future work

The work presented in this thesis has shown the potential of the combined theoretical and experimental approaches in order to understand, design and optimise coffee extraction processes, at both the consumer and the industrial level. Therefore, in order to keep on advancing the engineering understanding of coffee extraction, further research on the following areas would be recommendable:

- Optimise particle characterisation methods:
    - Accurately assess the contribution of oil droplets, gas bubbles and soluble particles to the particle distribution measurements obtained with the *wet* method. This would result in a new route to estimate the effective $d_{[3,2]}$ in coffee packed beds.

- Alternative routes to estimate the microstructure (porosity, tortuosity) of coffee particles. This would contribute to refine the estimation of effective diffusion coefficients from microstructural measurements.

- Deeper investigation of the flow rate non-steady state profile:

  - Developing an understanding of the effect of axial (compaction) and hydrodynamic pressure forces on the characteristics (size, sphericity) of the coffee grinds.

  - Independent investigation and modelling of each the phenomena that have been identified to contribute to the observed non-steady state flow rate profile, especially the effect of gas in the pore space of the bed. This would involve the development of a model coupling the kinetics of extraction of gas at the particle scale and the bed scale.

- Extraction at the particle and bed scale:

  - Applying the model to individual species.

- Upon implementation of the aforementioned points, the improved approach could be further applied to:

  - Study the mechanisms of extraction aroma molecules.

  - Study other attributes of the drink as a function of the extraction parameters, e.g. foam quality, mouthfeel.

Finally, in the longer term, the validated model describing the extraction of soluble solids and aroma molecules could be correlated to the results of sensory evaluation of the samples. This would eventually make a powerful mathematical tool to predict flavour and mouthfeel of coffee beverages.

REFERENCES

Aguilera, J. (2003). Solid-liquid extraction. In C. Tzia & L. George (Eds.), *Extraction optimization in food engineering* (1st ed.). New York: Marcel Dekker, Inc.

Aguilera, J., Michel, M., and Mayor, G. (2004). R : Concise Reviews / Hypotheses in Food Science Fat Migration in Chocolate : Diffusion or Capillary Flow in a Particulate Solid ? — A Hypothesis Paper. *Journal of Food Science*, *69*(7), 167–174.

Aguilera, J., and Stanley, D. W. (1990). Microstructure and Mass Transfer: Solid-Liquid Extraction. In J. Aguilera & D. Stanley (Eds.), *Microstructural Principles of Food Processing and Engineering* (2nd ed., pp. 325–341). Maryland: Aspen Publishers.

Albanese, D., Matteo, M. Di, Poiana, M., and Spagnamusso, S. (2009). Espresso coffee (EC) by POD : Study of thermal profile during extraction process and influence of water temperature on chemical – physical and sensorial properties. *Food Research International*, *42*(5-6), 727–732. doi:10.1016/j.foodres.2009.02.027

Anderson, B., Shimoni, E., Liardon, R., and Labuza, T. (2003). The diffusion kinetics of carbon dioxide in fresh roasted and ground coffee. *Journal of food engineering*, *59*, 71–78. doi:10.1016/S0260-8774(02)00432-6

Andueza, S., De Peña, M. P., and Cid, C. (2003). Chemical and sensorial characteristics of espresso coffee as affected by grinding and torrefacto roast. *Journal of Agricultural and Food Chemistry*, *51*(24), 7034–9. doi:10.1021/jf034628f

Andueza, S., Maeztu, L., Dean, B., de Peña, M. P., Bello, J., and Cid, C. (2002). Influence of Water Pressure on the Final Quality of Arabica Espresso Coffee. Application of Multivariate Analysis. *Journal of Agricultural and Food Chemistry*, *50*(25), 7426–7431. doi:10.1021/jf0206623

Andueza, S., Maeztu, L., Pascual, L., Ibáñez, C., de Peña, M. P., and Cid, C. (2003). Influence of extraction temperature on the final quality of espresso coffee. *Journal of the Science of Food and Agriculture*, *83*, 240–248. doi:10.1002/jsfa.1304

Andueza, S., Vila, A. M., de Peña, M. P., and Cid, C. (2007). Influence of coffee / water ratio on the final quality of espresso coffee. *Journal of the Science of Food and Agriculture*, *592*, 586–592. doi:10.1002/jsfa

Armstrong, R. T., Georgiadis, A., Ott, H., Klemin, D., and Berg, S. (2014). Critical capillary number: Desaturation studied with fast X-ray computed microtomography. *Geophysical Research Letters*, *41*(1), 55–60. doi:10.1002/2013GL058075

Bartel, C., Mesias, M., and Morales, F. J. (2015). Investigation on the extractability of melanoidins in portioned espresso coffee. *Food Research International*, *67*, 356–365. doi:10.1016/j.foodres.2014.11.053

Bear, J. (1988). *Dynamics of fluids in porous media* (2nd ed.). New York: Dover publications, INC.

Bee, S., Brando, C. H. ., Brumen, G., Carvalhaes, N., Kolling-Speer, I., Speer, K., … O.G, V. (2005). The raw bean. In A. Illy & R. Viani (Eds.), *Espresso coffee.The science of quality* (2nd ed., pp. 87–178). San Diego: Elsevier Academic Press.

Bekedam, E. . (2008). *Coffee brew melanoidins : structural and functional properties of brown-colored coffee compounds*. PhD. Wageningen University.

Bekedam, E. ., Schols, H. A., van Boekel, M. A. J. S., and Smit, G. (2006). High molecular weight melanoidins from coffee brew. *Journal of agricultural and food chemistry*, *54*(20), 7658–66. doi:10.1021/jf0615449

Bonnländer, B., Eggers, R., Engelhardt, U. ., and Maier, H. . (2005). Roasting. In A. Illy & V. Rinantonio (Eds.), *Espresso coffee.The science of quality* (2nd ed., pp. 179–214). San Diego: Elsevier Academic Press.

Borrelli, R. C., Visconti, A., Mennella, C., Anese, M., and Fogliano, V. (2002). Chemical characterization and antioxidant properties of coffee melanoidins. *Journal of agricultural and food chemistry*, *50*(22), 6527–33.

Bradbury, A. G. . (2001). Chemistry I: Non-volatile compounds: Carbohydrates. In R. J. Clarke & O. G. Vitzthum (Eds.), *Coffee Recent Developments* (1st ed., pp. 1–17). Oxford: Blackwell Science.

Buffo, R. a., and Cardelli-Freire, C. (2004). Coffee flavour: An overview. *Flavour and Fragrance Journal*, *19*(2), 99–104. doi:10.1002/ffj.1325

Caporaso, N., Genovese, A., Canela, M. D., Civitella, A., and Sacchi, R. (2014). Neapolitan coffee brew chemical analysis in comparison to espresso, moka and American brews. *Food Research International*, *61*, 152–160. doi:10.1016/j.foodres.2014.01.020

Cappuccio, R., and Liverani, F. (1999). Computer Simulation as a Tool to Model Coffee Brewing Cellular Automata for Percolation Processes; 2D and 3D Techniques for Fluid-dynamic Simulations. In ASIC (Ed.), *18th International Conference on Coffee Science* (Vol. 1999, pp. 173–178).

Caprioli, G., Cortese, M., Cristalli, G., Maggi, F., Odello, L., Ricciutelli, M., … Vittori, S. (2012). Optimization of espresso machine parameters through the analysis of coffee odorants by HS-SPME-GC/MS. *Food chemistry*, *135*(3), 1127–33. doi:10.1016/j.foodchem.2012.06.024

Caprioli, G., Cortese, M., Maggi, F., Minnetti, C., Odello, L., Sagratini, G., and Vittori, S. (2014). Quantification of caffeine, trigonelline and nicotinic acid in espresso coffee: the influence of espresso machines and coffee cultivars. *International Journal of Food Science and Nutrition*, *7486*(1465-3478 (Electronic)), 465–469. doi:10.3109/09637486.2013.873890

Carman, P. C. (1997). Fluid flow through granular beds. *Chemical Engineering Research and Design*, *75*, S32–S48. doi:10.1016/S0263-8762(97)80003-2

Carniglia, S. C. (1986). Construction of the Tortuosity Factor from Porosimetry. *Journal of catalysis*, *418*, 401–418.

Carpita, N., Sabularse, D., Montezinos, D., and Delmer, D. P. (1979). Determination of the pore size of cell walls of living plant cells. *Science (New York, N.Y.)*, *205*(4411), 1144–7. doi:10.1126/science.205.4411.1144

Cheng, N.-S. (2011). Wall effect on pressure drop in packed beds. *Powder Technology*, *210*(3), 261–266. doi:10.1016/j.powtec.2011.03.026

Corrochano, B. R., Melrose, J. R., Bentley, A. C., Fryer, P. J., and Bakalis, S. (2014). A new methodology to estimate the steady-state permeability of roast and ground coffee in packed beds. *Journal of Food Engineering*, *150*, 106–116. doi:10.1016/j.jfoodeng.2014.11.006

Crank, J. (1975a). *The Mathematics of Diffusion* (2nd ed.). New York: Oxford University Press.

Crank, J. (1975b). Diffusion in a sphere. In *The Mathematics of Diffusion* (2nd ed., pp. 80–103). New York: Oxford University Press.

Cussler, E. L. (2009a). Diffusion of interacting species. In E. L. Cussler (Ed.), *Diffusion. Mass transfer in fluid systems* (3rd ed., pp. 161–209). New York: Cambridge University Press.

Cussler, E. L. (2009b). *Diffusion.Mass transfer in fluid systems*. (E. . Cussler, Ed.)*Diffusion. Mass transfer in fluid systems* (3rd ed.). New York: Cambridge University Press.

Cussler, E. L. (2009c). Fundamentals of mass transfer. In E. L. Cussler (Ed.), *Diffusion. Mass transfer in fluid systems* (3rd ed., pp. 237–273). New York: Cambridge University Press.

Del Valle, J. M., and de la Fuente, J. C. (2006). Supercritical CO2 extraction of oilseeds: review of kinetic and equilibrium models. *Critical reviews in food science and nutrition*, *46*(2), 131–60. doi:10.1080/10408390500526514

Del Valle, J. M., Germain, J. C., Uquiche, E., Zetzl, C., and Brunner, G. (2006). Microstructural effects on internal mass transfer of lipids in prepressed and flaked

vegetable substrates. *The Journal of Supercritical Fluids*, *37*(2), 178–190. doi:10.1016/j.supflu.2005.09.002

Del Valle, J. M., Mena, C., and Budinich, M. (2008). Extraction of garlic with supercritical CO2 and conventional organic solvents. *Brazilian Journal of Chemical Engineering*, *25*(3), 532–542. doi:10.1590/S0104-66322008000300011

Dias, R., Teixeira, J., Mota, M., and Yelshin, A. (2006). Tortuosity variation in a low density binary particulate bed. *Separation and Purification Technology*, *51*(2), 180–184. doi:10.1016/j.seppur.2006.01.010

Dixon, A. G., Macdonald, B., and Olm, A. (2014). Modeling of packed bed reactors : hydrogen production by the steam reforming of methane and glycerol. In *COMSOL conference*. Boston.

Eggers, R., Ambrogi, A., and Schnitzler, J. von. (2000). Special features of SCF solid extraction of natural products: deoiling of wheat gluten and extraction of rose hip oil. *Brazilian Journal of Chemical Engineering*, *17*(3), 329–334. doi:10.1590/S0104-66322000000300009

Eggers, R., and Pietsch, A. (2001). Technology I: Roasting. In R. J. Clarke & V. O.G (Eds.), *Coffee Recent Developments* (1st ed., pp. 90–107). Oxford: Blackwell Science.

Endo, Y., Chen, D.-R., and Pui, D. Y. H. (2002). Theoretical consideration of permeation resistance of fluid through a particle packed layer. *Powder Technology*, *124*(1-2), 119–126. doi:10.1016/S0032-5910(01)00479-X

Espinoza-Perez, J. D., Vargas, A., Robles-Olvera, V. J., Rodriguez-Jimenes, G. C., and Garcia-Alvarado, M. A. (2007). Mathematical modeling of caffeine kinetic during solid–liquid extraction of coffee beans. *Journal of Food Engineering*, *81*(1), 72–78. doi:10.1016/j.jfoodeng.2006.10.011

Fabbri, A., Cevoli, C., Alessandrini, L., and Romani, S. (2011). Numerical modeling of heat and mass transfer during coffee roasting process. *Journal of Food Engineering*, *105*(2), 264–269. doi:10.1016/j.jfoodeng.2011.02.030

Favre, E. (1979). Capsule for beverage preparation.US4136202A. USA.

Fond, O. (1995). Effect of water and coffee acidity on extraction. Dynamics of coffee bed compaction in espresso type extraction. In ASIC (Ed.), *16th International Conference on Coffee Science* (pp. 413–421). Kyoto (Japan).

Frisullo, P., Barnabà, M., Navarini, L., and Nobile, M. A. Del. (2012). Coffea arabica beans microstructural changes induced by roasting : An X-ray microtomographic investigation. *Journal of Food Engineering*, *108*(1), 232–237. doi:10.1016/j.jfoodeng.2011.07.036

Geiger, R., Perren, R., Schenker, S., and Escher, F. (2002). Mechanism of volume expansion in coffee beans during roasting. In ASIC (Ed.), *19th International Conference on Coffee Science*. Trieste, Italy.

Gianino, C. (2007). Experimental analysis of the Italian coffee pot "moka." *American Journal of Physics*, *75*(1), 43. doi:10.1119/1.2358157

Giesche, H. (2006). Mercury Porosimetry: A General (Practical) Overview. *Particle & Particle Systems Characterization*, *23*(1), 9–19. doi:10.1002/ppsc.200601009

Gloess, A. N., Schönbächler, B., Klopprogge, B., D`Ambrosio, L., Chatelain, K., Bongartz, A., … Yeretzian, C. (2013). Comparison of nine common coffee extraction methods: instrumental and sensory analysis. *European Food Research and Technology*, *236*(4), 607–627. doi:10.1007/s00217-013-1917-x

Grosch, W. (2001). Chemistry III: Volatile Compounds. In R. J. Clarke & O. G. Vitzthum (Eds.), *Coffee Recent Developments* (1st ed., pp. 68–89). Oxford: Blackwell Science.

Hapgood, K. P., Litster, J. D., Biggs, S. R., and Howes, T. (2002). Drop penetration into porous powder beds. *Journal of colloid and interface science*, *253*(2), 353–66. doi:10.1006/jcis.2002.8527

Heilmann, W. (2001). Technology II: Decaffeination of Coffee. In R. J. Clarke & O. G. Vitzthum (Eds.), *Coffee Recent Developments* (1st ed., pp. 108–124). Oxford: Blackwell Science.

Hekmat, D., Mornhinweg, R., Bloch, G., Sun, Y., Jeanty, P., Neubert, M., and Weuster-Botz, D. (2011). Macroscopic investigation of the transient hydrodynamic memory behavior of preparative packed chromatography beds. *Journal of chromatography. A*, *1218*(7), 944–50. doi:10.1016/j.chroma.2010.12.092

Hofmann, T., Czerny, M., Calligaris, S., and Schieberle, P. (2001). Model Studies on the Influence of Coffee Melanoidins on Flavor Volatiles of Coffee Beverages. *Journal of Agricultural and Food Chemistry*, *49*(5), 2382–2386. doi:10.1021/jf0012042

Homma, S. (2001). Chemistry II: Non-volatile compounds, Part II. In R. J. Clarke & O. G. Vitzthum (Eds.), *Coffee Recent Developments* (1st ed., pp. 50–67). Oxford: Blackwell Science.

Huang, Z., Shi, X.-H., and Jiang, W.-J. (2012). Theoretical models for supercritical fluid extraction. *Journal of chromatography. A*, *1250*, 2–26. doi:10.1016/j.chroma.2012.04.032

Humbert, S., Loerincik, Y., Rossi, V., Margni, M., and Jolliet, O. (2009). Life cycle assessment of spray dried soluble coffee and comparison with alternatives (drip filter and capsule espresso). *Journal of Cleaner Production*, *17*(15), 1351–1358. doi:10.1016/j.jclepro.2009.04.011

International Coffee Organisation. (2016). International Coffee Organisation. Retrieved January 21, 2013, from http://www.ico.org/monthly_coffee_trade_stats.asp

Jaganyi, D., and Madlala, S. P. (2000). Kinetics of coffee infusion: a comparative study on the extraction kinetics of mineral ions and caffeine from several types of medium roasted coffees. *Journal of the Science of Food and Agriculture*, *90*(July 1999), 85–90.

Jaganyi, D., and Price, R. D. (1999). Kinetics of tea infusion: the effect of the manufacturing process on the rate of extraction of caffeine. *Food Chemistry*, *64*, 60–64.

Kassing, M., Jenelten, U., Schenk, J., and Strube, J. (2010). A new approach for process development of plant-based extraction processes. *Chemical Engineering and Technology*. doi:10.1002/ceat.200900480

King, W. D. (2008). The physics of a stove-top espresso machine. *American Journal of Physics*, *76*(6), 558. doi:10.1119/1.2870524

Kok, C., and Rudin, A. (1981). Relationship between the hydrodynamic radius and the radius of gyration of a polymer solution. *Makromolekulare Chemie-Rapid Communications*, *2*(11), 655–659.

Lanfrey, P.-Y., Kuzeljevic, Z. V., and Dudukovic, M. P. (2010). Tortuosity model for fixed beds randomly packed with identical particles. *Chemical Engineering Science*, *65*(5), 1891–1896. doi:10.1016/j.ces.2009.11.011

Lang, R., Yagar, E. F., Wahl, A., Beusch, A., Dunkel, A., Dieminger, N., … Hofmann, T. (2013). Quantitative Studies on Roast Kinetics for Bioactives in Coffee. *Journal of Agricultural and Food Chemistry*, *61*, 12123–12128.

Latham, J.-P., Munjiza, A., and Lu, Y. (2002). On the prediction of void porosity and packing of rock particulates. *Powder Technology*, *125*(1), 10–27. doi:10.1016/S0032-5910(01)00493-4

Leal, L. G. (2010). *Advanced Transport Phenomena*. New York: Cambridge University Press.

Lee, T. A., Kempthorne, R., and Hardy, J. K. (1992). Compositional Changes in Brewed Coffee as a Function of Brewing Time. *Journal of Food Science*, *57*(6), 1417–1419. doi:10.1111/j.1365-2621.1992.tb06872.x

Leloup, V., and Liardon, R. (1993). Analytical characterization of coffee carbohydrates. In ASIC (Ed.), *15th International Conference on Coffee Science* (pp. 863–865). Montpellier, France.

Leloup, V., Michieli, J. H. D. E., and Liardon, R. (1997). Characterisation of oligosaccharides in coffee extracts. In ASIC (Ed.), *17th International Conference on Coffee Science*.

Li, Y., and Park, C.-W. (1998). Permeability of Packed Beds Filled with Polydisperse Spherical Particles. *Industrial & Engineering Chemistry Research*, *37*(5), 2005–2011. doi:10.1021/ie970603s

Ludwig, I. A., Sanchez, L., Caemmerer, B., Kroh, L. W., De Peña, M. P., and Cid, C. (2012). Extraction of coffee antioxidants: Impact of brewing time and method. *Food Research International*, *48*(1), 57–64. doi:10.1016/j.foodres.2012.02.023

Macdonald, I. F., El-Sayed, M. S., Mow, K., and Dullien, F. A. L. (1979). Flow through porous media-the Ergun equation revisited. *Industrial & Engineering Chemistry Fundamentals*, *18*(3), 199–208. doi:10.1021/i160071a001

Masella, P., Guerrini, L., Spinelli, S., Calamai, L., Spugnoli, P., Illy, F., and Parenti, A. (2014). A new Espresso brewing method. *Journal of Food Engineering*, *146*, 204–208. doi:10.1016/j.jfoodeng.2014.09.001

Mateus, M., Lindinger, C., Gumy, J.-C., and Liardon, R. (2007). Release kinetics of volatile organic compounds from roasted and ground coffee: online measurements by PTR-MS and mathematical modeling. *Journal of agricultural and food chemistry*, *55*(25), 10117–28. doi:10.1021/jf071901v

Mateus, M., and Rouvet, M. (2007). Interactions of water with roasted and ground coffee in the wetting process investigated by a combination of physical determinations. *Journal of Agricultural and Food Chemistry*, *55*, 2979–2984.

Mayer, F., Czerny, M., and Grosch, W. (2000). Sensory study of the character impact aroma compounds of a coffee beverage. *European Food Research and Technology*, *211*(4), 272–276. doi:10.1007/s002170000169

Mazeau, K., and Rinaudo, M. (2004). The prediction of the characteristics of some polysaccharides from molecular modeling. Comparison with effective behavior. *Food Hydrocolloids*, *18*(6), 885–898. doi:10.1016/j.foodhyd.2004.04.004

Mestdagh, F., Davidek, T., Chaumonteuil, M., Folmer, B., and Blank, I. (2014). The kinetics of coffee aroma extraction. *Food Research International*, *63*, 271–274. doi:10.1016/j.foodres.2014.03.011

Moroney, K. M., Lee, W. T., O'Brien, S. B. G., Suijver, F., and Marra, J. (2015). Modelling of coffee extraction during brewing using multiscale methods: An experimentally validated model. *Chemical Engineering Science*, *137*, 216–234. doi:10.1016/j.ces.2015.06.003

Mota, M., Teixeira, J. A., Bowen, W. R., and Yelshin, A. (2001). Binary spherical particle mixed beds : porosity and permeability relationship measurement. The Filtration Society. Retrieved January 23, 2013, from http://repositorium.sdum.uminho.pt/handle/1822/1403

Navarini, L., Cappuccio, R., and Liverani, F. (2004). The Body of the espresso coffee : the elusive importance. In ASIC (Ed.), *20th International Conference on Coffee Science* (pp. 193–203). Bangalore, India.

Navarini, L., Colomban, S., Lonzarich, V., Rivetti, D., Brollo, G., and Suggi-Liverani, F. (2008). Hyper Espresso coffee extraction: adding physics to chemistry. In ASIC (Ed.), *22nd International Conference on Coffee Science* (pp. 296–309). Campinas (Brazil).

Navarini, L., Nobile, E., Pinto, F., Scheri, A., and Suggi-liverani, F. (2009). Experimental investigation of steam pressure coffee extraction in a stove-top coffee maker. *Applied Thermal Engineering*, *29*(5-6), 998–1004. doi:10.1016/j.applthermaleng.2008.05.014

Navarini, L., and Rivetti, D. (2010). Water quality for Espresso coffee. *Food Chemistry*, *122*(2), 424–428. doi:10.1016/j.foodchem.2009.04.019

Nemec, D., and Levec, J. (2005). Flow through packed bed reactors: 1. Single-phase flow. *Chemical Engineering Science*, *60*(24), 6947–6957. doi:10.1016/j.ces.2005.05.068

Nestle. (2013). The history of coffee. *Nestle Professional*. Retrieved May 18, 2015, from https://www.nestleprofessional.com/uk/en/BeverageExpertise/The_hottest_trends_in_Beverage/Pages/The_History_of_Coffee.aspx?UrlReferrer=https%3a%2f%2fwww.google.co.uk%2f

Nicoli, M., Rosa, M., and Lerici, C. (1990). Influence of some processing conditions on solid-liquid extraction of coffee. *Food science and technology-Lebensmittle-Wissenschaft & Technologie*, *23*(5), 386–389.

Nicoli, M., and Savonitti, O. (2005). Storage and packaging. In A. Illy & R. Viani (Eds.), *Espresso coffee.The science of quality* (2nd ed., pp. 230–258). San Diego: Elsevier Academic Press.

Nunes, F. M., and Coimbra, M. A. (2001). Chemical characterization of the high molecular weight material extracted with hot water from green and roasted arabica coffee. *Journal of agricultural and food chemistry*, *49*(4), 1773–82.

Nunes, F. M., Coimbra, M. A., Duarte, A. C., and Delgadillo, I. (1997). Foamability, Foam Stability, and Chemical Composition of Espresso Coffee As Affected by the Degree of Roast. *Journal of Agricultural and Food Chemistry*, *45*(8), 3238–3243. doi:10.1021/jf970009t

Ohresser, S., Eichler, P., Koch, P., and Raetz, E. (2010). Method for delivering faster a short coffee extract from capsule.US8231918 B2. Switzerland.

Oliveira, E. L. G., Silvestre, A. J. D., and Silva, C. M. (2011). Review of kinetic models for supercritical fluid extraction. *Chemical Engineering Research and Design*, *89*(7), 1104–1117. doi:10.1016/j.cherd.2010.10.025

Pacheco Ortiz, R. W., Benincá, C., and Zanoelo, E. F. (2015). Cyclically pressurized extraction of solutes from ground coffee: Kinetic experiments and modeling. *Separation and Purification Technology*, *141*, 256–262. doi:10.1016/j.seppur.2014.12.004

Parenti, A., Guerrini, L., Masella, P., Spinelli, S., Calamai, L., and Spugnoli, P. (2014). Comparison of espresso coffee brewing techniques. *Journal of Food Engineering*, *121*, 112–117. doi:10.1016/j.jfoodeng.2013.08.031

Peronius, N., and Sweeting, T. J. (1985). On the correlation of minimum porosity with particle size distribution. *Powder Technology*, *42*(2), 113–121. doi:10.1016/0032-5910(85)80043-7

Petkowicz, C. L. ., Milas, M., Mazeau, K., Bresolin, T., Reicher, F., Ganter, J. L. M. ., and Rinaudo, M. (1999). Conformation of galactomannan: experimental and modelling approaches. *Food Hydrocolloids*, *13*(3), 263–266. doi:10.1016/S0268-005X(99)00008-9

Petracco, M. (2001). Technology IV: Beverage preparation: brewing trends for the new millennium. In R. J. Clarke & O. G. Vitzthum (Eds.), *Coffee Recent Developments* (1st ed., pp. 140–162). Oxford: Blackwell Science.

Petracco, M. (2005a). Products of Chemistry Our Everyday Cup of Coffee : The Chemistry behind Its Magic, *82*(8).

Petracco, M. (2005b). Percolation. In A. Illy & R. Viani (Eds.), *Espresso coffee.The science of quality* (2nd ed., pp. 259–280). San Diego: Elsevier Academic Press.

Petracco, M. (2005c). The cup. In A. Illy & V. Rinantonio (Eds.), *Espresso coffee.The science of quality* (2nd ed., pp. 290–315). San Diego: Elsevier Academic Press.

Petracco, M. (2005d). Grinding. In A. Illy & R. Viani (Eds.), *Espresso coffee.The science of quality* (2nd ed., pp. 215–229). Elsevier Academic Press.

Petracco, M., and Liverani, F. S. (1993). Dynamics of fluid percolation through a bed of particles subjetc to physico-chemical evolution, and its mathematical modelization. In ASIC (Ed.), *15th International Conference on Coffee Science* (pp. 702–711).

Petracco, M., and Marega, G. (1991). Coffee grinding dynamics: a new approach by computer simulation. In ASIC (Ed.), *14th International Conference on Coffee Science* (pp. 319–330). San Francisco (USA).

Pittia, P., and Rosa, M. D. (2001). Textural Changes of Coffee Beans as Affected by Roasting Conditions. *Lebensm.-Wiss. u.-Technol*, *175*, 168–175. doi:10.1006/fstl.2000.0749

Pittia, P., Sacchetti, G., Mancini, L., Voltolini, M., Sodini, N., Tromba, G., and Zanini, F. (2011). Evaluation of Microstructural Properties of Coffee Beans by Synchrotron X-Ray Microtomography : A Methodological Approach. *Journal of Food Science*, *76*(2). doi:10.1111/j.1750-3841.2010.02009.x

Poling, B. E., Thomson, G. ., Friend, D. G., Rowley, Richard, L., and Vincent Wilding, W. (2008). Physical and Chemical Data. In D. Green & R. Perry (Eds.), *Perry's Chemical Engineers' Handbook* (8th ed.). New York: McGraw-Hill. doi:10.1036/0071511253

Rhodes, M. (2008). Fluid flow through a packed bed of particles. In *Introduction to particle technology* (2nd ed., pp. 153–165). Wiley.

Rohatgi, A. (2015). WebPlotDigitizer. Retrieved from http://arohatgi.info/WebPlotDigitizer

Romani, S., Severini, C., Fiore, A. G., and Pinnavaia, G. G. (2004). Quality of " Espresso " coffee: a study performed through Italian coffee shops. In ASIC (Ed.), *20th International Conference on Coffee Science* (pp. 521–525). Bangalore, India.

Salmas, C. E., and Androutsopoulos, G. P. (2001). A Novel Pore Structure Tortuosity Concept Based on Nitrogen Sorption Hysteresis Data. *Industrial & Engineering Chemistry Research*, *40*(2), 721–730. doi:10.1021/ie000626y

Samprovalaki, K., Robbins, P. T., and Fryer, P. J. (2012). Investigation of the diffusion of dyes in agar gels. *Journal of Food Engineering*, *111*(4), 537–545. doi:10.1016/j.jfoodeng.2012.03.024

Schenker, S., Handschin, S., Frey, B., Perren, R., and Escher, F. (2000). Pore Structure of Coffee Beans Affected by Roasting Conditions. *Journal of Food Science*, *65*(3), 452–457. doi:10.1111/j.1365-2621.2000.tb16026.x

Schwartzberg, H. (1987). Leaching—Organic Materials. In R. . Rousseau (Ed.), *Handbook of Separation Process Technology* (1st ed., pp. 540–577). Wiley.

Schwartzberg, H., and Chao, R. Y. (1982). Solute diffusivities in leaching processes. *Food Technology*, *36*(2), 73–86.

Scott, G. D. (1960). Packing of Spheres: Packing of Equal Spheres. *Nature*, *188*(4754), 908–909. doi:10.1038/188908a0

Sederman, A. ., Alexander, P., and Gladden, L. . (2001). Structure of packed beds probed by Magnetic Resonance Imaging. *Powder Technology*, *117*(3), 255–269. doi:10.1016/S0032-5910(00)00374-0

Sivetz, M., and Desrosier, N. W. (1979a). Development of coffee industry. In *Coffee technology* (pp. 19–30). Westport, Connecticut: Avi publishing company, inc.

Sivetz, M., and Desrosier, N. W. (1979b). Brewing technology. In *Coffee technology* (pp. 598–622). Westport, Connecticut: Avi publishing company, incsic.

Sivetz, M., and Desrosier, N. W. (1979c). Percolation: Theory and practice. In *Coffee technology* (pp. 317–372). Westport, Connecticut: Avi publishing company, inc.

Smith, R. F. (2001). A history of coffee. In M. N. Clifford & K. C. Willson (Eds.), *Coffee: botany, biochemistry and production of beans and bevearges* (1st ed., pp. 1–12). London&Sydney.

Sohn, H. ., and Moreland, C. (1968). The effect of particle size distribution on packing density. *The Canadian Journal of Chemical Engineering*, *46*.

Sovová, H., and Stateva, R. P. (2011). Supercritical fluid extraction from vegetable materials. *Reviews in Chemical Engineering*, *27*(3-4), 79–156. doi:10.1515/REVCE.2011.002

Spiro, M. (1993). Modelling the aqueous extraction of soluble substances from ground roast coffee. *Journal of the Science of Food and Agriculture*, *61*, 371–372. doi:10.1002/jsfa.2740610314

Spiro, M. (1997). Factors affecting the rate of infusion of black tea. In R. Schubert & M. Spiro (Eds.), *Chemical and Biological Properties of Tea Infusions* (pp. 38–62). Frankfurt/Main: Umwelt und Medizin.

Spiro, M., and Chong, Y. Y. (1997). The kinetics and mechanism of caffeine infusion from coffee: the temperature variation of the hindrance factor. *Journal of the Science of Food and Agriculture*, *74*(3), 416–420. doi:10.1002/(SICI)1097-0010(199707)74:3<416::AID-JSFA868>3.0.CO;2-0

Spiro, M., and Hunter, J. E. (1985). The kinetics and mechanism of caffeine infusion from coffee: the effect of roasting. *Journal of the Science of Food and Agriculture*, *36*, 871–876.

Spiro, M., and Jago, D. S. (1982). Kinetics and Equilibria of Tea Infusion.Part 3.-Rotating-disc experiments interpreted by a steady-state model. *J.Chem.Soc.Farady Trans.,1*, *78*, 295–305.

Spiro, M., and Page, C. M. (1984). The Kinetics and mechanism of caffeine infusion from coffee: Hydrodynamic aspects. *Journal of the Science of Food and Agriculture*, *35*(8), 925–930. doi:10.1002/jsfa.2740350818

Spiro, M., and Selwood, R. M. (1984). The kinetics and mechanism of caffeine infusion from coffee: The effect of particle size. *Journal of the Science of Food and Agriculture*, *35*(8), 915–924. doi:10.1002/jsfa.2740350817

Spiro, M., and Siddique, S. (1981). Kinetics and equilibria of tea infusion: Kinetics of extraction of theaflavins, thearubigins and caffeine from Koonsong broken pekoe. *Journal of the Science of Food and Agriculture*, *32*(11), 1135–1139. doi:10.1002/jsfa.2740321115

Spiro, M., Toumi, R., and Kandiah, M. (1989). The kinetics and mechanism of caffeine infusion from coffee: The hindrance factor in intra-bean diffusion. *Journal of the Science of Food and Agriculture*, *46*(3), 349–356. doi:10.1002/jsfa.2740460313

Stapley, A. G. F. (2002). Modelling the kinetics of tea and coffee infusion. *Journal of the Science of Food and Agriculture*, *1671*(July 2001), 1661–1671. doi:10.1002/jsfa.1250

Sympatec. (2015). Dispersing principle. Retrieved March 3, 2015, from https://www.sympatec.com/EN/LaserDiffraction/RODOS-M.html

Uquiche, E., del Valle, J. M., and Ihl, M. (2005). Microstructure-Extractability Relationships in the Extraction of Prepelletized Jalapeño Peppers with Supercritical Carbon Dioxide. *Journal of Food Science*, *70*(6), 379–386.

Uquiche, E., del Valle, J. M., and Ortiz, J. (2004). Supercritical carbon dioxide extraction of red pepper (Capsicum annuum L.) oleoresin. *Journal of Food Engineering*, *65*(1), 55–66. doi:10.1016/j.jfoodeng.2003.12.003

Voilley, A., and Simatos, D. (1979). Modeling the solubilization process during coffee brewing. *Journal of Food Process Engineering*, *3*(4), 185–198. doi:10.1111/j.1745-4530.1979.tb00238.x

Walstra, P. (2003). Polymers. In *Physical Chemistry of Foods*. New York: Marcel Dekker, Inc.

Wang, X., and Lim, L.-T. (2013). A Kinetics and Modeling Study of Coffee Roasting Under Isothermal Conditions. *Food and Bioprocess Technology*, *7*(3), 621–632. doi:10.1007/s11947-013-1159-8

Wang, X., and Lim, L.-T. (2014). Effect of roasting conditions on carbon dioxide degassing behavior in coffee. *Food Research International*, *61*, 144–151. doi:10.1016/j.foodres.2014.01.027

Weerts, A. H., Martin, D. R., Lian, G., and Melrose, J. R. (2005). Modelling the hydration of foodstuffs. *Simulation Modelling Practice and Theory*, *13*(2), 119–128. doi:10.1016/j.simpat.2004.09.001

Yu, A. B., and Standish, N. (1993, August). A study of the packing of particles with a mixture size distribution. *Powder Technology*. doi:10.1016/S0032-5910(05)80018-X

Zanoni, B., Pagliarini, E., and Peri, C. (1992). Modelling the aqueous extraction of soluble substances from ground roasted coffee. *Journal of the Science of Food and Agriculture*, *58*(2), 275–279. doi:10.1002/jsfa.2740580217

Zhang, C., Linforth, R., and Fisk, I. D. (2012). Cafestol extraction yield from different coffee brew mechanisms. *Food Research International*, *49*(1), 27–31. doi:10.1016/j.foodres.2012.06.032

Zou, R. P., Gan, M. L., and Yu, A. B. (2011). Prediction of the porosity of multi-component mixtures of cohesive and non-cohesive particles. *Chemical Engineering Science*, *66*(20), 4711–4721. doi:10.1016/j.ces.2011.06.037